Developing a Framework for Mixing Tube Tool Condition Monitoring of Abrasive Waterjet Systems

Danila Pietrow

A thesis submitted in partial fulfilment of the requirements for the degree of
Doctor of Engineering

The University of Sheffield

Faculty of Engineering

Department of Mechanical Engineering

Submission Date

June 12, 2024

Acknowledgements

First, I want to acknowledge my excellent supervisory team of Prof. Patrick Fairclough and Dr Kevin Kerrigan. Patrick, thank you for your continuous support and insightful feedback throughout. Your experience has helped me overcome many challenges and finish this EngD. Kevin, thank you for providing immense knowledge of the field and sharing your extensive network of industry contacts that enabled this research.

A special thanks goes out to Dr Mohamed Hashish, the godfather of the abrasive waterjet, who, despite his busy schedule, always made time to discuss my project direction. His input was invaluable, and I have huge respect for his knowledge and expertise.

I want to acknowledge the managerial team of the IDC, including Dr Hassan Ghadbeigi, Mrs Clare Clarke, Dr Pete Crawforth, and Dr David Curtis, for offering support during different stages of my research. Your collective contribution made a significant impact on my work.

Nicolas Duboust and David Tinker, your help was much appreciated during my preliminary data collection process and helped form the foundation of my methodology. Jerome Debout, Cedric Georges and the whole family at Aquarese - thank you for all your assistance and for providing your equipment on such short notice!

Polina, Nikita and Andrey thank you for helping me get to where I am today! Nikita, thank you for your amazing support throughout my EngD, you helped make my journey far less stressful. Mum and dad, I could not appreciate you more for giving me the opportunity to come to the UK. Dad thank you for encouraging me to pursue doctoral research - you couldn't have been more right in what the experience would provide.

To all my friends, thank you for never failing to motivate and inspire me. It's rare to find such genuine and passionate people and I am so happy to have met you all.

Chloe, I am forever grateful for your patience, endless curiosity, joy and for simply being the incredible person you are. I got my main research idea during one of our

many strolls together. Your positive energy has always lightened my days and helped me (finally) finish writing this thesis. Thank you for creating such a cosy environment at home and being a constant inspiration through the work you produce.

And of course, I have to thank the best doggo Maple for making me go on all those long walks in the Peaks where I got most of my analysis ideas and for all her daily rascal business that kept my months of writing fun.

Abstract

The abrasive waterjet machining process needs to be improved to increase its adoption in industry. The wear of the mixing tube affects cutting performance and must be considered for accurate machining. Frequent downtimes and subsequent costs can deter AWJ adoption. A wear monitoring system can help improve efficiency and lower costs by allowing for scheduled maintenance and better resource management. This thesis aimed to develop a framework for a real-time tool condition monitoring system that can predict mixing tube wear. Data collection challenges were identified to achieve this, and a data collection framework was designed. Wear time and a range of indirect sensor data was collected using the proposed methodology and analysed. The use of machine learning was explored to predict the mixing tube's exit diameter, a commonly used and direct measure of wear, and to classify the tool state using a 10% exit diameter growth as a wear threshold. Machine learning was used as the problem involved analysing indirect sensor data, which presented challenges such as non-linearity and multivariate relationships that are better addressed by machine learning techniques than traditional analytical methods. The performance of machine learning algorithms using only the sensor data was compared with simpler linear algorithms trained on recorded wear time. The sensor-based machine learning approaches were outperformed by the wear-time-based linear models when evaluated under controlled experimental conditions where variations such as part changes were not considered. For exit diameter prediction, 0.023 and 0.01 root mean squared error scores were obtained for machine learning and linear approaches respectively. For tool state classification, 0.7 and 1.0 F1-scores, which represent the harmonic mean of precision and recall, were obtained for machine learning and linear approaches respectively. However, a hybrid approach using machine learning models trained on both sensor and wear time data was found to achieve the best performance under changing conditions. In conclusion, this thesis proposed a foundation for building a tool condition monitoring system for the abrasive waterjet mixing tube.

Author Publications

Peer-reviewed conference paper

Danila Pietrow, J. Patrick A. Fairclough, Kevin Kerrigan. "A Framework for Tool Condition Monitoring of Abrasive Waterjet Systems". *Procedia CIRP* (2024), pp. 475-480. DOI: 10.1016/j.procir.2024.08.404.

Conference presentation

Danila Pietrow. "Abrasive Waterjet Nozzle Wear Prediction". *IDC Student Conference at AMRC* (2022).

Contents

Nomenclature

AI Artificial Intelligence

Al_2O_3 Aluminium Oxide

$AMRC$ Advanced Manufacturing Research Centre

ATD Additional Tube Dwell

AWJ Abrasive Waterjet

CB CatBoost

CFD Computational Fluid Dynamics

$CFRP$ Carbon-Fibre-Reinforced Polymer

CV Cross-Validation

EDM Electrical-Discharge Machining

$EngD$ Engineering Doctorate

ET Extremely Randomised Trees

FFT Fast Fourier Transform

GB Gradient Boosting Machines

HMI Human-Machine Interface

ID Internal Diameter

IQR Inter-Quartile Range

KMM Kernel Mean Discrepancy

KNN K-Nearest Neighbors

LASSO Least Absolute Shrinkage and Selection Operator

LGBM LightGBM

LogR Logistic Regression

LR Linear Regression

MAE Mean Absolute Error

MC Mixing Chamber

MI Mutual Information

MLP Multi-Layer Perceptron Neural Networks

MMD Maximum Mean Discrepancy

PCA Principal Component Analysis

PSD Power Spectral Density

RF Random Forests

Ridge Linear Least Squares with *l*2 Regularization

RMS Root Mean Square

RMSE Root Mean Squared Error

ROC − AUC Receiver Operating Characteristic - Area Under the Curve

SHAP Shapley Additive Explanations

Std dev Standard Deviation

STFT Short-Time Fourier Transform

SVM Support Vector Machines

TCM Tool Condition Monitoring

UHP Ultra High Pressure

WDC Wear Data Collection

XGB XGBoost

Chapter 1

Introduction

Automation can improve the efficiency and precision of cutting processes while lowering costs. Tool condition monitoring (TCM) is a method that can help address automation challenges in machining. TCM can enhance sustainability, productivity, and the final quality of machined components. Abrasive waterjet (AWJ) machining is one technology that can benefit from TCM and needs to be improved for better adoption in industry. This thesis aims to develop a framework for building an abrasive waterjet TCM system. The goal is to lay the foundation for tool path compensation and more accurate and sustainable AWJ machining.

In this thesis, the term "framework" refers to a structured, step-by-step approach for developing a real-time TCM system tailored for AWJ machining. This framework provides a clear methodology for data collection, data processing and model training, along with practical guidelines for implementation. These guidelines can be adapted to suit the unique requirements of different AWJ systems and users. The framework aims to bridge the gap between academic research and industrial applications by offering a clear, actionable method for developing predictive wear models. A framework for AWJ TCM is provided in the conclusions chapter.

This chapter introduces the AWJ process, followed by the idea of TCM and the challenges the industrial partner faces that this thesis aims to address. The motivations for the research are then discussed before the aims and objectives are presented. Finally, a brief thesis outline is presented.

1.1 Background

1.1.1 Abrasive waterjet (AWJ) machining

AWJ machining is a non-conventional cutting process. Cutting is manufacturing by removal of material [1]. Cutting performed using an automated machine, referred to as machining, is usually applied to parts in the near-net form as a final finishing operation before assembly or application. Unlike conventional machining methods, which involve direct physical contact between the tool and the workpiece, non-conventional machining refers to systems that do not have contact between the tool and the workpiece. Laser, electric discharge, ultrasonic and AWJ machining are all examples of non-conventional methods. The advantage of non-conventional processes is that they can cut hard and brittle materials, often with less damage to the workpiece and significantly reduced consumable costs compared to conventional cutting processes that use cutting tools.

The AWJ, patented by Dr Hashish in 1987, works by mixing abrasives with a high-velocity water stream [2]. Modern waterjets have multi-axis machining capabilities. Six-axis robotic arm and up to five-axis gantry systems are commercially available. A typical AWJ system, as seen in Figure 1.1, includes the nozzle, water catcher tank, intensifier pump and abrasive feeding system. In this thesis, "nozzle" refers to the AWJ cutting head unless otherwise specified.
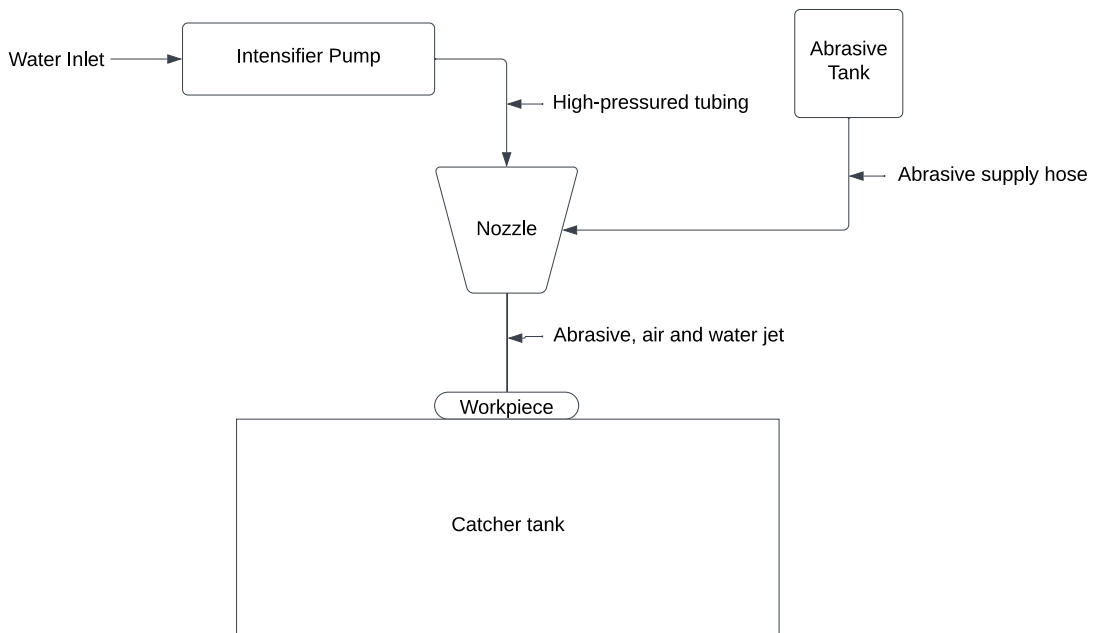

Figure 1.1: A schematic of a typical AWJ system and its key components.

Water is first supplied to the intensifier pump, where the water pressure is increased. Water is next brought to the nozzle through high-pressure tubing. Inside the nozzle, the water passes through three key components: the orifice, mixing chamber (MC) and mixing tube. The orifice first focuses the high-pressured jet of water. Next, abrasive particles are introduced from the abrasive tank to the MC, with the abrasive feed rate controlled by a metering disk in the abrasive tank. Finally, abrasives are mixed and accelerated by the water in the mixing tube before the jet leaves the nozzle. The water jet can then carry out the machining of the workpiece before the catcher tank collects the debris and dissipates the jet's energy.

The jet consists of a three-state flow of water, abrasives and air. When the AWJ is first switched on, a high-velocity water jet leaves the nozzle which removes some air from the MC [3, 4]. This creates vacuum, pulling air to the nozzle from the air inlet [4–6]. After the vacuum is established, the air can then act as a carrier for the abrasive particles when the operator switches on the abrasive supply. The water, abrasives, and air mixture then exit the tube, with the jet expanding horizontally into a cone.

The AWJ can generate high pressures of 6000 bar and has two common machining operations: cutting and drilling. Cutting refers to the process of removing material to form a desired geometric feature, while drilling is a specific process where a hole is created in a workpiece, employing either single location perforation or using the trepanning method.

The defining feature of AWJ machining is the use of abrasive particles. The most preferred abrasive in the industry for machining composites, metal, and glass is naturally occurring garnet [7, 8]. Garnet materials are a group of silicate minerals often used as abrasives [9, 10]. The main type of garnet used for abrasive application is almandine, which is Fe rich, due to its higher hardness and density relative to other garnet minerals [9–11]. Garnet effectively cuts a wide range of materials, leads to comparatively low mixing tube wear, doesn't produce harmful by-products and can be recycled. Garnet is a cost-effective and environmentally friendly choice for many applications [12, 13]. For extremely hard materials such as carbides or ceramics, harder abrasives such as aluminium oxide (Al_2O_3) may be required for effective machining as machining with garnet, although possible, would be relatively slow [8]. The use of Al_2O_3 abrasive leads to faster mixing tube wear due to it's higher hardness relative to garnet [7, 14].

The AWJ has several advantages over other non-conventional processes. It is non-chemical, non-thermal and non-electric, so it can machine a broad range of materials

3

without altering their physical properties. As a result, surface defects such as heat-affected zones and thermal cracking are completely eliminated [15]. Unlike laser and electric discharge systems, AWJs can machine reflective materials such as aluminium and non-conductive materials such as plastics and ceramics [16]. In addition, the AWJ has earned the label of a green machining process as it typically only uses water (non-toxic, readily available, and easily disposed of) and garnet (a non-reactive, biologically inert mineral) without producing toxic vapours common in composites machining or requiring lubricants which may impose health and safety issues [12, 15, 16].

A popular use case for AWJs is for machining composite materials such as carbon-fibre-reinforced polymer (CFRP). The AWJ has been used in many aircraft CFRP component machining applications. Some example components include [17]:

- Boeing 777: horizontal stabilisers

- Boeing 787: wing skins, vertical stabilisers, centre wing box, fixed leading edge

- Airbus 350XWB: wing spars

- Bell Helicopter V-22 Osprey: wing skins

Unique challenges are encountered when machining CFRP compared to conventional materials such as metals. Coolant application is problematic because the fibers can absorb moisture, leading to degraded mechanical performance of the finished part [18]. However, without coolant, tool-workpiece friction in conventional machining can cause thermal damage and matrix degradation [19]. In addition, carbon fibres are extremely abrasive, contributing to elevated tool wear rates [18]. Direct physical contact between the tool and the composite workpiece can produce further damage, such as delamination and fibre pull-out [18]. Hence, AWJ machining may be preferred over conventional machining methods, as it eliminates the need for traditional coolant application, limits thermal damage through cold cutting, and avoids direct contact between the tool and workpiece. While the jet of water does come into contact with the workpiece, its high-velocity impact leads to only momentary exposure, minimising the risk of moisture absorption.

Despite many listed advantages, the AWJ process has drawbacks. The process has high maintenance requirements and can struggle to hold dimensional accuracy, especially for thicker parts. Jet energy dissipates with increased part thickness, resulting in a cone with a wider exit compared to entry. This width deviation may be reduced by lowering the machining rate, which increases the machine running cost,

or by angling the tool to achieve a straighter edge on one side of the workpiece. As a result, the waterjet is often reserved for use on "difficult-to-cut" components [16].

As the shape of the water jet is controlled by the waterjet tool (the nozzle), the condition of the nozzle is the major factor that influences the dimensional accuracy and process's maintenance challenges.

1.1.2   Tool wear

One of the most important challenges in machining is the constant wear of tools. Tool wear refers to the gradual material loss of the tool due to regular operation. Tool wear is critical as it directly impacts the quality of the machined component. In AWJ machining, tool wear affects the precision and kinetic energy of the jet, reducing machining accuracy and surface quality [20, 21].

For AWJs, the tool is the nozzle, pictured in Figure 1.2. The nozzle has three key components: the orifice, MC and mixing tube. The orifice is typically 0.1 to 0.5 mm in diameter, with the diameter of the mixing tubes 2.5 to 5 times greater [7]. All three key nozzle components experience wear, however each component wears at a different rate. The lifespan of a typical commercial mixing tube, such as the ROCTEC 100 made by Kennametal's Rapid Omnidirectional Compaction (ROC) process [22], is approximately 50-100 hours when used under standard operating conditions with garnet abrasive [20]. The useful lifetime of the orifice varies, but if the recommended diamond material is used, lifetimes of 1000 hours are expected provided water is filtered and the water quality is good [23–25]. Finally, it is recommended that the MC be replaced every 500 hours, as this is standard industrial practice.

This thesis focuses on the wear of the mixing tube, which is the shortest-lived component. It experiences accelerated wear relative to other nozzle parts due to the high-velocity flow of large particles (relative to mixing tube internal diameter (ID)) in a narrow space, resulting in an erosive environment [7].

Mixing tube replacement costs play a significant role in waterjet economics, and improvements in wear monitoring are required for the growth of the technology [14]. It is not uncommon to have machining tools replaced prematurely in industry, with 20-50% of their useful life still remaining [26]. This methodology is known as preventative maintenance, the alternative to which is TCM or predictive maintenance.

High-pressure water

To pressure sensor

Abrasives and air

Orifice

Mixing Chamber

Nozzle body

Mixing tube

3-phase jet
(water, abrasives and air)
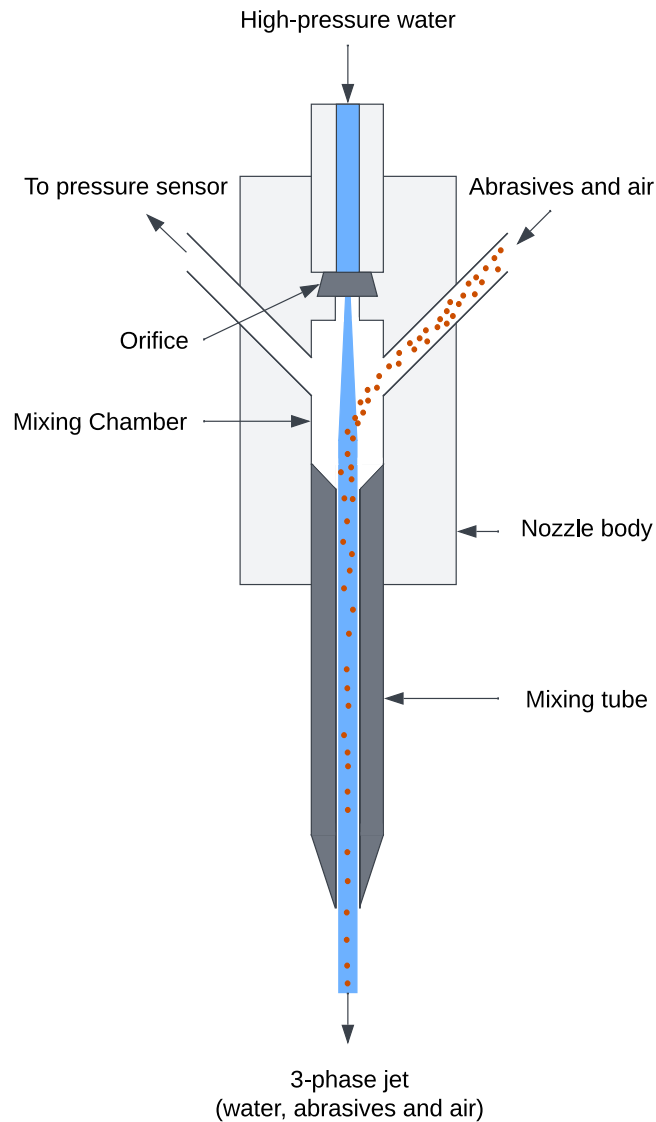
Figure 1.2: A schematic showing key components which make up the AWJ tool - the nozzle. The schematic includes an additional MC entry, which is part of some nozzle designs used for connecting vacuum assist technology or a pressure sensor.

1.1.3   Tool condition monitoring (TCM)

TCM is a vital aspect of modern manufacturing. TCM refers to using systems and technologies to monitor and assess the condition of tools in manufacturing processes. The main aim of TCM is to detect the wear and failure of the tool. TCM is used in machining to ensure tools are in optimal condition to reduce costs and increase production efficiency [27].

TCM can be carried out via either a direct or indirect approach. The direct ap-

proach measures the actual tool wear. Due to practical limitations, direct methods can often only be carried out by removing the tool and inspecting it in a laboratory. Practical limitations include poor illumination, use of cutting fluid and access problems during machining [28]. Indirect methods on the other hand, rely on measuring auxiliary variables via sensors, for example vibration, acoustic emission and temperature, during a machining process. The tool state and process conditions can influence these variables, and appropriate sensors can be used to measure them. The tool state can then be inferred from the measured data. To create an indirect TCM system, the following steps are used:

1. Attach sensor(s) to the machine and collect data.

2. Process the raw data and create features.

3. Feed the features to a decision-making system to make an inference.

After collecting data, the first step usually involves processing the raw sensors' signals to create usable features [29]. A "feature" refers to an individual measurable property of the observed signal, for example, the average vibration over a time period. Ideally, these features correlate with the tool condition. After the features are created and before the tool state is inferred, these features can be evaluated by a decision-making system [28]. For the decision-making system to make accurate predictions, a learning algorithm must be provided that is capable of performing a pattern association task that can map features to the appropriate tool state, such as a worn tool or a tool in good condition [29].

For AWJ mixing tube monitoring, direct monitoring methods include measuring the weight loss, measuring the exit diameter through either pin gauges or microscopy techniques, and studying the bore profile through destructive longitudinal sectioning or through radiometric techniques [14, 20, 21, 30]. The exit diameter and weight measurements are both non-destructive and simple to perform. Unlike weight loss measurements, exit diameter measurements do not require removing the mixing tube from the nozzle. However, all direct methods are inherently intrusive, lead to machine down time and disrupt the process.

Direct TCM methods have a high degree of accuracy, while indirect approaches are more practical but may lack accuracy [28, 31]. Indirect methods are usually considered more practical as they can be used online, continuously detecting changes to the measured signal. The constant signal observation allows indirect methods to be automated and carried out in real time. On the other hand, direct methods can

only be carried out intermittently and after process interruption, which is inefficient in terms of cost and time [31]. In addition, with a direct method, tool failure cannot be determined until after the machining cycle is completed, so potential damage, to the part being machined, cannot be prevented.

Considering the advantages of indirect TCM, the question remains as to why it is not yet widely applied. This question can be answered by understanding the challenges around indirect approaches. First, to build a monitoring solution, data has to be collected. The data collection comes at a cost. Collecting tool wear data usually entails expensive machining trials, especially when the collected data must include the full wear progression of the tool to capture the tool's failure point and observations during the full life cycle. The data trials are not only expensive but can also be time-consuming. Second, sensors used to collect the data and eventually monitor the process can be expensive and difficult to set up, with their data challenging to interpret. The sensors must also be non-intrusive to the machining process and capable of functioning online without interruption, sometimes in a harsh environment. They cannot restrict the working space and must be relatively maintenance-free and easily installed [31]. The sensors should also be versatile and capable of monitoring the tool condition under different process parameters. Finally, there is the challenge of designing the data collection trials. Not only are the scope, cost and sensor setup challenges considered at this stage, but also the potentially large input parameter spaces for different use cases must be accounted for, as well as the validation strategy for the proposed indirect system.

It's important to remember that indirect TCM aims to accurately predict the tool condition. This is not guaranteed before the expensive data collection takes place. As a result of this and the challenges described above, the application of indirect TCM in industry is challenging and rare.

1.2 Industrial context

The University of Sheffield Advanced Manufacturing Research Centre (AMRC) is a research centre working on machining, composites and future manufacturing needs. The centre bridges the gap between cutting-edge research and the day-to-day needs of industry. AMRC-sponsored Engineering Doctorate (EngD) research helps address problems framed by industrial members. An EngD is a four year long programme that offers PhD-level research. An EngD differs from a PhD by having a greater practical focus on industry outcomes over literature contributions with an additional

requirement that the projects are based around a real business case identified by an industrial partner. The EngD also has a significant taught component, with the EngDs offered by the Industrial Doctorate Centre at AMRC combining a first year of taught modules and background research with three subsequent years structured similarly to a traditional PhD.

The EngD research behind this thesis started from a problem framed by several AMRC members. It was identified that the AWJ process had to be improved to bring it closer to finishing rather than predominantly roughing operations for CFRP machining[1]. In many sectors, including aerospace, the machined components' final dimensional accuracy and surface finish are critical for the application. AWJ's tool path compensation capability must be developed to bring the AWJ technology closer to a finishing operation capable of producing higher-quality parts. A significant and unavoidable challenge affecting tool path compensation capability is tool wear. Tool wear monitoring requires development to address this. Currently, tool path compensation offset is measured by incrementally cutting a small test piece, measuring its dimensions, and calculating the difference between set and measured dimensions in a time-consuming process [32]. If the wear of the mixing tube is known or predictable, the tool offset may be inferred automatically. Mixing tube wear detection systems must therefore be developed as a foundation for smarter tool path compensation.

In addition, there is an increased demand for smart manufacturing with the transition to Industry 4.0 and the growth in machine learning. Process monitoring research is becoming progressively more important. No condition monitoring of mixing tube wear is currently in place for AWJ machining at the AMRC. Instead, mixing tubes are either replaced based on a preventative maintenance strategy or not monitored until a deterioration in the workpiece surface quality or machined dimensions is observed. This approach results in increased costs and wasted material. An online monitoring system of wear state is required, capable of continuous tracking in real-time.

1.3   Research motivation

In recent years, with the advent of the Internet of Things, there has been a surge in connected devices such as sensors, which has led to an explosion in the quantity of generated data [33]. The growth in computing power has also allowed more complex algorithms to be used for extracting insights from this generated data.

---

[1]Roughing involves removing the bulk of excess material from a workpiece while a finishing operation gets the workpiece to its final precise dimension with a desired surface finish.

For AWJ machining, research has focused on assessing the application of the available indirect sensors for their ability to differentiate between a worn and an unworn tool [34–41]. The research demonstrated that multiple sensors, via an indirect approach, can potentially monitor the AWJ process online in a non-intrusive manner. However, the ability to predict wear online using these approaches has seen limited research. Mohan et al. and Kim et al. took steps towards real-time process monitoring, but the approaches used had several limitations with no clear validation being performed [42, 43].

There is therefore a research gap in exploring the predictive capability of different indirect TCM methods. It is also unclear whether sensors can be used to predict the extent of tool wear in AWJ machining.

To develop a TCM system, data must be collected to build a model capable of inferring tool wear during machine operations. The specific challenges of data collection of the AWJ process have not been previously addressed, which may be the reason for a lack of research on TCM in AWJ machining beyond determining if a sensor has predictive potential. Therefore, a second research gap is present in developing a data collection system for building a monitoring application for the AWJ process, which addresses the present challenges.

Several challenges exist. First, the online system must be non-intrusive and capable of functioning without process interruption. Second, any indirect approach used must be able to function in a harsh waterjet environment, which includes high humidity (within the AWJ enclosure) and potential water and abrasive spraying during machining. Third is the challenge of a large input parameter space, which includes water jet, abrasive, and workpiece-specific parameters. Any proposed solution must be able to account for these and operate effectively under different parameter sets. Finally, considering a typical mixing tube has a life of 50-100 hours when using garnet abrasive, any data collection process which accounts for the full extent of tool wear can quickly become time-consuming and expensive [20].

Despite these challenges, a data collection framework must be developed to translate research into industry application in AWJ machining. Collected data could then be used to develop a process monitoring system. The research presented in this thesis aims to address the research gap in developing a data collection framework for building a monitoring application for the AWJ process and exploring the predictive capabilities of different indirect sensors in predicting mixing tube wear. The goal is to understand whether it is possible to predict the wear of the mixing tube.

Data collection framework design will address the mentioned challenges. Accelerated wear trials, using Al_2O_3 abrasive instead of garnet, will be used together with inexpensive sensors, with the aim of designing a feasible system for use in industry. The use of accelerated wear trials will be evaluated in their effectiveness for building a process monitoring solution for systems experiencing regular wear, with garnet. Data for this research is collected on industrial AWJ machines, ensuring findings represent real-world operating conditions.

Machine learning will be used as a tool to predict wear. Machine learning is selected for use as a decision-making system for TCM for multiple reasons. First, for a complex problem with a fluctuating environment such as AWJ TCM, that may otherwise necessitate a lot of fine-tuning with a traditional solution, machine learning requires less code, lower maintenance and can be automated during implementation[44]. Machine learning will be compared against simpler predictive approaches, such as using linear regression (LR) based on total tool wear time. While machine learning is an attractive tool, a simple solution can sometimes be more reliable and preferred, as simpler solution outputs are normally easier to interpret [27]. In addition, many stakeholders don't trust machine learning solutions, as they are seen as "black-box", and this approach will help evaluate whether it is worth investing in machine learning and an inherently more complicated setup [45].

This research has the potential for several technical impacts. First, it will establish a novel framework for mixing tube condition monitoring, which will serve as a foundation for tool path compensation and more accurate AWJ machining in a drive towards smarter manufacturing. This may help with AWJ adoption in industry. In addition, multiple sensors will be compared in their applicability for AWJ wear monitoring. This will help users of the process monitoring framework understand which sensor, or combination of sensors, is best to invest in. By studying the internal wear progression of the mixing tubes under multiple abrasives, previous research can be validated, and the wear process can be better understood.

From the economic and societal perspective, there are some additional potential impacts from this research. First, developing the AWJ machining solution helps improve an environmentally friendly machining process. By increasing the chances of technological adoption in industry, the environmental damage in industry may be reduced. Furthermore, developing a sustainable mixing tube replacement strategy with a dynamic end-of-life will allow users to get the maximum lifetime out of their tools - further improving the sustainability of the AWJ solution.

11

Finally, the research presented in this thesis will help address a research gap and help bring the process monitoring AWJ research closer to the manufacturing floor. At this stage, it is important to acknowledge that this is a complex problem. The objective of this EngD is not to develop a product that can be installed on any machine - the scope of this is too large. Instead, the objective is to develop a framework for building a mixing tube TCM system, acting as a foundation for creating a tool path compensation system.

1.4 Aims and objectives

The hypothesis of this thesis is that indirect sensor data from an accelerated wear trial can be used to accurately predict AWJ mixing tube wear using machine learning to reduce downtime and improve the sustainability of the process.

The aim of this thesis is to design a framework for building a mixing tube process monitoring system for the AWJ machining process. To achieve this aim, there are several objectives:

- To review the current literature on AWJ mixing tube wear and TCM development, to identify gaps in existing research.

- To develop a data collection methodology for building a dataset of indirect sensor data, which can then be used to train a model to infer mixing tube wear.

- To select suitable and inexpensive sensors for the data collection methodology that do not interfere with the machining process.

- To build a dataset using the designed methodology and explore changes in data with changing mixing tube wear.

- To study the wear progression of mixing tubes by studying the exit wear progression and internal wear profiles.

- To compare garnet and Al_2O_3 abrasives regarding the shape, size, density and flow to validate their similarities reported in literature, and to determine if accelerated wear with Al_2O_3 is comparable to regular wear with garnet.

- To explore the performance of different machine learning algorithms in their ability to both predict the exact mixing tube exit diameter in a regression task and to classify the state of the tool in a classification task using data from inexpensive sensors.

- To evaluate the feasibility of using machine learning and indirect data collection by comparing performance against simpler methods relying on monitoring total wear time.

- To assess whether machine learning models trained on data from accelerated wear trials can be used to make accurate predictions on mixing tubes worn using regular wear. In other words, can data be collected using a faster process to develop models that would be applicable in industrial conditions?

- To apply model explainability approaches on the best performing machine learning models to gain an insight into the relationships between individual features and model predictions.

1.5 Thesis outline

- Chapter 1 presented top-level AWJ and TCM background, discussed the industrial context and research motivations and provided the aims and objectives of this EngD.

- Chapter 2 reviews relevant research on AWJ mixing tube wear, challenges associated with monitoring mixing tube wear and the development of a TCM system.

- Chapter 3 first outlines the designed experimental methodology for the data collection trials before explaining each decision made. Sensor selection, an overview of collected data and the experimental setup are also discussed.

- Chapter 4 presents preliminary trial results. Within the chapter, the data collection methodology is evaluated, and the machine learning workflow is discussed.

- Chapter 5 includes data analysis of all collected data after the main trial was conducted. First, abrasive and mixing tube wear data that were collected after the main trials is presented and discussed. Next, the main trial experimental sensor data is visualised and explored for insights.

- Chapter 6 investigates using supervised machine learning for tool wear prediction and tool state classification. The effectiveness of using accelerated wear mixing tube data in making wear predictions on industry-worn mixing tubes is presented. Model explainability is explored. Finally, the effect and mitigation of data drift is discussed.

- Chapter 7 ties the designed methodology and explored monitoring strategies together to summarise their effectiveness, proposing a framework for building a TCM system for the AWJ machine. The chapter summarises the research findings and contributions to the field before discussing possible future research directions.

Chapter 2

Literature Review

After presenting the industrial context and motivation for this research, it is important to provide an overview of the literature to date and explain where this work fits within it. This chapter will review mixing tube wear and how to develop a wear monitoring system. The reviewed steps include selecting appropriate sensors, signal processing, and machine learning techniques. The main objective is to gain a better understanding of how wear occurs within mixing tubes and to explore and compare different ways of recording, monitoring, and predicting wear.

2.1 AWJ nozzle design

The AWJ nozzle design must be considered before exploring mixing tube wear to understand how parts further upstream have an impact on the mixing tube. A breakdown of the AWJ nozzle's key components, the mixing tube, orifice and MC was provided in Figure 1.2 in Chapter 1. A more detailed breakdown of additional components making up the AWJ nozzle and important issues associated with each one was created by Hashish and is presented in Figure 2.1 [25]. The additional components will not be addressed in this thesis, however their design parameters will be briefly discussed.

The Ultra High Pressure (UHP) water tube has to be fatigue resistant and correctly sized in order to produce a coherent jet [25]. The orifice holder has to withstand deformation under high-pressure loads and ensure accurate placement of the orifice for good orifice alignment[25]. A UHP seal has to be used in the orifice holder to seal the orifice. The seal is used to make sure no water leaks below and around the orifice which can greatly affect the orifice holder lifetime and the quality of the water jet [25]. The UHP seal keeps the pressure sealed during cutting, with wear to the part leading to leaks and a loss of UHP in the system, which may also result in pressure
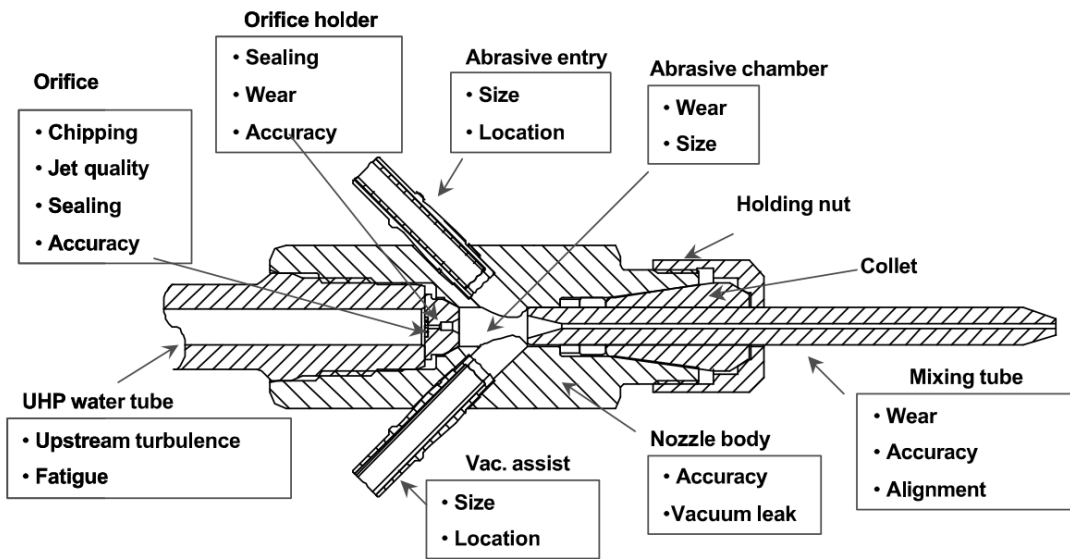
Figure 2.1: A schematic, created by Hashish, of the key components making up the AWJ nozzle, with a breakdown of important issues associated with each one [25].

inconsistencies [46]. The collet has to be accurately produced as it serves the important role of precisely holding the mixing tube in the nozzle body. Finally, the body of the nozzle provides the port connections for abrasive entry and potential additions such as a sensor for monitoring parameters downstream of the orifice or a vacuum assist part [25].

Vacuum assist is an additional vacuum suction part which can be added to the nozzle assembly. The concept was developed by Hashish et al. to draw more air to the nozzle and provide a more effective abrasive-carrying capacity [47]. Vacuum assist was designed for addressing challenges in precision drilling of small holes in fragile materials. Vacuum assist eliminates lag time between starting the jet of water and abrasives arriving in the MC, by establishing abrasive flow to the nozzle prior to starting the waterjet [25].

For the three main AWJ components, Hashish notes several important design considerations [25]. The orifice has to be fluid flow erosion resistant, must produce a coherent jet and be resistant to chipping from the impact of small particulates [25]. The MC requires a hard liner to reduce wear from the rush of abrasives entering the nozzle [25]. Finally, for the mixing tube, a conical area upstream is required to facilitate abrasive entry, and careful alignment with the orifice is crucial to ensure even wear [25]. The orifice is normally 0.1 to 0.5 mm in diameter, with the mixing tube diameter 2.5 to 5 times greater, to maintain an optimum mixing and cutting

16

performance [7, 14, 20, 24, 48–50].

2.2   Mixing tube wear

The AWJ functions by accelerating abrasive particles through the mixing tube part of the nozzle. The waterjet velocity can reach 850 m/s [51, 52], with individual abrasive particles capable of reaching around 80% of the waterjet's velocity [53]. This high-velocity water and abrasive flow, through a relatively narrow tube, leads to an erosive environment and thus mixing tube wear. The abrasives, while mixing with water, continuously impact the internal mixing tube walls, changing the mixing tube profile, progressing towards and eventually increasing the exit diameter [7, 20].

The lifetime of an AWJ mixing tube depends on numerous factors, but for a typical tube used in industry, such as the ROCTEC 100, around 50 to 100 hours of total useful life can be expected [20]. However, mixing tube lifetime is application-dependent, with precision drilling having a lower tolerance for wear compared to rough cutting [7]. If generalising, 10% exit diameter growth is within the tolerable limit, even though some applications may allow higher wear up to 25% [7].

Hashish observed two general wear patterns that can occur during mixing tube wear, as shown in Figure 2.2 [7]. A divergent wear pattern is observed if the abrasives are significantly harder than the mixing tube material [7, 25]. For example, when a soft mixing tube material is used, such as steel, with hard abrasives such as garnet or Al_2O_3. When the mixing tube is made of a hard material such as tungsten carbide, a convergent wear pattern occurs instead [7, 25].

Hashish also characterised the two dominant wear modes which occur within the mixing tube [7]. The two wear modes are abrasion at the downstream sections and erosion by particle impact at the upstream section of the mixing tube [7]. Abrasive wear is wear by material displacement caused by hard particles [54]. Erosive wear is the loss of material from a solid surface caused by the impact of abrasive particles [54].

The findings by Hashish are consistent with erosion models reported by Bitter, which suggest that two different material removal mechanisms cause wear by solid particle impact: a combination of abrasion and erosion at shallow impact angles and erosion at large impact angles (greater than 20º) [7, 55, 56]. At the upstream sections, Hashish suggested that particles have velocity components that are not parallel to the wall, as abrasives enter at different speeds and angles [7]. Consistent with Bitter, at these upper sections, larger impact angles will dominate, and therefore higher erosion

Figure 2.2: Possible wear patterns of AWJ mixing tubes – as observed by Hashish [7]. When using hard abrasives like garnet, a mixing tube made of hard material exhibits a convergent wear pattern, whereas a mixing tube made of soft material exhibits a divergent wear pattern.

wear would occur [55, 56]. At the downstream sections, Hashish suggested that the velocity vectors of the particles become parallel with the tube, assuming the tube's length is sufficient to allow the shallow angle impact to dominate towards the tube exit, which leads to a combination of abrasion and erosion [7].

The work by Hashish and Bitter helps to understand the reasons behind the observation of different wear patterns observed in AWJ mixing tubes [7, 55, 56]. At the upstream tube sections, where large-angle impacts dominate and greater erosion occurs, ductile and tough materials such as steel are likely to be more resistant to wear compared to brittle and hard materials such as tungsten carbide. Downstream of the mixing tube, harder materials are better suited to resist abrasion, as they will better resist shallow angle impacts. Considering these wear modes, a convergent pattern indicates that the mixing tube material threshold for hardness is greater

than its threshold for toughness [25]. Convergent wear will therefore be observed for harder materials that better resist abrasion wear, and a divergent wear pattern will be observed for materials that better resist erosion wear.

Ramulu et al. investigated the wear performance of tungsten carbide tools [57]. The research supported the wear modes observed by Hashish [7]. The authors longitudinally sectioned two worn mixing tubes in half via electrical discharge machining (EDM) and studied the inner profile via microscopy. The authors found that at the mixing tube inlet, erosion wear dominated, followed by erosion to abrasion transition in the mid-section of the tube and a combination of erosion and abrasion towards the tube exit [57].

For mixing tubes experiencing the convergent wear pattern, wave zones have been reported along the internal mixing tube profile [7, 13, 14, 48, 57–59]. Figure 2.3, taken from Kennametal's ROCTEC mixing tube brochure presents an example representation of the wave zones [59]. Simulation work carried out by Chen et al., Mingming et al., Kamarudin et al. and Long et al., which included abrasive particle tracing, may explain this phenomenon [60–63]. The studies observed that abrasives introduced to the mixing tube have a large velocity difference between the waterjet and individual abrasive particles. Due to the presence of many local turbulent vertices at the beginning of the mixing process, the abrasive movement is disorderly and results in collisions with the mixing tube wall while the particle is accelerated down towards the tube exit. The particle circumferential movement would gradually decrease as the abrasive particles merged with water. Supporting Hashish's theory on particle velocity vectors at different points in the mixing tube [7].

The conclusions are also supported by experimental evidence observed by Ramulu et al. on sectioned mixing tubes [57]. The authors found that oscillating wear decreased towards the mixing tube exit, attributing this to a decrease in the turbulence of the waterjet slurry (abrasive, water and air mixture).

Kennametal, the manufacturer of the ROCTEC mixing tubes, has also reported that the wave pattern observed can help understand if the waterjet is functioning as intended [59]. "Functioning as intended" refers to having an orifice that is well aligned with the mixing tube and having both the orifice and MC in good condition [59]. If the jet is misaligned, the stream will hit the tube wall, diminishing the cut quality and reducing the mixing tube life, causing an irregular inner tube profile to be observed [59]. The ROCTEC brochure states that a "good tube wear" pattern is one which is both "concentric and consistent from entry to exit showing a wave-like wear

AWJ Mixing Tube Wear Patterns
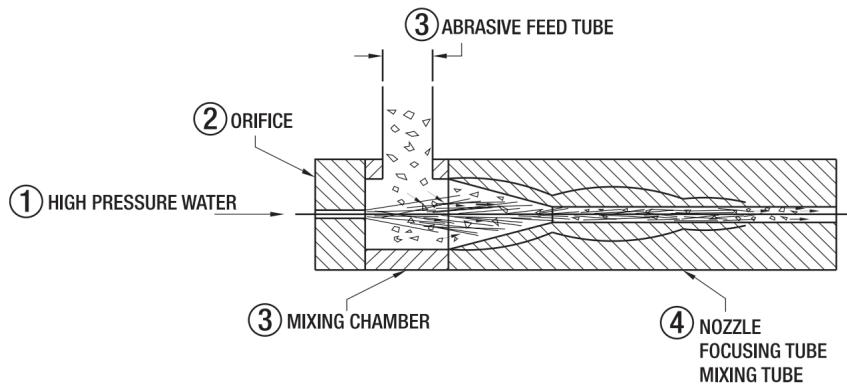
Figure 2.3: A schematic of the wave zone wear pattern expected to form during convergent wear of AWJ mixing tubes. The wave pattern is denoted by black curved lines along the tube's internal profile [59].

pattern" [59]. Examples of different wave patterns that can be observed on mixing tubes are presented in Figure 2.4.

If the jet is misaligned and allows the stream to hit the tube wall, the cut quality will diminish and the tube life will be shortened dramatically.

Good tube wear will be concentric and consistent from entry to exit showing a wave like wear pattern.

Figure 2.4: Longitudinally sectioned mixing tubes, showing examples of internal wear profiles under worn orifice or MC (top tube), orifice misalignment (middle tube) and of good consistent and concentric wear (bottom tube) taken from a ROCTEC brochure [59].

Hashish noted that the wave pattern observed inside the mixing tubes is more pronounced when the ratio of orifice diameter to mixing tube diameter is relatively low, resulting in stronger jet oscillations and lateral impacts [25]. In addition, Hashish noted that mixing tube misalignment could lead to blowout wear at the mixing tube exit, with the jet leaving the tube from its sidewall [25].

Unlike for conventional machining, where cutting edge radius is crucial, gradual mixing tube wear does not lead to sudden drops in performance [64]. However, mixing

tube wear has several negative effects on the machining process. Hashish reported that wear affects the efficiency of momentum transfer between the abrasives and water, which could reduce cutting performance [7]. Moreover, increases in the exit diameter due to wear affects the width of the cut and therefore machining precision [7, 65]. Nedic et al. found that an increase in the mixing tube working time led to more pronounced roughness of the machined surface for multiple materials [66]. Perec et al. and Hashish also found that increasing the exit diameter of the mixing tube increases the kerf width of cut, in a linear increasing trend [13, 67]. The kerf width is the variation in width of cut between the bottom and the top of a machined component. Kerf affects the surface finish as well as the required tolerance of the machined part [68, 69].

Finally, Hashish found that increasing the mixing tube diameter affects the power density of the jet [50]. A narrower mixing tube has a higher power density which leads to better cutting performance, with a faster volume removal rate, better depth of cut, narrower width of cut, and reduced surface waviness [50]. This suggests that a worn mixing tube with a larger exit diameter will have a lower power density compared to an unworn tube, which would result in lower performance.

2.3   Challenges of indirect monitoring of mixing tube wear

Data has to be collected to build an indirect monitoring system. There are several challenges associated with collecting data for the wear of the AWJ mixing tube. First, wear has to be measured in a repeatable and feasible manner. Wear measurements have to be performed using a direct method (as defined in Chapter 1) to build a monitoring system which uses an indirect approach. Second, data has to be collected for the entire tool life in order to capture the full extent of wear. The mixing tube has a relatively long life, and the data collection process can, therefore, become expensive in terms of time and cost. Finally, there is the challenge of a large input parameter space, which can further complicate and extend the data collection process.

2.3.1   Measuring mixing tube wear

There are several direct methods of measuring mixing tube wear. Different approaches can be split into several categories; measuring the exit diameter, measuring the inner profile and measuring the weight. The exit diameter can be measured via pin gauges and optical microscopy [20, 21]. The inner profile can be measured via destructive

longitudinal sectioning, radiometric techniques and epoxy casting [14, 21, 30, 70]. In addition to measuring the exit diameter and the profile of the tubes, the weight of the tube can also be used to measure wear [14, 20, 21].

Exit diameter measurements fail to capture the wear progression from the top of the tube. For tubes experiencing a convergent wear pattern, this is particularly relevant as the wear progresses from tube entry down towards the exit. Therefore, the exit diameter may fail to reflect the true extent of wear throughout the entire tube length, potentially leading to underestimations of wear severity. In addition, Nanduri et al. argued that exit diameter measurements are not a reliable indicator of mixing tube performance and wear [14, 20]. Instead, the authors suggested weight loss measurements are a better alternative, as weight loss has a linear correlation with mixing tube life unlike exit diameter measurements which are non-uniform. A limitation of this research is that the authors measured the exit diameter using pin gauges with incremental steps of 0.025 mm [14, 20]. The plots presented by the authors, shown in Figures 2.5 and 2.6 , where a "non-uniform" and non-linear wear progression was observed, have this non-linearity in steps of 0.025 mm. If pin gauges of a smaller diameter, for example 0.01 mm, were used instead, the authors may have come to a different conclusion. In addition, since the exit diameter correlates with machining quality, whether the pattern is linear or not does not disqualify the applicability of the method, provided it detects wear and can be used to build a monitoring system.
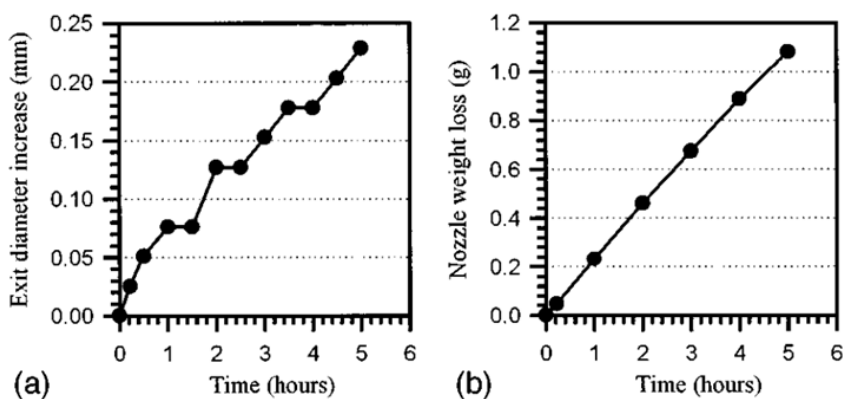

Figure 2.5: (a) Exit diameter increase and (b) nozzle weight loss of 76 mm long WC/Co mixing tubes worn using garnet abrasive. The mixing tubes had a starting ID of 1 mm. The figure is reproduced from Nanduri et al. [20].

The exit diameter measurements, via the pin gauge approach, are simpler and faster to perform in contrast to other methods. The pin gauge approach is also the
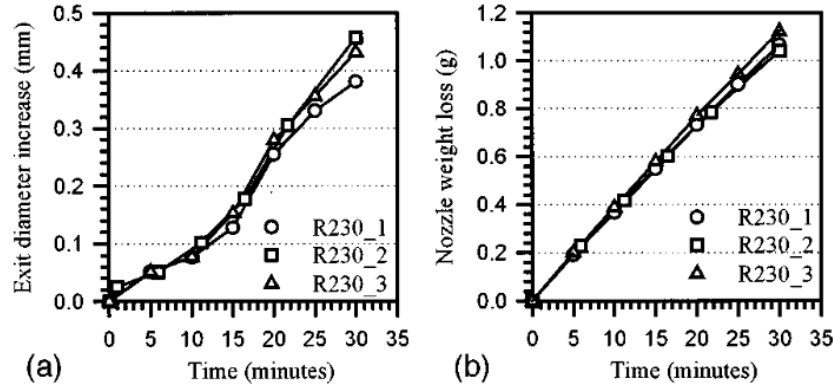
Figure 2.6: (a) Exit diameter increase and (b) nozzle weight loss of 76 mm long ROCTEC 100 mixing tubes worn using Al_2O_3 abrasive. The mixing tubes had a starting ID of 1 mm. The figure is reproduced from Nanduri et al. [20].

most practical as it is non-destructive and does not require any special preparation or laboratory equipment or the mixing tube to be removed from the machine. In addition, the pin gauge method does not cause a potential health risk due to radioactivity, unlike radiometric techniques [38]. The increase in exit diameter is also related to cutting performance, as it directly impacts multiple machining attributes, such as the width of cut and kerf [7, 13, 67]. Therefore, the exit diameter is an appropriate metric to monitor without necessarily detailing the exact wear profile.

Pin gauges can still be used to get an idea of the wear profile, for example, by using progressively larger pin gauges to build up a wear profile plot of different pin probing depths, such as the ones developed by Nanduri et al. seen in Figure 2.7 [14, 20]. However, this approach has several issues. First, it's more time-consuming as it requires removing the mixing tube from the machine and gauging the entrance of the mixing tube with multiple gauges. Second, mixing tubes come at varying lengths, and pin gauges may not be long enough, adding to the complexity of the setup. Finally, the pin gauges will fail to capture the wave pattern caused by wear, so the developed profile won't be completely accurate.

2.3.2 Accelerated wear of mixing tubes

A second challenge of data collection of wear for the AWJ process is the long life of the mixing tubes, which can lead to expensive data collection trials. A potential solution to this challenge is to accelerate the wear process. Accelerated wear can be carried out using either a soft mixing tube material (relative to abrasive) or harder abrasives [7, 21]. In industry, garnet abrasive together with tungsten carbide mixing

23
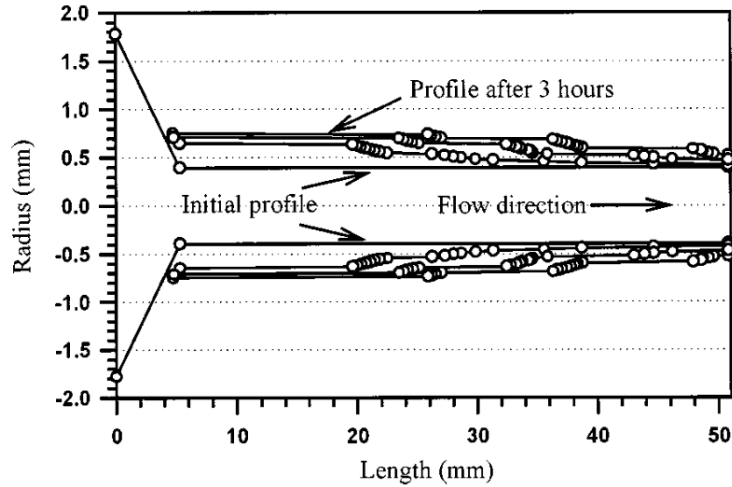
Figure 2.7: Changes to a tungsten carbide mixing tube's internal profile between 0 and 3 hours of wear, measured using progressively larger pin gauges from the top of the mixing tube. The figure is reproduced from Nanduri et al. [20].

tubes, such as the ROCTEC 100 created by Kennametal, are a common combination as they offer good cutting efficiency and an extended tool life [12–14]. For accelerated wear, a harder abrasive material such as Al_2O_3 or a softer mixing tube material such as steel are used.

The challenge of accelerated wear trials is maintaining a similar mixing tube wear profile between accelerated and regular wear. When developing a monitoring system, it is important to have representative wear. Garnet and tungsten carbide tube combination produces a convergent wear pattern [7]. Using a softer mixing tube material would not be suitable in replicating the wear process, as this would result in a divergent wear pattern being observed instead [7].

Hashish found that replacing garnet with Al_2O_3 may be a suitable alternative, as Al_2O_3 has a higher hardness but a similar density and particle shape [7, 50]. Particle shape and density are important. In a numerical study, Long et al. found that both properties may affect the velocity of the particles [63]. A less rounded shape of the abrasive (decreasing shape factor) and a lower abrasive density were found to result in higher particle velocity [63]. This means that abrasive particles will have more kinetic energy when travelling through the mixing tube if they have a lower shape factor and a lower density, potentially impacting the material removal inside the mixing tube. However, this may need further validation, as results were observed up to a density of 3500 kg/m³ for which particle velocity remained unchanged after

a density increase [63]. Meanwhile, the densities of Garnet and Al_2O_3 are 4100-4300 kg/m^3 and 3900-4100 kg/m^3 respectively [13, 58].

On the Mohs hardness scale, garnet has a hardness of 7.5-8, while Al_2O_3 has a hardness of 9. While wearing the mixing tube with Al_2O_3 will result in a convergent wear pattern, the higher hardness of the abrasive will lead to a greater degree of abrasion wear being observed [7]. Hashish et al. suggests that the contribution to erosion from both particles should remain similar [7]. The effectiveness of accelerated wear trials for a more feasible data collection process should therefore be assessed to see if data collected during an accelerated wear trial can generalise[1] to data from a regular wear trial despite differences in wear contributions.

Taggart et al., conducted research into using accelerated wear trials [71]. The authors found that using the harder abrasive on 76 mm long ROCTEC 100 mixing tubes with a 1.0 mm diameter at 365 MPa water pressure, 0.33 mm orifice diameter, 80 mesh abrasive and an abrasive flow rate of 7.6g/s resulted in the exit diameter growth rate increasing by almost 60 times from 0.00529 mm/hr for garnet, which was worn at a higher pressure of 379 MPa, to 0.305 mm/hr for Al_2O_3 [71]. Nanduri et al. completed further accelerated and regular wear tests of tungsten carbide tubes using Al_2O_3 and garnet abrasives [14, 20]. The authors concluded that the relative wear rates for both methods correlate well. This suggests that during the convergent wear pattern, the wear reaches the exit at a steady rate and wear is therefore relatively similar for both abrasives, albeit faster for Al_2O_3. This suggests accelerated wear trials are a suitable approach for tackling the data collection challenge of time and cost.

Perec et al., found that the wear difference between garnet and Al_2O_3 abrasive is not as great as shown by Taggart et al., with a 16 times exit diameter wear rate increase under the accelerated approach [13, 71]. The input mixing tube and orifice parameters between the two researchers were not the same, which may have contributed to the observed difference. Perec et al. presented cross-sectioned images of the mixing tubes, which appear to show poor wear that is not concentric and consistent, as described in Figure 2.4 [13, 59]. This suggests the jet was poorly aligned, and the wear was irregular, which also may have impacted the researchers' results.

Perec et al. observed that the particle size distribution for two different Al_2O_3 abrasives remained either unchanged after wear or had a slight reduction in median

---

[1]The term generalise is often used in the machine learning community when referring to a model's ability to perform well on new, previously unseen data rather than solely on the data it was trained on. In this case, the ability for data from an accelerated wear trial to make inferences from patterns seen during regular mixing tube wear.

particle size by approximately 15 μm [13]. This suggests little particle breakdown for the material. Meanwhile, in a separate study, Perec et al. found that garnet under the same pressure and with similar orifice and mixing tube dimensions had significant particle fragmentation [58]. The findings may contradict the observations by Hashish that the contribution to erosion from both abrasives should be the same [7]. Al_2O_3 may after all contribute more to erosion wear further along the tube as the particles may not fragment, maintaining their original size compared to the fragmenting garnet. This hypothesis is as yet untested. However, experimental and quantitative findings from slurry flow systems, where larger particles lead to higher erosion rates (as demonstrated by Lynn et al. and Clark et al.), may offer insight into the potential behaviour of non-fragmenting abrasives in abrasive waterjets [72, 73].

2.3.3 Abrasive waterjet input parameters

Another challenge of monitoring mixing tube wear is the broad range of input parameters available in AWJ machining. To monitor wear indirectly, data has to be collected using different parameters that may be applied by the user. Otherwise, the system may struggle to infer wear under new unseen conditions. The parameters that contribute to mixing tube wear can be split into two groups: process and design parameters [50]. The parameters and their effect on the wear rate are summarised in Table 2.1.

When designing a data collection system the extended list of input parameter options, summarised in Table 2.1, may become a challenge. However, studies have been undertaken to examine some of the possible variables. Literature shows that increasing the mixing tube length decreases the wear rate [7, 14, 50]. But, Hashish et al., argued that increasing the mixing tube length only delays the wear reaching the exit bore (during convergent wear), while the jet properties may still deteriorate [7]. However, Nanduri et al. found that increasing the length decreases the mixing tube weight loss rate per unit length as well [14].

Longer mixing tubes result in lower jet exit velocities due to increased frictional losses, as can be measured by Reynolds number and friction factor calculations. This reduced velocity could decrease the rate of material removal per collision and potentially reduces the overall wear rate of the tube. The relationship between tube length and wear characteristics can be hypothesized based on the idea that as the length increases, the abrasive jet loses more energy to friction, thereby reducing its erosive power. This phenomenon is supported by collected data from Nanduri et al., where

Table 2.1: Parameters affecting the mixing tube wear rate. Up/down arrows indicate that increasing the parameter value increases/decreases the wear rate.

Parameter Name	Effect of Increasing Parameter on Wear Rate	Additional Notes
Design Parameters		
Mixing tube to orifice diameter ratio	-	Ratio between 2.5 and 5 provides optimal cutting and mixing conditions [7, 14, 24, 48–50].
Orifice diameter	↑	[25].
Mixing tube length	↓	Slower exit bore growth with increasing length [7, 14, 50].
Mixing tube material hardness	↓	Abrasive material dependent, however generally, higher material hardness leads to greater wear resistance. [7, 57, 74, 75].
Orifice and mixing tube misalignment	↑	Misalignment causes accelerated and uneven wear [25, 32, 59, 76].
Distance from orifice to mixing tube	↑	[25, 77].
Mixing tube inlet angle	-	Higher inlet angles may lead to uneven wear, however generally no effect [14, 25, 78].
Process Parameters		
Abrasive material hardness	↑	[7, 14, 20, 71, 75].
Abrasive material density	↓	Results observed during a numerical study and not experimentally confirmed [63].
Abrasive particle size	↑	Larger particles have a higher kinetic energy and produce larger impact forces [7, 50, 75]. However, this effect is mixing tube material dependent [25, 50].
Abrasive particle shape factor	↓	Results observed during a numerical study and not experimentally confirmed [63].
Abrasive flow rate	↑	Increases wear rate, without changing wear pattern [14, 48, 50].
Waterjet pressure	↑	[14, 25, 50, 65].

the mixing tube weight loss rate per unit length decreases with increasing tube length [14].

Consequently, tube length is a critical parameter in AWJ machining that impacts the longevity of the mixing tubes. However, it is important to note that it's a complex system and additional factors outside jet velocity can influence wear rates. For example, Hashish et al. suggested that longer tubes may wear slower due to the abrasive particles having their velocity vectors align parallel to the mixing tube wall along the tube length, assuming the tube length is sufficient to allow for this [50].

Process parameters are abrasive-dominated. It is often the case that the waterjet user uses the same abrasive of the same size, therefore the key variable is water pressure. Water pressure changes may lead to increased particle fragmentation which may not only impact the wear rate but also the wear profile [14, 50]. Whether water pressure changes affect the wear profile is important to understand. This may become an additional challenge for data collection considerations for a process monitoring system, that is aiming to maintain a similar profile in the TCM system development as in production. Hashish et al. found that for garnet abrasive, increasing pressures beyond 207 MPa did not result in further significant fragmentation of particles [65]. Therefore, particle fragmentation beyond this pressure should not affect the wear profile.

Nanduri et al. found that for Al_2O_3 abrasive, up to 310 MPa water pressure, the mixing tube weight loss rate increased, but between 310-359 MPa began to plateau [14]. However, the range considered was limited up to 359 MPa, clearly further pressure increases should be considered. The work by Nanduri et al. nevertheless suggested that beyond approximately 310 MPa water pressure, wear becomes consistent inside the mixing tube for the Al_2O_3 abrasive.

Water pressure increase can also result in a reduced jet coherency which may impact the wear profile [65]. A coherent jet refers to a focused jet exhibiting minimal dispersion or deviation from its path. However, Hashish and Yanaida suggest that for orifice diameters greater than or equal to 0.381 mm, jet coherency may not deteriorate further with increasing water pressure beyond 350 MPa [65, 79]. This is due to the "critical Reynolds number" threshold (as defined by Yanaida) of 460,000 being crossed, indicating a transition in the jet's behavior where its core region length relative to its diameter becomes independent of variations in the Reynolds number. Suggesting that increasing water pressure beyond 350 MPa should not impact the wear profile due to jet coherency provided the orifice diameter is greater or equal to 0.381 mm. However, this conclusion is subject to limitations as the theoretical

model by Yanaida considered only water and air flowing through the tube without abrasive particles [79]. Addressing the presence of large abrasive particles, relative to the mixing tube's internal diameter, flowing in a fluid along a tube remains an unresolved challenge in fluid dynamics research [80].

To better understand the effects of different parameters on both abrasive and erosive wear, it can also be helpful to study wear models. Ramulu et al. acknowledged that wear models for the inside of an AWJ mixing tube have not been proposed. Instead, the authors suggested using well-established wear models, which, although not definitive, can help explain the wear mechanism inside ceramic tubes [57]. For abrasive wear, an appropriate model, which assumes all cracked material is removed, was proposed [81]:

$$\dot{V} \propto P^{1.5} \, K_c^{-0.5} H^{-0.625} \left(\frac{E}{H}\right)^{0.8} \tag{2.1}$$

where $\dot{V}$ represents the volume of material loss per unit length, P stands for the applied load and K_c and is the fracture toughness of the mixing tube, H represents the mixing tube hardness and E is the mixing tube material elastic modulus.

For erosive wear, the proposed model was [81]:

$$\varepsilon_v \propto v^2 \frac{\pi d^4}{12} \left(E\rho/K_c^2\right) \tag{2.2}$$

where ε_v represents the volume of material removed per impact, v is the impact velocity and d and ρ are the diameter and density of the abrasive particle, respectively.

From equation 2.1 and 2.2, it can be noted that pressure changes contribute to higher volumes of material removal for both abrasive and erosive wear, as increases in pressure would increase the applied load as well as the impact velocity. In addition, the choice of abrasive particle is significant, as increases in both density and particle size can result in greater erosive wear. The implications from these equations therefore support the earlier suggestion by Hashish to use Al_2O_3 abrasive, for accelerated wear, as a substitute for garnet, due to it's similar density and shape [7].

From experimental data, an additional model was deduced for the volume removed by a single particle by Nanduri et al. [14]:

$$V \propto (v \sin \alpha)^{1.9} d^{3.28} \left(\frac{H_p}{H_t}\right)^{7.12} K_t^{-1.3} \tag{2.3}$$

where V is the volume removed by a single particle, v, d, H_p, are the particle velocity, diameter, and hardness, respectively, α is the impact angle and H_t and K_c are the target material hardness and fracture toughness, respectively.

Unlike equations 2.1 and 2.2, equation 2.3 developed specifically for the AWJ cutting process, acknowledges that the ratio of particle hardness to mixing tube material hardness is also significant in defining the volume removal.

2.4 Developing a tool condition monitoring system

When developing an indirect TCM system, there are several key steps to consider. Abellan-Nebot et al. summarised these steps in a machining monitoring systems review [82]:

1. Sensors: which sensors to use? Take into account the cost, reliability and how intrusive the sensor is.

2. Signal processing: how to process the raw sensor signals?

3. Feature generation: which features to create? The raw signal has to be transformed into more useful "features" for a model to learn the relationships within the data. For example, time domain and frequency domain features may need to be created.

4. Feature selection: which combination of the created features is the most meaningful? This step can help develop a reliable and robust model.

5. Design of experiments: which experiment design is needed for modelling the process accurately? An effective approach is required to collect enough information for creating a monitoring system which can function in industry while keeping the cost and time required to a minimum.

6. Artificial intelligence (AI) technique: what AI method to select for modelling the process? A model which can learn the relationships between features is required. Dataset size, desired model accuracy, and the model nature may influence model selection.

Some of the challenges facing the design of the experiments step have already been addressed in the previous section of the literature review. The remainder of this chapter will focus on the other steps.

2.4.1 Sensor selection

The first challenge in developing an indirect AWJ TCM system is the sensor selection. For AWJ machining, the sensor approaches can be split into three groups: monitoring the workpiece response, focusing on the jet of water, or focusing on the nozzle itself.

Several authors have focused on measuring the workpiece response. Kovacevic et al. used a dynamometer to record the normal force experienced by a workpiece when machined with mixing tubes of a different wear state [30]. The authors found that wear correlated with increasing normal force observed, and severe wear can be detected with this approach. Hreha et al. used an accelerometer mounted directly on a steel workpiece and varied the mixing tube diameter [83]. The authors found that the RMS of the signal has the potential to detect wear as the amplitude peaks were seen to shift in the range between 100 and 200 Hz with changing mixing tube diameter. The work indicates that monitoring the workpiece response may be a viable solution for mixing tube wear detection. However, this approach of monitoring the workpiece directly has limitations. First, the response is workpiece dependent and therefore not robust. Second, as is the case with the approach used by Kovacevic et al., it's not practical - as the dynamometer may be damaged [30]. For the method described by Hreha et al., the approach is limited as it does not offer automated wear monitoring, as the sensors will need re-attaching to each new workpiece for wear detection [83].

A second sensor approach is to monitor the jet of water itself by observing the jet diameter. The jet diameter is influenced by water pressure, mixing tube wear, orifice condition and the alignment between the mixing tube and the orifice [32, 84, 85]. Prijatelj et al. used a through-beam optical vision system to detect the changes in focusing tube exit diameter [32]. While successful, the approach was shown to have a major practical limitation for monitoring applications. As the authors noted, the harsh environment of the AWJ machine meant the jet spray and abrasive sticking would cover the lens [32]. The lens would therefore need frequent cleaning, which would result in process intervention rendering this method impractical for online monitoring.

The final sensor approach is to focus on the nozzle itself. Kumar et al. found that an accelerometer attached to the nozzle can successfully detect differences in mixing tube diameters [34]. The authors observed that with increasing exit diameter wear, the dominant frequency amplitude tended to increase [34]. Jegaraj et al. also used an accelerometer mounted on the nozzle and found that this method can also be used to monitor the condition of the orifice [24]. Copertaro et al. were successful in detecting

31

changes in signal response from mixing tube wear with two accelerometers attached to the mixing tube, however the methodology used had practical limitations as it required the mixing tube to be machined to attach the sensors [41]. For an online monitoring application, this additional required machining step will add to the cost of the process.

Kovacevic et al. utilised temperature measurements via an infrared thermographer aimed at the mixing tube [35]. The study found that with increasing wear the mixing tube temperature peak will shift towards the tube exit and the peak temperature would decrease, due to a reduction in frictional forces between the internal mixing tube wall and the jet of water. The results are complementary to the data obtained by Bauer et al., who found that a worn mixing tube would result in a lower observed maximum mixing tube temperature [40]. Bauer et al. also found that changing the condition of the orifice from new to damaged would result in a temperature decrease, suggesting the orifice condition could also be monitored via optical thermography [40].

Zeng et al. showed that a vacuum sensor attached to the abrasive supply hose can be used to detect changes in the mixing tube exit diameter, with vacuum pressure increasing with an increasing exit diameter, abrasive flow rate and water pressure [36].

Louis et al. showed that airflow sensors can be used to monitor the waterjet, with airflow increasing with increasing mixing tube exit diameter and water pressure [37]. The results are consistent with findings by Hashish, who observed the airflow rate increasing with increasing pressure, mixing tube diameter, water flow rate and suction hose diameter and decreasing abrasive hose length [5]. Hashish et al. also observed that the effect of mixing tube length on airflow suction is insignificant [5]. Several other AWJ parameters impact the airflow. Zhang et al. stated that the amount of air flow that flows into the MC is dependent on the amount of air removed by the jet of water, amount of abrasive particles introduced and the restriction of the feed tube [4]. A worn orifice and an orifice of larger diameter would produce a wider jet, expelling more air from the MC per unit time [3, 4]. A worn mixing tube would have a larger cross-sectional area and would also allow the jet to remove more air [4]. Higher water pressure would also increase airflow, while the presence of abrasives in the abrasive hose or the reduction of the abrasive hose diameter would restrict the air passage, thus lowering airflow [3, 4].

Louis et al. notes a limitation of working with the airflow sensor - when attaching it within the abrasive hose it will be destroyed if abrasives are flowing through the

system [37]. The authors' results were based on data collected when the abrasive tank was empty. The authors suggested the airflow sensor cannot be utilised when abrasive is used, recommending the pressure loss measurements inside the hose to be recorded instead, as the measurements correlate well with airflow data [37]. Putz et al. found that airflow sensors can also be used for orifice defect and abrasive supply hose blockage detection [86]. Still, the authors noted the sensor setup had a similar limitation where it can only be used with the abrasive supply disconnected [86]. Despite limitations, airflow sensors are robust and can even be used for the detection of orifice misalignment and leakage in the abrasive hose [38].

Prabu et al., Kim et al., Mohan et al. and Bauer et al. all looked at using acoustic emission sensors to monitor mixing tube wear [39, 40, 42, 43]. Prabu et al. and Kim et al. looked at using the root mean square (RMS) values of acoustic emission sensors to monitor exit diameter wear progression [39, 43]. Both studies found a relationship between the RMS of the signal and mixing tube wear. Mohan et al. and Bauer et al. saw a change in measured signal with increasing exit diameter [40, 42]. Kim et al. and Mohan et al. proposed a monitoring solution of mixing tube wear based on their results [42, 43].

Kim et al. developed a basic software tool to classify the mixing tube condition into normal or damaged based on assigned RMS value limits [43]. However, the solution had several limitations for online monitoring. First, the approach relied on assigning RMS value limits for classification, which were based on a single set of tubes that were also used to generate the data for finding the limits. Whether this approach works on new tubes (unseen data) has not been validated. Second, judging from the paper's figures, it is difficult to find a difference in the RMS of the signal for different wear times (0, 40, 80 and 100 hours). The authors argue that with increasing mixing tube wear, without damage, the RMS of the signal decreases [43]. Yet their results seem to contradict that, as at 300 MPa pressure, the mean of the RMS signal for a tube worn for 80 hours appears to be slightly higher than for a new unworn mixing tube [43]. The lack of repeats further limits the validity of the findings. When the authors increased the pressure to 350 MPa it is harder to distinguish between a new and damaged tube, while the authors argued a large RMS change would be observed. Finally, the validity of the results is further questioned when studying the contradicting findings obtained by Prabu et al., where the mean RMS signal was found to increase, instead of decrease, with increasing mixing tube wear time (from 0 to 70 hours) [39]. The results by Prabu et al. are also consistent

with results obtained by Mohan et al. and Bauer et al., where the average amplitude of frequencies also increased with increasing exit diameter [39, 40, 42].

The monitoring solution proposed by Mohan et al. relied on using an artificial neural network trained on the frequency domain acoustic signals to predict the mixing tube exit diameter [42]. The authors quoted a prediciton accuracy of 96%, however the findings have limitations [42]. Namely, the authors used data from the same mixing tubes for training and evaluating the model performance. No clear validation was performed on unseen data. The waterjet is a complex process, there may be variations in the observed signal for different mixing tubes and the performance of this model on unseen data may be worse. The authors also collected data during aluminium machining. If a different workpiece material is used in the future the findings may not be as accurate if the recorded signal is effected. The same applies to the process parameters, with additional process parameters not explored. Overall, the proposed monitoring solutions by both Kim et al. and Mohan et al. have limitations, yet the acoustic emission sensor approach has shown potential for wear detection [42, 43].

The research that focused on using sensors to monitor the nozzle directly demonstrated promise for an AWJ non-intrusive online wear TCM system. However, the bulk of research has not evaluated the performance of indirect methods in predicting wear, instead concentrating on illustrating their potential in detecting changes in mixing tube ID [34–41]. Meanwhile, the work that did attempt to take the research a step further by evaluating a monitoring application had several limitations [42, 43].

Selected sensors for TCM must have a signal that allows tool wear detection [31]. From this review, it can be concluded that a variety of sensors are suitable for tool wear detection. When selecting an appropriate sensor, several parameters should be considered: the sensor should not interfere with the process or working space, it should be wear and maintenance free, and it should be resistant to dirt [31]. Finally, a multi-sensor approach may be the solution (recording more than one variable at a time), as several researchers found them to be more reliable than a single sensor system in conventional machining [27, 82, 87–89]. The use of multiple sensors is known as sensor fusion, with more than one sensor signal combined in a complementary manner for more robust predictions [90]. To benefit from sensor fusion in TCM, machine learning can be applied, which would allow linear or non-linear models to relate sensor data to the wear process [91].

2.4.2 Signal processing and feature extraction

Once the sensor data is collected, the data in most cases requires processing. The raw data is unlikely to be practically useful for wear identifications on its own, as unprocessed data contains high volumes of information [28, 92]. The signal is first processed and then converted into useful information in a process known as feature extraction. Extensive data collection can incur a high cost. A recent TCM review in milling has noted that more attention has to be given to sensor configuration and feature extraction as opposed to further trials for additional data collection [93]. Features which are sensitive to wear and not the workpiece material nor the process parameters selected are especially useful [94]. Finally, after the features are created, a process called feature selection is employed to choose only select features that aid the model in learning the valuable information from the data [28].

The first step on the raw data is signal processing (also known as pre-processing). Signal processing may include filtering, amplification, segmentation, signal transformation and resampling [28, 82]. Filtering may involve extracting relevant information from a signal, such as specific frequencies. Filtering may also involve noise removal. This can be achieved through the application of a moving average filter [95]. Amplification includes changing the amplitude of a signal to either reduce or enhance its strength. Segmentation refers to dividing a continuous signal into smaller segments, to extract relevant data; for example by removing data when the AWJ is not running between repeats. Signal transformation could entail transforming the signal into time-frequency or frequency domain, for example via Fourier transforms [28]. Finally, signal processing may include resampling - changing the sampling rate of the data.

Machine learning may require additional pre-processing steps, to be carried out after feature extraction, which include data cleaning, missing value handling and normalization [96, 97]. Data cleaning involves finding and correcting inaccurate data. This may involve missing value handling. Missing values in the dataset need to be filled (also known as imputed) or removed in order for some machine learning algorithms to be used [96].

There are multiple strategies for imputing missing values. First, they can be filled with single values such as the mean or median of their feature [98, 99]. Missing values can also be filled via interpolation (interpolating the values of the next available and previous data points), especially when the data is sequential, like time-series sensor data [96]. Finally, model-based imputation can be performed where a predictive model is trained using the missing data as a target to predict. For example, via the

k-Nearest Neighbors (KNN) algorithm, where the missing values are filled with the mean of the k values from the k most similar data points [100].

Processed data may also require normalisation, a requirement of several algorithms such as LR, which is a method by which data of a feature is scaled via min-max or z-score normalisation [96, 97]. Min-max normalisation scales the feature based on its maximum and minimum values, while z-score normalisation converts the data to have a standard normal distribution with a standard deviation (std dev) of 1 and mean of 0 [96, 97]. Equations 2.4 and 2.5 present the calculation for min-max scaling and z-score, respectively. Feature scaling may be necessary for some models that rely on distance-based calculations to ensure that all features contribute equally and are on a similar scale, preventing one feature from dominating the others.

$$X_{\text{normalized}} = \frac{X - X_{\min}}{X_{\max} - X_{\min}} \tag{2.4}$$

$$Z = \frac{X - \mu}{\sigma} \tag{2.5}$$

Once the data is processed, feature extraction takes place. Features can be extracted using time, frequency and time-frequency domains. The goal is to make features which describe the signal for the required task. Worden et al. found that both frequency- and time-domain features are useful for health monitoring and will be explored in more detail in this thesis [101]. Frequency domain features can be a useful addition to time-domain features, as they may capture patterns not present in the time-domain. To convert time-domain data to frequency domain, fast Fourier transform (FFT) are often used, which are a computational efficient algorithm for calculating discrete Fourier transforms [28, 102, 103]. When extracting frequency domain features, attention has to be paid to the sampling rate. As per the Nyquist theorem, to avoid introducing noise, the highest frequency that can be accurately represented is half of the sampling rate [104]. Time-frequency domain features can be extracted using short-time Fourier transform (STFT). Spectrograms can then be created, which can be used as inputs for computer vision models for TCM [105].

Common time-domain features include statistical features such as minimum, maximum, mean, std dev, RMS, skewness, kurtosis, peak-to-peak, shape factor and inter-quartile range (IQR) [28, 106–108]. Other time-domain features which have been used in fault diagnosis and TCM research include impulsive metrics, properties related to the peaks of the signal, which are: impulse factor, clearance factor and crest factor [107–110]. Zero crossing rate and RMS energy can also be informative for audio signals and TCM [111–113].

Common frequency domain features include the dominant frequency, statistical features of the power spectrum and band power ratios [28, 114]. Other potentially useful frequency domain features, which are less often explored, include spectral flatness and Shannon entropy [110, 115, 116]. Power-based frequency domain features can be calculated by utilizing the Power Spectral Density (PSD) method. PSD provides a frequency decomposition of the signal, allowing the user to understand the distribution of power across different frequency components. PSD is beneficial when random effects can obscure the underlying phenomenon [117]. PSDs are often computed using the Welch method, which involves dividing the signal into overlapping segments and averaging their periodograms [117, 118]. Choosing lengths of segments[2] is a compromise between frequency resolution with longer segments and estimate reliability with shorter segments which produces more averages and therefore a decrease in variance [117, 119].

Table 2.2 summarises several time and frequency domain features and how they are calculated. The table is not exhaustive, with some statistical features not included.

Finally once the data has been processed and features created, the features require selection to reduce the dimensionality of the dataset, and to help the model learn the relationships within the data [82]. Feature selection can also help simpler models be more robust on small datasets [82]. Feature selection can be carried out via feature ranking or subset selection. Ranking uses a metric to rank the features and eliminate the features with a low score. For example, via correlation index ranking or mutual information (MI) scores [120–123]. Multiple ranking metrics can be used together to build a better understanding of feature strengths. For example, the Pearson-correlation coefficient, used by Quan et al. during a tool wear condition study, only measures the linear dependence between the feature X and the target y [123]. MI scores can be used to complement the linear ranking method, as they provide additional information about the non-linear relationships and dependencies between features and the target variable [120, 124].

Subset selection is another option for feature selection, which is more computationally expensive as it searches up to all the sets of possible feature combinations for the optimal subset [82]. This can be done via different algorithms, for example, neural networks [31]. The Least Absolute Shrinkage and Selection Operator (LASSO) model can also be used [125]. LASSO applies a regularisation process to penalize the

---

[2]The segment length refers to the duration of individual portions in which the input time-domain signal is divided. Each segment undergoes computation using a modified periodogram, and the average of these periodograms constitutes the spectral estimate.

Table 2.2: Equations for several time and frequency domain features.

Features	Equation
Time Domain	
RMS	$x_{\mathrm{rms}} = \sqrt{\frac{1}{N} \sum_{i=1}^{N} x_i^2}$
Shape factor	$\frac{x_{rms}}{x_m}$
Impulse factor	$\frac{x_p}{x_m}$
Clearance factor	$\frac{x_p}{\left(\frac{1}{N} \sum_{i=1}^{N} \sqrt{|x_i|}\right)^2}$
Crest factor	$\frac{x_p}{x_{rms}}$
Zero crossing rate	Number of times the signal crosses the zero baseline per unit time.
Frequency Domain	
Dominant frequency	Frequency component with the highest amplitude in the PSD.
Spectral flatness	$\frac{\sqrt[N]{\prod_{i=1}^{N} x_i}}{\frac{1}{N} \sum_{i=1}^{N} x_i}$
Shannon entropy	$-\sum_{i=1}^{n} p_i \log_2 p_i$

Where N is the total number of samples in the signal, x_i represents the value of the signal or power spectrum at the i-th frequency bin in the PSD, x_m is the mean absolute value of the signal, x_p is the maximum absolute value of the signal, and p_i represents the normalized probability of the i-th frequency component in the PSD.

coefficients of regression features, shrinking some of them to zero. LASSO can be used for feature selection, as it can identify which features are irrelevant for modelling the process, as they will have a coefficient equal to zero. LASSO can be tuned to adjust the strength of the penalty on the coefficients. The larger the parameter, the higher the number of coefficients of features are shrunk to zero.

An alternative method to feature selection could be to use principal component analysis (PCA) to reduce the dimensionality of the data [126]. PCA identifies the axes that account for the largest amount of variance, using as many axes as the number of dimensions in the dataset [44]. To determine the number of dimensions to reduce the dataset to using PCA, one typically selects the number of dimensions that retain a

specified percentage of the total variance. This percentage is often determined based on the desired level of information preservation. A common approach is to set a threshold, such as retaining 95% or 99% of the variance, ensuring that the reduced dataset still captures the majority of the original information [44]. PCA analysis only models linear relationships within the data. Kernel PCA can be used to perform complex nonlinear projections for dimensionality reduction [44].

2.4.3 Machine learning

Machine learning, a subset of AI, can be used to build a TCM system based on indirect sensor data. Machine learning focuses on the development of algorithms (models) to enable computers to learn from and make predictions on data. Machine learning is a key component of AI because it provides the means for machines to learn and improve their performance without being explicitly programmed for specific tasks. Machine learning has been used in a variety of TCM research in machining [127].

TCM systems require reliable machine learning models capable of learning relationships between process variables and the prediction target during machining. Model selection depends on the number of data points available, desired model performance and the nature of the model [82]. For TCM, while artificial neural networks are often discussed, a simpler system is less likely to fail and can sometimes be just as accurate [27]. To select a model several factors need to be understood, including: different types of machine learning tasks to solve for, how to evaluate model performance and which models are available.

The two main categories of machine learning tasks are supervised and unsupervised learning. In supervised learning, the algorithm is provided with a labeled dataset, meaning the input data features are associated with a corresponding output data, known as target or label [44]. The goal of a supervised algorithm is to learn the relationships between the input and output data to make predictions on new unseen data when the target variable is not provided. For unsupervised learning, the input data does not have a specific target associated with it. The goal is to discover patterns without specific guidance.

The two fundamental types of supervised machine learning tasks are classification and regression. Classification involves predicting a specific category or class. For example, in TCM it can be predicting if the tool is worn or not (binary classification). Regression has the goal of predicting a continuous numeric output. For example, in TCM this may be predicting the exit diameter of a mixing tube.

To evaluate model performance, you require a metric and a validation strategy. Accuracy and F1 score are two popular methods for classification tasks, with mean absolute error (MAE) and root mean squared error (RMSE) popular for regression tasks [44, 128, 129]. Using both metrics at once can be beneficial to gain a more comprehensive understanding of the models' performance.

Accuracy measures the proportion of correctly classified instances out of the total number of instances in the dataset. Accuracy can be calculated using 2.6.

$$\text{Accuracy} = \frac{\text{Number of Correct Predictions}}{\text{Total Number of Predictions}} \tag{2.6}$$

The F1 score is a combination of precision and recall. Precision measures the accuracy of positive predictions, for example for all instances predicted as worn, how many are actually worn? Recall measures the ability of the classifier to capture all positive instances, for example of all the instances that are actually worn, how many did the model correctly predict as worn? The F1 score balances precision and recall. The F1 score ranges from 0 to 1, 1 indicating perfect recall and precision. F1 score can be calculated using equations 2.7 - 2.9, where TP stands for true positive, FP for false positive and FN for false negative. TP instances are correctly predicted positive instances, FP instances are actually negative but are incorrectly predicted as positive by the model and FN instances are actually positive but are incorrectly predicted as negative by the model.

$$\text{Precision} = \frac{TP}{TP + FP} \tag{2.7}$$

$$\text{Recall} = \frac{TP}{TP + FN} \tag{2.8}$$

$$F1 = \frac{2 \times (\text{ Precision } \times \text{ Recall })}{\text{Precision } + \text{ Recall}} \tag{2.9}$$

For classification tasks, accuracy is a valuable metric when the class being predicted is balanced, in other words it has a similar number of target instances for each class. Accuracy is valuable as it is easy to interpret. However, for imbalanced classification problems, the F1 score is a better choice as it takes into account both precision and recall. For imbalanced problems, accuracy can be misleading, as a model that always predicts the majority class may still achieve a high accuracy.

For regression, MAE measures the average absolute difference between predicted and actual values, while RMSE quantifies the square root of the average squared difference between predicted and actual values. MAE treats all errors equally and is

suitable as a simple and easy-to-understand error metric. It is easily interpretable as it's expressed in the same units as the target variable. RMSE squares the errors before summing, making it better suited than MAE when larger errors are undesirable. MAE and RMSE can be calculated using equations 2.10 and 2.11 respectively, where n is the number of observations, y_i is the actual value and $\hat{y}_i$ is the predicted value.

$$MAE = \frac{1}{n} \sum_{i=1}^{n} |y_i - \hat{y}_i| \tag{2.10}$$

$$RMSE = \sqrt{\frac{1}{n} \sum_{i=1}^{n} (y_i - \hat{y}_i)^2} \tag{2.11}$$

As mentioned earlier, to evaluate the performance of machine learning models, you require both a metric to measure the quality of predictions and a validation strategy to assess how well the model generalises to unseen data. In machine learning the model is trained on a training dataset and evaluated on a test dataset. A validation set may also be used to experiment with different modelling strategies before evaluating performance on unseen data. A validation set is used to avoid data leakage and to provide an unbiased assessment of the model's generalisation capabilities. It ensures that the model's performance is not over-optimised for the test dataset and helps in fine-tuning hyperparameters (model configuration settings) and selecting the best model among different candidates. Data leakage, which occurs when information from the test set unintentionally influences the modelling process, can lead to overly optimistic performance estimates. The use of a separate validation set helps mitigate this risk and promotes more reliable model evaluation [44].

Two validation strategies are common, including a hold-out test set and cross-validation (CV). Hold-out validation involves splitting the dataset into two separate portions, with one used for training and one for testing a model. CV involves dividing the dataset into subsets (folds) and training the model on each subset in turn, and testing the performance on the remaining data. The result is the average of the k-number of folds. CV can be stratified to ensure that each fold maintains a similar distribution of target classes as the original dataset, providing a more robust evaluation of the model's performance across different subsets of the data.

Two concepts to pay attention to when evaluating model performance are overfitting, and underfitting [44]. Overfitting occurs when the model is too complex in relation to the quantity of data or present noise. For example, if a deep neural network detects subtle patterns in the data, but the training dataset is too small or too

noisy, the model will likely detect patterns in the noise itself and wont generalise to new instances. Overfitting can be overcome by simplifying the model, acquiring more data or reducing noise. Underfitting is the opposite of overfitting, where the model is too simple for the data structure. Here, more powerful or less constrained models or better features are required.

2.4.4 Model selection, tuning & explainability

Once the metric and validation strategy are picked, the next step is model selection. Various model types can be considered, each with distinct learning mechanisms. Linear models, for instance, operate on the principle of fitting a linear relationship between input features and the target variable. Examples of linear models include LR, Support Vector Machines (SVM), linear least squares with l2 regularization (Ridge) and Logistic Regression (LogR) [130, 131].

Tree-based models, such as random forests (RF) and extremely randomised trees (ET), partition the feature space hierarchically, building decision trees [44, 131–133]. RFs generate several decision trees, each using different subsets of features and data samples. The final prediction is then determined through a collective decision-making process. Due to the different samples and variables considered, each tree is different from each other and the trees are uncorrelated. So, when combined, much of the variance is ruled out [132]. ETs introduce additional randomness during the splitting process, resulting in a more varied ensemble [133]. This ensemble methodology enhances robustness and mitigates overfitting [132].

Additional tree-based models include gradient-boosting algorithms, which focus on building decision trees sequentially, where each tree corrects the errors of its predecessor [132]. Different implementations of this approach exist, including gradient boosting machines (GB) provided by scikit-learn, XGBoost (XGB), LightGBM (LGBM) and CatBoost (CB) [131, 134–137]. In a comparison between XGBoost, LGBM and CB by Alshari et al., LGBM was found to be the fastest algorithm to run, while CB edged performance over the other two algorithms [138].

Other algorithms include deep learning models. Examples include multi-layer perceptron (MLP) neural networks which have multiple layers for pattern recognition and pre-trained neural network TabPFN, which had its model weights pre-trained for classification tasks on tabular data [131, 139]. Finally, there are proximity-based models such as KNN [131, 140].

In machine learning, there is no one solution that will fit every problem [44]. Applying multiple models to see which works best for a given problem is therefore a

viable approach. In previous TCM research in machining, a variety of models have been used, from linear to tree-based to deep learning models [42, 141–145].

In addition to using single models, models can be combined to form an ensemble, through a process known as ensemble learning or ensembling [109]. Ensemble learning refers to the technique of combining several individual models to create a more robust model with a reduced overall variance. The idea is that diverse models, when ensembled, can compensate for each other's weaknesses and outperform any individual model [146]. Different ensembling strategies exist, such as stacking, where multiple diverse models are trained, and their predictions are used as input features for a meta-model [44]. A simpler averaging of predictions of multiple models can also be used [147].

Signal time domain data can also be converted to images via gramian angular summation field or gramian angular difference field and time-frequency domain data can be converted to spectrograms via STFT. Computer vision tasks such as convolutional neural networks can be used on these images to classify the state of the tool [105]. This approach was used by Martínez-Arellano et al. for tool wear classification and achieved an accuracy of 80% [148].

Machine learning algorithms may require hyperparameter optimisation for improved performance on different datasets [149–151]. Especially when using default settings offered by common machine learning libraries [149, 152, 153]. The challenges of optimisation include having a high-dimensional configuration space and it not always being clear which parameters are important to optimise [149]. These challenges are especially true for tree-based and deep-learning architectures [154].

There are multiple hyperparameter optimisation methods available, including grid search and random search [132, 149, 154, 155]. Grid search, also known as full factorial design, is limited by the fact that the number of evaluations grows exponentially with the increase in the configuration space, as the method evaluates each combination of user-specified hyperparameter values exhaustively [132]. A simple alternative to grid search is random search, which randomly samples configurations until a set search budget is reached [155]. A limitation of random search is that it doesn't use information from prior experiments to select the next parameters. Finding the best set of parameters relies on randomness unless every parameter is exhaustively searched [132].

An alternative to grid search and random search is Bayesian optimisation. Unlike the previous two described optimisation strategies, Bayesian optimisation does not treat each hyperparameter configuration independently, instead determining the next

values based on the previous results [132, 154, 156]. This helps avoid many unnecessary evaluations, allowing for the optimiser to find the optimal set of hyperparameters within fewer iterations than grid search or random search. To select the next hyperparameters, Bayesian optimisation uses a surrogate model [157]. This model helps in detecting the optimal hyperparameter values, which are then evaluated in the real objective function [154]. The model is updated iteratively until the maximum number of iterations is reached. Common surrogate models include the Gaussian process and RF [132, 149, 154].

Once the models make predictions, their output can be considered black-box, as the internal processes employed by the models to make predictions are often complex and difficult for humans to interpret. Model explainability is focussed on explaining the behaviour of models from input to output in human terms, for example, via feature importance or Shapley additive explanations (SHAP) [158, 159]. The purpose of model explainability is to create an understandable solution which can communicate machine learning results and make them more trustworthy [158].

Feature importance is the most used technique for interpreting models as they provide a simple and intuitive explanation of relative feature contributions to predictions, suggesting which features matter most to a model and offering a comparison between each feature [159]. Feature importance is also straightforward to implement as many machine learning libraries and frameworks, such as scikit-learn, provide built-in functions for calculating and visualizing feature importance [131].

However, unlike SHAP plots, feature importance does not suggest how each feature matters to a model [160]. Medium importance could suggest a medium effect for all predictions or a larger effect for a few predictions. SHAP leverages the game theory concept of Shapley values to optimally assign feature importance [159, 161]. SHAP provides a detailed approach to understanding feature importance via summary plots, allowing the user to understand how the model makes decisions for individual instances.

2.5   Overview of literature

The literature review has covered mixing tube wear, challenges facing AWJ data collection for TCM and the development of TCM systems via machine learning. The review has shown that an extensive body of previous literature has been published on the use of different sensors in their ability to differentiate between a worn and an unworn mixing tube. However, the accuracy of the sensors in predicting wear in

a monitoring application has not been evaluated on independent data. In addition, multiple challenges facing data collection during the development of such a monitoring application have not been addressed. Therefore a research gap exists in developing a framework for data collection which addresses these challenges. The use of machine learning is not in itself novel in TCM, but there is limited application of different machine learning approaches in AWJ machining.

This thesis aims to address the research gaps by developing a novel framework for data collection to address the outlined challenges, collecting the data and building and evaluating different machine learning approaches to predict the exit diameter and classify the state of the mixing tube tool in AWJ machining.

Chapter 3

Experimental methodology

This chapter aims to propose a trial design for data collection in order to develop a TCM system framework for AWJ machining. The designed data collection approach, which is aligned with the literature review, can then be used to build a dataset for training and evaluating the performance of different models in predicting wear.

In this chapter, focused on the experimental methodology, the framework for data collection if first proposed, then the decisions behind the methodology are explained. Sensor selection is then discussed before an overview of the data collected. Finally, the experimental setup for data collection is presented and the chapter is summarised.

3.1 Data collection methodology design

3.1.1 Trial design overview

Designing the data collection methodology is a crucial step to develop a TCM system. The data requires collection under conditions similar to the ones applied in industry. In this section, the designed methodology will first be presented, including the parameters selected, before each decision is explained in more detail in the next section.

The mixing tubes used were tungsten carbide ROCTEC 100 tubes manufactured by Kennametal, with an ID of 1.02 mm. This is a standard durable mixing tube used in industry and research [13, 14, 20, 71, 162].

The data was collected with the following steps to build a dataset for process monitoring:

1. Change abrasive to Al_2O_3.

2. Install new mixing tube and secure it in place with a collet and holding nut.

3. Record the mixing tube exit diameter using steel pin gauges with 0.01 mm increments.

4. Collect data using the connected sensors under a dwell cycle at varying pressures (3000, 3500, 4000, 4500 and 5000 bar) for 3 repeats, for 5 seconds each.

5. Wear the mixing tube for 5 or 10 minutes (tube dependant) at 4000 bar pressure, an abrasive feed rate of 7.55 g/s and an orifice with a diameter of 0.406 mm. The waterjet was run straight into the catcher tank.

6. If the tube is worn to the designated wear time, repeat steps 3-4 and finish data collection for that tube. Otherwise, repeat steps 3-6.

7. Go back to step 2 unless all mixing tubes have been worn.

With this approach, data was collected on each mixing tube without taking the tubes off until the wear cycle was complete, as the exit diameter measurements could be done without needing to disassemble the nozzle. This data collection approach will be referred to as the wear data collection (WDC).

Once all the mixing tubes were worn, additional data collection was carried out using the steps below:

1. Install the mixing tube and secure it in place with a collet and holding nut.

2. Collect data using connected sensors under a dwell cycle without abrasive feed at varying pressures (3000, 3500, 4000, 4500 and 5000 bar) for 3 repeats, for 5 seconds each.

3. Go back to step 1, and repeat the process for each mixing tube.

This additional process will be referred to as an "additional tube dwell" (ATD) process.

Table 3.1 shows the mixing tube numbers and the duration each was worn for during WDC. The table also includes the interval at which data was collected, whether the tubes were worn during a preliminary or main trial and the length of the tube. The original plan involved wearing additional tubes for 90 minutes. However, due to issues with the machine at the time, this data collection failed and was removed from the methodology.

In addition to the tubes listed in Table 3.1, several other tubes worn using a regular wear approach with garnet were obtained and are listed in Table 3.2. These

Table 3.1: ROCTEC 100, 1.02 mm ID mixing tubes to be worn using Al_2O_3 abrasive as part of the data collection effort to build a TCM system for the AWJ process.

Tube Number	Wear (minutes)	Interval (minutes)	Trial	Length (mm)
1	60	10	Preliminary	101.6
2	60	10	Preliminary	101.6
3	15	5	Main	101.6
4	30	10	Main	101.6
5	45	5	Main	101.6
6	60	10	Main	101.6
7	75	5	Main	101.6
8	90	10	Main	101.6
9	60	10	Main	76
10	60	10	Main	76

tubes were worn by other researchers and were kindly provided for this research. The mixing tubes supplied by Dr Hashish were not labeled, but all had been initially worn for 40 hours, with several used further to 70 hours of wear as the tubes were found to be in acceptable condition at the time.

A comparison of wear conditions for the mixing tubes used in this study is presented in Table 3.3. The mixing tubes used in this thesis will be referred to by their respective tube numbers seen in Tables 3.1 and 3.2 throughout the remainder of this thesis.

The tubes in table 3.1 will be worn for WDC, while the tubes in both Tables 3.1 and 3.2 will have additional data collected on them using the ATD approach.

3.1.2 Trial design decision making

With the trial design proposed, this section will provide more detail on the chosen: wear measurement approach, wear method, wear duration, mixing tubes used, data collection phases and the parameters selected.

Exit diameter measurements are chosen as a direct measurement of wear to be linked with the sensor response, as they are easy to perform and therefore most relevant to a practicing engineer. To build an indirect wear monitoring system, data has to be collected via an indirect approach (i.e. a sensor) and linked with a direct

Table 3.2: Mixing tubes supplied by other researchers, worn using garnet abrasive.

Tube number	Wear (hours)	Supplied by	Length (mm)
11	40	The AMRC	101.6
12	40/70	Dr Hashish	152.4
13	40/70	Dr Hashish	152.4
14	40/70	Dr Hashish	152.4
15	40/70	Dr Hashish	152.4
16	40/70	Dr Hashish	152.4
17	40/70	Dr Hashish	152.4
18	40/70	Dr Hashish	152.4
19	40/70	Dr Hashish	152.4
20	40/70	Dr Hashish	152.4

Table 3.3: A comparison of mixing tube details and parameters used to wear each tube investigated in this thesis.

	Mixing tube provider		
	WDC Tubes	The AMRC	Dr Hashish
Mixing tube details			
Manufacturer	Kennametal	Kennametal	Kennametal
Type	ROCTEC 100	ROCTEC 100	ROCTEC 500
Material	Tungsten Carbide	Tungsten Carbide	Tungsten Carbide
Starting ID (mm)	1.02	1.02	1.02
Length (mm)	76, 101.6	101.6	152.4
Wear parameters used			
Water pressure (bar)	4000	4000	6000
Abrasive type	Al_2O_3	Garnet	Garnet
Abrasive size (mesh)	80	80	50
Abrasive flow rate (g/s)	7.55	5.32	9.07
Orifice ID (mm)	0.406	0.406	0.381

measurement of wear. As was outlined in Chapter 2, measuring mixing tube wear is a challenge. Exit diameter measurements fail to capture wear along the entire profile of the tube, however they are fast, simple, practical, non-destructive and cheap to perform when pin gauges are used [14, 20, 38, 78]. In addition, exit diameter measurements correlate with machining quality so are an effective representation of wear [7].

For data collection, accelerated wear using Al_2O_3 was chosen. As outlined in Chapter 2, a challenge regarding data collection of wear of the mixing tubes is the long lifetime of the tubes. Running an AWJ for over 50-100 hours to collect wear data on one tool would be expensive, require a long time, use a large quantity of abrasive, result in additional AWJ component wear and may potentially result in too few data points to build a meaningful TCM system. A solution of accelerated wear trials was explored in Chapter 2. To keep the process as similar as possible to industrial conditions, accelerated wear trials require using the same mixing tube material but a harder abrasive. Changing the mixing tube to a softer material can result in a different wear pattern being observed [7]. To maintain the convergent wear pattern, Al_2O_3 abrasive is selected - a good substitute for garnet which is typically used for AWJ machining [14, 20]. Al_2O_3 has a similar density and shape to garnet but is much harder. Higher hardness of the abrasive results in the mixing tube life being reduced from 50-100 hours to around 1 hour [14, 20]. Al_2O_3 was shown in literature to contribute to greater abrasive wear inside the mixing tube, and to fragment less than garnet which may effect the wear pattern [7, 13, 58]. While not ideal, the great reduction in mixing tube life means this accelerated wear approach for developing a TCM system will be explored in the thesis.

The wear times chosen in Table 3.1 were based on the figure that constitutes a "worn" tube, the data observed by Nanduri et al. and the data presented in a Kennametal ROCTEC brochure [14, 162]. Hashish noted that what constitutes a "worn" tube depends on the application, however generally 10% exit diameter wear is a tolerable limit [7]. Hashish also noted that for certain applications, 25% may be passable [7]. It is important to keep these figures in mind when wearing the tubes during data collection. The tubes must be worn past the "worn" threshold so that the data from the full extent of wear can be used to build a TCM system. The goal for the TCM system is to make the AWJ more accurate, with greater wear the cutting performance will decrease [7, 13, 65–67]. Considering the drop in performance, and the additional time taken to wear the tubes past the 25% mark, 10% exit diameter growth will be used as the wear threshold, beyond which the tube will be classed

as worn. Using the data presented by Nanduri et al. and a Kennametal ROCTEC brochure, it was estimated that it would take approximately 60 minutes to surpass the wear threshold of 10% [14, 162]. The machining was extended 50% beyond the limit to ensure the worn threshold was surpassed.

The tubes' wear times, presented in Table 3.1, were staggered up to 90 minutes. This allowed the preservation of tubes at different stages for analysis after the wear trial. 10-minute intervals were selected to balance the quantity of data collected and the duration of the trials. For certain tubes, data was collected every 5 minutes instead - to test the robustness of machine learning models when testing performance on shorter time intervals. Ten tubes were worn in total to balance the quantity of data collected and the cost of the trials.

Two tubes of shorter length were worn to assess the effect of tube length on prediction accuracy. Initially, the plan was to wear longer tubes of a similar size to the ones provided by Dr Hashish, however none were available at the time for purchase.

The preliminary trial was carried out to test the proposed methodology before organising a larger data collection trial. This allowed assessing whether the accelerated wear approach works and if wear can be predicted during the dwell cycles. The tubes were worn for 60 minutes to allow both tubes to be worn within the time the machine was available. Wearing both tubes for the same period of time also provided an evaluation of the consistency of exit diameter wear, internal profile wear and the measured response.

The ATD data was collected during the main trial, as it could provide several benefits. First, it can help determine whether taking the tubes on and off affects the measured sensor response. Second, this effort can help extend the dataset for training machine learning models. Third, this data can be evaluated for training machine learning models against collecting data during the wear process. Collecting the data during the wear process is more time-consuming, as data is collected more frequently. Potentially, collecting the data post-wear on tubes worn up to a different time point is sufficient. Finally, with the ATD method data can be collected on additionally provided tubes, shown in Table 3.2, or on changes in both orifice and MC condition. Data can be collected from the additional tubes worn using regular wear to understand the difference with WDC tubes, and to evaluate the performance of machine learning models trained on accelerated wear data in making predictions on tubes worn in a regular wear process. This comparison will help determine whether

this framework of accelerated WDC can be used to build a TCM system for industrial purposes.

Finally, several factors had to be considered when selecting the process parameters to vary during data collection. For the experimental work to be industrially relevant, the process parameters had to relate to those found in the real manufacturing process. In addition, the large input parameter space had to be considered. As discussed in Chapter 2, the input parameter space includes design and process parameters. These are presented in Table 2.1. A robust TCM system has to be able to function under varying parameters.

However, varying every parameter will result in a large number of variations for a design of experiments, quickly adding to the time and cost factor of the data collection process. When determining which parameters to take into consideration, it's crucial to assess the likelihood of practical changes for individual waterjet users and identify the parameters that can potentially influence the wear profile. In case of indirect monitoring, the influence on wear rate is less significant provided the wear profile remains consistent. The changing wear rate should not affect the sensors' recorded response. However, alterations to the wear profile itself could have an impact on the observations captured by the sensors.

Most parameters should remain the same for a common AWJ user from the design parameters. For example, a tool centre point checking system controls the alignment between orifice and mixing tube, and so this is expected to remain unchanged. The parameter that may change depending on application is the tube length.

From the process parameters, although each parameter may affect the wear rate, not all parameters will have the same impact on the wear profile. The abrasive is normally unchanged, with garnet preferred [12, 13]. So the abrasive material parameters should stay the same. Particle size may vary in practice, with 80 mesh abrasive being the standard size used, however other mesh sizes, for example 120 mesh, may be used for certain applications [40]. Varying the abrasive size would be unfeasible in this study, as it would require repeating every trial with two different abrasives and machine time is limited. As 80 mesh abrasive is the most often used, this sole particle size will be explored.

The final process parameters to account for are waterjet pressure and abrasive flow rate. The abrasive flow rate is controlled via a metering disk and can be adjusted for different applications. However, changes in the flow rate only impact the wear rate and not the wear profile [14, 48, 50]. Pressure changes impact the kinetic energy of each particle, the particle fragmentation and the turbulence of the jet [65, 79, 81]. However,

while the theoretical models are limited, beyond approximately 300-350 MPa waterjet pressure the jet coherency and particle fragmentation were suggested by Hashish and Yanaida to not change [65, 79]. Based on equation 2.2, water pressure can indirectly impact the wear profile by altering the impact velocity of the abrasive particles. This may result in higher erosive wear, potentially impacting the wear profile, especially closer to tube entry. However, towards the tube exit, where abrasive wear is dominant, the changes are therefore assumed not to be significant. The assumption made in this study will be that changes in water pressure, above 300 MPa, will not impact the wear profile. So the tubes can be worn at one pressure, and for data collection, the response can be recorded under a different pressure, assuming it will not impact the wear profile, provided the pressure is above 300 MPa (3000 bar).

The tubes were worn at 4000 bar, using Al_2O_3 abrasive, an abrasive feed rate of 7.55 g/s, an abrasive mesh size of 80 and an orifice ID of 0.406 mm. They had data collected during a "dwell" cycle at varying water pressures between 3000 and 5000 bar at 500 bar increments for 3 repeats at each pressure, without abrasive.

The water pressure, abrasive mesh size and abrasive feed rate were chosen based on parameters used for industrial machining within the AMRC, and following a discussion with Dr Hashish for standard parameters used by waterjet customers. The selection is intended to be representative of the cutting operation used in manufacturing. It allows the gathered dataset and developed TCM system to be validated in a typical industrial environment. The parameters are also similar to those used by Dr Ashworth et al. for their wear trial at the AMRC on tube no. 11 used in this research [70]. Dr Ashworth et al. used a lower abrasive flow rate, however, a higher flow rate than the one used by Dr Ashworth et al. is typically required for metal and composite machining [70].

The orifice diameter was selected based on the following: first, it was the size available at the AMRC, so it removed the cost of purchasing a new one. In addition, it was the same orifice size used by Dr Ashworth et al., so allowed for the tubes to be compared [70]. Finally, the orifice size complied with the ideal ratio of 2.5-5 of orifice diameter to mixing tube diameter suggested in literature [7, 14, 24, 48–50].

Finally, the data collection process involved collecting data during a "dwell" cycle. In previous research, data was collected with abrasives flowing through the system [34–43]. However, data can be collected in a novel manner during the dwell cycle. The dwell cycle is a stage of waterjet machining when the jet is started, but the abrasive supply is not turned on. This stage is performed before waterjet machining operations to generate a vacuum in the nozzle, which will draw abrasives to the

nozzle [4–6]. Recording data during the dwell cycles allows for tool state prediction before the machining process begins, making the approach highly practical for real-time process monitoring. Additionally, this approach offers the potential to build a foundation for tool path compensation in waterjet machining. The tool can be offset for better performance if the exit diameter is predicted before machining. Finally, with the dwell cycle, additional data can be collected with only water flowing through the system, without further wearing the tube.

The dwell cycle can be used to gather data under varying water pressures to build a dataset for process monitoring. As noted, the assumption is that above 3000 bar pressure, the wear profile does not change. So the tubes are worn under a singular pressure of 4000, but data is collected (when abrasives are not flowing) under varying pressures. The data under additional pressure was fast to collect and increased the dataset size without affecting how the tube was worn. The additional data can be used to study the effect of water pressure on the sensor response and to help the machine learning models learn patterns within the data.

The parameters not considered included the traverse feed rate of the machine as well as the angle at which the machining takes place. The assumption was made that neither of these parameters affects the wear profile inside the tube.

The wear of other component parts in the nozzle, namely the orifice and MC, may influence both the wear pattern inside the mixing tube as well as the response of the sensor [3, 4, 86, 162]. To account for this, ATD tests were carried out with a MC and orifice change to more worn components.

3.1.3 Sensor selection

As discussed in Chapter 2, there are a variety of sensors available for wear detection of the AWJ mixing tube. When choosing a sensor for building a TCM system, it is important to consider the sensor reliability, cost, ease of use and intrusive nature of the process. The selected sensors for TCM in this thesis include an airflow sensor, pressure sensors and a condenser microphone.

In this work, both pressure and airflow sensors are considered as they are capable of detecting changes in mixing tube exit diameter [3–5, 36, 37]. As the jet of water is turned on, a negative pressure is generated inside the nozzle, causing air entrainment [3, 4, 25]. The air suction is key for pulling abrasives to the nozzle (when the abrasive supply is switched on) through the supply hose [4–6]. As the mixing tube wears, and the exit diameter increases, a greater vacuum in the nozzle is created and the airflow increases [3, 4].

In literature, authors noted setup issues when using the airflow sensor [37, 86]. However, if the setup can be improved this sensor is a good option for monitoring wear. The airflow sensor is a suitable choice for TCM as it offers a low-cost solution, can detect multiple failures, is inexpensive, and can be mounted in a non-intrusive way where the sensor or its wiring won't get damaged or interfere with the nozzle.

In literature, airflow sensors were added to the abrasive supply hose, limiting the sensor's use to when the abrasive supply is disconnected [37, 86]. Instead, here the sensor was placed at the air inlet near the abrasive tank, as shown in Figure 3.1. This position allows the sensor to work online with abrasive flowing through the system without damaging it. This proposed solution overcomes the challenge of designing a non-intrusive and practical monitoring system.
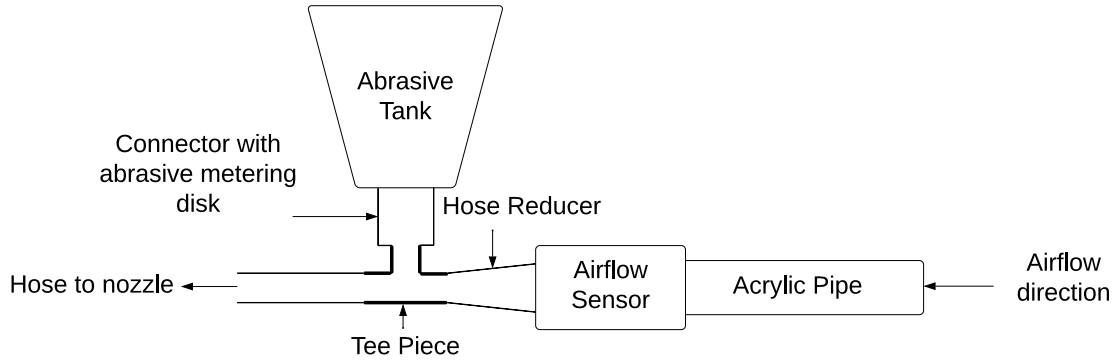

Figure 3.1: Drawing of the airflow sensor setup.

Pressure sensors are also considered and have been shown in previous research to be capable of detecting exit diameter wear by monitoring the negative pressure (vacuum) inside the MC part of the nozzle and the pressure changes in the abrasive hose [36, 37]. Again these sensors are inexpensive and simple to use. In addition, this sensor comes pre-installed on the machines used for data collection for this thesis. In addition to the nozzle pressure sensor, most waterjets have additional pre-installed sensors on the machine. The additional sensors record: water pressure, water flow rate and abrasive flow rate. Unfortunately, the machines used in this research did not have abrasive flow rate monitoring installed, however water flow rate and pressure were recorded. As nozzle pressure, water pressure and water flow rate sensors were installed on both machines used in this thesis, with the data recorded into the same database, this data will be collectively referred to as machine data.

In literature, acoustic emission approaches were popular [39, 40, 42, 43]. Acoustic emission sensors are expensive and difficult to set up, as they can interfere with the nozzle movement and may be damaged if not protected from the harsh water and

abrasive environment. However, a condenser microphone, also used by Mohan et al., can be used instead of an acoustic emission sensor for a simpler and cheaper setup [42]. Acoustic emission sensors may be better suited than microphones for the task overall, as they are capable of detecting high-frequency acoustic signals. Higher-frequency variations in signal amplitude, above 20kHz, have been noted to be more prominent when studying an increase in nozzle diameter than lower-frequency variations [42]. In addition, acoustic emission sensors are often more robust and better suited for harsh environments. Unlike condenser microphones that are sensitive to environmental factors which can impact their performance, with humidity being a crucial one, as the AWJ enclosure is full of water droplets. Nevertheless, a condenser microphone is worth trialling for a TCM system when factoring in cost, the intrusive nature of setup and ease of use. A condenser microphone would work by capturing the changes in the acoustic signature created by variations in the mixing tube wear.

Finally, accelerometers are suitable for wear detection [24, 34, 41]. However, accelerometers are expensive and difficult to setup similar to acoustic emission sensors, as they require being attached close to the source - i.e. onto the nozzle itself. Although this approach was considered, it was not possible to implement this within this research project.

3.2 Overview of collected data

Two data collection trials were carried out: a preliminary trial at the AMRC facilities in the UK and a main trial at the Aquarese facilities in France. The preliminary trial was carried out to evaluate the proposed data collection framework. The main trial was carried out for additional data collection to validate the findings of the preliminary investigation. Due to the main trial being abroad and the availability of support offered by Aquarese, carrying out the data collection in one visit was not possible, and the main trial was split into two phases. During the second phase of the main trial, a condenser microphone was added inside the AWJ enclosure to the ATD data collection process. In addition, three extra Dr Hashish tubes were brought to France for testing. Finally, the shorter-length mixing tubes (tubes 9 and 10) were also worn during the second phase of the main trial.

A summary of the sensor data collected during the trials is presented in Table 3.4. Figure 3.2 summarises the measurement chain associated with each sensor during data collection. Two pressure sensors were used during the thesis aside from the water pressure sensor; one sensor was connected to the nozzle via tubing to a nozzle
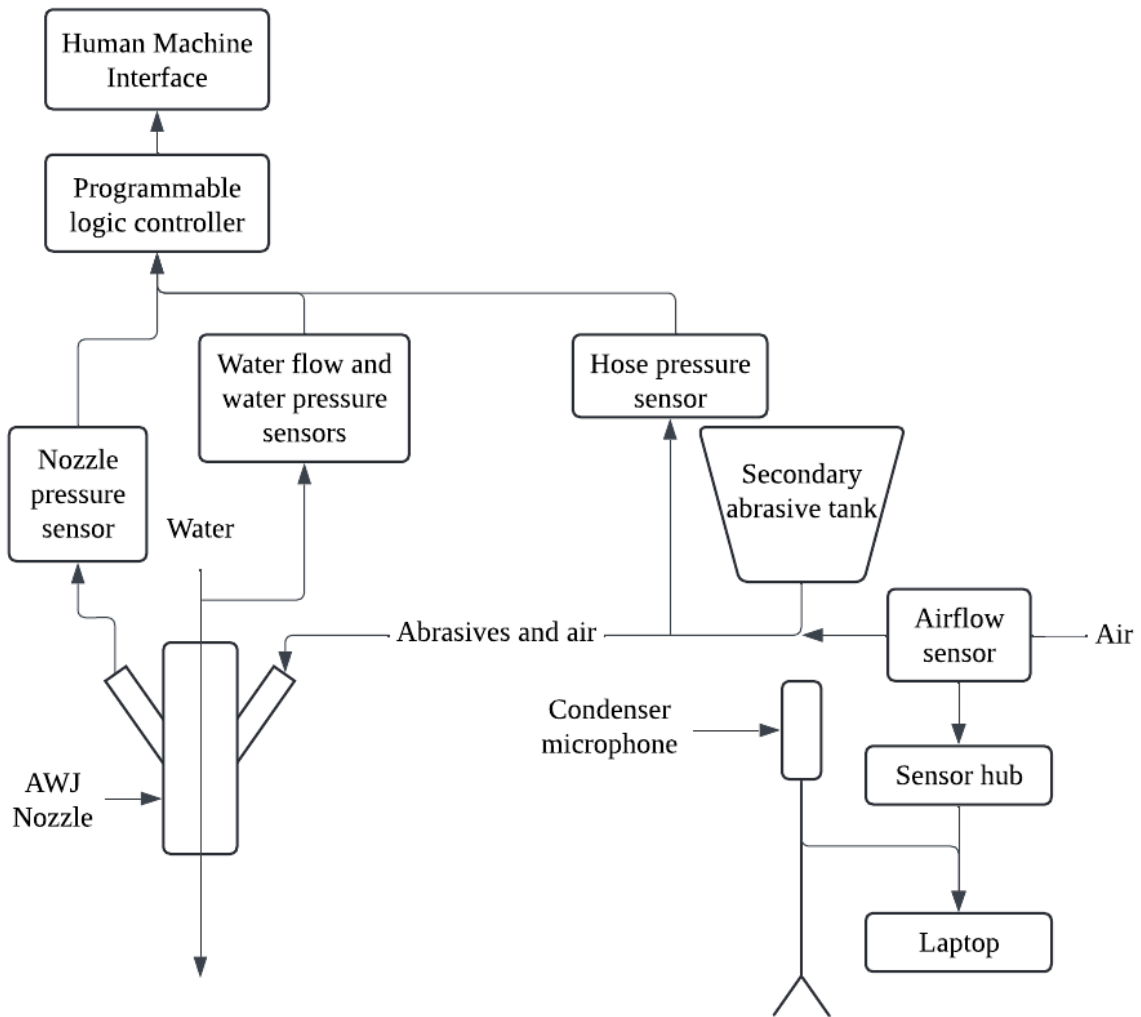
Figure 3.2: Schematic of the sensor configuration for data acquisition, illustrating the raw data recording pathways for each sensor.

body port connection, with a second sensor attached to the abrasive supply hose. In Table 3.4, the nozzle pressure data is missing for several tubes. For tubes 4, 6, 7, 8, this was caused by a crimp in the hose between the sensor and the nozzle. The hose was later adjusted to avoid the issue re-occurring. For tube 2, data loss was caused by a database failure during the preliminary trial, which also corrupted pressure and water flow rate recordings. In addition, orifice change data was collected for only a few tubes due to a machine fault which prematurely halted data collection during the first phase of the main trial.

The order of wear for the mixing tubes during Phase I was not in numerical order. It was 6, 4, 8, 7, 5, 3. During Phase I WDC, issues with pump pressure were observed, along with inconsistencies in the tracked airflow signal. At the end of Phase

Table 3.4: Overview of all sensor data collected. Orifice and MC columns indicate ATD data collection under the orifice and MC change to a worn component. The worn orifice used in the main trial Phase I is the same orifice used for WDC during the preliminary trial. "Machine" sensors include nozzle pressure, water pressure and water flow rate sensors.

Trial:	Preliminary	Main – Phase I			Main – Phase II		
Data collection:	WDC	WDC	ATD	Orifice	WDC	ATD	MC
Sensor							
Airflow	✓	✓	✓	✓	✓	✓	✓
Machine	✓	✓	✓	✓	✓	✓	✓
Pressure (hose)		✓	✓	✓	✓	✓	✓
Microphone						✓	✓
Mixing tube							
1 - 60 min	✓*		✓	✓		✓	✓
2 - 60 min	✓*, **		✓	✓		✓	✓
3 - 15 min		✓				✓	✓
4 - 30 min		✓**		✓		✓	✓
5 - 45 min		✓				✓	✓
6 - 60 min		✓**		✓		✓	✓
7 - 75 min		✓**				✓	✓
8 - 90 min		✓**		✓		✓	✓
9 - 60 min			✓***		✓	✓	✓
10 - 60 min			✓***		✓	✓	✓
11 - 40 hrs			✓			✓	✓
12 - 40/70 hrs			✓			✓	✓
13 - 40/70 hrs			✓			✓	✓
14 - 70/70 hrs			✓			✓	✓
15 - 40/70 hrs						✓	✓
16 - 40/70 hrs			✓			✓	✓
17 - 40/70 hrs			✓			✓	✓
18 - 40/70 hrs			✓			✓	✓
19 - 40/70 hrs						✓	✓
20 - 40/70 hrs						✓	✓

* A worn orifice was used during this data collection process.
** Nozzle pressure data may be completely or partially missing for this tube.
*** Data collected before tube was worn - wear at 0 minutes.

I, a water leak was observed above the nozzle and the water jet kept failing with the

nozzle overheating, which concluded Phase I data collection. Before beginning Phase II, the nozzle was re-assembled and checked for blockages. However, after wearing mixing tube 9, the water leak and pump pressure issues resulted in machine failure. The source of the problem was found to be the orifice holder and its UHP seal after troubleshooting by a technician. After changing the orifice holder and UHP seal, the AWJ became stable, and the pump, which was previously struggling to control its pressure, began operating as intended. The collected data can give a better insight into when the issue began. However, the part change during Phase II of the main trial caused a significant change in the recorded sensor response.

During the main trial, mixing tubes were worn to incrementally increasing wear times. This allowed for ATD data to be collected on tubes at different wear times, further expanding the collected dataset size. In addition, ATD data could be collected when changing the orifice and MCs to a component with a longer use time. Allowing for a better understanding of how wear on each part affects the sensor response and prediction accuracy. Finally, wearing the mixing tubes by a different amount of time, allowed for the wear profiles inside the mixing tubes to be studied after the completion of the trials.

After the data collection trials were completed, additional data could be collected on the worn mixing tubes. The exit diameter was imaged using a Jiusion HD 2MP USB digital microscope. The used MCs were also imaged via the USB microscope. In addition, the weight of the mixing tubes was collected using an analytical balance. Both optical microscope images and weight measurements of the mixing tubes were completed before and after the trials took place. These measurements allowed for wear consistency and progression to be studied. The condition of the available orifices was studied using a Nikon optical microscope.

In addition, the mixing tubes were machined longitudinally using EDM to study the internal wear profile progression. The mixing tubes were machined with an offset equal to half the EDM wire thickness to obtain one perfect half. A trained technician carried out EDM. EDM was carried out on all tubes, including those provided by the AMRC and Dr Hashish. Photography of the sectioned tubes was then carried out using a 12MP iPhone XR camera secured via a tripod above the mixing tubes. The camera was held in place while imaging every tube, with the photos taken via a Bluetooth remote controller to minimise the risk of camera motion.

Both garnet and Al_2O_3 abrasives were also studied. A Malvern Panalytical Mastersizer 3000 was used to analyse the size distribution of the abrasive particles. The Mastersizer uses laser diffraction to measure particle size distribution after dispersing
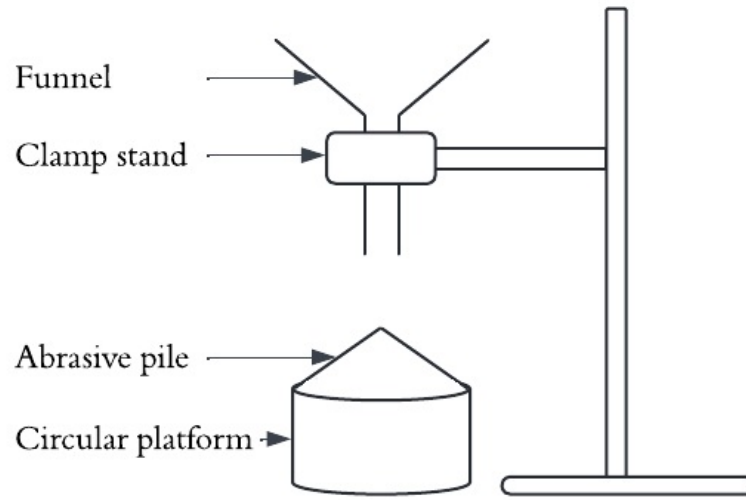
Figure 3.3: Schematic of the setup used to measure the angle of repose of abrasive particles.

the particles in either an air cell (for dry powder dispersion) or liquid. In the case of liquid dispersion, sonication can be employed to facilitate rapid particle dispersion. The particle size measurement range of the Mastersizer 3000 is from 10 nm to 3500 μm. For Al_2O_3 abrasive the particle size distribution was measured before and after waterjet use, to find the average abrasive size and evaluate whether the particles fragment during the wear process. The air cell was used for dispersing the dry garnet and Al_2O_3 samples, while the liquid cell was used for dispersing the Al_2O_3 sample recovered from the bottom of the abrasive water jet (AWJ) catcher tank after waterjet use.

A Nikon optical microscope was used to compare the shape of the abrasives. Helium pycnometry, via the Micromeritics Accupyc II, was used to measure the density of both abrasives. The flowability was compared using an angle of repose tests to evaluate whether either abrasive will flow better through the abrasive hose, ensuring both are similar without irregularities in flow.

For angle of repose measurements, each abrasive sample was poured through a funnel onto a circular platform of a known diameter, using the setup seen in Figure 3.3. Once a cone pile filled the base of the platform, the height of the abrasive pile peak was measured in mm using a digital caliper. The angle of repose was calculated using equation 3.1, where h is the height of the pile and d is the diameter of the platform. Five repeats were conducted for height measurements.

$$\text{angle of repose } = \tan^{-1}\left(\frac{2h}{d}\right) \tag{3.1}$$

3.3 Experimental setup and tool wear measurement

For the data collection to be relevant, it had to be carried out on machines used in industry, such as the one used by the AMRC in the UK. The AWJ available at AMRC is supplied by Aquarese and has a 6-axis Staubli TX200 robotic arm. This machine was used for the preliminary data trial. For the main trial, the same machine available in the Aquarese facilities in France was used, however the machine had a shorter abrasive hose length, which may have impacted airflow data [5]. Figure 3.4 shows the Aquarese waterjet enclosure for the machine based in France. The pictured human-machine interface (HMI) is used to operate the waterjet. Both waterjets used in this thesis are capable of machining at 6000 bar pressure and come preinstalled with a pressure sensor connected to the nozzle via a pneumatic hose, as shown in Figure 3.5. Professional technicians carried out the data collection under the supervision of the authors for the preliminary data collection trial. For the main trial, the author of the thesis was trained to operate the machine.

During the initial stages of the main trial, the catcher tank had a hole cut through at the bottom which caused trial delays and damage to the machine. The catcher tank is designed to withstand damage. However, potentially due to a harder abrasive (Al_2O_3) being used, no material being machined and the jet being stationary, the tank was damaged flooding the factory floor. For further data collection, the bottom of the catcher tank underneath the nozzle position was reinforced with two steel billets to prevent further damage. The nozzle was raised further above the catcher tank, and the water level was increased. Figure 3.6 shows an empty catcher tank with reinforced steel billets. Protective shields were added to the sides of the catcher tank to reduce overflows and prevent flooding of the factory floor during jet operation, caused by the raised water level.

Steel pin gauges were used to measure wear. The exit diameter size was determined by incrementally increasing the pin gauge size in 0.01mm diameter steps until a pin gauge could no longer fit into the exit diameter. The exit diameter was then decided by adding +0.01 mm to the last pin gauge diameter capable of fitting through the mixing tube exit. A schematic of the pin gauging process used to measure the AWJ mixing tube exit diameter is shown in Figure 3.7.
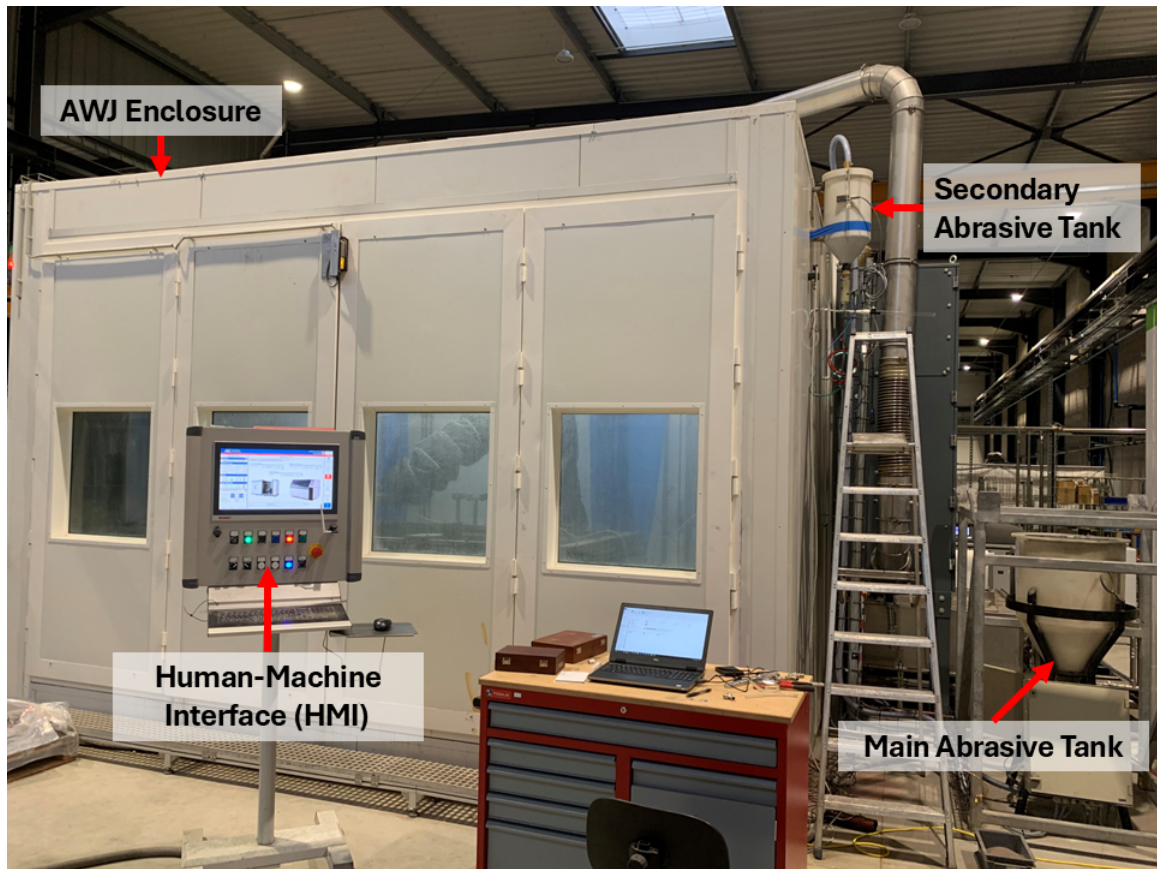
Figure 3.4: Photo showing the waterjet enclosure and data collection setup on the Aquarese 6-axis waterjet in France.

When recording the weight post data collection trials, the mixing tubes were first dried and cleaned with a high pressure air hose to remove any residue abrasive.

A ruby orifice and a pre-installed MC were used for the preliminary trial, as these were available at AMRC. Both components had previously been used for up to 230 hours. The exact use time has not been recorded, but the AWJ itself was not used for over 230 hours, and both parts were purchased new. For the main trial, a new diamond orifice and a new MC with 0 operational hours were used instead. A maintenance procedure provided by Aquarese was used to install either one of the nozzle parts. The nozzle on both machines was Paser IV, which is self-aligning and does not suffer misalignment issues between orifice and mixing tube which can impact performance [25, 32, 59, 76].

The mixing tubes had a spacer attached during both trials, a component designed to reduce the distance between the orifice and mixing tube, following a recommendation from Aquarese and the technicians at AMRC. The use of a spacer lowered the wear rate of the mixing tubes [25, 77].
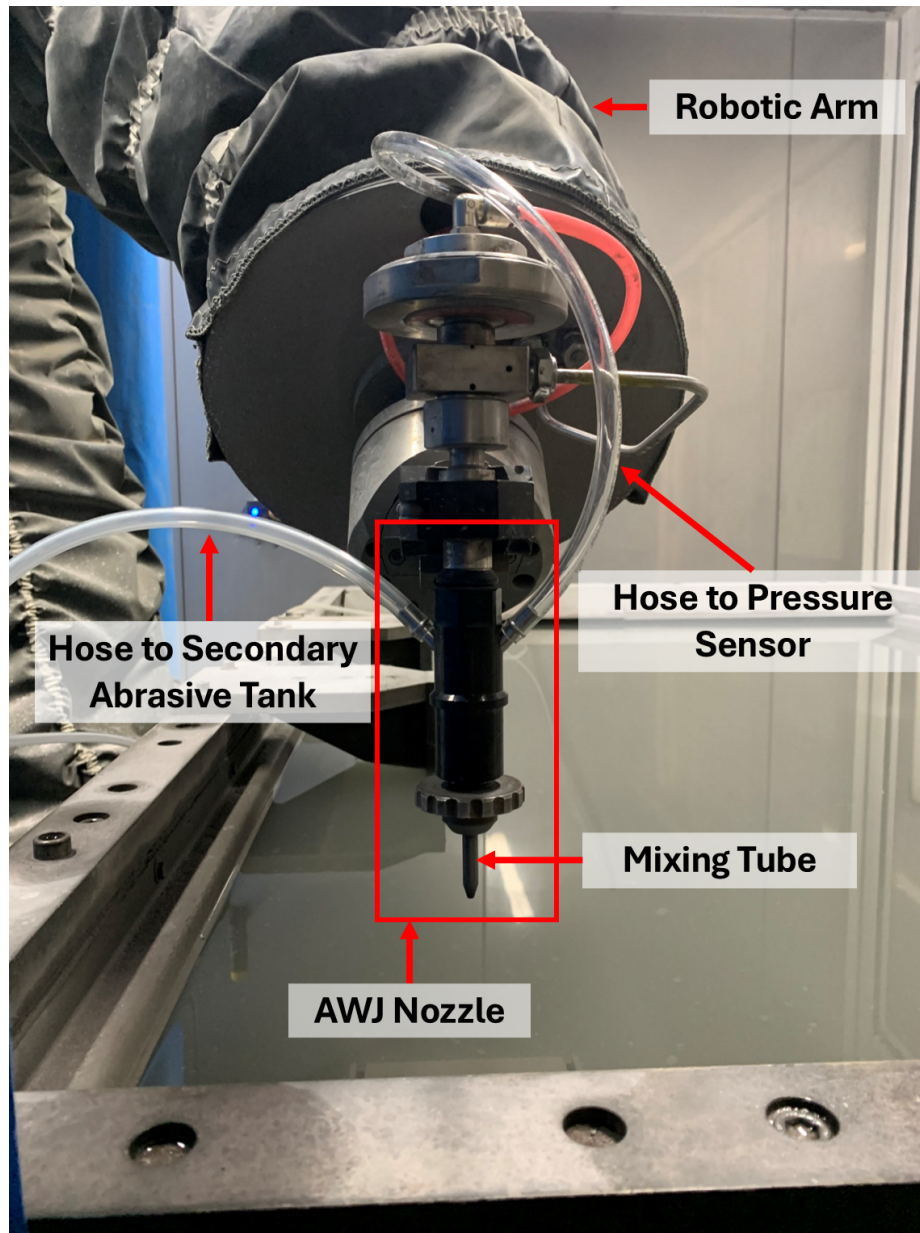
Figure 3.5: Photo of the nozzle on the Aquarese 6-axis AWJ in France.

The Al_2O_3 abrasive used was F080, brown fused alumina supplied by Kuhmichel. The supplier's informational sheet on brown fused alumina is provided in Appendix A. The F080 abrasive is size 80 on the FEPA scale, with a grain size range of 150-212 μm. The supplier did not directly offer 80 mesh Al_2O_3 abrasive, however F080 size was ordered as it provided equivalent grain size. 150-212 μm range approximates to 100 - 70 mesh, with the median value of 181 μm equivalent to 80 mesh. The garnet used for analysis was ClassicCut™80, 80 mesh abrasive supplied by GMA Garnet. A datasheet for this abrasive is provided in Appendix B
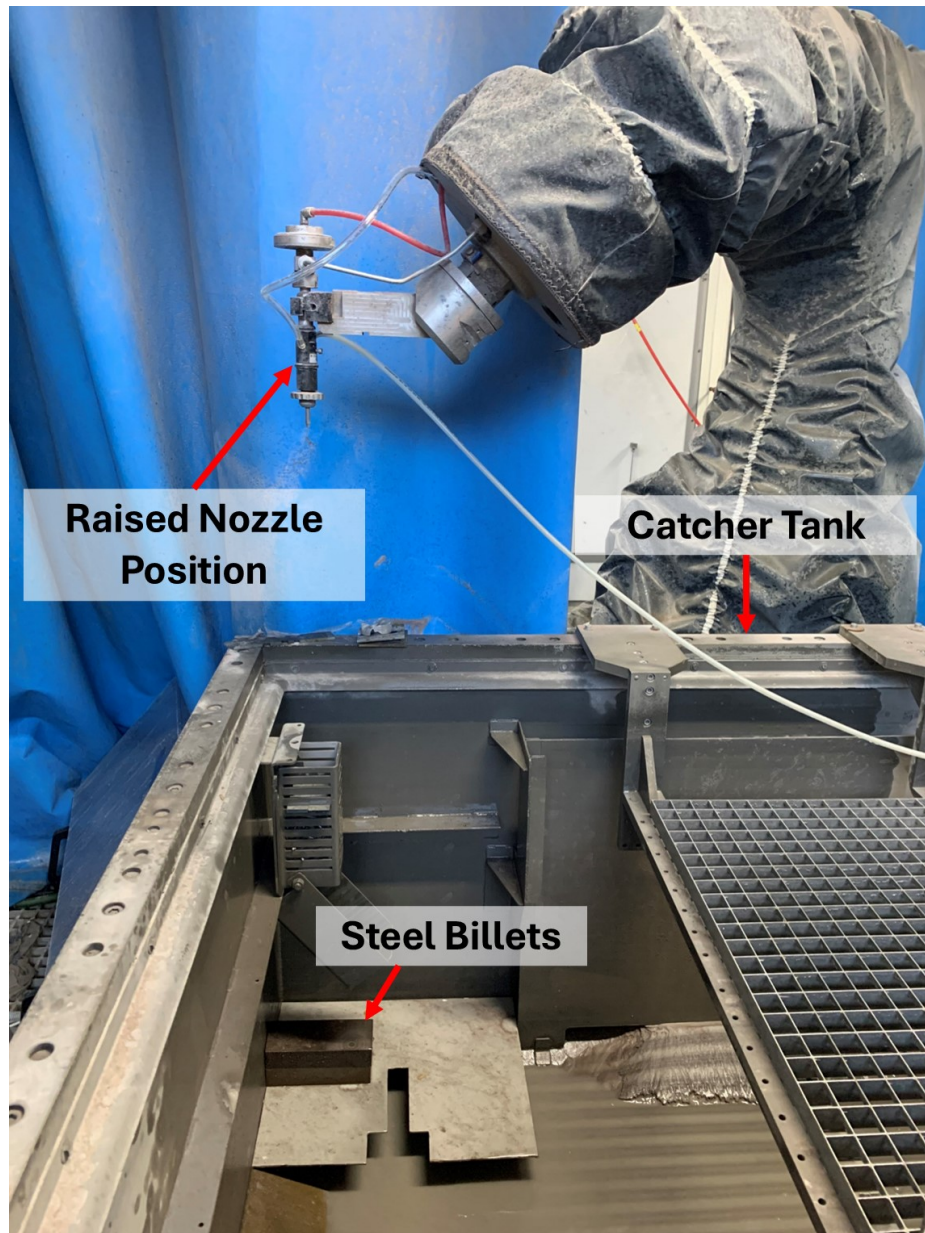
Figure 3.6: Photo of the empty catcher tank after it was cut through and reinforced with welded steel billets.

For data collection, airflow, pressure, water pressure and water flow rate sensors as well as a condenser microphone were used. The airflow sensor was attached at the air inlet to a tee piece via a custom 3D-printed pipe reducer, as shown in Figure 3.8. An acrylic pipe of the same ID was attached to the sensor to provide laminar airflow. The pipe was 300 mm long, as recommended by the sensor supplier. The airflow sensor was an SFM3000 $\pm$200 slm sensor from Sensirion. An extract of the datasheet for the sensor is available in Appendix C. The sensor is temperature-compensated.
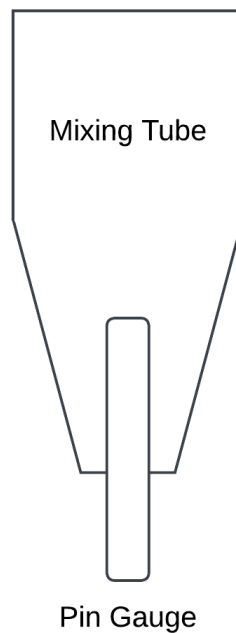
Figure 3.7: Schematic illustrating the measurement of a mixing tube's exit diameter using a pin gauge.

Airflow data was recorded at 100 Hz for the preliminary trial and the first phase of the main trial. A higher 2000 Hz sample rate was used in the second phase of the main trial after upgrading to a new computer with an Intel® Core™ i7 processor and 32GB of RAM, replacing the previous system with the same processor but 16GB of RAM. The new computer could handle the increased data collection rate without data loss, which was attributed to hardware issues in the earlier setup rather than system specifications. Airflow data was recorded using the SEK-ControlCenter software provided by Sensirion, with the sensor connected to the computer via the SEK-ControlBridge microprocessor. Appendix D includes an extract of the technical guide for the microprocessor.

The nozzle pressure, water pressure and water flow rate sensors are pre-installed on both the AWJs. The abrasive hose pressure sensor was installed on request by Aquarese technicians for the main trial, as seen in Figure 3.8. The nozzle and abrasive hose pressure sensors were a PA3029 pressure transmitter manufactured by IFM and pre-installed on the nozzle, as seen in Figure 3.5. Machine data was recorded by the Aquarese system and accessed via the HMI. The water pressure sensor used was HP-2 by WIKA, with the water flow rate recorded with an 8081 water flow rate transmitter
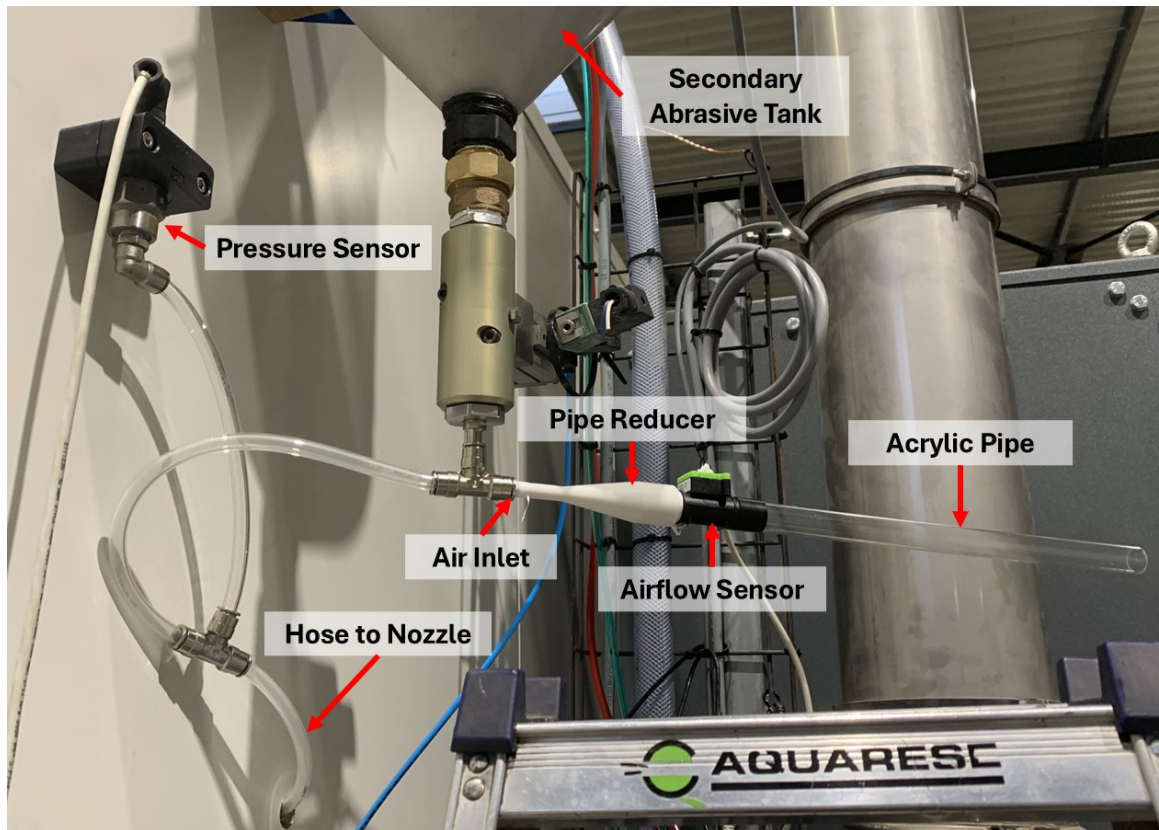
Figure 3.8: Photo showing the airflow and hose pressure sensor setup used during the main trials.

by Burkert.

The pressure, water pressure and water flow rate sensors had data collected at 5 Hz during the preliminary trial. For the main trial, a custom script was written by Aquarese for faster data collection at 50 Hz. Datasheet extracts for the pressure, water pressure and water flow rate sensors can be found in Appendices E, F and G respectively.

A C-1U USB condenser microphone by Behringer, with a 40 Hz to 20 kHz frequency range, was added inside the enclosure for the second stage of the main trial. A user manual extract which includes microphone specifications can be found in Appendix H. The microphone was connected directly to the PC for data collection at a 48 kHz sampling rate using Audacity software for data recording. In audacity, the recording level meter was lowered to 45%, based on output monitoring when the waterjet was running at both the lowest and highest pressures of 3000 and 5000 bar. Recording level adjustment was carried out to prevent clipping and distortions in the recording as recommended by the software documentation [163]. The microphone

had a cardioid polar pattern, so it was directed at the nozzle. The microphone was mounted firmly in a reproducible location with a tripod to ensure its position remained the same at all times. A microphone extension arm was used to reduce undesired reflections from the tripod. To prevent vibrations from influencing the measurement, a shock mount with a screw thread connection was used. A clear plastic bag was secured around the microphone to protect it from the humid environment. A silica pouch was placed inside the plastic bag to reduce moisture buildup further. A humidity strip was placed inside the bag and monitored throughout the data collection process. The microphone was placed 287 cm from the nozzle inside the enclosure. At this distance, the microphone had enough space to be secured in place, and to reach the connection wire fed to the enclosure which was plugged in to the data collection laptop.

There were two different data collection mediums - the HMI and a personal computer. The data between the HMI and personal computer required time synchronisation, which involved daily synchronisations with a common time server as well as post-processing. During post-processing, corrections relied on key events - the dwell cycles. An instant signal magnitude change marked the beginning of the dwell cycles. Averaging time differences between 15 repeats per recording cycle smoothed out the sampling rate differences ensuring consistent temporal alignment for accurate analysis. After completion, time synchronisation was validated via data visualisation.

After the setup was complete, an additional mixing tube was used to test the system, and the sensors were functioning as expected.

3.4   Methodology summary

This chapter presented the data collection framework for building a TCM system for the AWJ mixing tube tool, along with an overview of the collected data and experimental setup. Following the proposed methodology, a dataset was gathered ready for analysis which will be discussed in the following chapter. The outlined framework has several limitations, which include:

- The pressure changes are assumed to produce no changes to the wear profile.

- Only one abrasive flow rate is considered.

- Orifice and MC conditions are assumed to stay the same without degradation during accelerated wear trials.

- It is assumed that the wear profiles inside the mixing tubes obtained in practice, with a varying traverse nozzle feed rate and machining angle, will be the same as those obtained with the nozzle stationery, machining at a 90º angle relative to the water catcher tank.

Chapter 4

Preliminary Data Collection & Results

Following the development of a data collection methodology, data was collected and analysed to test the proposed framework. The referred-to framework describes the use of an accelerated wear approach, collecting data during dwell cycles and using indirect methods to monitor mixing tube wear. This chapter will present the work conducted after the collection of preliminary trial data. The preliminary trial aimed to understand whether the proposed data collection methodology works and whether sensors have the potential to predict mixing tube wear. In this chapter, the framework is first evaluated before the machine learning pipeline and results are presented. During framework evaluation, raw data is analysed to get a better understanding of the data and to gain an insight of potential issues of the process before evaluating machine learning performance.

The preliminary dataset included only two worn mixing tubes. With a small dataset, a secondary objective was to evaluate how well machine learning can perform with limited data. In addition, machine learning based on sensor data was compared against a simpler approach - measuring the wear time of the mixing tube only, to understand whether using machine learning is feasible or if a more basic approach to TCM of the mixing tube exists. As described in Chapter 3, the preliminary trial involved wearing the mixing tubes for 60 minutes each at 4000 bar water pressure, with data recorded under dwell every 10 minutes. The water pressures used were between 3000 and 5000 bar, with responses recorded for 3 repeats of at least 5 seconds each per water pressure setting using airflow and pressure sensors.

4.1 Data collection framework

4.1.1 Wear data

Figure 4.1 presents the wear progression of two tungsten carbide mixing tubes. The observed exit diameter wear progression suggests the accelerated approach successfully reduced the tool life as expected following the literature review [7, 14, 20]. For both mixing tubes, the "wear threshold", beyond which the tool is considered worn, was crossed within 60 minutes of wear [7]. The "wear threshold" of 1.10 mm was determined by calculating a 10% exit diameter increase from a starting diameter 1.00 mm. The actual initial exit diameters were measured as 0.98 and 1.00 mm ± 0.005mm for each tube via pin gauges, with the manufacture stating that the initial exit diameter for the provided tubes may vary between 0.97-1.02 mm.
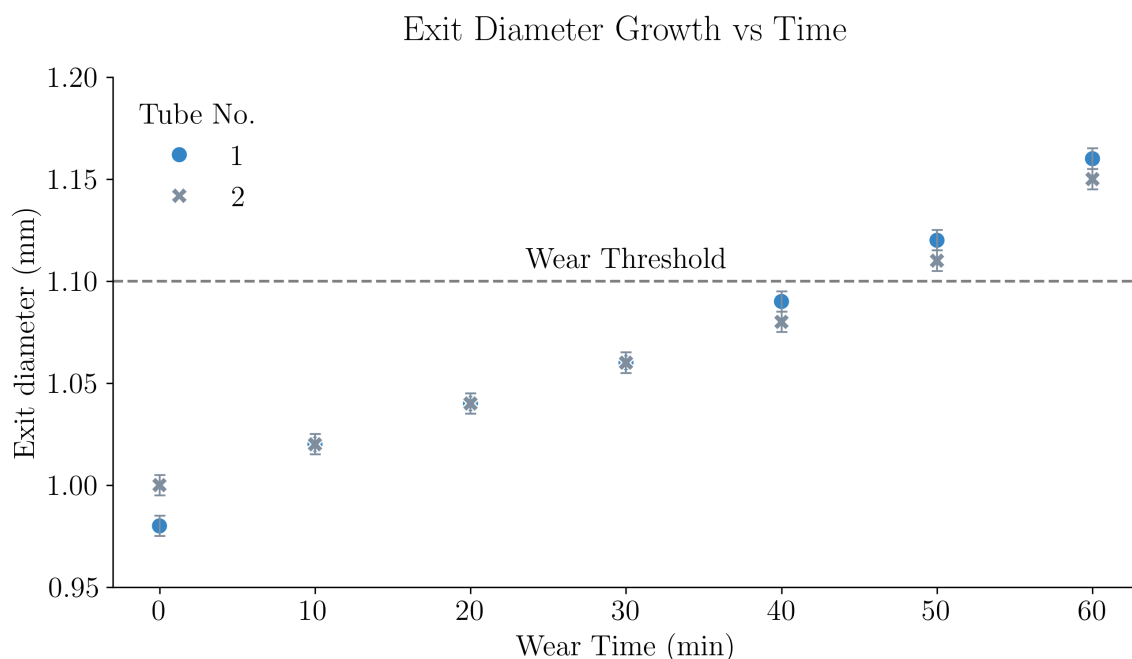

Figure 4.1: Comparison of exit diameter growth of two ROCTEC 100 mixing tubes during accelerated wear. Linear regression slopes for tubes 1 and 2 were 0.0028 ± 0.0001 mm/min and 0.0024 ± 0.0002 mm/min respectively, representing the exit diameter growth rates with their associated uncertainties.

Figure 4.1 suggests that the exit diameter wear progression is linear, which is inconsistent with a previous study which found a non-linear trend for the same accelerated wear approach using Al_2O_3 abrasive [14, 20]. As previously mentioned in Chapter 2, the authors used a larger pin gauge increments of 0.025 mm to measure the exit diameter, as opposed to 0.01 mm increments used in this thesis [14, 20].

Larger pin gauges may not have picked up subtle increases in the exit diameter over their recorded exit diameter growth range of 0.00-0.25 mm [14, 20]. The exit diameter wear progression observed during accelerated wear in Figure 4.1 resembles the wear progression during regular wear reported by Nanduri et al. (Figure 2.5). This similarity supports the thesis hypothesis that accelerated wear can serve as an effective alternative to regular wear. The hypothesis is further supported in Chapter 5, where similarities in abrasive flow, size, shape, and density between garnet and Al_2O_3 are observed.

While there is a difference in the growth rates between the two tubes, the difference is relatively small. The calculated gradients suggest the exit diameter growth between both mixing tubes is consistent. First, this suggests the wear process in AWJ machining is stable. Second, even though the sample size is small, this trend suggests that simple methods, such as recording the time the mixing tubes are used for, may perform well for TCM purposes relative to more complicated approaches such as machine learning algorithms based on sensor data. This will be further investigated later in this chapter.

Table 4.1 presents the mixing tube weight data. The weight change is similar for both tubes, with the final weight after 60 minutes of wear within 0.030 ±0.001 grams. Similar to the exit diameter data, this suggests the wear process is consistent as even after experiencing a high wear rate for 60 minutes, the mixing tubes had a similar end weight. For tube 2, the final weight is smaller, even though the exit diameter is also smaller. Potentially, tube 1 experienced greater internal profile wear.

Table 4.1: Mixing tube weight data.

	Weight (g ±0.001)	
	Tube 1	Tube 2
Pre-trial	61.297	61.362
Post-trial	58.481	58.451
Prct. change	-4.59%	-4.75%

4.1.2 Airflow data

A sample of collected airflow data is shown in Figure 4.2. Airflow data was collected at 100 Hz. This sample rate had lower storage requirements and reduced the bandwidth required by the recording equipment compared to the available 2000 Hz sample rate.

However, it offered a reduced resolution of the process. Due to limitations of the computer used for data collection at the time, recording at a sampling rate higher than 100 Hz was not feasible, as it would cause instability and data loss.
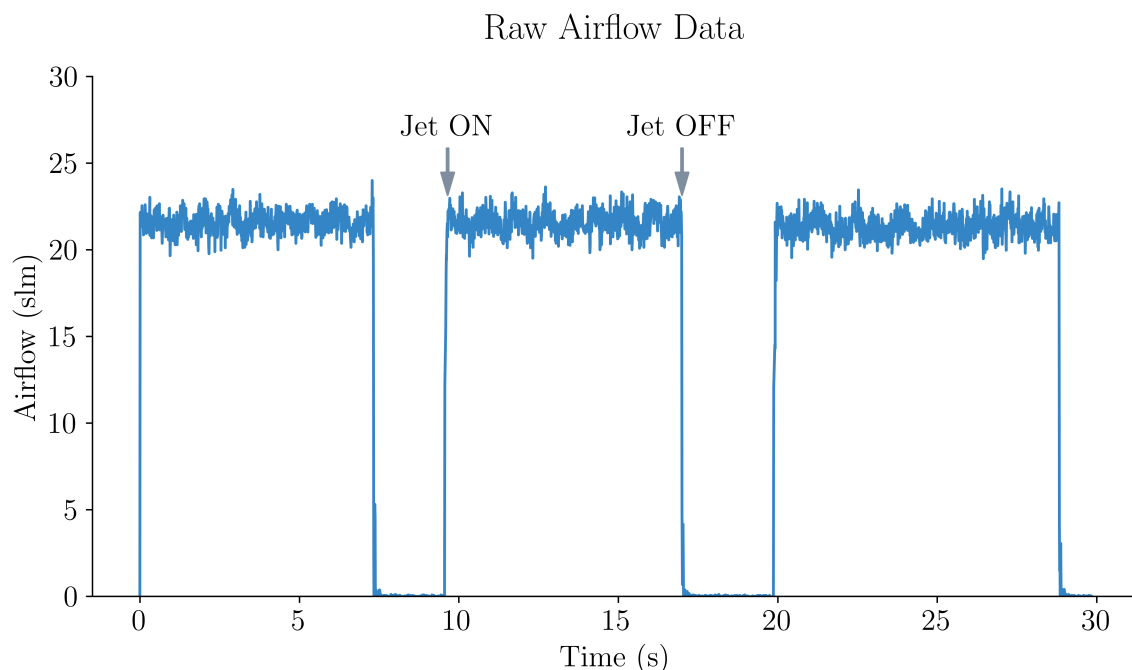
Raw Airflow Data

Figure 4.2: Airflow signal during three dwell cycles at 4000 bar water pressure of an unworn mixing tube 1.

Changes in the airflow signal are observed as the water jet is turned on and off, as seen in Figure 4.2. The three observed events each account for a repeat during the dwell cycle. The airflow signal's magnitude is seen to rapidly increase when the waterjet is turned on and rapidly decrease when the waterjet is turned off. In addition, the signal exhibits an oscillatory pattern. Suggesting the air is drawn into the waterjet at a varying rate. This may be due to pulsations caused by the intensifier pump. Finally, the average airflow appears to be similar for all three dwell recordings, as expected.

Figure 4.3 shows the relationship between average airflow and the exit diameter. The airflow average is calculated for 4 seconds of dwell data after the jet is turned on. Three repeats were recorded at each exit diameter. The data suggests that airflow increases with growing exit diameter, as expected following the literature review [4]. The increases in exit diameter allow a wider jet to leave the mixing tube, carrying out more air. Based on these results, the airflow sensor is suitable for use as an indirect method for AWJ process monitoring, as the signal changes with changing wear. An

anomaly is observed at 1.09 mm exit diameter (40 minutes of wear) for tube 1's first repeat in Figure 4.3. Observation of the raw airflow signal of the anomaly suggests it was likely caused by a temporary abrasive blockage caused by manual operation of the jet cycle, with the blockage cleared away by the jet before the second dwell cycle was run.
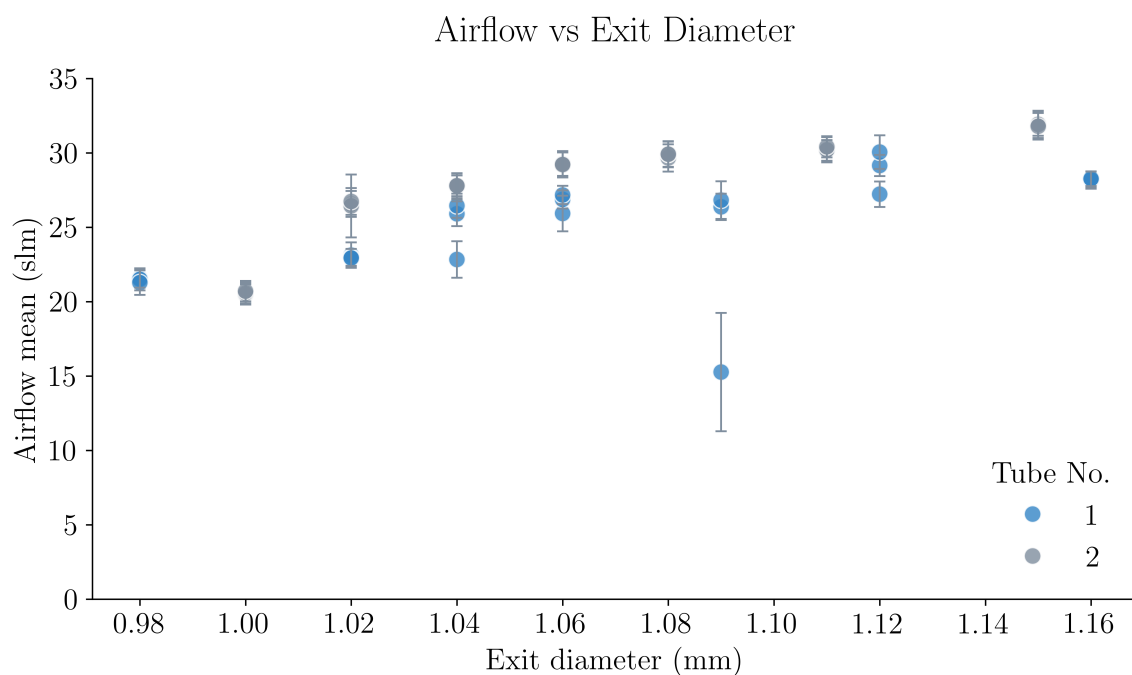

Figure 4.3: A comparison of the average airflow signal, with increasing exit diameter. The error bars are for one standard deviation of the data for each repeat.

When comparing the recorded airflow data between mixing tubes 1 and 2 in Figure 4.3, the data appears to vary more between repeats for tube 1. Meanwhile, tube 2 repeats are relatively consistent with each other. During data collection, it was observed, on the HMI dashboard, that the water pressure pump did not always stabilise at the required water pressure before the operator ran the dwell cycle. This could have resulted in lower airflow for the start of the signal, reducing the average of the recorded response. However, this will have only caused differences in the first repeat at that pressure, as for the second repeat, the pump pressure would have stabilised. For tube 1, there appears to be a variation between all 3 repeats for some measurements. Figure 4.4 provides additional information on the data. It appears that the existing issues for mixing tube 1 were cleared up before recording tube 2 dwell data. Namely, the recordings became consistent between repeats and 4000 bar water pressure measurements resulted in greater airflow than for lower water pressures.
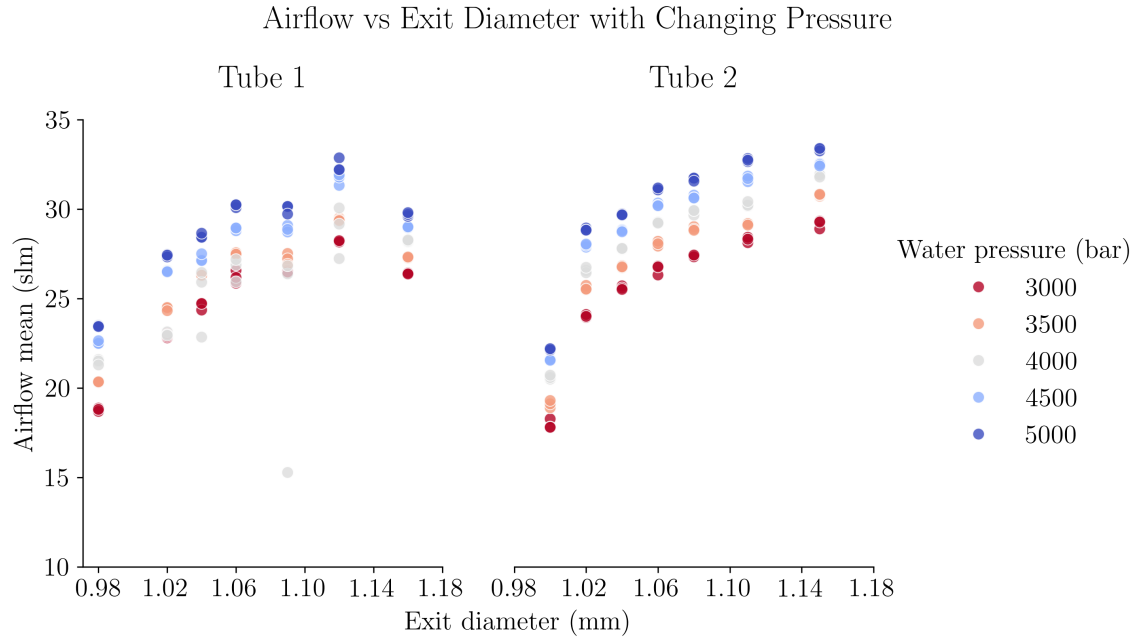
Figure 4.4: Two subplots showing the changing airflow at different water pressures and exit diameters for two preliminary trial mixing tubes.

The variations in data could be caused by an abrasive blockage near the mixing chamber or humidity in the abrasive supply hose. Humidity would have caused abrasives to clump together. Humidity issues can only be fixed by drying out the supply hose, for example, via an air hose. Otherwise, the issue persists, with the abrasive slowly accumulating and further blocking the supply hose. Since the issue was fixed without intervention, the data suggests humidity was not the cause for varying airflow, as it would not have cleared away on its own. Therefore, dry abrasive blockage was likely causing problems with the airflow.

Abrasive blockage may have been caused by poor machine operation by the technician. After each wear cycle, data was first recorded at 4000 bar water pressure. Figure 4.4 suggests 4000 bar water pressure recordings were the most unreliable, as for tube 1 the measurements were lower than 3500 or 3000 bar water pressures. The issue with the data may have been caused by failing to flush the abrasive after the wear cycle, which is done by letting the water jet run for sufficient time until all abrasive clears out from the abrasive hose. Failing to flush the abrasive, can cause abrasive build up in the hose. Therefore, at the start of dwell recordings, when the jet is powered on, the remaining abrasive in the supply hose is first cleared through the nozzle by the generated vacuum before only water and air exist in the system, resulting in a lower initial airflow. However, the build-up may not all clear up if some

moisture begins to clump non-flushed abrasive together during the start of the jet cycle, which may have affected further recordings as well. The data seen in Figure 4.4 supports this hypothesis.

For the data collection process to be effective going forward, several adjustments need to be made to the operating procedure. The operator has to ensure the high-pressure pump reaches the desired water pressure value and stabilises before starting the water jet. In addition, after each wear cycle, all abrasives must be allowed to clear through the hose before the water jet is turned off to avoid blockages forming. This can be done by turning off the abrasive supply and leaving the jet on for several additional seconds until the abrasive hose is clear.

In Figure 4.4, the final dwell runs for mixing tube 1, and the first dwell runs for tube 2 also appear to lie outside the general trend of the other data. To verify if the observed trend is accurate, more data has to be collected.

The implication of poor data quality is that any trained machine learning models may perform poorly. For example, as seen in Figure 4.3, at 1.04 mm exit diameter for mixing tube 2 at 4000 bar water pressure, the mean of the signal is higher than mixing tube 1's 1.06 mm recordings or even the 1.09 mm recording at the same water pressure. So, if training machine learning models on data from mixing tube 1 to predict the exit diameter of mixing tube 2 the model may perform poorly.

In order to improve the performance of machine learning models, frequency domain analysis and subsequent feature generation from this analysis is employed as an addition to the time domain analysis. Frequency domain features may contribute to the models' overall predictive accuracy by providing a more nuanced understanding of the underlying patterns associated with wear-related variations. It also showed potential in previous AWJ monitoring research for wear detection [42]. Figure 4.5 shows the PSD of the airflow signal and how the frequency distribution is impacted by mixing tube wear. The PSD not only provides a clear representation of the signal's frequency distribution but also serves as a powerful tool for detecting subtle changes in the signal's characteristics as wear progresses.

In Figure 4.5, the PSDs were computed using Welch's method using the SciPy library, with a default segment length of 256, the default Hann window and the default 50% point overlap between segments [118, 164]. A full list of the Python libraries used in this thesis is provided in Appendix I. For the box plots, the line inside the boxes represents the median power, with the box itself representing the interquartile range - 50% of the distribution of PSD values. For tube 1, two peaks around approximately 1 Hz went to 0.2 slm^2/Hz and one peak at 40 minutes of wear

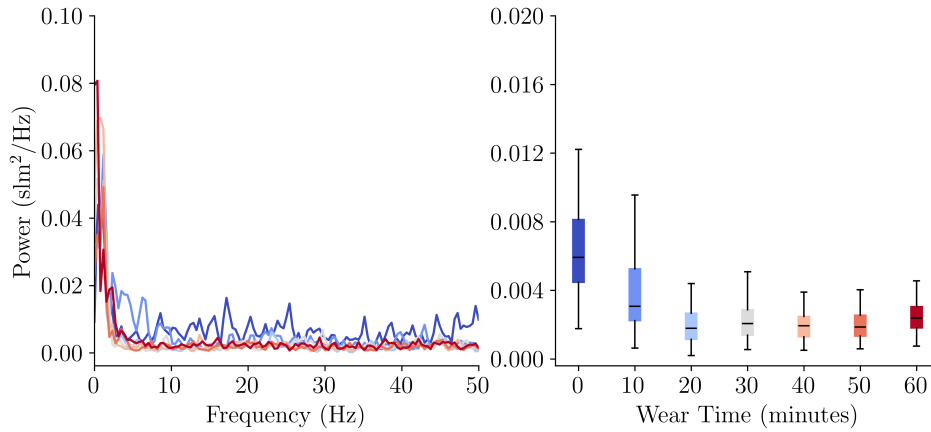Change in Airflow PSD with Increasing Mixing Tube Wear
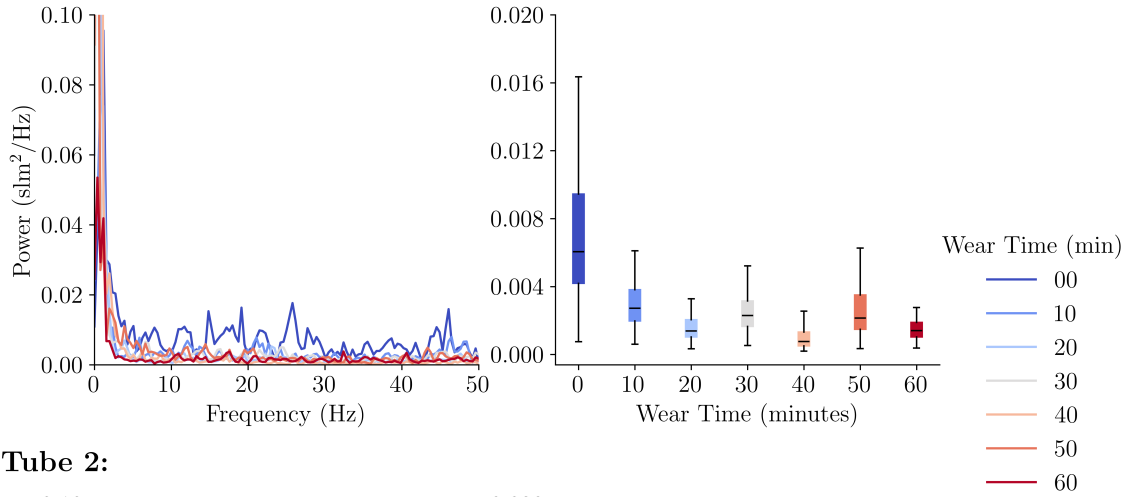
Figure 4.5: The figure depicts the dynamic changes in PSD of the airflow signal with increasing wear time on the mixing tubes. The plotted data is for 4 seconds of dwell, collected at 100 Hz and 4000 bar water pressure with the plotted PSD averaged over three dwell repeats. The two top subplots are for mixing tube 1 data, with the two bottom subplots for mixing tube 2 data. For both mixing tube 1 and 2, on the left is a line plot representing the PSD at different wear times and on the right right is a box plot, providing a concise summary of the PSD distribution at each wear time.

to approximately 1.8 slm^2/Hz. The y-axis was, however, limited to 0.1 slm^2/Hz range for better presentation purposes.

Figure 4.5 shows that with changing wear time, the PSD of the airflow signal changes. Specifically, the median amplitude is seen to decrease up to 20 minutes of wear for both mixing tubes, followed by subsequent fluctuations in the median value. A gradual reduction of the box sizes on the box plots is also observed, suggesting a higher variability in the PSD across different frequencies during the initial wear

period before stabilization at longer wear times.

The changes in median power and power distribution seen at the early stages of wear in Figure 4.5 may be a result of the system's higher sensitivity to wear-induced changes at the beginning. During early wear stages, the higher PSD may be due to the mixing tube's smoother surface causing more noticeable turbulence and distinct airflow variations. As wear progresses and the surface roughens, the airflow becomes more uniform, resulting in a lower PSD. This speculation suggests that the system's sensitivity to wear-induced changes is more pronounced initially, leading to higher PSD values.

After the initial wear stage has passed, the observed fluctuations in the median amplitude of the airflow PSD suggest a complex relationship between wear and the airflow signal. This complexity could stem from various factors such as surface roughness and the evolving wear patterns. The implications for predictive maintenance are that the observed patterns in the frequency domain can serve as indicators of the wear process, which could aid in the development of machine learning models for wear prediction.

Figure 4.6 displays the variations in the total power of the airflow signal in the frequency domain with changing water pressure and exit diameter. A decreasing trend in total power is observed with increasing mixing tube exit diameter. The results further support the creation of frequency domain features to help machine learning models detect patterns in the data between the airflow sensor signal and mixing tube wear. The relationship between changing water pressure and total power appears more complex. More data is required to further understand this relationship.

4.1.3 Machine data

The nozzle pressure data is presented in Figure 4.7. The sampling rate could not be increased on the machine, which led to lower temporal resolution data. Nevertheless, as Figure 4.7 shows, changes in pressure inside the nozzle are experienced when the jet is powered on. The three observed events each account for a repeat during the dwell cycle runs. The pressure data is consistent between all three measurements. Due to its low sensor resolution and sampling rate, the sensor cannot detect slight variations in the signal, as the resultion is only 0.01 bar.

Figure 4.8 gives a broader insight into how the nozzle pressure signal changes with changing mixing tube wear and water pressure. The average of the nozzle pressure signal is calculated for 4 seconds of dwell data from the point the jet is turned on. Some data for tube 2 is missing - a result of a database failure on the AWJ machine.
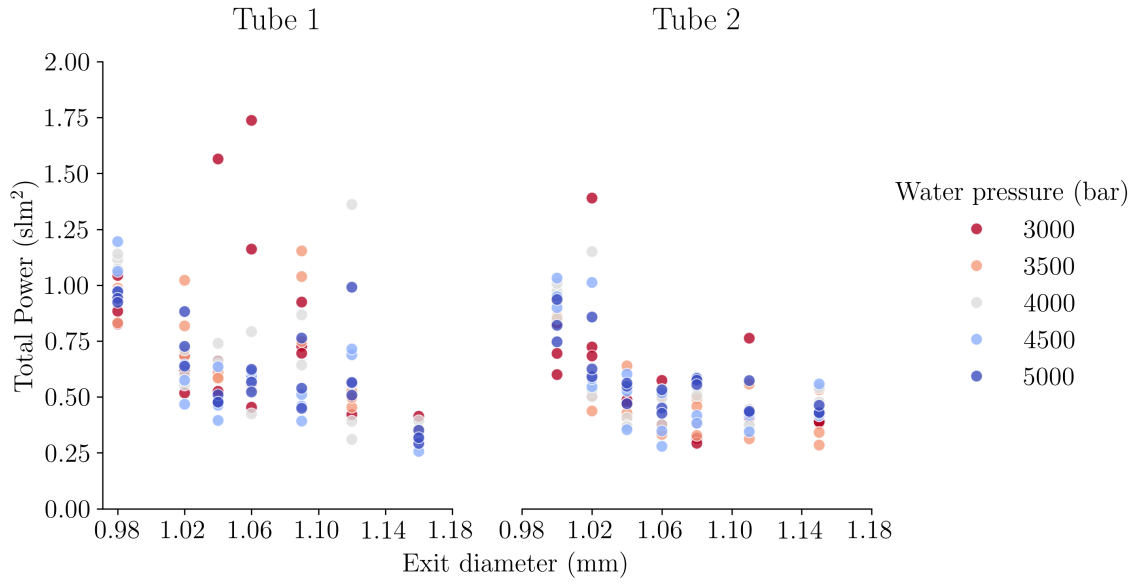
Figure 4.6: A scatter plot displaying the relationship between airflow total power in the frequency domain and exit diameter for two mixing tubes. Each point represents data from a singular dwell cycle under varying water pressure. For tube 1, a singular data point at 1.09 mm exit diameter falls outside the set y-axis range at approximately 6 slm^2. This point is an outlier, as indicated earlier by figures in the time domain.

Figure 4.7: Nozzle pressure during three dwell cycles at 4000 bar water pressure of an unworn tube 1 mixing tube, recorded at a 5 Hz sampling rate.

Figure 4.8: Subplots showing average nozzle pressure at different water pressures and exit diameters for two mixing tubes, with three repeats per pressure.

The general trend in Figure 4.8 appears to be that the vacuum increases in the nozzle with increasing exit diameter, as expected following the literature review [36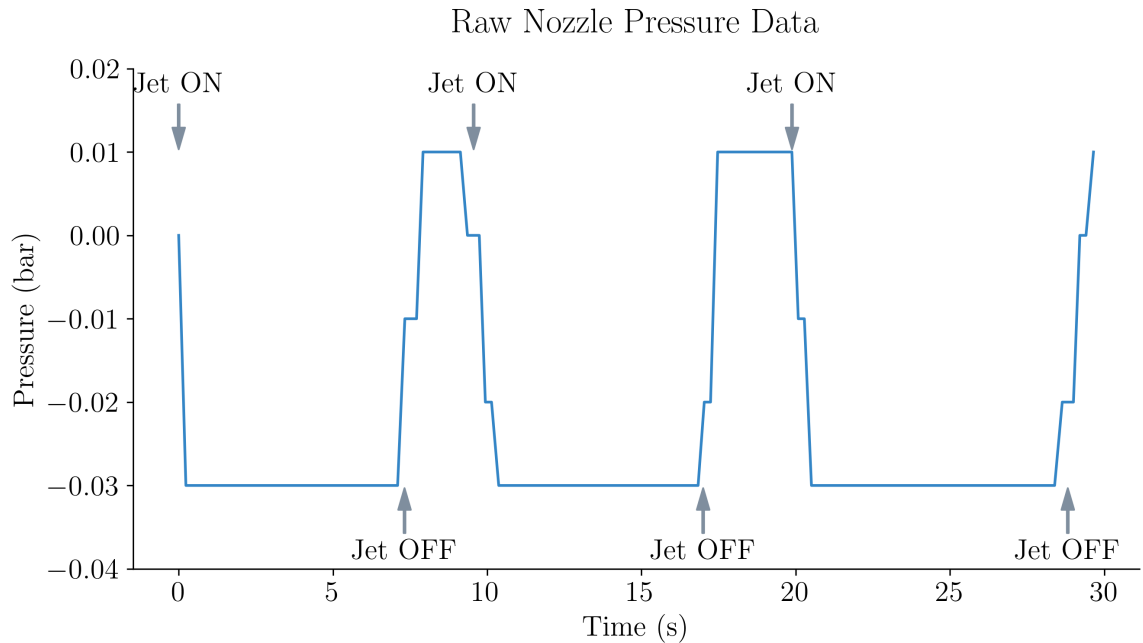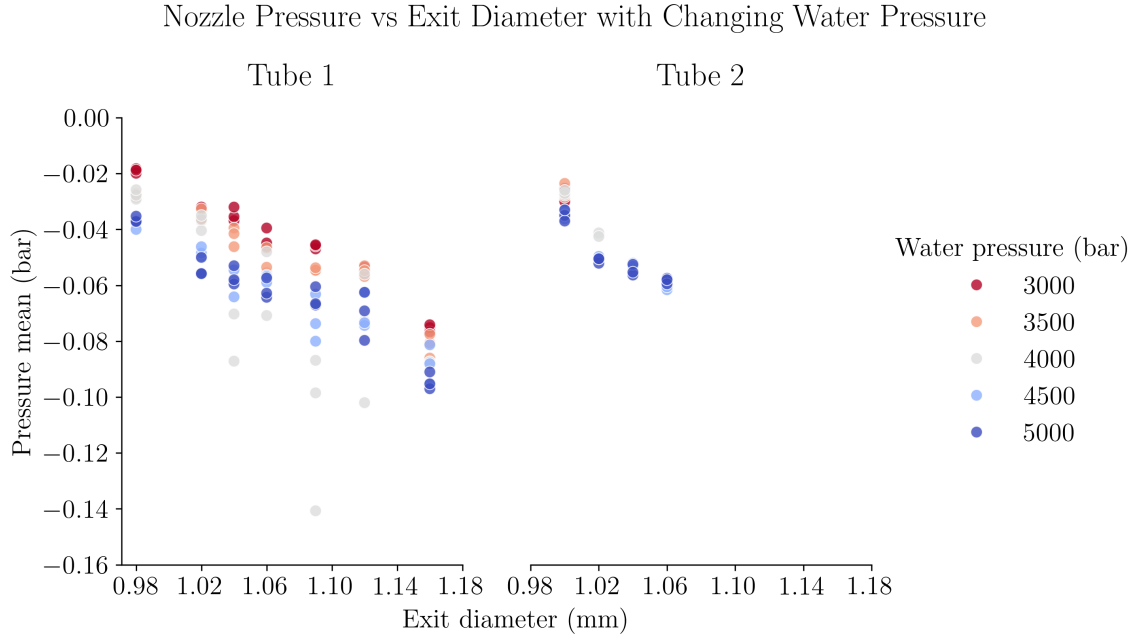]. The data suggests that using a pressure sensor to measure the vacuum inside the nozzle is a suitable approach for TCM of the mixing tube - as a difference in response is observed with changing wear

A key observation from Figure 4.8 is that there is a large percentage of data missing for mixing tube 2. Therefore, although the existing data appears similar, comparing the consistency in data between the two mixing tubes is challenging. Software installed by the waterjet manufacturer collects the data which can be downloaded from the provided database. A majority of the data for mixing tube 2 was missing when the database was accessed after the trial. The reason for this database failure is unknown. After the preliminary trial there was no machine access or resources available to reproduce the data before the main trials.

There are several implications for the analysis and future data collection from this database failure. First, for the machine learning evaluation, using nozzle pressure data would be problematic, as 67% of the dwell recordings have missing data. It would be possible to fill the missing data using different approaches, however with such a large percentage of data missing this may not lead to the best outcome. Second, a different approach must be considered for future trials to avoid a similar missing data error.

One that would allow collected data to be immediately seen as it's being saved to a file.

For mixing tube 1, Figure 4.8 supports observations seen by the airflow sensor. Namely, that an anomaly exists for one recorded repeat at 40 minutes wear for mixing tube 1 and after 20 minutes of wear there are issues with the data quality. The anomaly is worth omitting from the machine learning analysis, especially as the dataset is relatively small where the models don't have much information to learn patterns from, therefore potential noise should be reduced.

The final data collected during the preliminary trials was the water pressure and water flow rate data. For the same reasons as for the nozzle pressure sensor, mixing tube 2 data is largely missing. Figure 4.9 presents a sample of water pressure and flow rate data. Water pressure is seen fluctuating. This may be a result of an intensifier pump being used. This data supports an earlier theory on airflow data in Figure 4.2, where data fluctuations were attributed to fluctuating waterjet pressure.
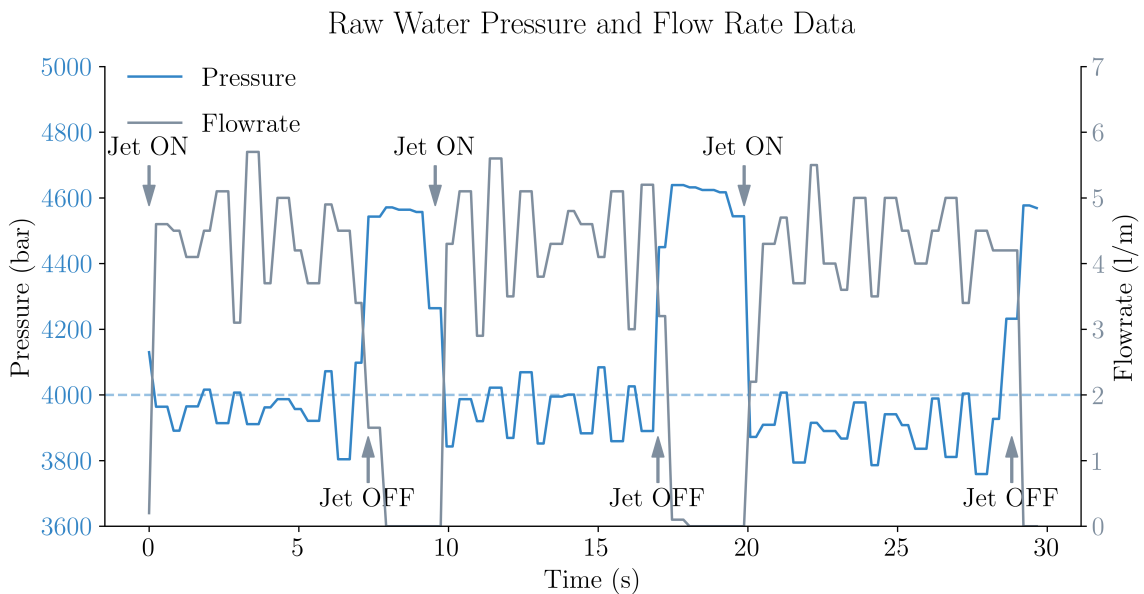
Figure 4.9: Water pressure and water flow rate readings during AWJ dwell cycles on an unworn mixing tube 1. The AWJ was set to run at 4000 bar water pressure, as indicated by the dashed line on the plot.

Figure 4.9 suggests that the average actual water pressure at which the AWJ operated was lower than the set pressure. Table 4.2 shows the actual average pressures at which data was recorded.

Figure 4.10 shows a general trend of water flow rate with increasing water pressure. The relationship between water flow rate and exit diameter appears less obvious. More

Table 4.2: Comparison of set AWJ water pressure and the average of the recorded water pressure over 5 second dwell measurements.

Water Pressure (bar)	
Set	Observed
3000	3019
3500	3501
4000	3867
4500	4481
5000	4953

data requires collection before conclusions are drawn.
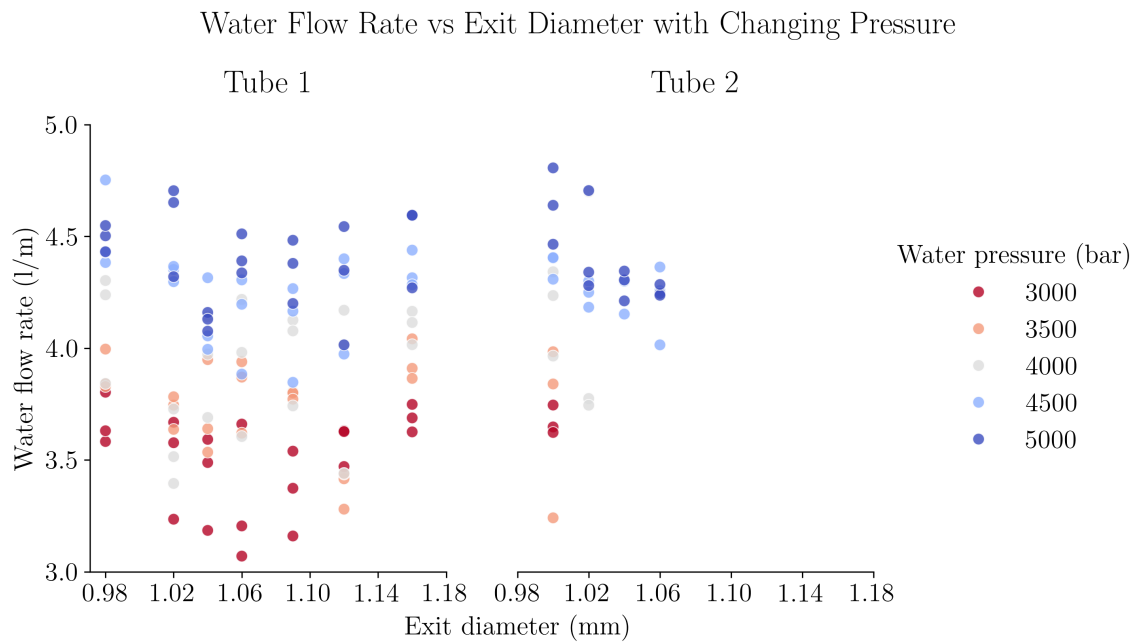
Figure 4.10: A scatter plot displaying the relationship between average water flow rate and exit diameter for two mixing tubes with changing water pressure. Each point represents data from a singular dwell cycle.

4.1.4 Data collection framework summary

The wear data presented in Figure 4.1 shows that the accelerated wear approach was successful. The 10% wear threshold was crossed within 60 minutes of wear, and the wear rate between the two mixing tubes was relatively consistent. The raw airflow and nozzle pressure data in Figures 4.2 and 4.7 suggest the dwell approach can be

used for TCM. Both pressure and airflow sensors are suitable for wear detection as indicated by Figures 4.4 and 4.8, as the exit diameter growth results in changes in the signal, and there appears to be a pattern to those changes.

These findings suggest that the framework is promising for TCM applications. However, the collected data had issue and the process can be improved. Airflow data was not consistent, and there were potential issues with the data quality. Furthermore, the dataset so far is limited to only two mixing tubes - the dataset needs to be expanded to validate the current findings. Whether data collection imperfections or differing internal wear profiles caused differences in the collected data between the two tubes discussed earlier has to be confirmed with further work. More data has to be gathered to see if data is stable and consistent for equivalent wear, otherwise TCM models could make mistakes. But crucially, a difference in the signal could still be seen with increasing wear which is a promising sign for developing a TCM system.

4.2 Exit diameter prediction and tool state classification

4.2.1 Data preparation and feature extraction

Before machine learning models can be trained, the data first has to be prepared into a suitable format. This involves first formatting data for processing, before transforming raw continuous sensor data into a structure suitable for machine learning models to learn from, through a process known as feature extraction. The goal is to create features that capture the important information in the data, so machine learning algorithms can learn patterns and make predictions.

The structured format that can be used is a simple table, with each column representing a derived feature from the raw data, for example airflow mean, and each row representing an observation, for example a single repeat of a dwell cycle. Tabulating data reduces the size of the input, extracts relevant information, speeds up model training and can help interpret the model output.

To tabulate the data, Python was used. Python offers a rich ecosystem of open-source libraries and frameworks for both data processing and machine learning. To process data with Python, the first step was to load the required libraries. The Python libraries used for data pre-processing include: Numpy and Pandas [165, 166]. The data was first read with Pandas. Next, data had it's time synchronised between the HMI and the personal computer as described in Chapter 3. Next, data was split

into individual dwell repeats. Before feature extraction was carried out, skip and hold (start and end) times were defined for segmenting the data. The skip time defined how much time at the beginning of the jet dwell cycle recording to omit. The hold time defined how many seconds of data to use for feature extraction from the start time. The default time used here was 0 seconds of skip time and 4 seconds of hold time. Using different times was also trialled for machine learning and is discussed later in this chapter.

Once only the segmented data remained, features were extracted on that segment. This process was repeated on all dwell cycle repeats until all data was processed. Therefore, 105 rows of data were extracted for each mixing tube - seven dwell cycle sets between 0-60 minutes of wear at five different water pressures with three repeats for each pressure. However, as an anomaly existed for mixing tube 1 at 40 minutes of wear at 4000 bar water pressure, that row of data was removed prior to model training.

As discussed in Chapter 2, time and frequency domain features can be extracted. These features can be extracted from all the collected sensor data, including airflow, nozzle pressure, water pressure and water flow rate recordings. As a large percentage of machine data is missing, this data is not used for the preliminary analysis. For water pressure, set input parameter values can be used instead. The preliminary machine data also has a low resolution, so is not well suited for frequency domain features engineering. Frequency domain features on low-resolution data could lead to misinterpretation of the underlying patterns. They can introduce noise, as per the Nyquist theorem, which suggests that the highest frequency that can be accurately represented is half of the sampling rate, which would be 2.5 Hz in the case of machine data which had a sample rate of 5 Hz [104]. Instead, not creating these features reduces the complexity of the relatively small dataset - potentially benefiting the model. Frequency domain features were still created using the airflow signal, which had a higher sampling rate of 100 Hz.

Table 4.3 summarises all the extracted features, following on from the literature review. To carry out feature extraction, Python's Pandas and Scipy libraries were used [166, 167]. A full list of the Python libraries used in this thesis is provided in Appendix I. Three different frequency bands were utilised to calculate the PSD ratios: low, medium and high. The bands were split by dividing the frequency range into three equal parts between 0 and 50 Hz. Next, the total power of each band was calculated by summing the power of each frequency in the band and subsequently dividing the value by the total power.

Table 4.3: Summary of all extracted features from the raw preliminary trial data.

	Extracted Features
Mixing tube	Wear time.
Airflow - Time Domain	Mean, max., min., std dev, RMS, skewness, kurtosis, peak to peak, IQR, shape factor, crest factor, impulse factor and clearance factor.
Airflow - Freq. Domain	Dominant frequency, total power, PSD power peak, PSD skewness, PSD kurtosis, PSD low frequency ratio, PSD medium frequency ratio, PSD high frequency ratio, spectral flatness and shannon entropy.
Water Pressure	Set input value.

With the features extracted, the next stage was to carry out feature selection. However, before this took place, the training and test sets were split to avoid data leakage. Data from mixing tube 1 was used for training and validating model performance while mixing tube 2 was used for final evaluation. To avoid information "leaking" into the set of data that was used for evaluating the true model performance, all decisions about modelling the data were first validated on the training set via CV.

4.2.2 Feature selection

Feature selection involves choosing a subset of relevant features to improve model interpretability and performance while reducing the dimensionality of the data and therefore reducing the risk of overfitting. The challenge of feature selection lies in finding the balance between retaining important features and removing irrelevant ones. For TCM, the goal is also to identify features which eliminate the need for continuous measurement of wear.

There are multiple ways to carry out feature selection, as discussed in Chapter 2. For example, a model can be used to identify useful features or a manual method of feature evaluation can be carried out [28, 31, 82, 123, 125]. First the manual approach was used as it allows to unpack the relationships between the created features and the target (the exit diameter for prediction). Manual feature selection helps make the modelling process more "grey-box" instead of "black-box". The manual methods relied on the combination of correlation analysis and MI scores.

A correlation heatmap is presented in Figure 4.11. The correlation heatmap is useful for feature selection as it can help identify which features have a strong relationship with the target and help detect multicollinearity - a situation where two or more features are highly correlated. A correlation coefficient of 1.0 signifies a perfect positive linear correlation, while -1.0 indicates a perfect negative linear correlation. A correlation coefficient of 0 suggests no linear relationship between the variables. High correlation among features can reduce the performance of machine learning models. First, because having multicollinear features increases the dimensionality of the dataset without necessarily providing additional information. Second, machine learning models may struggle to distinguish the individual impact of correlated features on the target variable. Addressing multicollinearity is important and can be carried out by removing or combining highly correlated features.

However, as mentioned in Chapter 2, correlation analysis only looks at linear correlation. Other patterns might exist between the target and the features. MI scores, which measure the dependency between two random variables, can complement correlation heatmaps during the feature selection process [120, 124]. An MI scores plot for both regression and classification is shown next to a correlation plot in Figure 4.12 showing the relationship between features and target variable (exit diameter). The MI scores were calculated using Python's Scikit-Learn library [131]. A full list of the Python libraries used in this thesis is provided in Appendix I.

Figure 4.12 suggests that there are several features which have linear correlation and are relevant to the target variable. Wear time in particular stands out as a strong feature related to the exit diameter. In addition, basic time-based statistics of the airflow signal, such as the minimum value, not only correlate strongly with wear but also have a relatively high MI score. Frequency domain features correlate less with the exit diameter in comparison to time domain features, however total power stands out as a strong feature judging by the MI scores.

Figure 4.12 also suggests that water pressure may be a weak feature as it has a low MI score and Pearson correlation. However, this perhaps highlights the disadvantage of making decisions based solely on correlation and MI score analysis. Data analysis carried out earlier in the chapter is useful here, which suggested in Figures 4.4 and 4.6 that water pressure affects the airflow signal in both time and frequency domains. Removing it as a feature may therefore negatively impact the model performance, as this feature may be useful in combination with other features even though it does not on it's own relate to the exit diameter.
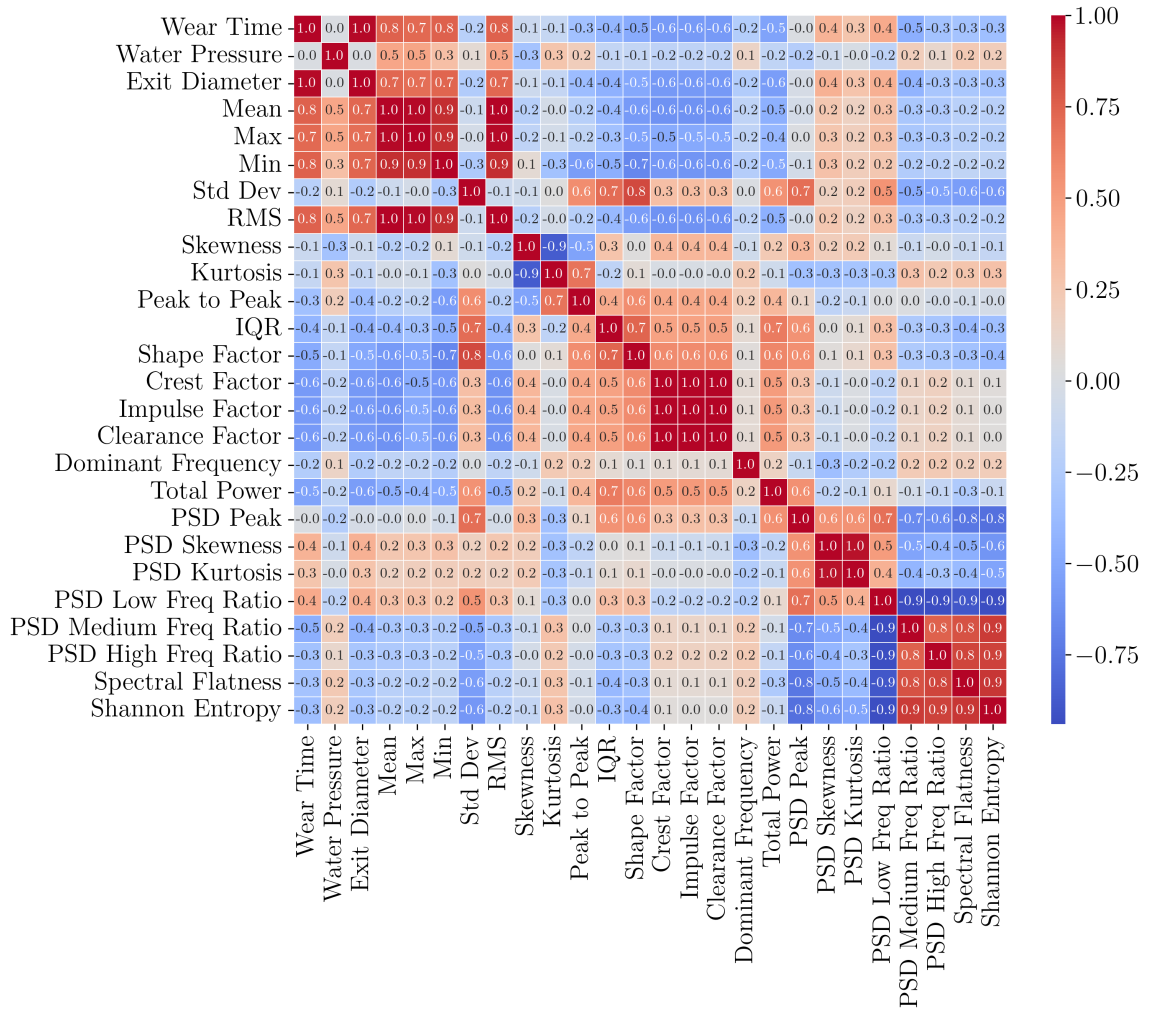
Figure 4.11: Correlation heatmap, using Pearson correlation coefficient, of created features from mixing tube 1 data. Apart from water pressure and wear time, all time and frequency domain features are for the airflow sensor data.

Figure 4.11 can be studied for multicollinearity and used in combination with Figure 4.12 to make decisions on features to drop from the dataset. In Figure 4.11, a big cluster of time-domain features correlate highly with each other, including the mean, minimum, maximum and RMS of the signal. Although the min. value of the signal has the highest correlation, and better regression MI score, keeping the mean or RMS might be better. As from the data analysis, where blockages were present, or water pressure was not allowed to fully build up, the min. of the signal may have been most affected at the start of the recordings. The RMS and mean would have stayed more consistent - giving the signal a better representation. As the RMS feature has a slightly higher MI score, it was kept with other multicollinear features dropped.

Another multicollinear cluster is observed for frequency domain features in Figure

Correlation and Mutual Information Scores between Features and Target
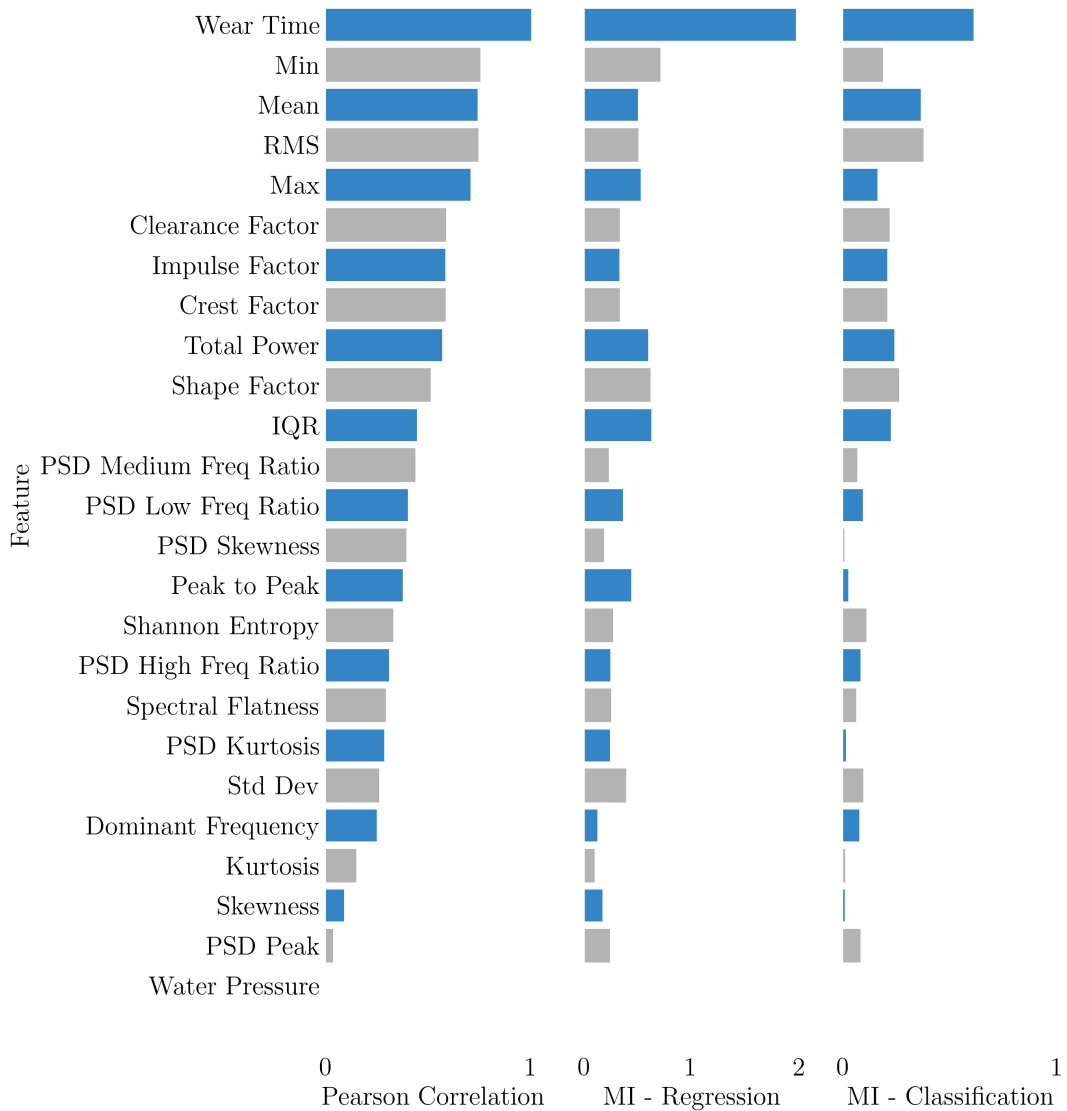
Figure 4.12: Subplots showing the correlation and MI scores of each feature with exit diameter. MI scores for regression used a continuous target (exit diameter), while classification used a binary target: exit diameters $\geq$1.10 mm were classified as 1 (worn), otherwise 0.

4.11 between the PSD frequency band ratios, spectral flatness and Shannon entropy. Aside from PSD low frequency ratio, all of these features were dropped, as although the PSD low frequency ratio feature has only the second highest correlation value, it stands out on the MI scores plots in Figure 4.12.

In addition, features: std dev, skewness, crest factor, impulse factor and PSD kurtosis were dropped due to multi-collinearity and their lower MI score and/or correla-

tion, when compared to their multicollinear features: shape factor, kurtosis, clearance factor, clearance factor, PSD skewness respectively. The PSD Peak feature was kept, as both features it was multicollinear with were dropped.

Finally, Figure 4.12 suggests that many remaining features have a low MI score for the classification task - however, the same features will be used for both regression and classification, as the features still show a linear relationship with the target and may be useful. Table 4.4 summarises which features were selected to keep for machine learning and which features were dropped following manual feature selection.

Table 4.4: Manual feature selection summary.

	Features
Keep	Wear time, water pressure, RMS, kurtosis, peak to peak, IQR, shape factor, clearance factor, dominant frequency, total power, PSD peak, PSD skewness, PSD low frequency ratio.
Drop	Mean, max., min., std dev, skewness, crest factor, impulse factor, PSD kurtosis, PSD medium frequency ratio, PSD high frequency ratio, spectral flatness, shannon entropy.

4.2.3   Machine learning

After the preliminary data has been prepared for machine learning and the features selected, the next stage is to decide on the machine learning approach. Specifically, the machine learning modelling method, the metrics and data splitting strategy for evaluation to use. The machine learning task is supervised, where the target is labelled. The TCM prediction may be suitable for either regression or classification type, so both were explored. Following the research motivations set out in Chapter 1, regression can benefit tool path compensation, while classification can be used for developing a sustainable mixing tube replacement strategy by predicting whether the tool is worn or not. 1.10 mm exit diameter was selected as the threshold for wear – a 10% increase from the initial starting diameter of approximately 1.00 mm. The goal of testing both approaches, namely classification and regression, was to evaluate whether the data is better suited for one type of problem. MAE and RMSE were used to evaluate regression performance. For classification F1 score and accuracy were used. Due to the target imbalance presented in Figure 4.13, greater attention

was paid to the F1 score when assessing classification model performance. For regression, as larger errors were unfavourable, RMSE was the preferred metric. MAE and accuracy were still used to get a better understanding of model performance on the small dataset.
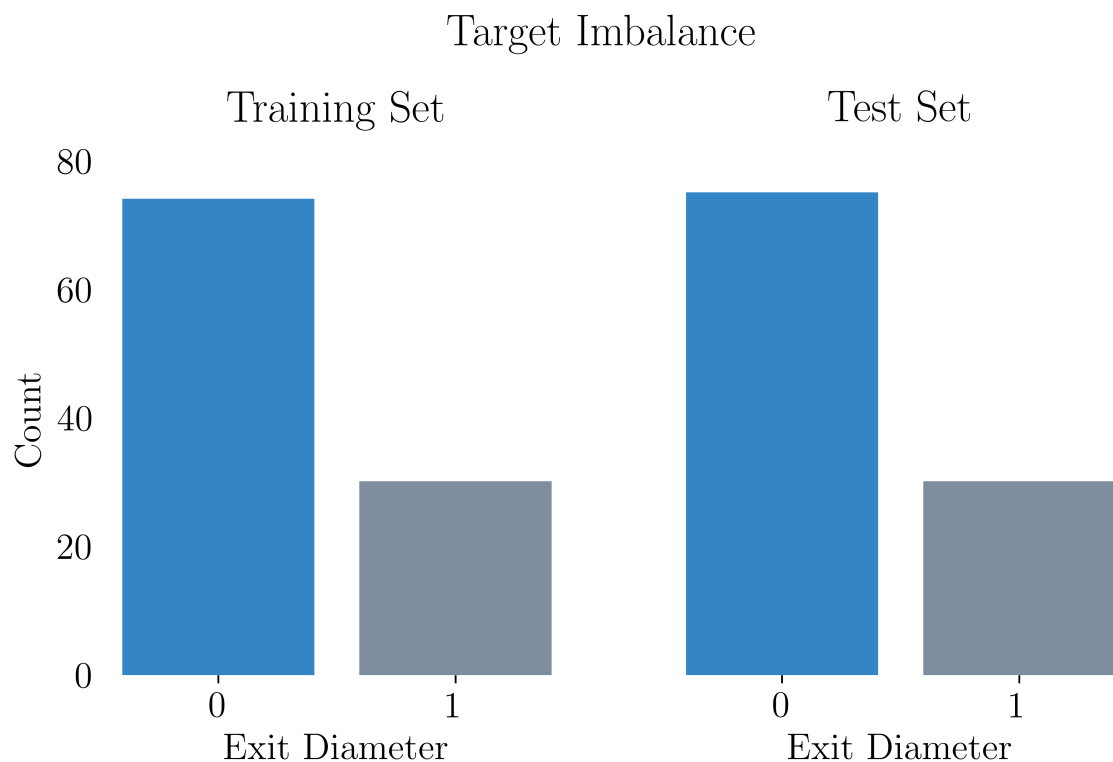
Figure 4.13: Count of "worn" (0) and "unworn" (1) mixing tube rows in the data for both training and test sets. The mixing tubes were classed as "worn" after the exit diameter equalled or exceeded 1.10 mm.

There is a range of algorithms that may be used for both classification and regression, as discussed in the literature review. Multiple algorithms were evaluated to gain a better understanding of the prediction potential for this problem. The algorithms can be split into three categories, each with its own advantages: linear, tree and other. Linear approaches trialled include LR, LogR, Ridge and SVM algorithms. Linear algorithms are notable for their simplicity and are well-suited for scenarios where the relationships between features and targets are linear. Tree algorithms tested include ET, RF, and a variety of gradient-boosting machines. The gradient boosting machines included: XGB, LGBM, CB and scikit learn's GB. Tree algorithms excel at capturing non-linear relationships and handling decision boundaries, making them more flexible compared to linear methods. The final "other" category includes deep

learning methods, such as scikit-learn's MLP and a pre-trained transformer on tabular data TabPFN, as well as instance-based method KNN. Deep learning methods can extract intricate patterns, while KNN can excel when decision boundaries are not well-defined, and data can be better modelled via a proximity of data points approach. Not all mentioned models were used for both regression and classification, as some models are only suitable for one type of training. TabPFN and LogR were used for classification only, while LR was used for regression only.

All machine learning models were trained using their default hyperparameters, which are available in the models' documentations [168–172]. A full list of the Python libraries used in this thesis is provided in Appendix I. The only exception was scikit-learn's MLP, which used two hidden layers of 5 neurons each, reduced maximum iterations of 100 and increased regularization of 0.001. These parameters were selected due to a small dataset size to avoid overfitting. Not tuning the MLP architecture is a limitation, however model tuning was outside the scope for the preliminary trial data analysis, therefore a simple architecture was used for the tabular data.

In addition to machine learning, a basic model was developed for both regression and classification using wear time as a sole feature. The aim was to use a basic approach as a baseline for machine learning. All the machine learning algorithms tested would rely solely on airflow data and set water pressure without using wear time as a feature. Wear time data was not used in order to assess the ability of the machine learning algorithms to predict wear when mixing tube usage is not being tracked, which can be found in practice in industry. For regression, the basic wear time-only model was trained using LR. For tool state classification, LogR was used instead.

Before training the models, all data was standardized through z-score normalization, using equation 2.5, as discussed in the literature review [96, 97]. This step is standard practice and is crucial when using algorithms that are sensitive to the scale of input features, such as linear and deep learning algorithms. The scaling was applied based on the mean and standard deviation calculated on the training set for both final hold-out validation and CV experimentation.

Several experiments were run to test the best modelling approach, before the final evaluation. Five CV splits were used, stratified on wear time.

The experiments were conducted to check whether any of the following would improve the models' performance:

- Denoising the raw data

- Selecting a different raw data skip and hold time for extracting features.

- Ensembling best models.

Denoising was carried out by calculating the moving average on the raw airflow data over a certain window size (number of data points) [95]. The moving average filter smoothed out short-term fluctuations and was done prior to feature generation. Multiple window sizes were used, including 5, 10, 25, 50 and 100. A window size of 5 achieved the highest CV performance. The effect of denoising on the training set performance is visualised in Figure 4.14. RMSE and F1 score metrics were selected for evaluation of performance, to penalise larger errors and to account for class imbalance. A lower RMSE and a higher F1 score indicate better performance. For regression, the performance decreased for most models. For classification, the results were mixed. Several models, such as TabPFN and GB algorithm, saw notable improvements past 0.9 F1 score. For the final evaluation, it may be worth testing how well denoising performs on classification.

Effect of denoising on model performance
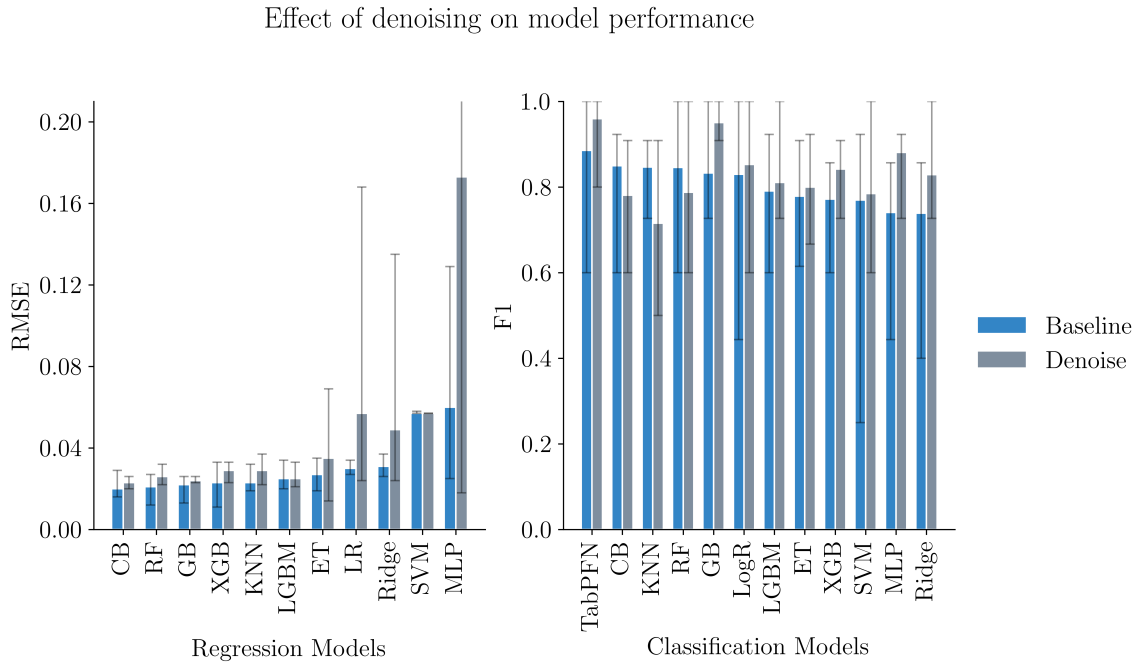
Figure 4.14: Effect of using a moving average filter of size 5 over the raw airflow data on regression model performance. The presented scores for each model are the average of five CV folds stratified on wear time. The error bars indicate the range of scores over the 5 CV folds.

The originally selected skip and hold times were 0 and 4 seconds on the raw airflow data for each dwell cycle repeat. As seen in Figure 4.14, the baseline models

which performed well for both regression and classification tasks were the CB and RF algorithms. The performance of the RF algorithm with altering skip and hold times is presented in Figure 4.15. The experiment suggests that the initial selected times were good for both regression and classification. While CB marginally outperformed the RF algorithm, CB is more prone to overfitting than RF, and the evaluation dataset is small, meaning overfitting is a concern [173]. Therefore, RF was chosen for evaluating hold and skip times.

Effect of hold and skip time on model performance of RF Algorithm
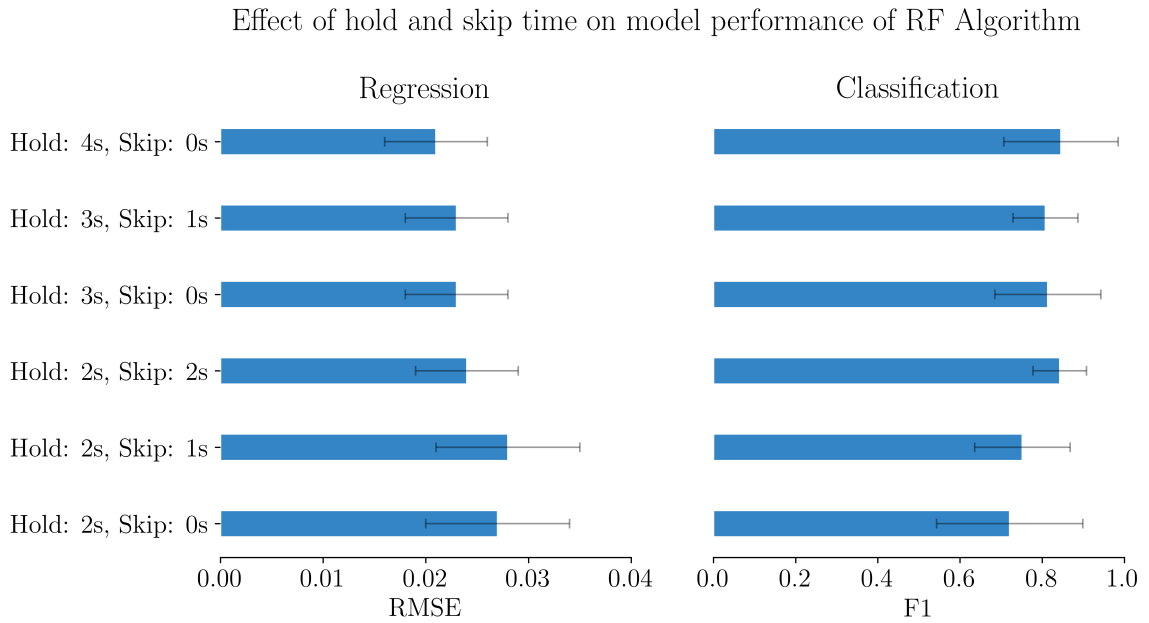
Figure 4.15: Effect of altering the raw airflow dwell data segmentation times prior to feature generation on RF algorithm performance. The performance is averaged over five CV folds. The error bars represent one standard deviation of the results from the five folds.

For ensembling, two different approaches were trialled. The first approach involved selecting the best of each of the three categories of models, namely linear, tree and other, and combining them via averaging the prediction. The best models were selected separately for regression and classification, evaluated using RMSE and F1 score respectively. For the second approach, the best individual models were selected based on the RMSE and F1 scores, irrespective of their model category. The first approach benefitted from diversity, while the second approach benefited from predictive capability. Table 4.5 lists the best-performing algorithms for both approaches, their corresponding metric performance over CV and the final score obtained via ensembling.

Table 4.5: Model ensembling results.

Regression models	RMSE	MAE	Classification models	F1 score	Accuracy
Approach 1: best models from each model category					
LR	0.030	0.025	LogR	0.830	0.912
CB	0.020	0.016	CB	0.850	0.922
KNN	0.023	0.017	TabPFN	0.886	0.941
Ensemble	0.022	0.017	Ensemble	0.915	0.952
Approach 2: best models overall					
RF	0.021	0.016	CB	0.850	0.922
GB	0.022	0.015	KNN	0.847	0.913
CB	0.020	0.016	TabPFN	0.886	0.941
Ensemble	0.018	0.014	Ensemble	0.858	0.923

Table 4.5 demonstrates that ensembling can improve performance. Approach 2 worked better for regression, while approach 1 achieved a better F1 score for classification. For final model evaluation, the model combination from approach 2 was used for regression, and model combination from approach 1 was used for classification.

Several other experiments were possible to conduct. For example tuning the best models' hyperparameters, using other models and conducting dimensionality reduction via PCA. However, due to this only being a preliminary investigation, they were deemed out of scope.

The experimentation stage suggested that it's worth testing whether denoising data will better classification performance and whether ensembling can yield more accurate predictions.

For final model performance evaluation on the test set, in addition to obtaining performance on the standard dataset, several extra changes were also tested to evaluate the effect of several decisions. These could later be used to help the machine learning decision-making for the main trial analysis. The aim was to understand the following:

- Does algorithmic feature selection outperform manual feature selection?

- If evaluating the model performance only on 4000 bar water pressure data, the pressure the mixing tubes were worn at, are results different?

- If both training and evaluating model performance solely on 4000 bar water pressure data, does model performance decrease? In other words, is there value in collecting additional dwell data at other water pressures?

- How does including wear time as a feature for the machine learning algorithm impact performance?

- For classification, does denoising raw data make a significant impact?

For algorithmic feature selection, the LASSO algorithm was used [125]. LASSO-selected features were used for both regression and classification. The adjustable "alpha" parameter, which determines regularisation strength, was changed in a systematic progression from 1 to 0.000001. The best alpha value was determined via stratified CV on the training set, with the final selected value of 0.0001. For feature selection, all features with non-zero coefficients were kept. The LASSO selected features are shown in Figure 4.16. An interesting observation is that the water pressure data was kept, even though, as discussed earlier, Figure 4.12 suggests that it is not a useful feature. There are some notable differences with manually selected features. For example, several multicollinear features were kept, especially the cluster of time-domain features RMS, min., max. and mean.
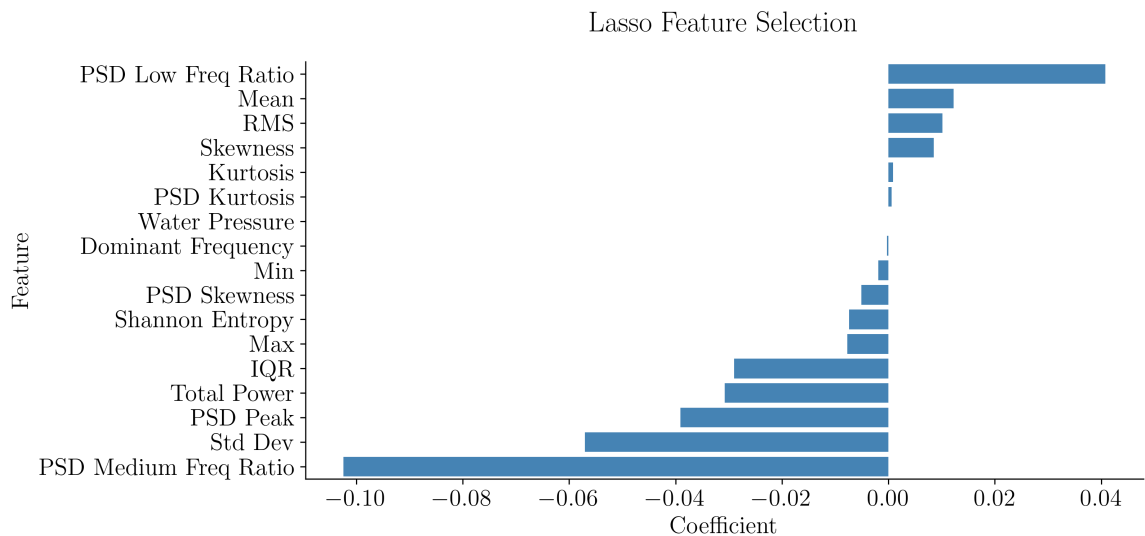

Figure 4.16: LASSO selected features and their corresponding coefficients with the alpha hyperparameter set to 0.0001. The water pressure coefficient was low, at -0.000024.

Finally, to enhance the credibility of the final results, a random seed parameter was introduced for every model where the generation of random parameter weights could

potentially influence the outcomes. This random seed parameter was systematically altered five times (using seeds 45-49), and the final model score was determined as the average across all five seed variations. This approach aimed to ensure robustness and consistency in the results despite a small dataset of two worn mixing tubes, mitigating the impact of random variations and enhancing the overall trustworthiness of the study's conclusions.

4.2.4 Results

Figure 4.17 presents the machine learning results of the preliminary trial. The models were trained on data from mixing tube 1 and evaluated on data from mixing tube 2. The error bars illustrate the variability and robustness of the model performance.
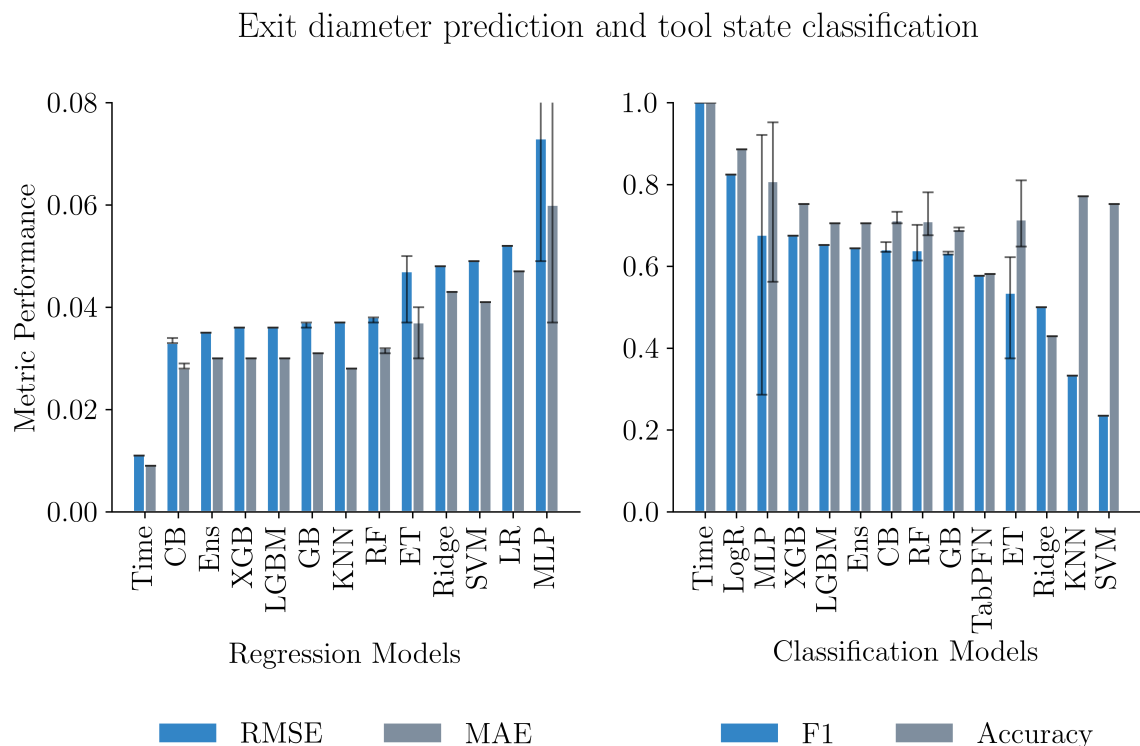
Figure 4.17: Comparison of model performance when predicting the exit diameter (left) and classifying the state of the tool (right). Each model was retrained 5 times, each time using a different random seed, to obtain the final score. The error bars indicate the range of predicted scores across these 5 random seeds. For the MLP model, the upper range of error was 0.12 for RMSE and 0.10 for MAE, with these values left out of the figure for clarity of the rest of the plot. "Ens" denotes ensemble performance. The regression ensemble included RF, GB and CB. The classification ensemble included LogR, CB and TabPFN.

The machine learning performance in Figure 4.17 is lower compared to the CV scores seen in Figure 4.14. Data issues observed earlier in the chapter may be the explanation for lower performance. These issues may have introduced noise to the training dataset. With the small dataset size, lower performance is expected as the models can only learn the relationships they observe in the training set.

The time model, using simple models based on wear time data only, outperformed all sensor data-based machine learning algorithms for both regression and classification, as shown in Figure 4.17. The findings indicate that a simple approach to tracking the mixing tubes' operational duration may prove sufficient and potentially more effective for wear detection than more complex methodologies.

However, it's crucial to acknowledge the limitations imposed by the small dataset, which included only two worn tubes. A larger dataset collected using a refined data collection process may produce different results. Especially if there is a greater variation in the exit diameter over time than observed in this preliminary study, as seen in Figure 4.1. Or if the noise in the airflow data is reduced. Furthermore, models solely based on wear time may not adequately adapt to changes in the process. For instance, issues such as blockages, poor abrasive flow or process parameter adaptations could worsen the time-based models' performance in practice. These issues will reduce performance as they would impact the wear rate.

For regression, Figure 4.17 shows the smallest attained RMSE and MAE of 0.033 and 0.028, respectively, for the CB algorithm. 0.033 mm wear would equate to approximately 8 hours of machining time during regular wear at 3000 bar water pressure and an abrasive feed rate of 6g/s [162]. The input parameters are not an exact comparison, but this figure indicates the rough tool life error from this prediction – if using the exit diameter as a threshold for deciding the condition of the tool.

The predictions made by the CB algorithm are plotted against true exit diameter values in Figure 4.18. The figure suggests the model generally overestimated wear at the beginning of the wear process and began underestimating the wear once the true values crossed the worn threshold of 1.10 mm. The regression approach performance needs improving. With the current predictions, unworn mixing tubes may be replaced prematurely, while worn mixing tubes may not always have wear detected, as indicated by Figure 4.18.

Figure 4.17 indicates weaker ensemble performance compared to some individual models for both classification and regression. More complex ensembling methods should be assessed for improving model performance on a larger dataset.

CatBoost Regression Predictions on the Test Set
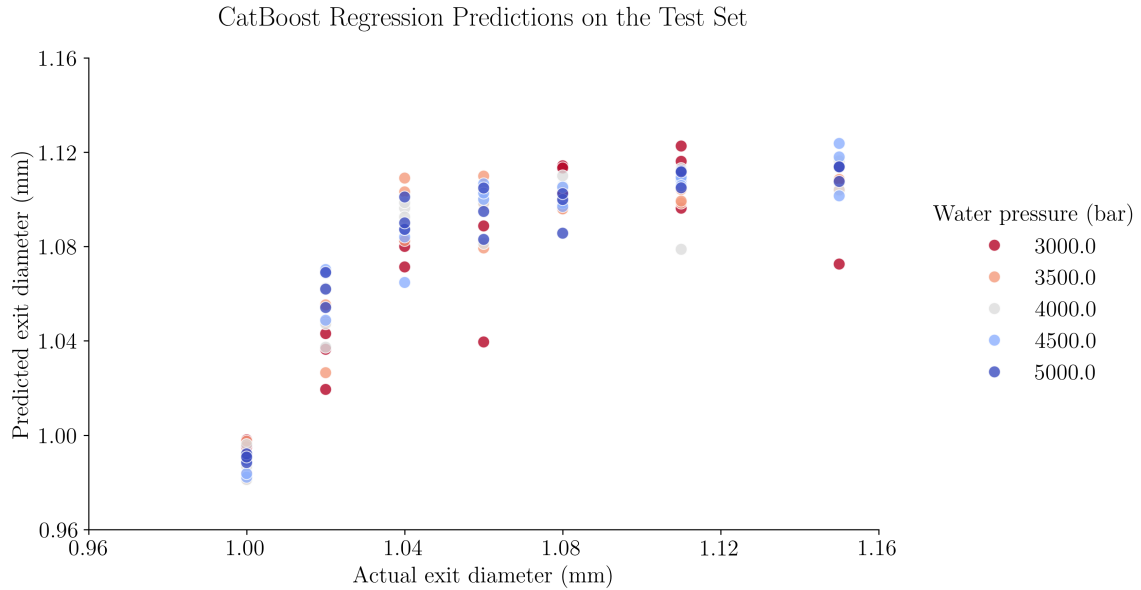
Figure 4.18: Exit diameter predictions made by the CB algorithm trained on mixing tube 1 data and evaluated on mixing tube 2 data.

For classification, Figure 4.17 indicates that the LogR algorithm worked particularly well. Table 4.19 compares the predictions made by the LogR algorithm and the true values. The model made 12 errors, suggesting 2 worn mixing tubes were not worn when they were and prematurely identifying 10 mixing tubes as worn. In general, classification appears a more reliable approach on the preliminary data. The best classification model, LogR, makes fewer errors around the wear threshold boundary, as seen in Table 4.19, compared to the best regression model, CB, as seen in Figure 4.18.

Additional obtained results are presented in Tables 4.6 and 4.7 showing regression and classification model performance respectively. The results evaluate the effect of several decisions on model performance. The "Baseline" column presents the results found in Figure 4.17. The "LASSO" column presents the results of using LASSO feature selection prior to model training. "Test 4000" column contains performance when only using 4000 bar water pressure dwell data in the test set. "Only 4000" column shows results when 4000 bar water pressure dwell data only is used for both training and testing model performance. The "Time Feature" column includes metric scores for each model when wear time was added as an additional feature to the existing feature set. The classification table has an additional column "Denoise", for model performance when the raw data has been smoothed using a moving average filter of size 5.

97

Confusion Matrix of LogR Predictions
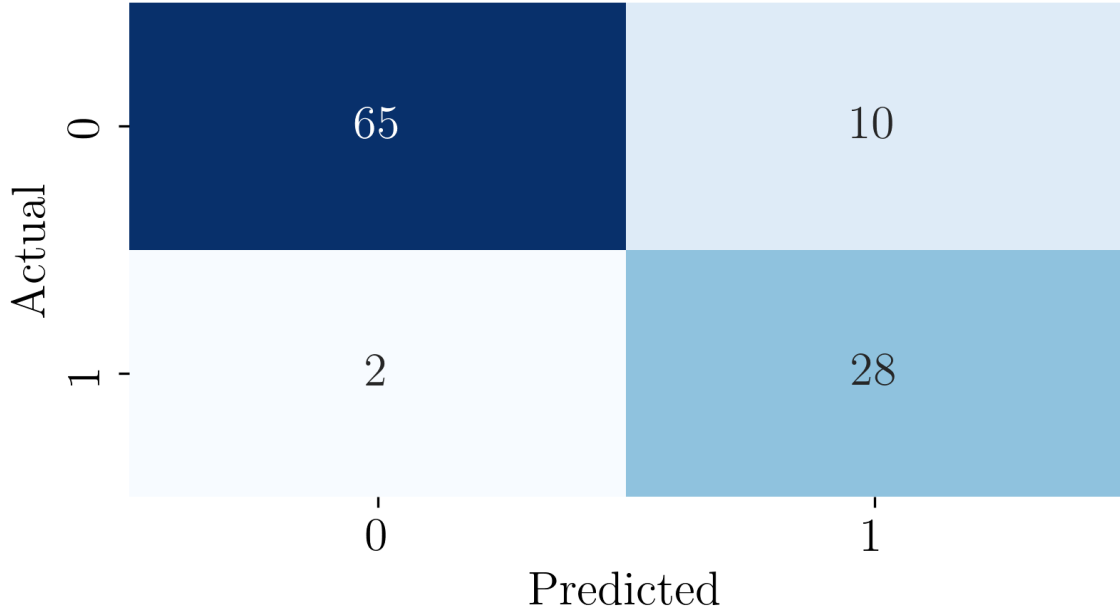
Figure 4.19: Break down of predictions made by the LogR algorithm and the actual classes for mixing tube 2. The model made 93 correct predictions and 12 errors. 0 represents the negative class (not worn), and 1 represents the positive class (worn).

Table 4.6: Regression model performance (RMSE) on the test set after dataset changes. Blue and grey cells indicate increased and decreased performance, respectively, relative to the 'Baseline' score.

	Baseline	LASSO	Test 4000	Only 4000	Time feature
LR	0.052	0.087	0.054	0.144	0.015
Ridge	0.048	0.061	0.050	0.062	0.014
SVM	0.049	0.049	0.049	0.049	0.049
ET	0.047	0.052	0.045	0.051	0.010
RF	0.038	0.033	0.041	0.050	0.010
GB	0.037	0.033	0.037	0.045	0.010
XGB	0.036	0.033	0.039	0.038	0.010
LGBM	0.036	0.030	0.041	0.048	0.016
CB	0.033	0.030	0.034	0.035	0.015
MLP	0.073	0.051	0.072	0.118	0.041
KNN	0.037	0.030	0.035	0.039	0.010
Ens	0.035	0.031	0.037	0.041	0.009

Tables 4.6 and 4.7 show that algorithmic feature selection using LASSO improved both regression and classification performance for multiple models. Going forward

Table 4.7: Classification model performance (F1 score) on the test set after dataset changes. Blue and grey cells indicate increased and decreased performance, respectively, relative to the 'Baseline' score.

	Baseline	LASSO	Test 4000	Only 4000	Time feature	Denoise
LogR	0.824	0.912	0.769	0.714	1.000	0.707
Ridge	0.500	0.513	0.500	0.545	0.561	0.378
SVM	0.235	0.235	0.000	0.000	1.000	0.630
ET	0.535	0.541	0.474	0.513	0.715	0.565
RF	0.639	0.655	0.594	0.571	0.960	0.608
GB	0.632	0.529	0.571	0.571	1.000	0.662
XGB	0.675	0.592	0.667	0.571	1.000	0.644
LGBM	0.652	0.530	0.600	0.000	1.000	0.645
CB	0.641	0.684	0.588	0.571	1.000	0.608
MLP	0.677	0.455	0.727	0.602	0.775	0.708
KNN	0.333	0.769	0.286	0.500	1.000	0.523
TabPFN	0.577	0.652	0.571	0.727	1.000	0.725
Ens	0.644	0.737	0.588	0.714	1.000	0.716

to the main trial TCM model development, LASSO feature selection will be utilised instead of manual feature selection. Not only did LASSO improve performance, it is also faster to implement.

Evaluating data on the test set consisting of only 4000 bar water pressure dwell data led to a reduction in performance, especially for classification. This experiment was carried out to understand whether the assumption of varying water pressure between 3000 and 5000 bar does not change the wear profile of the mixing tubes, does not lead to misleading model performance when evaluated on multiple water pressures (despite being worn using only singular pressure) if the assumptions in future work is proven to be incorrect. Overall, best performing models suggest the baseline results did not see major performance change. For CB, regression performance dropped from 0.033 RMSE to 0.034, and for classification, LogR F1 score dropped from 0.824 to 0.769. Therefore, if the assumption is proved to be incorrect, the overall conclusions from this study should not be misleading.

When comparing "Test 4000" and "Only 4000" columns in Tables 4.6 and 4.7, the results for many algorithms suggest there is a benefit in collecting additional dwell data at additional water pressures, as performance tended to decrease for "Only 4000" when removing the additional training data rows.

The effect of data denoising for classification is inconclusive when studying Table 4.7. The performance does improve for some models. However, the performance of the best-performing model, LogR, decreases.

When adding the wear time feature to machine learning algorithm datasets, performance begins to match the basic time models' for both regression and classification. For regression, the time model had a RMSE of 0.011 and a F1 score of 1.0. This result highlights the importance of tracking the use time of mixing tubes in industry. However, as the performance of machine learning models still did not exceed basic time models' performance, even when wear time was added as a feature, basic models stand out as a clear choice for future TCM applications. However, this still requires further validation after a larger dataset is gathered.

For future work, selecting a limited number of models could be beneficial to further the analysis and optimise model performance. Having fewer models would allow for model optimisation and tuning. To assist with model selection, it would be useful to understand which categories of models performed well on the existing dataset for both regression and classification. Table 4.8 summarises the best scores for each model under varying processing conditions. For regression, the two compared processing conditions were baseline and LASSO feature selection. For classification, the compared conditions included baseline, LASSO feature selection, and data denoising. The use of the wear time feature for model training was excluded from the comparison. The baseline processing condition had manual feature selection and no denoising performed.

Several insights can be drawn from Table 4.8. Tree models and KNN combined with LASSO feature selection stand out for the regression task. For classification, LogR stands out as the best model. The "other" model category stands out for classification as the models outperform other linear and tree algorithms. Intricate non-linear relationships in the data may explain why deep learning models MLP and TabPFN, together with KNN are performing well.

Based on the results, the following algorithms were selected for further work for both classification and regression: RF, LGBM and KNN. LogR was also selected for classification. RF is selected because the algorithm is less prone to overfitting than gradient-boosted trees while still showing strong performance in Table 4.8. LGBM is selected over CB and XGB. While LGBM had similar performance, the algorithm is significantly faster to train and tune [138]. KNN and LogR are selected based on their performance. MLP performed well on the classification task; however, the algorithm is more complicated and time-consuming to tune and offers lower potential for model explainability [132, 173].

Table 4.8: Summary of best regression (RMSE) and classification (F1) performances for each model. The regression (Reg.) and classification (Class.) conditions indicate the processing step used to achieve the best scores during evaluation.

Model	RMSE best	Reg. Condition	F1 Score Best	Class. Condition
LR/LogR	0.052	Baseline	0.912	LASSO
Ridge	0.048	Baseline	0.513	LASSO
SVM	0.049	Baseline	0.630	Denoise
ET	0.047	Baseline	0.565	Denoise
RF	0.033	LASSO	0.655	Denoise
GB	0.033	LASSO	0.662	Denoise
XGB	0.033	LASSO	0.675	Baseline
LGBM	0.030	LASSO	0.652	Baseline
CB	0.030	LASSO	0.684	LASSO
MLP	0.051	LASSO	0.708	Denoise
KNN	0.030	LASSO	0.769	LASSO
TabPFN			0.725	Denoise
Ens	0.031	LASSO	0.737	LASSO

4.3   Overview of preliminary results

In this chapter, preliminary trial data was presented, machine learning methodology for regression and classification laid out and preliminary results presented. The designed data collection framework, discussed in Chapter 3, was successful. Accelerated wear was achieved, 10% exit diameter growth exceeded, and signal change observed for airflow and pressure sensors during the dwell cycles. Exit diameter growth was linear and consistent between both mixing tubes.

However, the data collection process was not without issues and can be improved. Specifically, the operator has to ensure the water pressure pump stabilises at the required pressure before running the dwell cycle and abrasive has to be allowed to flush out of the system before the jet is turned off after the completion of the wear cycle. In addition, the machine based data collection to populate the machine database failed. Future data collection efforts should focus on a more reliable data recording approach.

The collected dataset was small in size, imposing several limitations on final conclusions. However, the final model performance was still good after feature generation and selection. The best-obtained RMSE of 0.030, under LASSO feature selection, equated to approximately 8 hours of tool life for the regression task. While for classification the best model made only 12 errors out of 105 predictions, with a worn tube not identified as such only twice. Nevertheless, the performance was worse than for a basic time model, which achieved a RMSE of 0.011 and made no errors on the classification task.

A basic time model may therefore be the TCM solution required for the AWJ users. To validate this conclusion, a larger dataset is required as at the moment only one mixing tube is used for training each model, with each model fitting to the data patterns seen on that tube only. Taking into account the observed data collection issues, especially for mixing tube 1, which was used for training the models, performance is likely to improve with a larger dataset. Especially if the noise in the data is reduced. The impact of a larger dataset is explored later in this thesis and supports the argument for more complex TCM approaches (see Figure 6.19, Chapter 6) as the performance of time models may deteriorate.

Additional experimentation suggested that advanced techniques such as algorithmic feature selection, raw data denoising and model ensembling have the potential to benefit model performance. The assumption that the wear profile does not change between 3000 and 5000 bar water pressure was shown to only be a minor limitation

if proven incorrect in future work, as the model performance was comparable when not using the additional data in the evaluation test set.

Overall, the results showed that two mixing tubes can be used for indirect TCM with airflow sensors to predict wear. The results provided valuable insights into the predictive capabilities of airflow data. Although the performance was outmatched by a basic time model, this chapter makes an original contribution by quantifying the extent to which airflow sensors can predict mixing tube wear.

Finally, when discussing model performance, it is important to consider the trustworthiness of the results. Throughout the analysis, multiple strategies were employed to ensure the reliability of the drawn conclusions. Specifically, suitable metrics were chosen, together with a reliable evaluation strategy, which for the test set included using multiple random seeds and averaging the final scores of 5 iterations during model learning. In addition, data analysis was carried out prior to and post-feature generation to better understand the interaction of individual features with the target instead of simply supplying the data to the models and evaluating the results.

Chapter 5

Data Analysis

Once the preliminary data trial and analysis took place, the main trial was conducted. The main stage of the data collection effort was split into two phases, as detailed in Chapter 3. During the main phase additional mixing tubes were worn and data recorded. After the main trial was completed, supplementary abrasive and mixing tube analysis was carried out. The aim of this chapter is to explore this additional collected abrasive, mixing tube and experimental data for data quality validation and understanding purposes before supplying machine learning algorithms with data. Additional objectives include confirming previous research findings discussed in the literature review and further TCM analysis following preliminary work in Chapter 4.

Following on from Chapter 4, both the data collection method and machine learning application for TCM require several improvements. While the data collection methodology developed in Chapter 3 was shown to work, the orifice used had previously been worn for an unknown operational time, up to 230 hours. As it was a Ruby orifice, with a lower useful life compared to Diamond, orifice condition may have accelerated the wear rate, and potentially caused uneven wear of the mixing tubes. The condition of the orifice and mixing tubes requires assessment. In addition, the wear process itself needs to be better understood by studying the wear of the mixing tubes.

Several observations from Chapter 4 require validation. A linear exit diameter growth trend was observed, with wear consistent between tubes. Using a new orifice, a larger data collection effort would confirm the observed trend and whether the wear threshold is crossed within 60 minutes of wear.

Multiple limitations were addressed for the data collection framework improvement following the Chapter 4 analysis. First, the machine sensors' sampling rate was increased for better data resolution. Second, data was missing in the preliminary trial following a database error. A new, improved system was implemented to ensure data

collection reliability. Furthermore, the operator was required to monitor the pump pressure and abrasive in the supply hose throughout data collection. Ensuring the dwell cycles are not run before the pump reaches the required pressure and that no abrasive remains in the abrasive hose after the wear cycle.

For TCM, Chapter 4 suggested that both air and pressure sensors may be used for indirect monitoring of mixing tube wear. However, it was identified that several improvements are required, including a larger dataset size and better machine learning model performance. Additional sensors to monitor the process were added to assess whether this improves performance.

This chapter is split into three sections. First a trial overview is provided, before post-trial data of abrasive particles and nozzle components is analysed. Finally, the experimental sensor data is explored.

The abrasive particles are studied first. The aim was to confirm the findings from the literature review. Namely, garnet and Al_2O_3 abrasives are compared for similarities in density, shape and size. The abrasive are also compared for their flow properties to make sure both have consistent flow inside the abrasive supply hose. Particle fragmentation of Al_2O_3 was also studied.

Next, orifice and MC analysis is conducted using optical microscopy scans to compare new and worn states. As the parts were imaged after the main trial was completed, these images illustrate if the components got damaged during the accelerated wear trials. The wear progression of the final nozzle component, the mixing tube, is analysed next for consistent wear patterns as described in literature. The tubes worn via the accelerated wear approach are also compared with tubes worn using regular wear.

After the additional post-trial analysis is completed, data collected during the main trial phase is explored via data visualisation. Wear evolution and raw sensor data is explored. The trial had several challenges, the context of which is presented next. The data quality is studied before concluding the chapter.

5.1 Main trial overview

Before starting the analysis, it is important to recall the changes between each of the three data collection stages, as discussed in Chapter 3. After the preliminary trial, the following changes were made before Phase I of the main trial:

- A different AWJ was used. This waterjet was also a 6-axis AWJ provided by Aquarese, similar to the one used at the AMRC.

- An Additional pressure sensor was added, attached to the abrasive supply hose.

- A custom script for recording machine sensors' data was written by Aquarese. This script allowed for a higher sampling rate of 50 Hz and for automatic data logging saved to a hard drive to avoid data loss.

- The author of this thesis was trained to run the AWJ, allowing for more control over the data collection process.

After Phase I, the following changes were implemented before Phase II of the main trial:

- Airflow was recorded at 2000 Hz due to the availability of a better laptop.

- A condenser microphone was added for ATD recordings.

In addition, as mentioned in Chapter 3, after wearing mixing tube 9 during Phase II, the UHP seal and orifice holder part failure resulted in a component change by an Aquarese technician. It was observed that the part change helped stabilise the water pressure pump, allowing pressure to stay high without requiring constant manual resetting after each dwell cycle. However, it also had an impact on the responses recorded by the network of sensors.

As mentioned in Chapter 3, there were several other issues with the main trial. First, a hole was machined at the bottom of the AWJ tank. Second, a crimp in the hose between a pressure sensor and the nozzle caused data loss. Finally, the initial plan of using a high-speed camera and an accelerometer and conducting aluminium machining could not be carried out due to the trial being held abroad and being limited by export control and time.

5.2 Post-trial analysis

5.2.1 Abrasive particles

The abrasive change from garnet to Al_2O_3 allowed for accelerated AWJ mixing tube wear. The implications of this change are important to understand. Therefore, garnet and Al_2O_3 abrasive particles were investigated to validate the findings discussed in the literature review.

Hashish suggested that Al_2O_3 is a suitable alternative to replace garnet for the purpose of accelerating mixing tube wear [7]. Hashish argued, that this change will

keep the wear pattern convergent and therefore consistent with regular wear, yet will accelerate the time required to wear the tubes. According to Hashish, while Al_2O_3 has a higher hardness that will accelerate wear, it also has a similar density and particle shape as garnet [7, 50]. As discussed in the literature review, both density and shape are important [57, 63, 81]. Long et al. observed in a numerical study, that a less rounded particle shape and a lower density may result in higher particle kinetic energy [63]. Which may have been one of the contributing factors to the damage AWJ catcher tank during the main trial data collection process.

Figure 5.1 presents a comparison of the particle shapes of the two abrasives through optical microscopy. In the images, multiple abrasive particles for each material are present. The images show garnet particles have a more rounded profile, while Al_2O_3 particles have sharper edges. Both particles appear similar in terms of circularity. The images suggest the overall shape is similar, but due to lower roundness, Al_2O_3 abrasive may have had higher particle kinetic energy when travelling through the mixing tube according to the numerical study results by Long et al. [63]. The implications for wear from higher kinetic energy of Al_2O_3 abrasive is a greater contribution to abrasive and erosive wear considering equations 2.1 and 2.2 [57, 81]. Greater particle angularity would also result in higher wear rates [54].

| (a) Garnet | (b) Al_2O_3 |
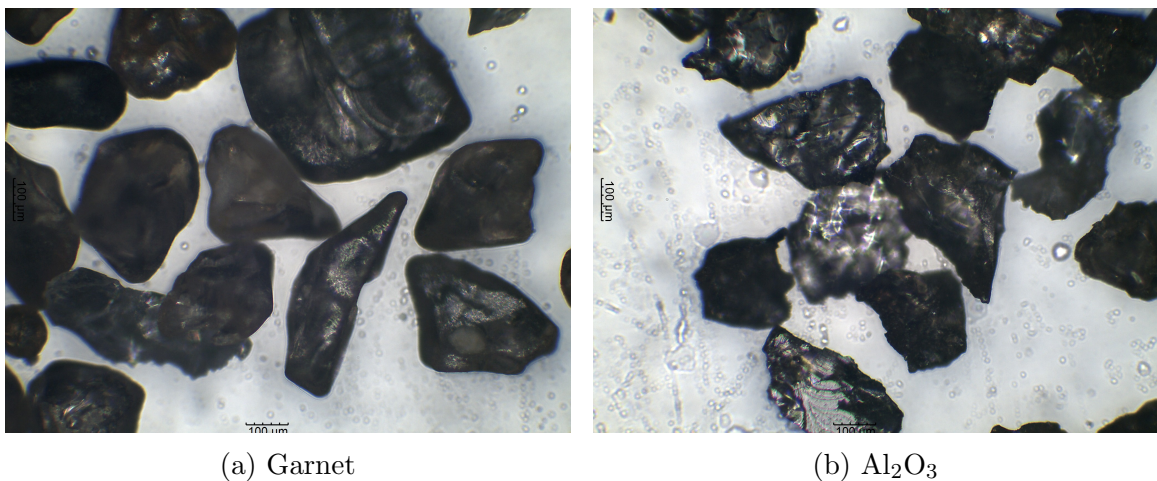
Figure 5.1: Optical microscopy images of garnet and Al_2O_3 abrasive particles under x10 magnification, for shape comparison.

The physical characteristics property sections on the supplier datasheets for the two abrasives, provided in Appendices A and B, support the roundness observations. The grain shape is described as angular for brown fused alumina (Al_2O_3) and sub-angular for garnet, suggesting garnet has a lower roundness.

107

Optical microscopy was deemed sufficient to study the particle shape. However, given the observed results, a more comprehensive approach involving the capture of additional images of individual particles and subsequent analysis using software, such as the open-source tool ImageJ, to compute shape descriptors like circularity and roundness for quantitative shape characterisation may have provided a better understanding of particle shape.

Table 5.1 compares the density of the two abrasives. Both densities are similar, as expected after the literature review. The lower density of Al_2O_3 would increase it's kinetic energy inside the mixing tubes, as suggested by Long et al., however due to the small difference this effect would be insignificant [63]. Despite their slight differences in shape and density, both Al_2O_3 and garnet abrasives are similar. Therefore, as suggested in the literature and assumed for the creation of the data collection framework, Al_2O_3 is a suitable substitute for garnet in terms of increasing the particle hardness while maintaining similar shape and density [7].

Table 5.1: Density of garnet and Al_2O_3 abrasive, measured using helium pycnometry and averaged over five repeats.

	Al_2O_3	Garnet
Density (g/cm^3)	3.9674	4.0998
Std dev (g/cm^3)	0.0011	0.0015

Figure 5.2 compares the abrasive size distribution. Although only Al_2O_3 abrasive was used to wear mixing tubes 1-10, mixing tube 11 was worn using garnet. A sample of garnet used for wearing tube 11 was used to calculate the particle size and to understand potential differences before comparing the internal profiles of the mixing tubes. Based on Figure 5.2 Al_2O_3 abrasive has a higher average, median and maximum particle size. The larger size of Al_2O_3 would contribute to greater abrasive and erosive wear [54].

In Table 3.3 in Chapter 3, literature suggested 80 mesh (177 μm) abrasives were used for accelerated wear tubes and for the tube supplied by the AMRC, while Dr Hashish supplied tubes were worn using 50 mesh abrasive (297 μm). Figure 5.2 implies that the true abrasive size for accelerated wear tubes using Al_2O_3 abrasive was closer to 50 mesh (297 μm), while the garnet's median mesh size was 60 mesh (250 μm). Therefore, the process parameters between the three separate mixing tube sets worn by different researchers are more similar than initially thought. An abrasive
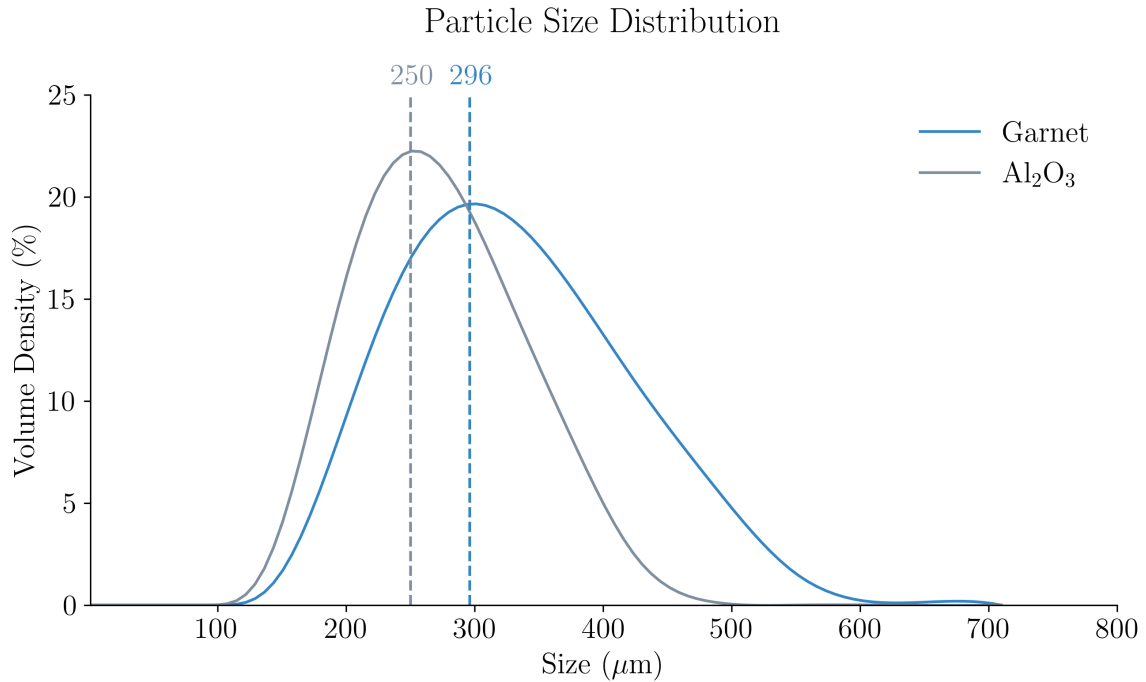
Figure 5.2: Distribution of particle size for unused garnet and Al$_2$O$_3$ abrasive, obtained using a Mastersizer over 20 repeats. The dashed lines indicate the median particle size of each abrasive.

sample was not available from Dr Hashish, but it would be unlikely to be a mesh size larger than 50 (297 μm), considering the ID of the mixing tubes is 1.02 mm.

Figure 5.3 shows how the particle distribution changes for Al$_2$O$_3$ abrasive before and after the wear of mixing tubes. A significant particle distribution shift is observed, with particle mean, median and maximum size reducing after use. This contradicts the results discussed in the literature review, where an investigation by Perec et al., using the same mixing tubes and pressure as in this study, reported little particle fragmentation with the particle size distribution maintaining approximately the same median value [13]. Lack of particle fragmentation could result in greater differences in observed wear profiles between Al$_2$O$_3$ and garnet abrasives, which would be a limitation for the designed TCM data collection framework. Larger-diameter particles align slower with the axial flow direction, increasing erosion at the lower sections of the mixing tubes [7]. However, Figure 5.3 suggests the particles do fragment, similar to garnet [58]. Therefore, the absence of fragmentation isn't a limiting factor for designing an accelerated wear trial approach based on Al$_2$O$_3$ abrasive.

A limitation of the fragmentation results displayed in Figure 5.3 is in the process of collection of the used abrasive samples. While the catcher tank was cleared before
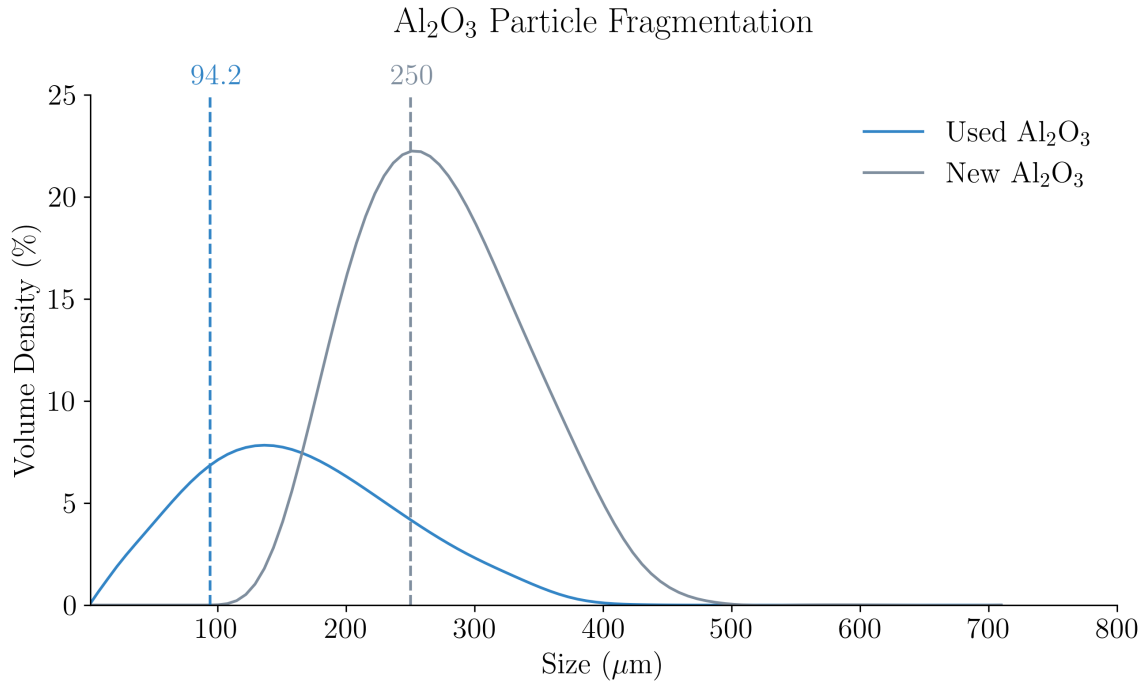
Figure 5.3: Comparison of particle size distribution for Al_2O_3 before and after use. The after use sample was collected from the bottom of the AWJ catcher tank after the tank was drained of water. The dashed lines indicated the median particle size. The data was obtained over 20 measurements using a Mastersizer.

the abrasive change was carried out, mixing tube material, as well as fragmentation of the steel billets protecting the bottom of the tank, may have contaminated the sample. A breakdown of present material, for example, by determining the elemental composition of the material through the use of X-ray fluorescence measurements, would have strengthened the conclusions.

A comparison of abrasive flowability, via the angle of repose measurements, is given in Table 5.2. Abrasive flow differences may impact how well the abrasive travels through the abrasive supply hose. From a practical standpoint of designing data collection trials to accelerate wear, good abrasive flow is crucial to avoid blockages and ensure good mixing with water inside the mixing tubes. The angle of repose measures the steepest angle at which a pile of granular material remains stable without sliding. A higher angle of repose would indicate that the material has a higher resistance to sliding (or flowing) due to friction between particles. Angle of repose is higher for angular particles which have less rounded edges. Table 5.2 demonstrates similarity in the angle of repose between Al_2O_3 and garnet, implying similar flow performance is expected during AWJ operation. For practical implementation, Al_2O_3 is therefore

a suitable alternative to garnet. Al_2O_3's higher angle of repose could be due to it's shape, which as observed in Figure 5.1, is less rounded.

Table 5.2: Comparison of abrasive flow through the angle of repose test. Data for five repeats is presented. Equation 3.1 was used to calculate the angle of repose. For both abrasives, the std dev of the height measurements was 0.1 mm.

	Al_2O_3	Garnet
Base diameter (mm)	48	48
Heap height (mm)	14.0, 14.0, 14.2, 14.2, 14.1	14.0, 14.1, 13.8, 14.0, 14.1
Average angle of repose (°)	30.43	30.26

To summarise, Al_2O_3 is a suitable substitute for garnet as stated in literature and hypothesised in Chapter 3 [7]. Analysis of abrasive particles confirmed similarities in shape and density between Al_2O_3 and garnet. However, minor differences were present between the two abrasives. Al_2O_3's less rounded shape and lower density could lead to higher kinetic energy inside the mixing tube [63].

The particle size of both abrasives was larger than 80 mesh on average, which would result in faster wear. In addition, contrary to the literature review, Al_2O_3 was shown to fragment during the wear process, but this observation had some limitations [13]. Finally, a similar angle of repose suggested similar performance can be expected for the two abrasives during AWJ operation.

5.2.2 Wear of nozzle components

Figure 5.4 displays the state of wear of the two orifices used in this research. As discussed in the literature review, the orifice has to withstand chipping and erosive wear from the water flow [25]. Both orifices appear in good condition, with no chipping observed. The significance of this finding in the context of this research is that for preliminary trial and orifice change data, orifice wear should not be a contributing factor if a change in recorded signal or mixing tube wear profile is observed. In addition, as the parts were imaged after the completion of all data collection trials, Figure 5.4 illustrates that the proposed methodology using accelerated wear did not damage the orifices.

The state of wear of the two used MCs is pictured in Figure 5.5. The worn MC, provided by Aquarese, appears to have significant wear at the upper section, above the chamber where abrasive particles enter. The wear may have been caused by using a damaged orifice or from abrasives entering the chamber from the supply hose and

(a) Diamond Orifice   (b) Ruby Orifice
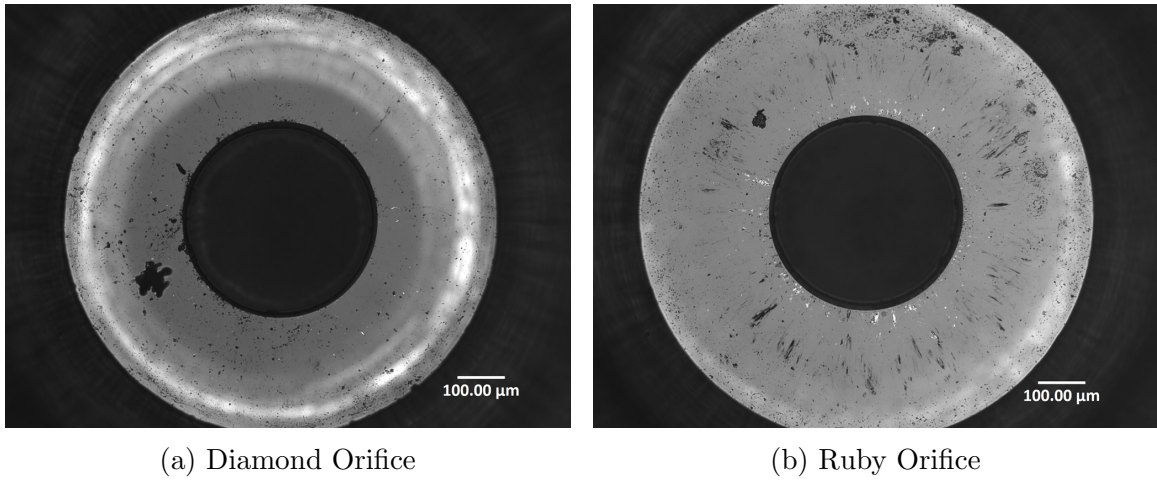
Figure 5.4: 10x magnification optical microscopy images of diamond and ruby AWJ orifices after the completion of the data collection trials. The measured diameters were 0.406 and 0.405 mm for diamond and ruby orifices, respectively.

colliding with the MC wall. The MCs could not be sectioned for a more detailed analysis of the interior profile. However, as a change in the state of wear between the two parts is observed, they can be compared for their effect on the sensors' signal to understand how wear of the second fastest-wearing machine component, the MC, may affect mixing tube wear monitoring. The MC used for the preliminary trial was not available for imaging.

(a) MC new   (b) MC worn

Figure 5.5: USB microscopy photos of two MCs taken at Aquarese. The worn mixing tube was installed prior to collecting MC change data as detailed in Table 3.4

For the initial assessment of mixing tube wear, weight data can be analysed. Figures 5.6 shows how the weight loss changed for mixing tubes with increasing wear time. A linear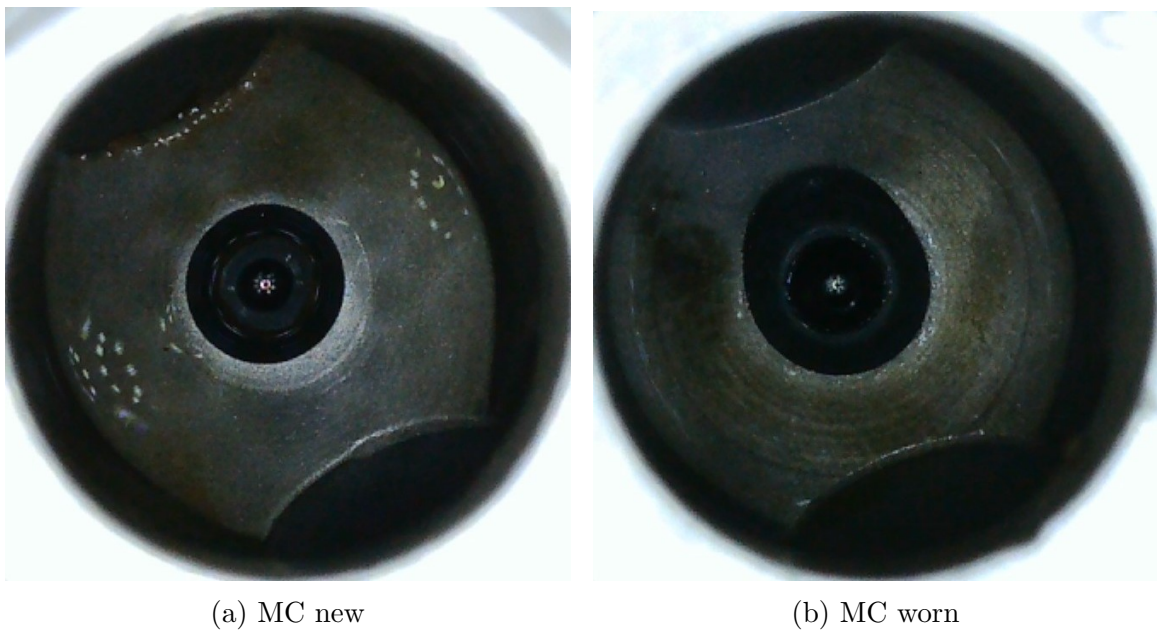 trend is observed between wear time and weight, confirming the observation of previous work on accelerated mixing tube wear [14, 20]. The weight change appears consistent between tubes worn for the same period of time. This is supported by Figure 5.7 and Table 5.3, which show a progressive increase in the percentage weight change for mixing tubes worn for increasing periods of time. Consistent wear is favorable indication for TCM, as it suggests the process is repeatable and consistent and therefore has potential for reliable monitoring.
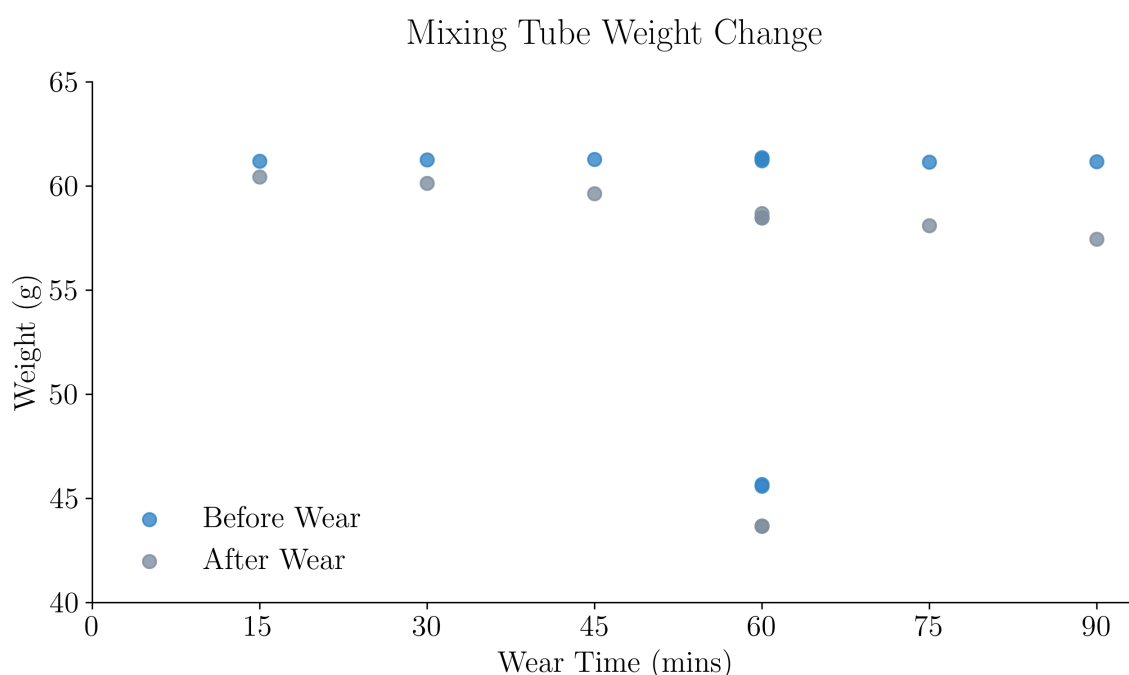
Figure 5.6: Mixing tube weight before and after accelerated wear trials. For each wear time, only one tube was worn, except at 60 minutes, where five tubes were worn: two in the preliminary trial and three in the main trial, including two shorter tubes (76 mm). Measurement uncertainty was 0.001 grams.

When studying the specific data of tubes worn for 60 minutes, in Table 5.3 and Figure 5.7, there are two notable observations. First, the weight change differs between tubes of the same length worn on two separate AWJs (mixing tubes 1-2 and mixing tube 6). Second, for tubes of the same length, worn on the same machine (tubes 1 and 2 as well as tubes 9 and 10), the weight change is very similar, and the tubes begin to converge to a similar post-trial weight even when the starting weight slightly differs. Weight differences between two AWJs is an indication that transferring a TCM system built on data from one machine, to another machine, could
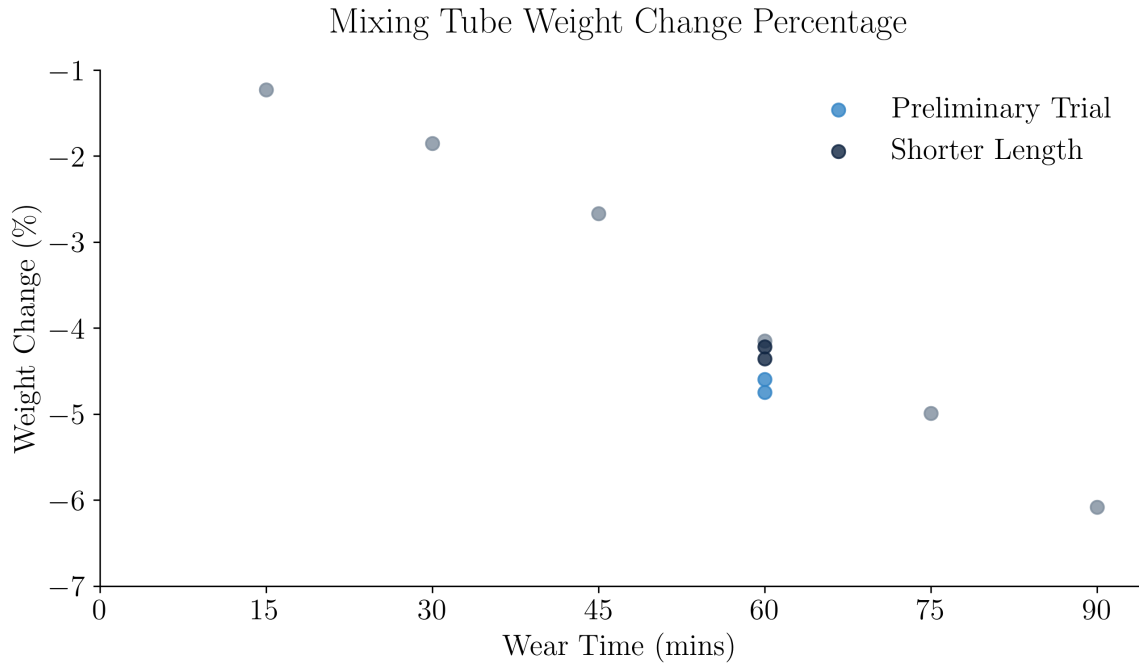
Figure 5.7: Mixing tube percentage weight change before and after accelerated wear trials. The "Preliminary Trial" mixing tubes 1 and 2 were worn on a different AWJ. The "Shorter Length" mixing tubes 9 and 10 were worn during the main trial but were of shorter length at 76 mm long.

Table 5.3: Mixing tube weight data for tubes worn using Al_2O_3 abrasive, before and after the wear trial. Each tube was washed, dried and cleared of residue with an air hose before measurement.

Tube No.	Wear Time (min)	Trial	Weight (g) Before	After	Weight Change (%)
3	15	Main - I	61.177	60.423	-1.23
4	30	Main - I	61.255	60.119	-1.85
5	45	Main - I	61.265	59.630	-2.67
1	60	Preliminary	61.297	58.480	-4.60
2	60	Preliminary	61.363	58.449	-4.75
6	60	Main - I	61.203	58.660	-4.15
7	75	Main - I	61.135	58.084	-4.99
8	90	Main - I	61.160	57.439	-6.08
9	60	Main - II	45.584	43.662	-4.22
10	60	Main - II	45.663	43.673	-4.36

be problematic. Weight change similarity between tubes of the same length on the same machine, however, is a positive sign for developing a TCM system. It again suggests consistency to the AWJ wear process, where factors such as the alignment

and securing of the mixing tube do not have a significant impact on the wear itself. This may have been a result of using a nozzle with a collet and holding nut parts as pictured in Figure 2.1, which serve the purpose of precisely aligning the mixing tube [25]. Overall, the weight data is an encouraging sign that the data collection approach designed in Chapter 3 is reproducible.

Mixing tube exit diameter wear uniformity can be studied using USB microscopy photos in Figures 5.8 and 5.9. Poor wear can be caused by MC and orifice wear as well as orifice or mixing tube misalignment [25, 32, 59, 76]. If any tubes had been exposed to poor wear conditions, the recorded data for that tube may have been affected. It's therefore important to study the wear progression uniformity. As discussed in the literature review, a "good" tube wear pattern is consistent and concentric [59]. In addition, the exit diameter has to be circular without blowout wear [25]. While internal profiles of the tubes will be studied later in this Chapter, the exit diameters observed in Figure 5.8, further support weight data in Figures 5.6 and 5.7 and suggest "good" wear has occurred for accelerated wear tubes as the exit diameter growth appears to have been consistent, uniform and without blowout wear. The collected data for all tubes should therefore not have been impacted by poor mixing tube wear.

After studying the exit diameter, studying the internal profiles of the tubes is useful for further validation of the quality of wear and to analyse the wear progression. The internal profile can be studied by conducting destructive machining through EDM. Figures 5.10, 5.11 and 5.12 show digital photos of mixing tubes which were machined longitudinally in half via EDM. The photos were taken with a tripod-mounted camera and a Bluetooth camera remote to maintain a consistent scale between the tubes.

Figure 5.10 compares the wear progression for tubes worn with Al_2O_3 abrasive. From the photos, a gradual increase in the diameter of the internal profile is observed with increasing wear time. All tubes show consistent and concentric wear, as defined by the mixing tube manufacturer [59]. This suggests normal wear has occurred in the absence of a damaged orifice or mixing tube misalignment. For mixing tubes 7 and 8, the wear profile appears to become less consistent closer to the mixing tube exit. This could be a result of prolonged wear which could be impacting the jet inside the mixing tube.

A wave pattern is observed forming in the mixing tubes with increasing wear, as shown in Figure 5.10. This observation aligns with findings from previous literature [7, 13, 14, 48, 57–59]. Image edge analysis of the EDM photos in Figure 5.10 can
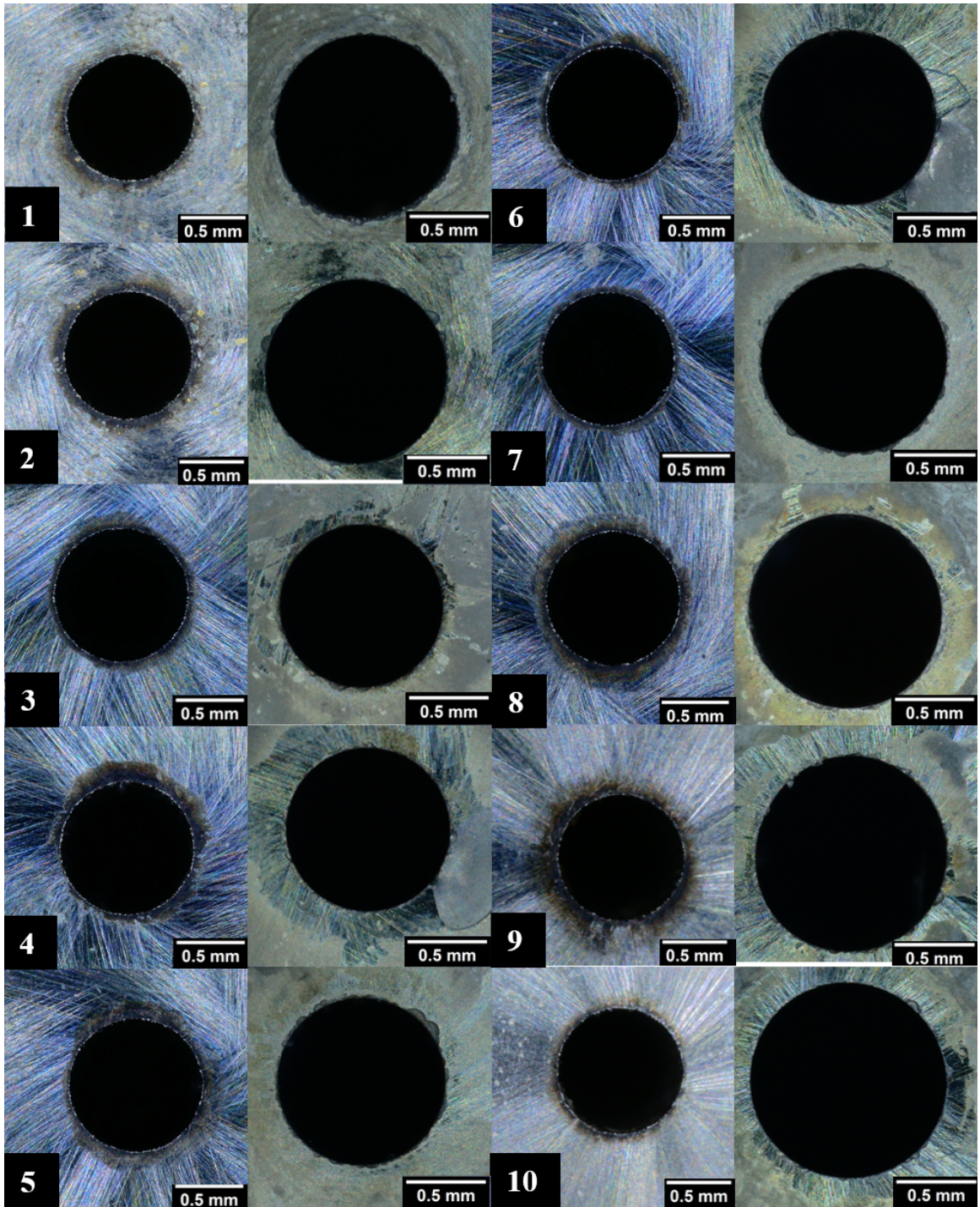
Figure 5.8: USB microscopy photos of tubes 1-10 before and after wear. For each tube (numbered), the left photo was taken before the wear trial and the right after the wear trial.

help compare the wave patterns of the mixing tubes and track their development with increasing wear.
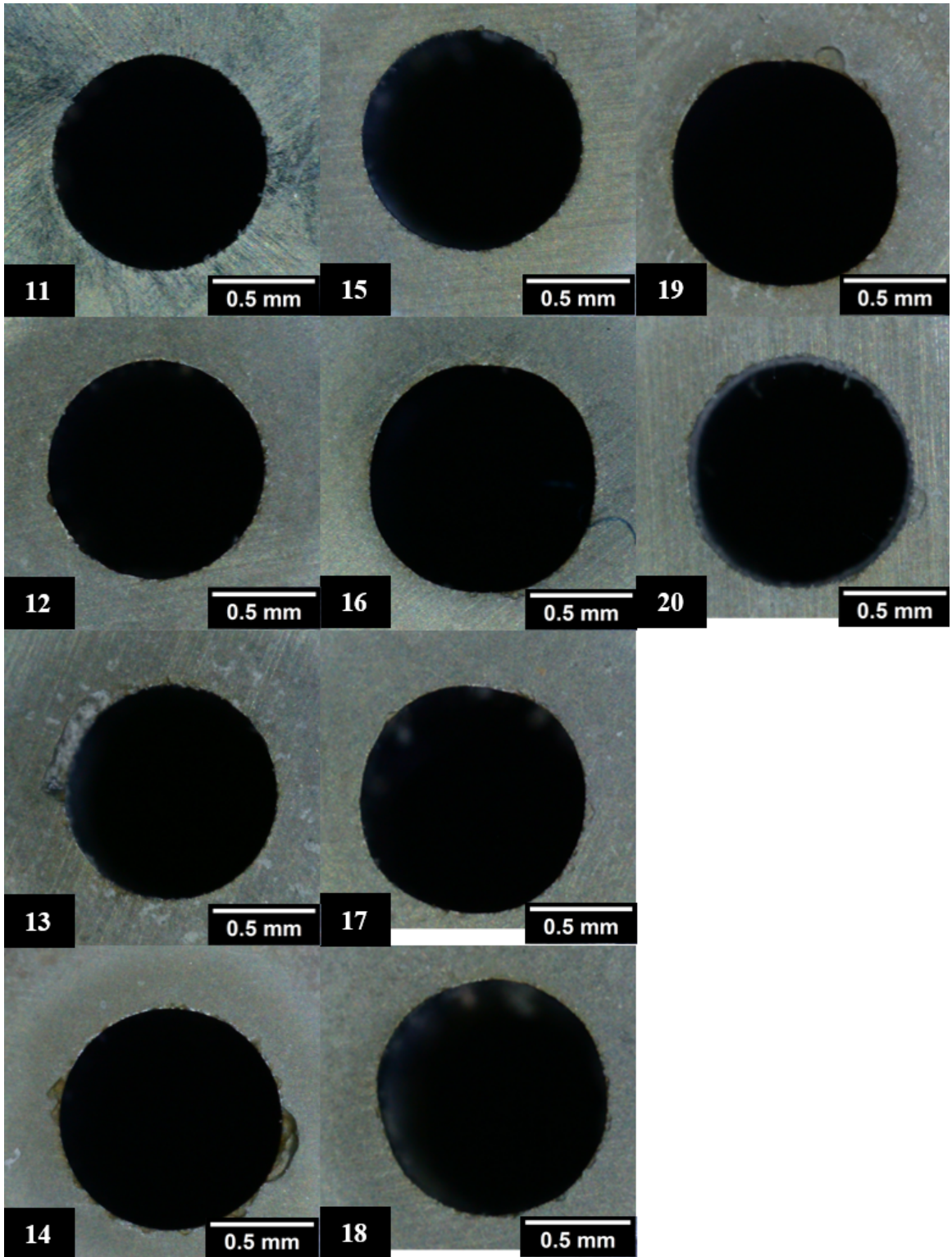
Figure 5.9: USB microscopy photos tubes 11-20 after the completion of the main trial.
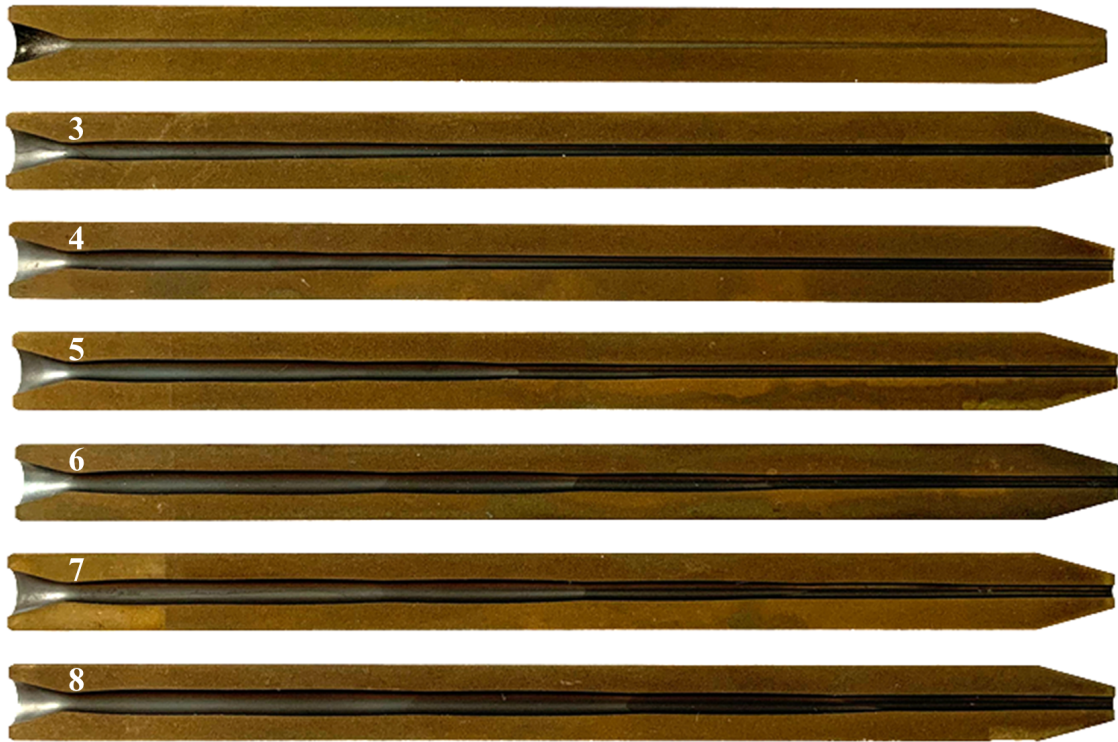
Figure 5.10: Wear progression of AWJ mixing tubes displayed in order from 0 to 90 minutes. The unnumbered tube was brand new and not used in the trials. Numbered tubes were worn during the first phase of the main trial.

Internal profile contours for mixing tubes 3 to 8 are shown in Figure 5.13. To generate the contours from EDM images, the mixing tube wall was first removed using an automatic background remover in Adobe Photoshop leaving the internal profile of the image only. The processed images were then converted to binary format. Contours were detected using OpenCV's findContours function. The largest contour, representing the wear profile, was then extracted. It should be noted that the contours may have been affected by misalignment in the photography process, such as the tubes not being perfectly perpendicular during imaging.

The internal profiles, plotted in Figure 5.13, suggest that with increasing wear time, both the wave diameter and the wavelength of the pattern increase. The data suggests that the abrasive particles exhibit oscillatory motion as they travel down the mixing tube, evidenced by the wave pattern of the red 90-minute tube contour in Figure 5.13. This pattern could be influenced by various factors, such as the inlet angle and flow instabilities. However, these findings are inconclusive and wave analysis can be explored in further work.

All mixing tubes in Figure 5.10 also have a convergent wave pattern, with wear
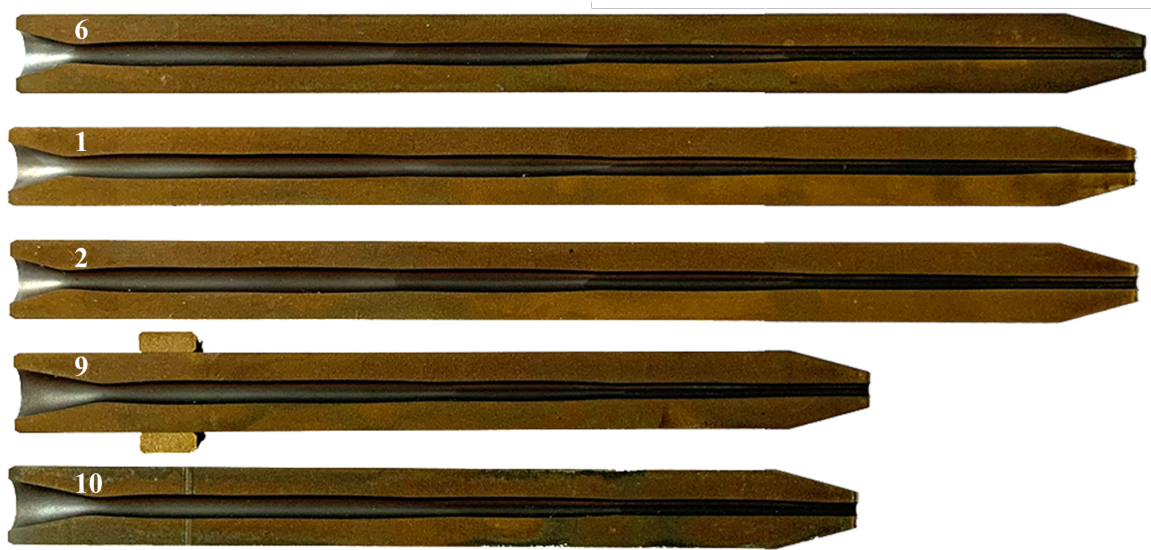
Figure 5.11: Comparison of wear between mixing tubes worn for 60 minutes. Tubes 1 and 2 were worn during the preliminary trial. For tube 9 a brass ring is present after being machined. This brass ring was originally present on all mixing tubes, however, contrary to other tubes it failed to come off for tube 9 post EDM.

Figure 5.12: Comparison of wear between mixing tubes subjected to regular and accelerated wear using garnet or Al_2O_3 abrasives. Tube 5 was worn using accelerated wear, with all other tubes worn using regular wear.
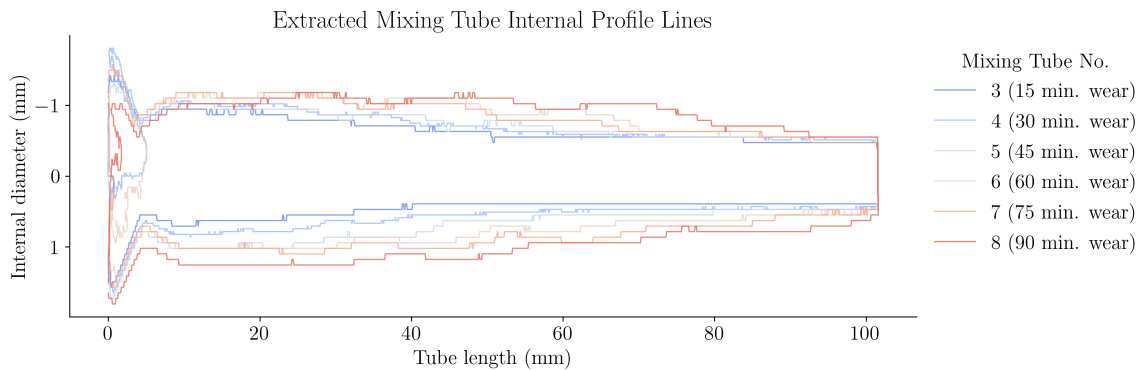
Figure 5.13: Internal wear profile contours of mixing tubes 3-8 (15-90 minutes of wear).

starting upstream of the mixing tube and developing towards the mixing tube exit. The results in Figure 5.10 are as hypothesised during the data collection framework development. Replacing garnet with Al_2O_3 abrasive, maintained the convergent wear pattern which is representative of the regular wear process when using garnet abrasive [7]. The implications for the data analysis are that the collected data can be trusted not to have been affected by poor mixing tube wear.

Figure 5.11 shows the wear progression of mixing tubes all worn for 60 minutes using Al_2O_3 abrasive. Similar to Figure 5.10, a convergent wear pattern is observed with wave zones for all mixing tubes. Figure 5.11 can be used to study multiple factors. The consistency of wear can be studied by comparing same length tubes from the same trial (tubes 1 and 2 from preliminary and tubes 9 and 10 from main trial). The difference in wear profile from using two separate AWJs can be studied by comparing tube 6 with two preliminary trial tubes 1 and 2. Finally, the effect of length on internal wear profile growth can be studied by comparing tubes 9 and 10 with tube 6, which were all worn on the same machine under the same process conditions during the main trial.

Wear consistency can be assessed by studying the wave profile in Figure 5.11, which suggests the tubes wear in a consistent fashion. The profile images support the conclusions drawn after analysing the mixing tube weight data in Table 5.3. This implies the wear process is repeatable, which is a positive implication for TCM if the recorded signal is also repeatable. However, there appear to be slight differences in wave lengths between several tubes. These findings are inconclusive and could benefit from wave analysis in further work.

As the overall wear patterns are similar, for TCM this means the application has potential to be transferable for data collected on separate machines. For length

120

changes, Figure 5.11 indicates that the overall profile is similar, however a difference in the wave shape is observed. A longer conical area at the upstream section of the tubes may be the reasons for variations in shape of the wear profile. As mentioned in the literature review, the conical area facilitates abrasive entry and affects how even the wear is inside the tubes [25]. In Figure 5.11, wear does appear more even along the profile at the upstream section of tubes 9 and 10, in comparison to tubes 1, 2 and 6. Overall, similar to Figure 5.10, there is consistency in how the wear develops inside the mixing tubes.

Figure 5.12 shows the wear progression of tube 5, worn via accelerated wear, and all mixing tubes worn using regular wear assessed in this thesis. Tube 5 is included to compare it with tube 11 worn for an equivalent period of time with a different abrasive, using data from previous research and discussions with Kennametal researchers to equate 1 hour of regular wear to 10 minutes of accelerated wear [14]. In addition, tube 11 can be compared with tubes 12-20, with some worn for the same period of time, to see how tubes may differ when worn for the same length of time, using regular wear, under different parameters by different researchers. Lastly, tubes 12-20 can be again compared for wear consistency. When comparing the mixing tubes, it is important to account for different process parameters aside from the change in abrasive. The effect of process parameters on mixing tube wear rates was presented in Table 2.1 in Chapter 2. In Chapter 3, Table 3.3 compared the process parameters used by each researcher. As a short summary, tube 11 had a smaller particle size used, as seen in Figure 5.2, which would have lowered the wear rate. Tubes 12-20 were ROCTEC 500 mixing tubes with a longer useful life. These tubes were also worn under higher waterjet pressure and a faster abrasive flow rate, which would result in faster wear. Tube 11 had the lowest abrasive flow rate. Finally, tubes 12-20 used a smaller orifice size (0.001" smaller) which would result in slower wear.

Figure 5.12 reveals that mixing tube 5 had more pronounced wear than tube 11. The harder abrasive had a greater wear contribution upstream of the mixing tube. The upper section pattern of mixing tube 5 is more similar to the patterns of mixing tubes supplied by Dr Hashish (12-20). However, the wear profiles of mixing tubes 12-20 appear to have less distinct waves upstream compared to mixing tubes worn using Al_2O_3 abrasive displayed in Figure 5.10. While this may result from differences in parameters used (see Table 3.3) or from different nozzle designs, the longer conical shape at the abrasive entry of the mixing tubes may have contributed. As mentioned in the literature review, the conical area facilitates abrasive entry, which may have impacted the velocity vectors of the abrasives upstream of the tube [25].

121

The shorter conical shape at a sharper angle for the shorter mixing tube may result in particle velocity vectors that are less parallel to the waterjet than for the longer conical shape, leading to greater erosive wear and a more distinct wave profile [7]. The effect of conical shape on abrasive particle trajectory requires further research. Furthermore, due to the observed differences between tubes worn using the accelerated wear approach and tubes worn using the regular wear method, any TCM system developed on data gathered on mixing tubes worn using Al_2O_3 abrasive would require validation on data collected from mixing tubes worn using garnet. This will ensure the proposed approach can be implemented in practice, where the wear profile of mixing tubes may differ.

Despite mixing tube 11 being worn for 40 hours, its internal profile shown in Figure 5.12 appears more similar to the unworn mixing tube shown in Figure 5.10 than to other mixing tubes worn using regular wear. While there is a difference in parameters used to wear the two sets of mixing tubes, it is possible mixing tube 11 may have experienced less wear due to process inconsistencies such as poor abrasive flow. Mixing tube 11's material is also less wear resistant than of mixing tubes 12-20 as displayed in Table 3.3, further supporting this hypothesis since mixing tubes 12-20 had more internal wear shown in Figure 5.12.

Figure 5.14 compares the exit diameters of the additional mixing tubes worn using a regular wear approach supplied for the research in this thesis. Mixing tube 11 is expected to have a larger exit diameter for equivalent wear time than mixing tubes 12-20 due to its shorter length. As discussed in the literature review, for shorter-length mixing tubes experiencing a convergent wear pattern, wear reaches the exit faster [7, 14, 50]. This is not the case and supports the hypothesis that the wear process was likely affected by process inconsistencies.

From both Figures 5.12 and 5.14, it is difficult to gauge which mixing tubes supplied by Dr Hashish were worn for 40 hours and which for 70 hours. From the wear plot, mixing tubes 16-20 can be classed as longer wear tubes as they all cross the wear threshold boundary and have a larger exit diameter compared to mixing tubes 12-15. At 40 hours, the mixing tubes supplied by Dr Hashish were deemed in good condition, which is why some tubes were worn for longer (70 hours) by the original users. So it's possible to assume that the mixing tubes with a larger exit diameter were the ones that were worn for a longer period of time. However, EDM photography in Figure 5.12 shows a similar wear profile between mixing tubes 16 and 12, despite an exit diameter difference of 0.06 mm. In addition, despite mixing tube 19 having an exit diameter of 1.10 mm, its profile wear upstream is less than that
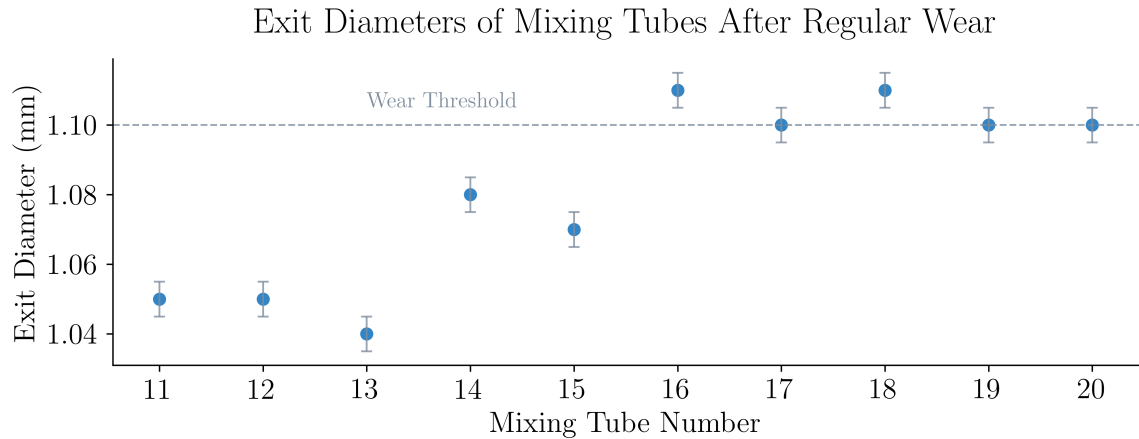
Figure 5.14: Exit diameter of mixing tubes 11 - 20 worn using parameters detailed in Table 3.3. The dashed line indicates the identified wear threshold of 10% exit diameter wear. The error of each measurement is ±0.005 mm.

of most other mixing tubes, as suggested by Figure 5.12. Suggesting that mixing tube 19 may have been subject to less wear time despite a larger exit diameter. The disparities imply that the wear process is inconsistent for regular wear, as either the internal wear profile or the exit diameter growth for the same machining time was inconsistent. For TCM, this suggests time tracking may not be accurate, as wear may be inconsistent for some mixing tubes.

To summarise, orifice, MC and mixing tubes used for data collection in this thesis were all studied for wear. Both orifices were in good, similar condition. The worn MC had visually more wear compared to the new MC used to wear the mixing tubes in the main trial. For the mixing tubes, all tubes worn using Al_2O_3 abrasive had consistent wear, which was comparable to "good" wear patterns described in literature [59]. This was evident through weight, exit diameter and internal profile analysis. However, the wear patterns of mixing tubes worn using garnet were not as consistent. Going forward, the validation strategy used in machine learning must account for this difference to understand the transferability of any model for use in industry.

5.3   Exploratory data analysis

This section will analyse the collected data from the machining trials. Collected data is important to understand before feeding it to different models for TCM, so this section will explore data for insights to frame the machine learning approach. A summary of all collected data is given in Table 3.4 in Chapter 3.

The data was processed in a similar manner to Chapter 4. Data was first read by using the Pandas library [166]. Next, the data recordings had their time synchronised via the methodology described in Chapter 3. Data was next split into individual repeats before features could be extracted. Once features were extracted, 11 data points caused by operator errors were removed together with the anomaly identified in Chapter 4. For a detailed list of all excluded data please refer to Table J.1 in Appendix J. A breakdown of the total number of recorded dwell cycles for each trial is given in Table 5.4. Each counted recorded dwell cycle was for a singular repeat. For each one of these repeats, features can be extracted to form one row of data for machine learning.

Table 5.4: Summary of total recorded dwell cycles. The "Change" column includes data collected after an orifice or MC part change. 11 recordings affected by operator error and the anomaly identified in Chapter 4 were not included in this summary.

Trial	Mixing tubes worn	Dwell cycles recorded			
		WDC	ATD	Change	Total
Preliminary	2	209	0	0	209
Main - Phase I	6	760	165	104	1029
Main - Phase II	2	209	300	299	808

5.3.1 Raw data visualisation

The first step of the data analysis process is to introduce the data. Figure 5.15 displays the exit diameter progression for all worn tubes during accelerated wear data collection trials. Similar to Figure 4.1 in Chapter 4, and as hypothesised during the data collection trial design, the wear threshold of 1.10 mm exit diameter wear was crossed within the wear time range of the accelerated trials. For mixing tubes which crossed the wear threshold, a more detailed comparison of when the threshold was crossed is provided in Table 5.5. Figure 5.15 shows that mixing tubes worn during the preliminary trial, and shorter tubes, had a faster exit diameter growth rate. Table 5.6 provides a comprehensive comparison of both weight loss and exit diameter growth rates for each mixing tube.

Figure 5.15 suggests that the exit diameter wear progression is linear at first, however at larger exit diameters the wear rate accelerates. This is observed via increasing distance between plotted points for tubes 8-10, with increasing wear time in Figure 5.15, and is supported by the progressively increasing exit diameter growth rate with wear time shown in Table 5.6. There also appears to be a fast wear rate at
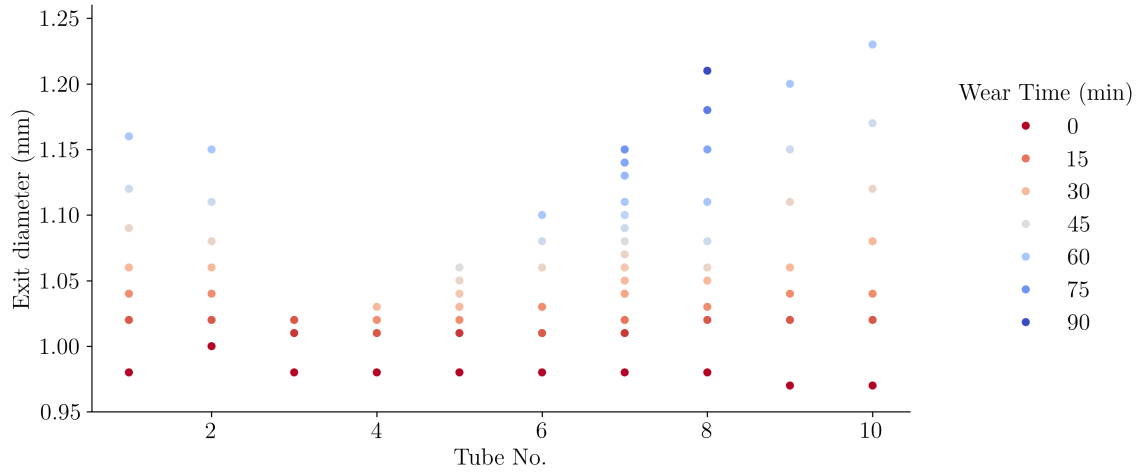
Figure 5.15: Exit diameter growth of mixing tubes worn using Al_2O_3 abrasive. Mixing tubes 1-2 were worn during the preliminary trial, with the remaining tubes worn during the main trial. Mixing tubes 9-10 are of shorter length. Mixing tubes 3, 5 and 7 had the exit diameter measured every 5 minutes, with all other mixing tubes worn at 10-minute intervals.

Table 5.5: Time for the mixing tube to cross the 1.10 mm exit diameter wear threshold during accelerated wear. The "Time Crossed" and "Exit Diameter" columns show measurements after the wear threshold was exceeded.

Trial	Mixing Tube No.	Length (mm)	Time Crossed (min)	Exit Diameter (mm)
Preliminary	1	101.6	50	1.12
Preliminary	2	101.6	50	1.11
Main - Phase I	6	101.6	60	1.10
Main - Phase I	7	101.6	55	1.10
Main - Phase I	8	101.6	60	1.11
Main - Phase II	9	76	40	1.11
Main - Phase II	10	76	40	1.12

the beginning of the tool life, reaching around 1.02 mm within the first 5-10 minutes of wear, as seen in Figure 5.15. The relatively high exit diameter growth and weight loss rates seen in Table 5.6 for the shortest wear time of 15 minutes supports this trend observation. The initial fast wear acceleration may be related to the mixing tube design or manufacturing process, while later-stage wear acceleration may be a result of the abrasive particles failing to align their velocity vectors with the jet of water due to increasing variations in the tube profile, as seen in Figure 5.10, and

125

Table 5.6: Wear rates of worn mixing tubes, where E. D. is exit diameter. The weight loss and exit diameter growth rates were calculated by taking into account the first measurement and final measurements.

Tube No.	Wear Time (min)	Weight Loss (g/hour)	E. D. Growth (mm/hour)
1	60	2.82	0.180
2	60	2.91	0.150
3	15	3.02	0.200
4	30	2.27	0.100
5	45	2.18	0.107
6	60	2.54	0.120
7	75	2.44	0.136
8	90	2.48	0.153
9	60	1.92	0.230
10	60	1.99	0.260

therefore causing more and more mixing tube wall collisions and greater wear which propagates from top to bottom [7, 50].

Initial more linear wear pattern would benefit simple TCM systems, such as linear models based on wear time, to approximate the exit diameter. This was the case in Chapter 4, where mixing tubes were worn for 60 minutes. However, once the exit diameter approaches and exceeds the wear threshold, lack of linearity and consistency, as seen between tubes 9 and 10, may begin to affect predictions. This will be more significant for shorter tubes that have a faster exit diameter growth rate.

Mixing tubes worn during the preliminary wear trial, crossed the wear threshold sooner and had a faster wear rate as shown in Tables 5.5 and 5.6. The preliminary trial was conducted on a separate AWJ to the main trial with a different orifice used. However, as suggested by Figures 5.4 and 5.11 in the previous section, neither orifice wear nor mixing tube alignment should have made an impact on the wear rate. As suggested by Figure 5.11, the wear pattern is also consistent with mixing tubes worn during the main trial. By studying the airflow rates, the difference can be inferred. A greater airflow would result in better abrasive entrainment and higher abrasive flow rates, which would increase the wear rate without impacting the wear profile [14, 48, 50]. Airflow increases with increasing pressure, mixing tube diameter, water flow rate and suction hose diameter and lower suction hose length [3–5]. As all parameters apart from hose length were comparable between both trials, the shorter hose length of the preliminary trial may have resulted in greater airflow and therefore greater abrasive flow rate and greater wear.

The average airflow at 0 minutes of wear for each mixing tube is compared in Figure 5.16. Mixing tubes 1-2 were worn on a separate AWJ. Mixing tube 10 was worn after a part change during the main trial.
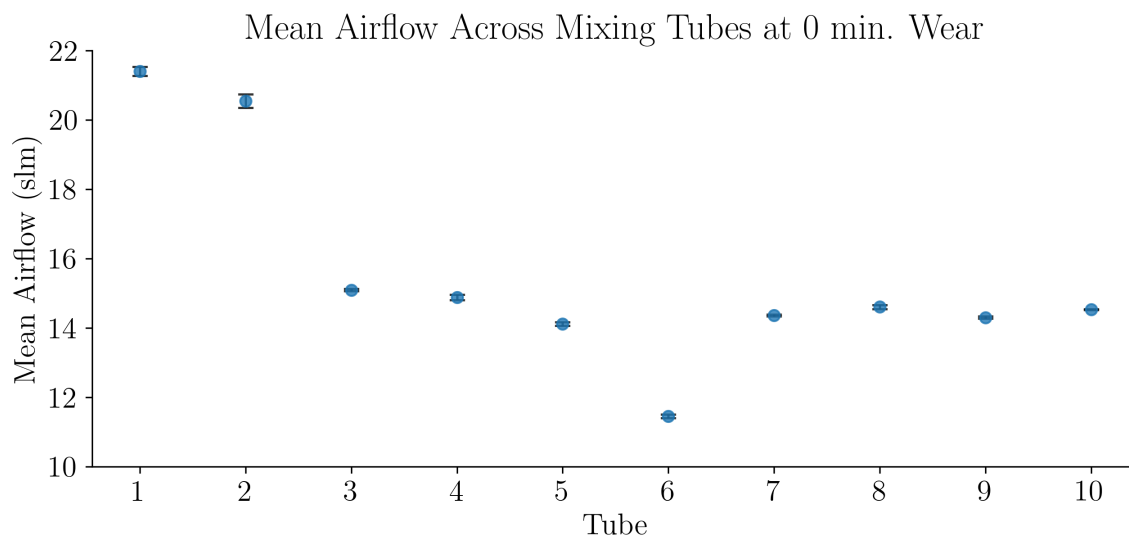
Figure 5.16: Average airflow during AWJ dwell cycles at 0 minutes wear at the start of the WDC trials. Values are averaged over three repeats at 4000 bar water pressure, with error bars showing standard deviation.

Despite similar starting exit diameters, as seen in Figure 5.15, preliminary trial mixing tubes 1-2 do have greater airflow. As discussed, a short hose length may have been the cause. Wear of other nozzle components may have also resulted in the observed difference. This disparity in airflow may have caused the difference seen between the two trials in the wear rate. Figure 5.16 also supports the observations by Hashish et al. discussed in literature, that the effect of mixing tube length on airflow suction is insignificant [5]. Both mixing tubes 9 and 10 have a similar airflow rate at 0 minutes of wear, despite having a shorter mixing tube length of 76 m.

Table 5.6 shows that for shorter tubes, the exit diameter growth rate is higher, as expected after the literature review [7, 14, 50]. Hashish stated longer mixing tube length delays the time wear reaches the exit bore for convergent wear patterns [7]. The weight loss rate is lower for shorter tubes as seen in 5.6, however this is length dependent and the percentage weight change for mixing tubes 9-10 was greater as seen in Table 4.1.

The exit diameter growth rate of 0.230 and 0.260 mm/hour of the two 76 mm mixing tubes is lower than the 0.305 mm/hour exit diameter growth rate observed by Taggart et al. [71]. Taggart et al. used the same mixing tube, mixing tube diameter

and abrasive flow rate and had a smaller 80 mesh abrasive size, a smaller orifice diameter of 0.33 mm and a lower water pressure of 3650 bar with the mixing tube worn for 25 minutes [71]. As suggested by Table 2.1 in Chapter 2, the expectation would be for a lower wear rate due to a smaller orifice diameter and lower particle size (following observations in Figure 5.2) and lower pressure. The difference could be machine-dependent or due to the difference in the nozzle, with a newer version of the Paser IV nozzle head used to wear mixing tubes 9-10 as opposed to the Paser III head used by Taggart et al. [71]. The implications for TCM of this difference and the differences discussed earlier between preliminary and main trials when using different equipment are that any designed TCM system may be machine-dependent and require validation on a separate setup. This would be particularly true for time-based approaches, which may be more sensitive to wear rates, unlike machine learning methods, which may be capable of learning other patterns within the data. Figure 5.15 further supports using more complicated approaches due to a lack of consistency in exit diameter growth rates between mixing tubes worn on the same machine.

The raw data for each sensor used is presented in Figure 5.17, comparing the effect of both mixing tube wear and water pressure on the sensor response. All sensors except for water pressure see a notable change in recorded magnitude with changing wear. Changes in water pressure affect the response on each sensor. As noted in Chapter 4, while water pressure does not correlate highly with wear, as seen in Figures 4.11 and 4.12, it does impact the magnitude of the recorded signal and therefore influences other features which are used to detect wear. It may be important for systems using different water pressures to keep this feature during TCM and not remove it.

In Figure 5.17, water pressure appears to fluctuate in a wave pattern. As noted in Chapter 4, this may explain the fluctuations in airflow and audio signals. Although different data segmentation times were explored in Figure 4.15 in Chapter 4, skipping 0.5s of data may be worthwhile to avoid the initial turning on of the jet affecting the generated features.

Figure 5.18 shows the sensor data in the frequency domain. PSD is used in this thesis for feature generation as it provides a meaningful representation of the signal, which is less sensitive to noise. All sensors see a change in the PSD with changing wear apart from water flow, which, as seen in Figure 5.17, is more pressure dependent.

The machine data exhibits reduced variability in both the time and frequency domains when compared to airflow and audio data. Consequently, only total and peak power features will be extracted from the machine data within the frequency
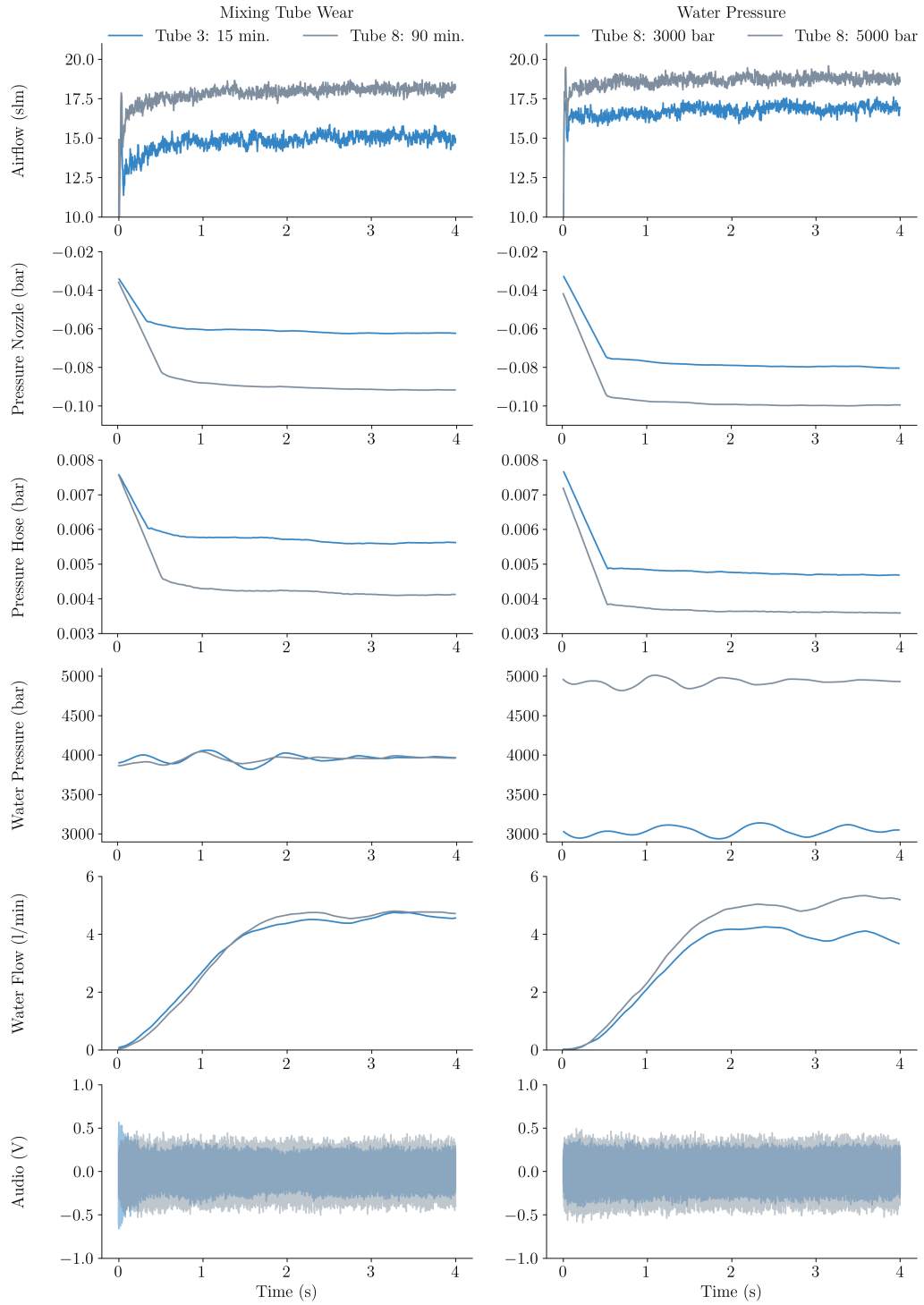
Figure 5.17: Raw data in the time domain of each sensor used during ATD data collection during Phase II of the main trial. The data is segmented from the beginning of the dwell cycle. The plots on the left compare the effect of mixing tube wear under 4000 bar water pressure, and the plots on the right compare the effects of water pressure on the sensors' response.
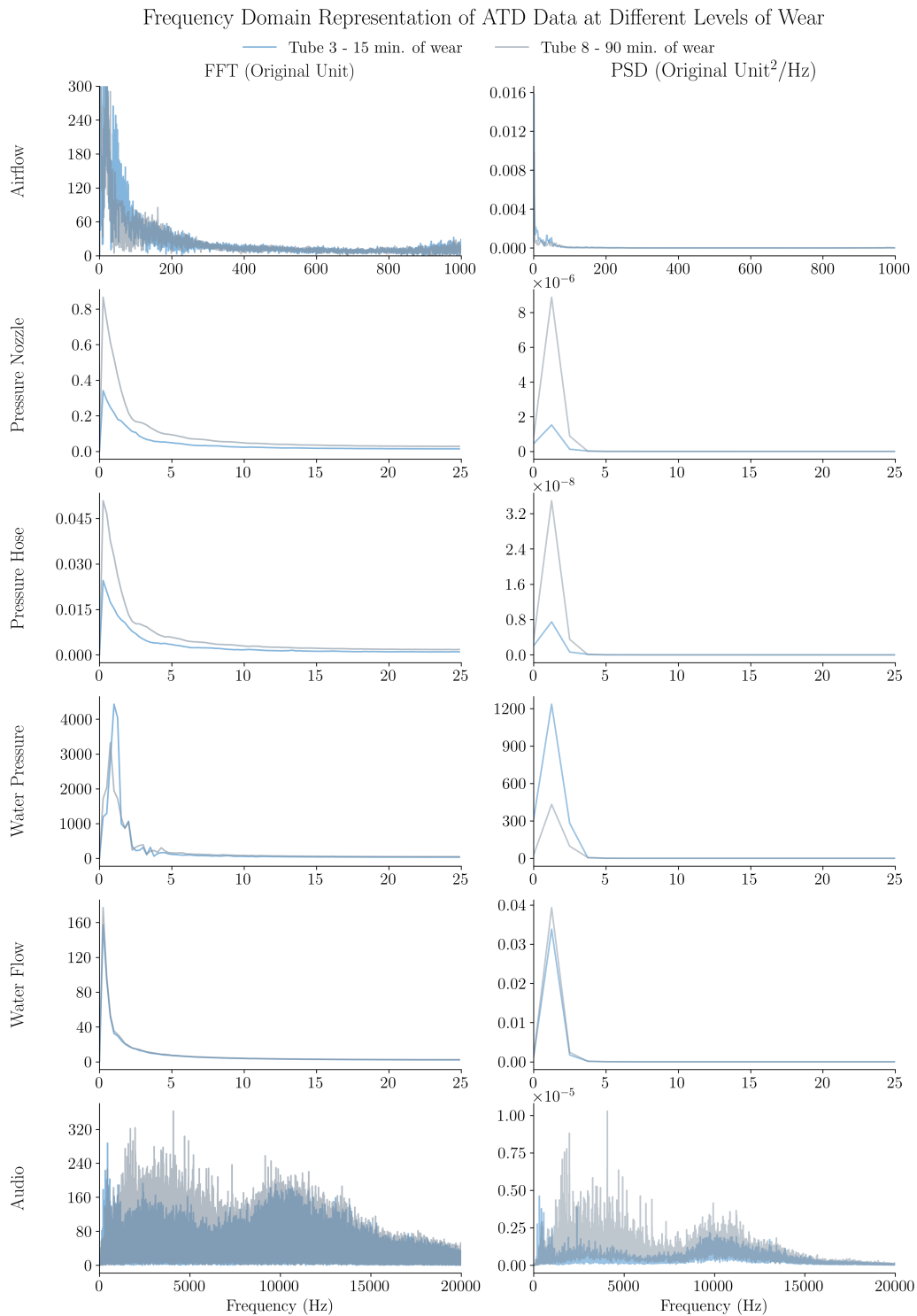
Figure 5.18: Raw data in the frequency domain over 4 seconds of recording for each sensor used during ATD data collection during Phase II of the main trial. The plots on the left show how the amplitude of each frequency varies with mixing tube wear for each sensor following FFTs, while the plots on the right display the PSD of each sensor calculated using the Welch method over 10 segments. For each sensor, the DC component of the signal was first removed prior to FFT application by subtracting the mean from each value.
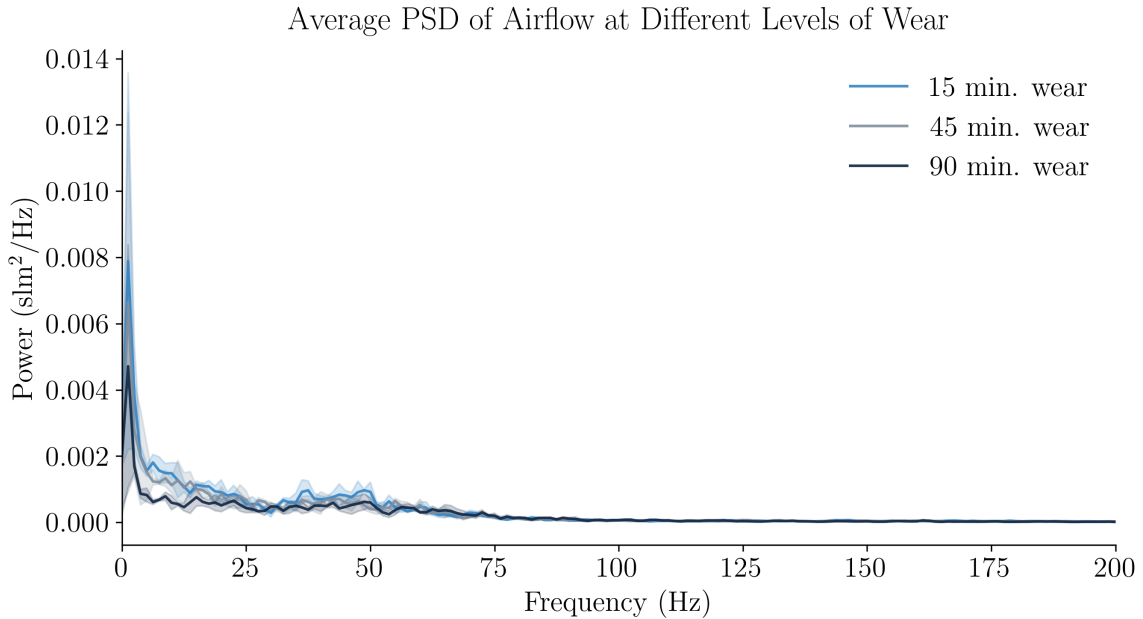
Figure 5.19: Variation in the airflow PSD with increasing mixing tube wear in the 0 - 200 Hz frequency range. The shaded region represents the error, which is 1 standard deviation of the data.

domain. In the time domain, central tendency features such as RMS, std dev, and mean, alongside maximum and minimum values, will be extracted. This simplification is adopted to avoid unnecessarily increasing the dimensionality of the data.

For Phase II of the main trial, airflow data was sampled at 2000 Hz. However, the majority of available data (from the preliminary trial and Phase I of the main trial) in this thesis had the airflow sensor sampled at 100 Hz. In Figure 5.18, the frequency domain data of the airflow sensor has the greatest variation in the 0-200 Hz range. Figure 5.19 looks at the variation in the airflow PSD in the 0-200 Hz frequency range. With changing wear, the greatest power difference is observed in the 0-50 Hz range, which can be obtained from a 100 Hz sampling rate. Figure 5.19 suggests that using a 100 Hz sampling rate for the airflow sensor will be sufficient for generating meaningful frequency domain features to monitor wear, with a higher sampling rate not required.

To summarise, wear data and raw sensor data were studied in the time and frequency domain. The wear was shown to be non-linear, with accelerated wear at the beginning and towards the end of mixing tube life. The wear rate was different between the two different AWJs used for data collection. Raw data suggested that the response of the applied sensors is water pressure and wear dependent. In the frequency domain, water flow, nozzle pressure, and abrasive hose pressure sensors

were less informative in comparison to airflow and audio sensors, which had a higher sampling rate.

5.3.2 Data quality and limitations

After presenting the raw data, validating the data quality before feature generation is important. This step is crucial in any research study as it ensures that the data collected is reliable, accurate, and consistent. Without proper data validation, the results obtained from data analysis could be misleading and potentially lead to incorrect conclusions. In the context of this thesis, data quality validation is especially crucial due to the issues faced during data collection. Namely, a part failure resulted in nozzle component replacement, as discussed in Chapter 3.

Inconsistencies in the airflow sensor data can be studied to assess data quality. Checking just one sensor provides a quick way to confirm the consistency of the collected data. The airflow sensor was chosen as airflow data was available for all trials and had no missing data.

According to the trial notes taken during data collection, the issues with the nozzle were first observed during the wear of mixing tube 5, after 30 minutes of wear. The issues continued when wearing mixing tube 3 and later conducting ATD and orifice change tests. Both mixing tubes 3 and 5 were the last to be worn during the main trial's Phase I, with mixing tubes 4 and 6-8 already worn. Data can be compared before and after the problem onset to look for inconsistencies.

Figure 5.20 compares how the average airflow evolved for each mixing tube with increasing wear time. Before discussing machine issues, it is worth acknowledging that overall (except for several recordings), the airflow data is more consistent between repeats and between pressures than seen for mixing tube 1 in the preliminary trial, as shown in Figure 4.4. This indicates that the suggested changes in Chapter 4 successfully improved the data collection process.

Regarding part issues, Figure 5.20 suggests that for mixing tube 5, the issue did not affect the airflow progression trend. However, data for mixing tube 3 appears more unstable. Starting from mixing tube 8, a drop off for several dwell recordings appears at 3000 bar water pressures. In addition, after wearing mixing tube 8, the airflow average appeared to decrease for the mixing tubes that followed. Potentially, the part issue started earlier than first observed. This may have impacted the collected data after wearing mixing tube 8.

Figure 5.21 compares the raw airflow signal at 3000 bar pressure for mixing tube 8 when the anomalies were first observed at 40 min. wear. The airflow data for the
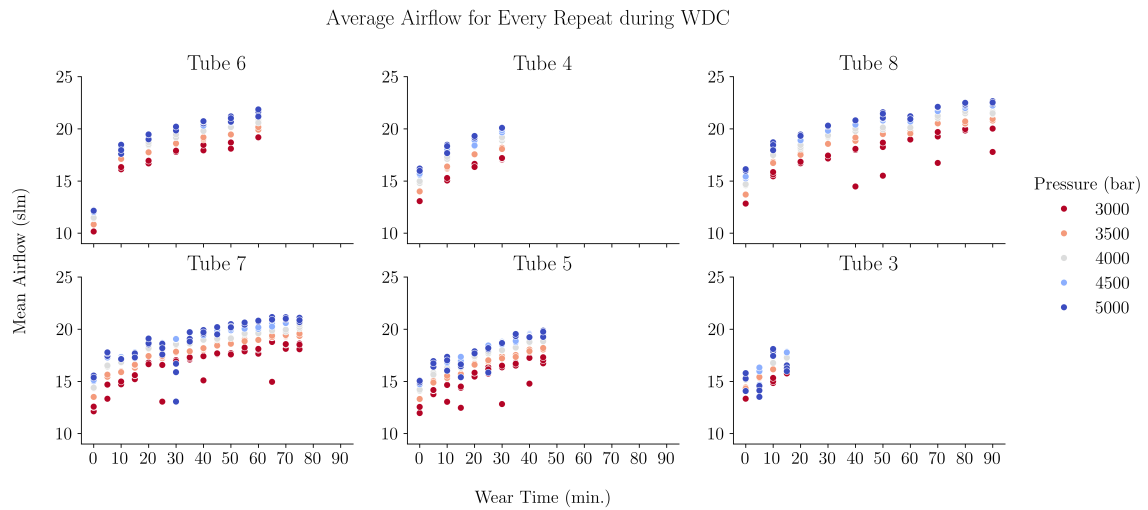
Figure 5.20: Average airflow for each dwell repeat at different water pressures taken during Phase I of the main trial WDC. The figures are arranged in trial wear order: 6, 4, 8, 7, 5, 3. The airflow average is calculated from the jet start over a 4-second segment. The water pressure values plotted are for input pressure, not measured pressure.

repeats at 40 and 50 minutes of wear gradually builds up to a stable plateau, unlike previously seen airflow data, which quickly reached a stable airflow. The issue is not water pressure related, as the water pressure data is similar between all repeats, as seen in Figure 5.21. The issue could be blockage or humidity-related. However, the consistency suggests it's likely a result of orifice holder and UHP seal damage, which was detected at a later stage. Wear of both components can affect the jet coherency as discussed in the literature review [25]. The issue got worse with time, supported by Figure 5.20, showing increasing average airflow inconsistencies with time on the machine. Eventually, the issue was observed during the trials when wearing mixing tube 5, with part failure occurring at the start of Phase II of the main trial.

While both the orifice holder and UHP seal were replaced, the data suggests the UHP seal was likely the culprit in the observed issues. The function of the UHP seal is to prevent high-pressure water from leaking out of the nozzle and to allow the pressure to be maintained during operation [25, 46]. UHP seal damage can result in pressure loss and inconsistencies. The integrity of the UHP seal is crucial for maintaining a consistent and reliable cutting process.

Examination of Figure 5.20 reveals that the data most affected was at the highest and lowest pressure values. High-pressure recordings were likely affected due to failures of the seal to maintain the required pressure. In the case of low pressures, it is plausible that since data collection was initially run at these levels, the pump

133

Raw Airflow and Water Pressure Data for Mixing Tube 8 at Different Wear Times
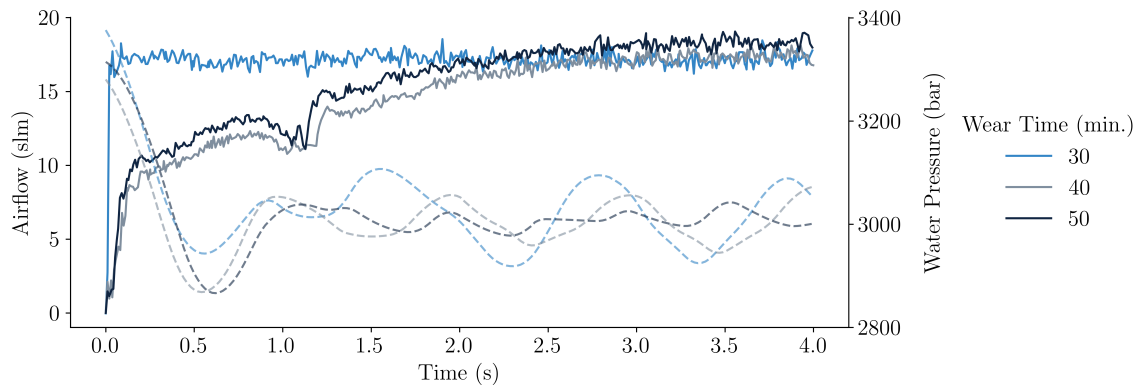
Figure 5.21: Raw airflow (solid line) and water pressure (dashed line) data during the first dwell repeats at 3000 bar pressure for mixing tube 8 at different wear times.

needed time to compensate for leaks before achieving stability for further recordings. Figure 5.21 showed the effect on the airflow at low pressures. Figure 5.22 presents raw airflow data at high pressures and accompanying water pressure and water flow rate data to check if either influences the observed airflow suction. Airflow instantaneously reaches a stable value for normal operation (mixing tube 8 at 30 min. of wear). For mixing tube 7, at the same water pressure, airflow takes around 100 ms before having a significant increase and around 1 s to reach a stable value. Despite similar wear time, there is also a significant difference in the average airflow between both recordings, with their water pressure and water flow rate similar. For mixing tube 5, the airflow data has erratic increasing and decreasing patterns and appears even more unstable.

The issues with the UHP seal introduced noise to the dataset as seen in Figures 5.20, 5.21 and 5.22. As the part was not replaced until complete nozzle failure after wearing mixing tube 9 during Phase II, all ATD and orifice change data of Phase I and partial WDC data were affected. The implication for TCM was that some unreliable data should be excluded to ensure the accuracy of subsequent analyses. Appendix J provides a detailed list of all excluded data.

From this analysis, the airflow sensor appears to offer good potential in detecting issues in the AWJ process. As discussed in the literature review, the airflow sensor is robust. It can be used in AWJ machining to detect mixing tube wear, orifice damage and misalignment, as well as blockages and leaks in the abrasive supply hose [5, 36–38]. The sensor may have further potential in fault diagnosis of the AWJ process.

As the orifice holder with the UHP seal were changed during data collection, it
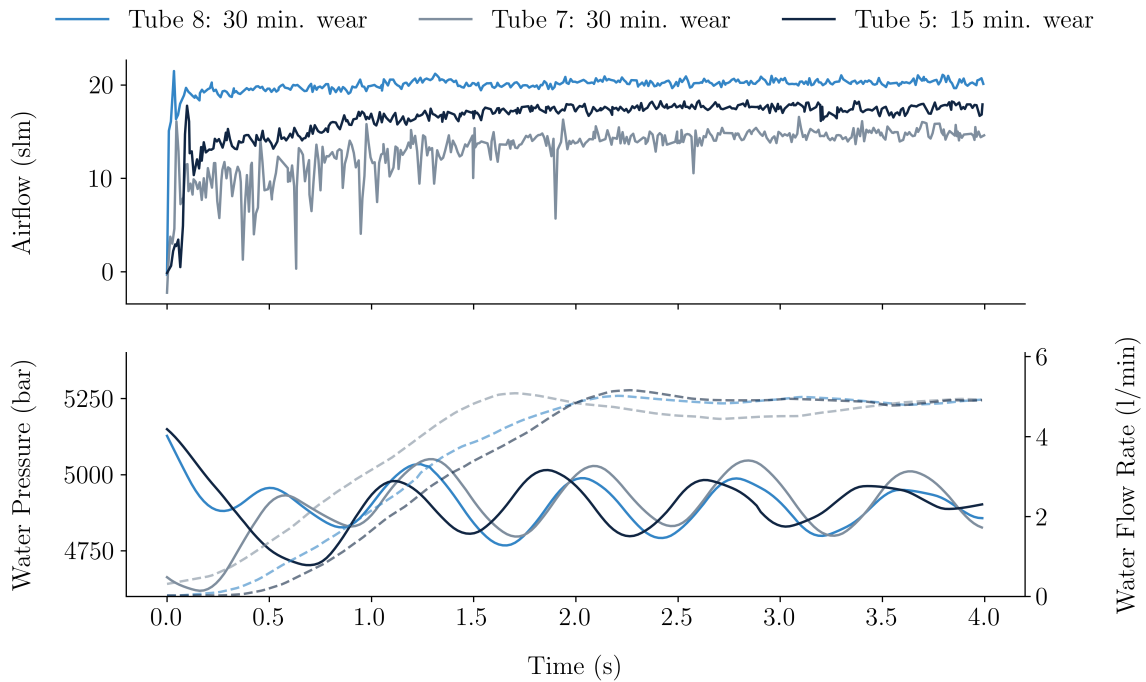
Figure 5.22: Two subplots, with raw airflow data (top plot) and raw water pressure (bottom plot solid line) and water flow data (lower plot dashed lined) visualised. Three repeats are selected at 5000 bar input water pressure. The first repeat for mixing tube 8 is used as an example of airflow data during normal operation. The second and third repeats are selected as examples of inconsistent airflow signals based on data in Figure 5.20.

is important to assess the effect of this change on the recorded signal. From Figure 5.16, it was evident that an AWJ machine change impacted the airflow signal. Figure 5.23 displays how the part change affected the recorded airflow signal. First, data is consistent, as seen by the low deviation between repeats throughout the data collection trials. However, the figure suggests that the part change significantly lowered the airflow, as a reduction is observed from Phase I WDC to Phase II ATD and from Phase I ATD to Phase II ATD. For TCM, this implies any developed model has to be able to account for data drift over time as the recorded signal may change with changing wear on other nozzle components, not just the change in wear of the mixing tube. The limitation of this observation is the lack of data to account for the effect of replacing the mixing tube on its airflow signal. Mixing tube 10 offers the only comparison, as its Phase II WDC and ATD data were collected after the part change. There is a small difference in airflow, but not as significant as the observed effect from the part change for other mixing tubes. The nozzle is designed for precise alignment

of the mixing tube using the collet and the nut, and this may have helped reduce the change in airflow when taking the tube on and off. Further work is required to assess the effect of replacing the mixing tube on the observed airflow signal.

Average Airflow of Each Repeat at 4000 Bar Pressure Per Data Collection Stage

Figure 5.23: Average airflow at 4000 bar water pressure for each recorded repeat at different dwell data collection stages including ATD and WDC to compare the effect of UHP seal and orifice holder part changes on the recorded airflow signal. For WDC data, the values at maximum wear time for that mixing tube are taken. During Phase I ATD cycles, mixing tubes 9 and 10 had undergone 0 minutes of wear.

Figure 5.23 also offers valuable insights into what affects the airflow signal. Mixing tube 11 had an exit diameter of 1.05 mm as seen in Figure 5.14, but its wear profile showed few signs of wear in Figure 5.12. In Figure 5.23, despite having a similar exit diameter as mixing tubes 5 (1.06 mm) and 3 (1.03 mm), it had a lower airflow rate. This suggests that the airflow response is not just exit diameter-dependent implying the sensor is suitable for tracking overall wear of the mixing tube, not just the exit diameter wear. The same applies to mixing tube 19, which had a larger exit diameter of 1.10 mm but an internal wear profile which appeared less worn compared to other mixing tubes of similar exit diameter, as seen in Figure 5.12. This data suggests that the airflow sensor may possibly not detect a larger exit diameter if the wear upstream is smaller than expected, which means mixing tubes might be harder to predict as worn even though their cutting performance may be affected. As the literature review suggested, an exit diameter increase reduces the cutting performance of a mixing tube [7, 13, 65, 67]. However, the effect on the cutting performance of these tubes requires further validation. Specifically, further work can investigate if cutting performance changes for the same exit diameter with changing wear upstream of the mixing tube.

Figure 5.24 compares the effect of changing the orifice and MC components on the observed airflow signal. After the literature review, it was expected that an orifice

with greater wear would increase airflow [3, 4]. Limited Phase I data suggests the orifice change led to a reduction in airflow signal, implying that the diamond orifice used during ATD and WDC had greater wear than the Ruby orifice replacing it. Although the diamond orifice was measured to have a slightly larger diameter (0.001 mm larger as identified in Figure 5.4) the observed airflow data may be unreliable due to significant nozzle performance instability and water leaking during Phase I orifice change runs. For the MC change in Phase II, replacing the part with a more worn component resulted in an airflow increase. As the wear of both parts can influence the signal, they should be considered in the evaluation strategy for the TCM system.
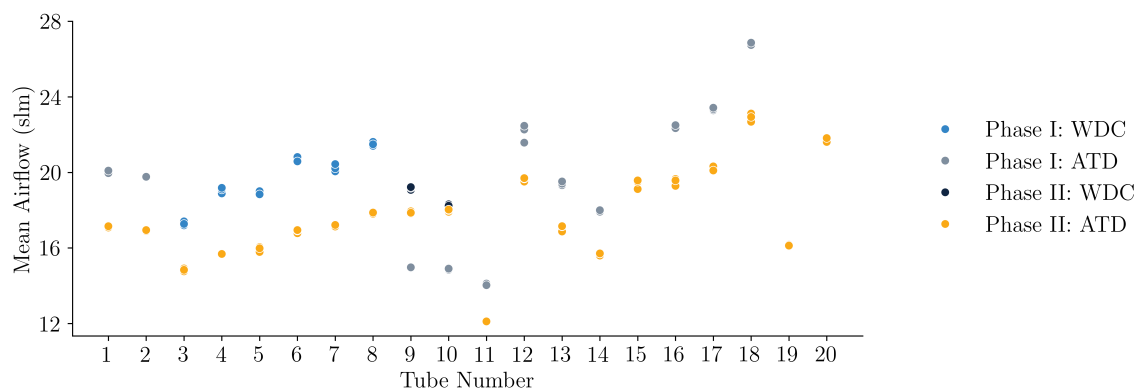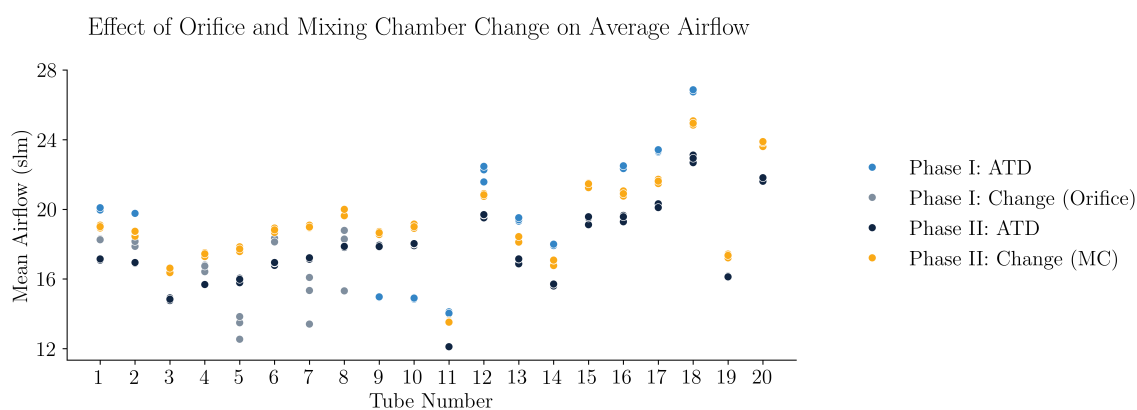

Figure 5.24: Average airflow at 4000 bar water pressure for each recorded repeat at different dwell data collection stages to compare the effect of nozzle part changes on the airflow signal. During Phase I ATD cycles, mixing tubes 9 and 10 had undergone 0 minutes of wear.

To summarise, the data quality was assessed by studying the changes in the airflow signal. Data collection improvements suggested at the end of Chapter 4 improved the consistency of the collected data. Raw data visualisation suggested that the first 0.5s of the recording may have to be removed during segmentation. The recorded airflow data also suggested that the monitored sensors' response changes from machine to machine, after part replacement and due to nozzle component wear. The length of mixing tubes, assuming a similar wear stage, does not affect airflow. Despite improvements to the data collection process, the raw data had inconsistencies. These were likely caused by wear on the orifice holder and UHP seal. The data most affected was at high and low pressures. A shift in the data was observed after the UHP seal and orifice holder were replaced. Based on a small data sample, the effect of taking a mixing tube on and off was not as significant, suggesting the data shift occurred due to the part change. As the recorded data magnitude shifted under multiple

circumstances, it is essential to account for possible domain shifts when developing a TCM system.

5.4 Data analysis overview

This chapter aimed to explore the additional collected data to validate the assumptions made after the literature review, to explore the raw data and to assess the data quality. First, abrasive and mixing tube wear analysis was carried out before presenting the raw sensor data and checking the data for inconsistencies.

The abrasive analysis confirmed the hypothesis after the literature review that Al_2O_3 is a suitable substitute for garnet abrasive due to similarities in shape, density and flow. Contrary to the literature review, and similar to garnet behaviour, Al_2O_3 abrasive particles were found to fragment during the mixing tube wear process [13, 58]. However, the collected Al_2O_3 abrasive particle sample may have been contaminated, so this requires further validation.

The two used orifices were found to be in similar condition, while the worn MC had substantial wear observed under a USB microscope. All mixing tubes had consistent wear patterns, without blowout wear on the tube exit and with a wave wear pattern on the internal profile, as expected for a "good" wear pattern described in literature [59].

Contrary to the observations in Chapter 4, the mixing tube wear trend was found to be non-linear. Accelerated wear occurred at the beginning and towards the end of mixing tube life. Similar to Chapter 4, the wear threshold of 10% exit diameter wear was crossed within the wear time range used.

All used sensors were seen to have a change in response with increasing wear. The data quality was improved after recommendations at the end of Chapter 4. However, due to nozzle component wear, data inconsistencies remained. The observed sensor magnitude was seen shifting with changing parts, nozzle component wear and when using separate AWJs.

The proposed data collection framework outlined in Chapter 3 was successful in building a comprehensive dataset on mixing tube wear while being feasible. However, due to the potential for data drift under varying circumstances, machine learning systems may struggle during application if data drift is not accounted for. The data validation strategy has to be carefully designed to account for possible changes in data distributions in order to assess the true potential of machine learning.

Chapter 6

Mixing Tube Wear Prediction

After collecting and analysing the data, the next stage is to predict wear. As observed in Chapter 4, machine learning performs well. However, simpler approaches, such as using linear models on tool wear time data, have the potential to outperform more complicated methodologies. In Chapter 4, the conclusions were limited by a small dataset. Different modelling approaches can be evaluated further with a more comprehensive dataset collected.

The main aim of this chapter is to understand whether the use of machine learning is feasible in predicting wear for mixing tubes worn using the same abrasive (Al_2O_3) and to test model generalisation performance on mixing tubes which were worn using a different abrasive (garnet). The goal is to first understand the machine learning potential on the accelerated trial data, before verifying performance on industry worn mixing tubes. The hypothesis is that machine learning will outperform time models on this larger dataset.

In Chapter 5, we observed variations in the AWJ data with changing conditions. For a developed TCM framework to be industrially relevant, the approach must demonstrate adaptability to shifts in data distributions, as these are likely to occur in practice. Therefore, the end of this chapter will address data drift. Specifically, whether it affects predictions and whether it can be mitigated. The hypothesis is that data drift affects performance and can be mitigated.

6.1 Evaluation strategy

Before predicting wear, it is first important to consider several problem design choices, including the problem type, metrics to use, validation strategies and model selection. Similar to Chapter 4, predicting mixing tube wear is carried out via both regression and classification. Via regression, the exact exit diameter can be predicted, which can

be useful for applying an offset during tool path compensation. With classification, it is possible to test if a mixing tube should be replaced. Of course, the regression task could also be used to assess the state of the tool; however, if the regression models struggle, classification may offer an alternative.

RMSE and F1 score were chosen as the metrics to assess model performance for regression and classification, respectively. RMSE is used to penalise large errors, and F1 score is used to account for the imbalance in the dataset between worn and unworn data.

A breakdown of all available data after the exclusion of several recordings is shown in Table 6.1. Each recording is for a singular dwell cycle repeat. The total recordings per state at the bottom of the table show the imbalance between worn and unworn samples. A total of 44 data points were excluded, due to operator errors and data unreliability, to avoid them affecting the evaluation process. The "Change" data from Phase I of the main trial was also removed, due to poor AWJ condition. For a detailed list of all excluded data please refer to Table J.1 in Appendix J.

Due to the observed changes in the data with part changes, the validation strategy requires careful consideration. The assumption is that data drift is not present for testing model performance. Therefore, train and test data should come from the same distribution, in other words, from mixing tubes worn using the same nozzle components of the same state. The train and test splits are presented in Table 6.2, with sample counts per split presented in Table 6.3.

For evaluating the performance of machine learning on data collected under the same conditions, dataset 1 was used. The mixing tubes were split to account for target imbalance while providing enough mixing tubes in both sets for robust evaluation. All mixing tubes were of the same length, worn using the same abrasive (Al_2O_3), worn and tested on the same machine without any part changes.

For evaluating generalisation performance datasets 2-3 were used. Mixing tubes worn using Al_2O_3 abrasive and the accelerated wear approach formed the training set while mixing tubes worn using garnet formed the test set. As a part change occurred during the trials, two datasets were created to evaluate generalisation performance, as the data was available and there was also additional sensors added in Phase II of the main trial, which could be used in dataset 3.

Table 6.1: Total recordings per mixing tube making up the final dataset, split by trial, data collection event and unworn (0) and worn (1) mixing tube states. The "Change" event identifies the data collected after an orifice or MC part change.

Trial:	Preliminary		Main - Phase I				Main - Phase II					
Event:	WDC		WDC		ATD		WDC		ATD		Change	
Tool state:	0	1	0	1	0	1	0	1	0	1	0	1
Mixing Tube												
1	74	30	0	0	0	15	0	0	0	15	0	15
2	75	30	0	0	0	15	0	0	0	15	0	15
3	0	0	53	0	0	0	0	0	15	0	15	0
4	0	0	59	0	0	0	0	0	15	0	15	0
5	0	0	144	0	0	0	0	0	15	0	15	0
6	0	0	90	15	0	0	0	0	0	15	0	14
7	0	0	158	73	0	0	0	0	0	15	0	15
8	0	0	87	58	0	0	0	0	0	15	0	15
9	0	0	0	0	0	15	59	43	0	15	0	15
10	0	0	0	0	0	15	54	45	0	15	0	15
11	0	0	0	0	15	0	0	0	15	0	15	0
12	0	0	0	0	15	0	0	0	15	0	15	0
13	0	0	0	0	15	0	0	0	15	0	15	0
14	0	0	0	0	15	0	0	0	15	0	15	0
15	0	0	0	0	0	0	0	0	15	0	15	0
16	0	0	0	0	0	15	0	0	0	15	0	15
17	0	0	0	0	0	15	0	0	0	15	0	15
18	0	0	0	0	0	14	0	0	0	15	0	15
19	0	0	0	0	0	0	0	0	0	15	0	15
20	0	0	0	0	0	0	0	0	0	15	0	15
Total per state	149	60	591	146	60	104	113	88	120	180	120	179
Total per event	209		737		164		201		300		299	
Total per trial	209		901				800					
Total						1910						

Table 6.2: Break down of data making up the training and test sets. Dataset 1 is for testing performance on Al_2O_3-worn mixing tubes only. Datasets 2 and 3 are for evaluating generalisation performance on garnet-worn mixing tubes. Dataset 2 uses data before the worn nozzle component change, and Dataset 3 uses data after the worn nozzle component change.

Dataset No.	Train/Test Set	Mixing tubes	Trial	Event
1	Train	5, 6, 8	Main - Phase I	WDC
1	Test	3, 4, 7	Main - Phase I	WDC
2	Train	3-8	Main - Phase I	WDC
2	Train	1, 2, 9, 10	Main - Phase I	ATD
2	Train	9	Main - Phase II	WDC
2	Test	11-20	Main - Phase I	ATD
3	Train	10	Main - Phase II	WDC
3	Train	1-10	Main - Phase II	ATD
3	Test	11-20	Main - Phase II	ATD

Table 6.3: Total samples making up the train and test sets for each evaluated dataset. The worn column indicates the percentage of samples with the exit diameter greater than or equal to 1.10 mm.

Dataset No.	Train/Test Set	Total Samples	Worn
1	Train	394	19%
1	Test	343	21%
2	Train	899	28%
2	Test	104	42%
3	Train	249	60%
3	Test	150	50%

6.2   Machine learning pipeline

In order to predict mixing tube wear, the following pipeline was used:

1. Pre-process the raw sensor data.

2. Extract feature and build a tabular dataset.

3. Drop identified unreliable data.

4. Split the data into training and test sets.

5. Handle missing values.

6. Reduce dataset dimensionality.

7. Select training algorithm.

8. Tune hyperparameters of the selected algorithm on training data via stratified CV.

9. Train the model on the full training set using the best parameters identified during hyperparameter tuning.

10. Make predictions on the test data and evaluate performance using RMSE metric for regression and F1 score for classification.

Throughout the pipeline, the chosen CV strategy, when used, included a stratified 5-fold CV, stratified on wear time for regression and on the target for classification. In addition, standardisation of data was applied throughout the pipeline and was done using training data only to avoid data leakage. Finally, where applicable, a random seed for model initialization was set to ensure all results were reproducible.

During data pre-processing, the data was segmented to the desired duration after a set skip time, and if chosen, the data was also denoised via a rolling mean window. For airflow, the data from Phase II of the main trial was also resampled to a 100 Hz sampling rate, following observations in Chapter 5.

During Chapter 4, it was found that denoising airflow data can help classification. For segmenting the data, a 4-second duration performed best during CV with a 0-second skip time at the start of the dwell cycle. In Chapter 5, it was identified that using a skip time of 0.5s to avoid inconsistencies at the start of the dwell cycle should be tested as well. The effect of using a skip time of 0.5s and denoising the raw airflow

data on the larger dataset for predicting mixing tube wear will be explored later in this section.

For feature extraction, both time and frequency domain features were created, as well as several additional features. A summary of all created features is given in Table 6.4. Only basic time and frequency domain features were created for machine sensors following the data analysis in Chapter 5. For the preliminary trial data, no frequency domain features were extracted for machine data due to the low sampling rate. These values were counted as missing. Not all sensors were available for each trial, as indicated by Table 3.4 in Chapter 3, which further contributed to missing values in the created dataset. Ratio features were created as to help capture interactions between two features which can be difficult for models to learn.

Once the data was tabulated, there was some missing data. In order to use this data for machine learning, the missing values had to be handled. One option was to drop all the features with missing data. However, if only a small percentage of data is missing, it would mean removing a lot of potentially useful information for the models. The alternative to dropping this data was to impute the missing values. There are multiple ways of doing this, for example, by using the mean of that feature within the training set or using an algorithm such as KNN for imputation [100]. The choice was dataset-dependent. For dataset 1, where a large percentage of nozzle pressure data was missing, the choice was to drop this data. For datasets 2-3, KNN imputation was applied.

With the features extracted, the next step of the pipeline was to reduce the data dimensionality. Feature selection can be carried out at this stage. Following the results of Chapter 4, the LASSO algorithm was used to carry out automatic feature selection. In addition, PCA was explored together with Kernel PCA to assess whether these alternatives were better suited for the task in comparison to LASSO.

When using LASSO for feature selection, similar to Chapter 4, the best alpha parameter was first selected via CV performance. When the alpha parameter was selected, the LASSO algorithm was fit on the whole training set before removing features with a coefficient of 0. Sample CV performance on Dataset 1 training set with changing alpha parameter is presented in figure 6.1. While LASSO may keep multicollinear features as seen in Chapter 4, it also can offer performance improvement as seen in Table 4.7, is faster to implement and can be used within a pipeline for different datasets unlike manual feature selection.

LASSO was carried out on regression target only, with selected columns chosen for both regression and classification. While this approach creates a unified feature

Table 6.4: Extracted features from the provided dataset for predicting mixing tube wear. Machine sensors include nozzle pressure, abrasive hose pressure, water pressure and water flow sensors (not all are available for each trial as indicated in Chapter 3).

| | Sensor | | |
Time Domain Features	Airflow	Machine	Audio
Mean	✓	✓	
Maximum	✓	✓	
Minimum	✓	✓	
Std Dev	✓	✓	
RMS	✓	✓	
Skewness	✓		
Kurtosis	✓		
Peak to Peak	✓		
IQR	✓		
Shape Factor	✓		
Impulse Factor	✓		
Crest Factor	✓		
Clearance Factor	✓		
RMS Energy			✓
Zero Crossing Rate			✓
Mean Absolute Amplitude			✓
Peak Absolute Amplitude			✓
Frequency Domain Features			
Total Power	✓	✓	✓
Power Peak	✓	✓	✓
Dom Freq	✓		✓
Power skew	✓		✓
Power kurt	✓		✓
Power low freq ratio	✓		✓
Power med freq ratio	✓		✓
Power high freq ratio	✓		✓
Spectral flatness	✓		✓
Shannon entropy	✓		✓

Ratio features: Pressure nozzle to airflow, water flow to airflow, water pressure to water flow, water pressure to airflow, water pressure to pressure nozzle, water pressure to pressure abrasive hose.

Additional features: Tube length, set input pressure, pressure change between abrasive hose and nozzle
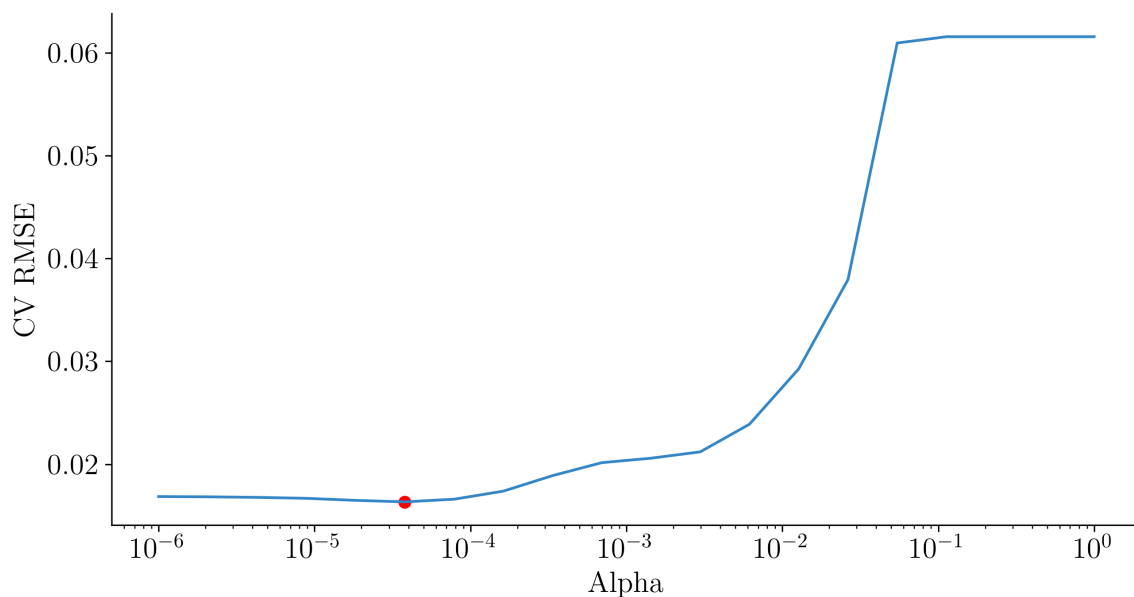
CV RMSE Score with Changing Alpha Parameter

Figure 6.1: LASSO CV performance on dataset 1's training set. The performance is shown for pre-processed data with a 4-second segment and 0-second skip time. 20 alpha values were evaluated in total, spaced evenly on a log scale between 1 and 0.000001. The alpha value which achieved the best CV performance on dataset 1 is marked by a red dot on the plot.

set, improves interpretability, simplifies the feature selection process and ensures consistency across both tasks, it has some limitations. It assumes common information between tasks, while features that are important for predicting the regression target are not necessarily the same as those important for classification, potentially limiting classification performance. Nevertheless, as seen in Table 4.7 in Chapter 4, this approach can still improve the performance of classification algorithms over manual feature selection; therefore, it was applied in this chapter.

For verification purposes, LASSO was also tested for feature selection on a classification target to achieve an optimal F1 score. The predictions were converted to binary classes using a threshold of 0.5 after applying a sigmoid function to the predictions, which compressed predictions between 0 and 1. The best F1 score was achieved using the same alpha value as for regression, resulting in the same features being picked for classification, further supporting the use of one unified feature selection approach for both regression and classification.

PCA was tested for dimensionality reduction due to the large feature space as indicated by Table 6.4 and the popularity of the method in dimensionality reduction

applications [44]. Kernel PCA was trialled, too. Unlike PCA, it is capable of capturing non-linear relationships in the data by using a kernel function [44]. Kernel PCA is, therefore, suitable for datasets with complex non-linear structures. The performance of MLP in Chapter 4 suggested this might be the case for this dataset.

When using PCA techniques, a key parameter to select is the number of components and the number of dimensions to reduce the data to. An example of PCA in use on dataset 1 is shown in figure 6.2. When selecting the number of components, it is common to examine the cumulative explained variance as a function of the number of components. The final selected number should capture a sufficiently high percentage of the total variance, often aiming for a threshold of at least 95% [44].
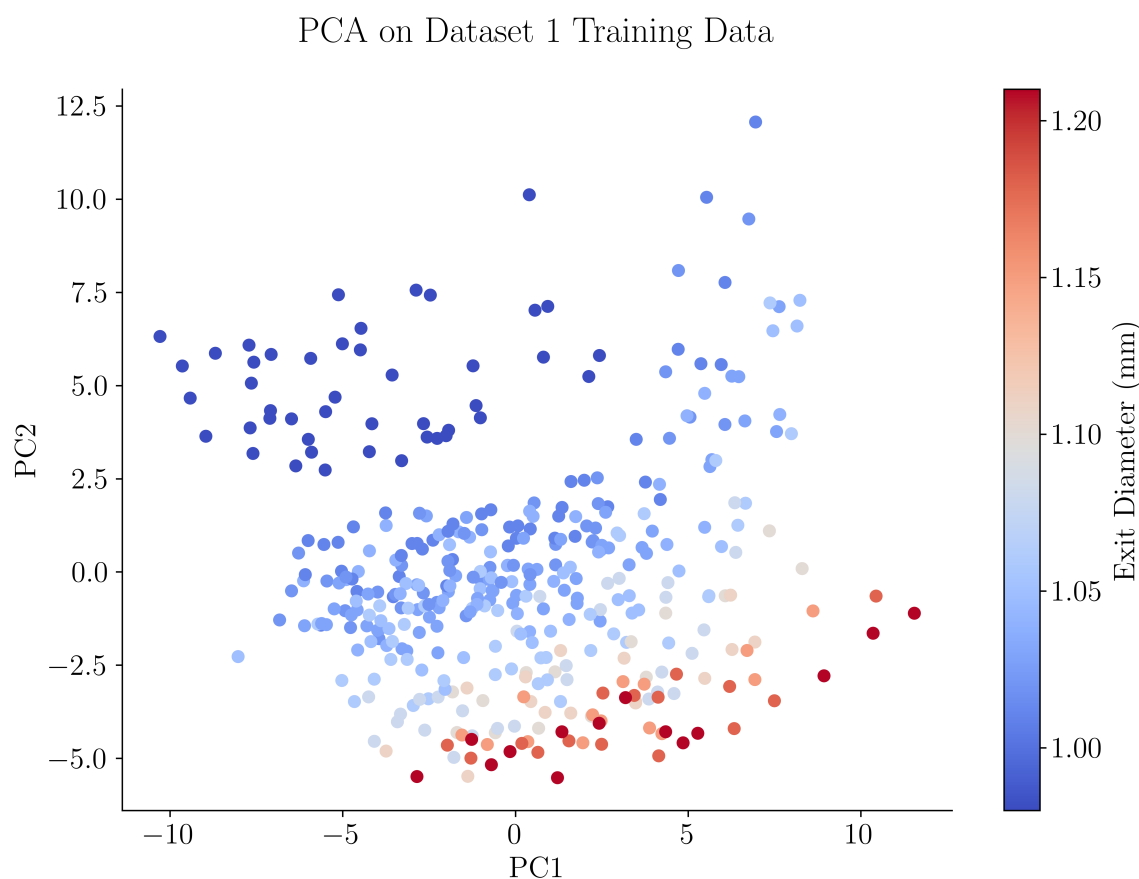
Figure 6.2: PCA visualisation of 2 principal components calculated using scikit-learn's library, employing default parameters and random state 42, on dataset 1 [131]. The data is coloured by the exit diameter of the mixing tubes.

The detailed pipeline steps have several changeable variables for pre-processing and dimensionality reduction. Before conducting time-consuming hyperparameter optimisation, each approach was compared on training data from dataset 1. The

comparison was carried out to select one approach to use at each pipeline stage. RF algorithm was chosen for use during comparison with n_estimators (number of trees parameter) set to 1000. RF was selected as it is less prone to overfitting provided enough trees are used [173].

Figure 6.3 provides the variable selection results. LASSO outperformed PCA and Kernel PCA for regression and classification and will be used for dimensionality reduction within the modelling pipeline for the remainder of this thesis. The performance between all tested pre-processing steps was similar for both regression and classification. The decision was made to use a dataset with 0.5 second skip time at the beginning of recordings to avoid unreliable data caused by pump issues, for example as seen in figure 5.16, affecting generated features. Figure 6.3 further supports the presence of complex non-linear relationships in the data, as Kernel PCA outperformed PCA in both regression and classification tasks. This may explain why, in Chapter 4, most best-performing algorithms were non-linear models.
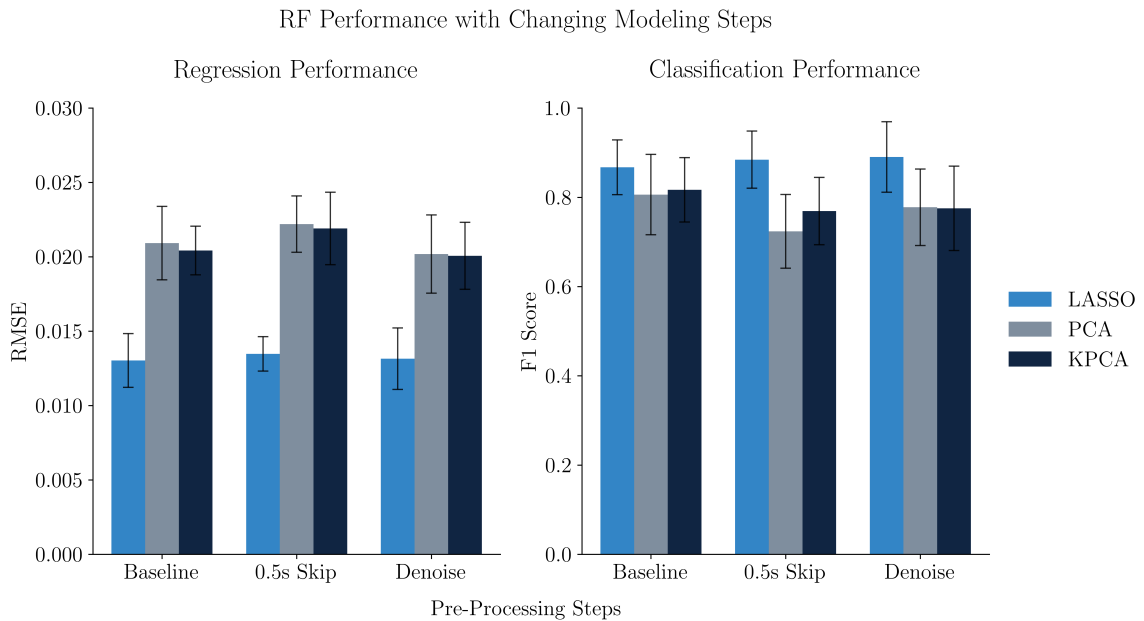
Figure 6.3: Performance of RF algorithm averaged over 5 CV folds for regression (left) and classification (right) under changing pre-processing steps and dimensionality reduction methods. The uncertainties are represented by the standard deviation of the CV scores.

RF, LGBM, KNN and LogR (for classification only) were the selected models to apply based on the results and discussion in Chapter 4. A hybrid approach of using machine learning models with wear time as a feature was also added to the analysis,

to assess the benefit of recording wear time of the mixing tubes when sensor-data is also available.

In addition to the selected models and similar to Chapter 4, ensembling of models was used to try and improve prediction performance on the test data. While ensembling via prediction averaging offered potential in the preliminary investigation in Chapter 4, more advanced ensembling via stacking was also tested. Stacking was carried out using the StackingRegressor and StackingClassifier classes in Python provided by the scikit-learn library [131, 174, 175]. The final estimators in the stacking algorithm were RF for regression and LogR for classification. Ensembling was done using all the tested models - RF, LGBM and KNN for regression and RF, LGBM, KNN and LogR for classification.

The final pipeline step to discuss is hyperparameter tuning. Hyperparameter tuning was carried out as the default settings offered by common machine learning libraries may not yield the best model performance [149, 152, 153]. There are various approaches to hyperparameter tuning, as discussed in the literature review [132, 149, 154, 155]. However, the state-of-the-art choice is to use Bayesian optimization [132, 154]. Bayesian optimisation via the Gaussian Process can be implemented using the scikit-optimize Python library and the BayesSearchCV class [176, 177]. A full list of the Python libraries used in this thesis is provided in Appendix I. Within BayesSearchCV, the F1 score and RMSE metrics were optimised using CV for each algorithm to find the best parameters. When optimising the hyperparameters, only the training data was used. The optimisation was run across 100 iterations. This provided a good balance for exploration (searching across the hyperparameter space) and exploitation (focusing on promising regions) without requiring an unfeasible amount of computer resources and time.

When choosing parameters to tune, selecting the most impactful parameters is important to avoid having a large parameter space to optimise. For RF, a higher number of trees (n_estimators in scikit-learn) will achieve better results [131, 132, 178]. However, this comes at a computational cost, and beyond a certain threshold, there are diminishing returns [178]. For LGBM, only a few parameters are most impactful given a fixed number of iterations and learning rate [132, 179]. Therefore, the optimal number of trees and iterations were first calculated for RF and LGBM on dataset 1 via CV on the training set to reduce the parameter search space before conducting hyperparameter tuning. Figure 6.4 presents the results. The results suggest that for RF, setting n_estimators to 100 is sufficient, while for LGBM, 500 was chosen to ensure the model was not underfitting the data.
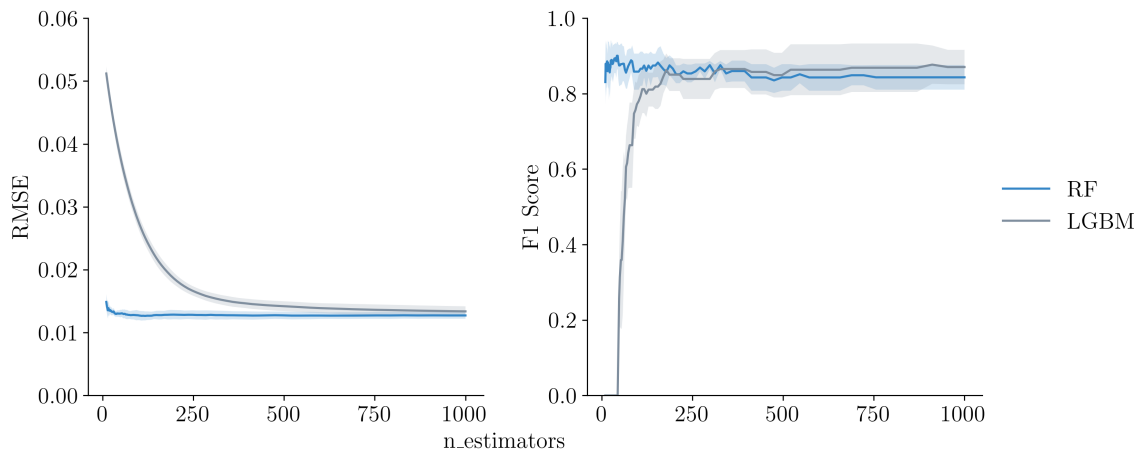
Figure 6.4: CV performance for regression (left) and classification (right) of RF and LGBM algorithms with increasing n_estimators parameter (trees/iterations). For LGBM, the learning_rate was set to 0.01. The shaded region represents the standard deviation of the 5-fold CV scores.

With the number of trees and iterations selected, the remaining hyperparameters to tune and their corresponding search spaces are provided in Table 6.5. Several parameters were introduced for classification to compensate for the target imbalance present in the data. For RF, the hyperparameters were chosen using a detailed chapter on hyperparameter tuning of RF in a book by Banachewicz et al. and a publication by Probst et al. which agreed with Banachewicz et al. on the most important parameters to tune [132, 178]. For LGBM, the book by Banachewicz et al. was again used, together with an article by Ozaki on tuning LGBM [132, 179]. In order to prevent over-fitting, the LGBM documentation was referred to, with num_leaves, min_data_in_leaf and max_depth added to the hyperparameters-to-tune list [180]. For tuning KNN, the scikit-learn documentation was referenced together with a publication by Yang et al., with parameter k (the number of nearest neighbours) identified as the most crucial hyperparameter [131, 154]. Finally, for LogR, the publication by Yang et al. and the book by Banachewicz et al. were used, with the coefficient "C" being an essential parameter to tune, which determined the regularisation strength of the model [132, 154].

With the machine learning pipeline outlined, the next stage was to feed the selected datasets and machine learning algorithms through the pipeline to select features using the LASSO algorithm and fine-tune each model on each training set before

Table 6.5: Summary of hyperparameters and search spaces tuned via Bayes optimisation for each algorithm. The "Class. Only" column indicates hyperparameters specific to classification.

Model	Parameter	Class. Only	Search Space
RF	min_samples_leaf		Integers 1 - 1000
RF	max_features		"sqrt", "log2", None
RF	bootstrap		True, False
RF	class_weight	✓	"balanced", "balanced_subsample", None
LGBM	feature_fraction		Real numbers 0.01 - 1.0
LGBM	num_leaves		Integers 2 - 512
LGBM	min_data_in_leaf		Integers 1 - 300
LGBM	bagging_fraction		Real numbers 0.01 - 1.0
LGBM	bagging_freq		Integers 0 - 10
LGBM	lambda_l1		Log scale between $1e^{-8}$ - 10
LGBM	lambda_l2		Log scale between $1e^{-8}$ - 10
LGBM	max_depth		Integers 1 - 16
LGBM	min_gain_to_split		Real numbers $1e^{-3}$ - 15
LGBM	max_bin		Integers 32 - 255
LGBM	scale_pos_weight	✓	Log scale between $1e^{-6}$ - 500
KNN	n_neighbors		Integers 1 - 100
KNN	weights		"uniform", "distance"
KNN	p		Integers 1 - 5
KNN	algorithm		"ball_tree", "kd_tree", "brute"
LogR	C		Log scale $1e^{-3}$ - 4
LogR	penalty		"l2", None
LogR	solver		"lbfgs", "liblinear"
LogR	max_iter		Integers 50 - 1000
LogR	class_weight	✓	"balanced", None

making predictions.

6.3 Prediction performance under the same wear conditions

TCM performance was first evaluated on data collected under the same conditions to understand the machine learning performance potential before applying the models on tubes worn using a regular wear approach. Figure 6.5 presents the results for dataset 1. Multiple modelling approaches are used, including different algorithms, ensembling methods, simple wear time-based methods, hyperparameter optimisation and adding the wear time feature to machine learning algorithms. For regression, performance improved with the new and larger dataset in comparison to the preliminary results seen in Chapter 4. LGBM was the best-performing model. Classification performance was lower compared to the preliminary performance, and LogR remained the clear best-performing algorithm.

Model performance on Dataset 1 (Identical Wear Conditions between Train and Test Set)
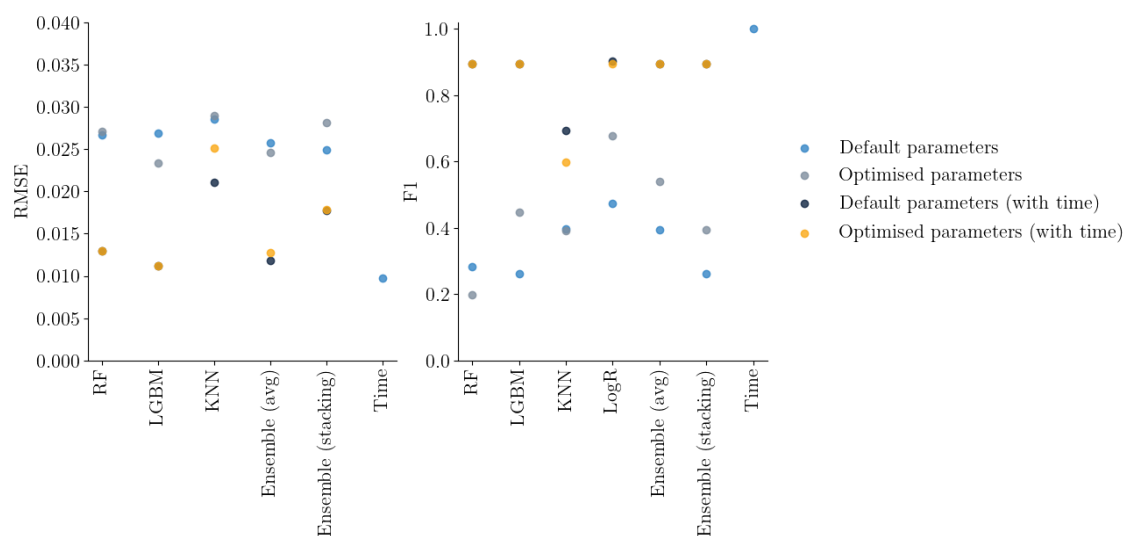
Figure 6.5: Machine learning performance on dataset 1, for regression (left) and the mixing tube state classification (right) with different modelling approaches. Ensemble (avg) refers to prediction averaging ensembling, while ensemble (stacking) involves using a stacking algorithm.

To help interpret the results and better understand why performance for regression improved and decreased for classification, it could be useful to do an error analysis on the best-performing algorithms. Figure 6.6 shows the true and predicted exit diameters. The model appears to be under-predicting the exit diameter. Predictions deviate the most for mixing tube 7 at higher exit diameters. The model also under-predicts for mixing tube 3 while over-predicting for mixing tube 4. The training

dataset was made up of mixing tubes 5, 6 and 8, with mixing tubes 6 and 8 having higher airflow at the same exit diameters than mixing tubes 3 and 7 as suggested by Figure 5.20 in Chapter 5. This noise, likely caused by the onset of the part issue discussed in Chapter 5, may have influenced the results due to slight data drift. Predictions at higher exit diameters appear most affected. The confusion matrix in Figure 6.7, produced using LogR predictions for the classification task, appears to suggest that this deviation, especially for the larger exit diameters, may have impacted classification, as the model begins making errors on "worn" mixing tube dwell recordings. Greater target imbalance may have also affected the performance of the classification algorithm. Therefore, while performance decreased for classification, it was likely affected by the present part issue. To overcome this, data drift mitigation strategies may be appropriate in further work.

Predicted vs Actual Exit Diameter on Dataset 1 using LGBM
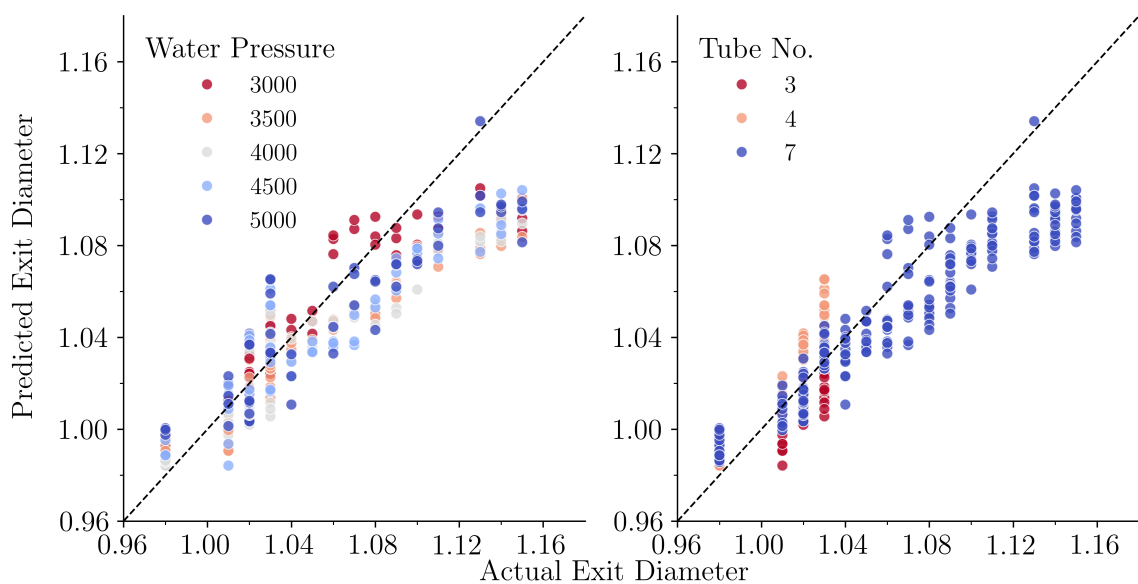
Figure 6.6: LGBM predicted versus actual mixing tube exit diameters per dwell cycle, shaded by water pressure (left) and mixing tube number (right).

Figure 6.5 suggests hyperparameter optimisation improved performance for the strongest algorithms and made a significant impact on classification in particular. For several models, optimisation lowered performance. This appears to have impacted KNN and RF algorithms in particular. Figure 6.8 depicts how each model converged over the 100 iterations to optimised parameters. The plot suggests that enough iterations were used for tuning both RF and KNN algorithms. The lack of

153
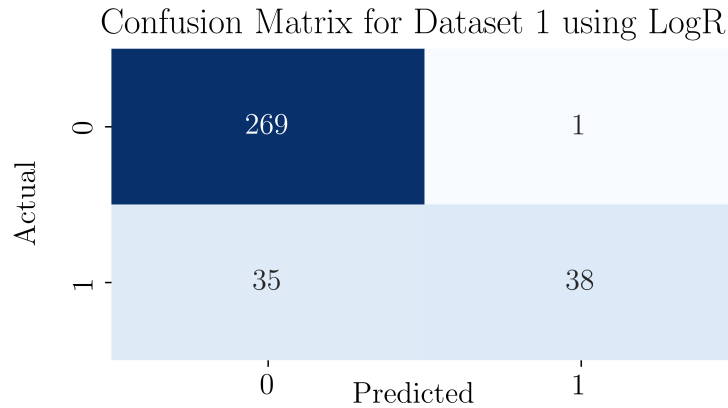
Figure 6.7: Confusion matrix of predicted and actual mixing tube states, with 1 denoting the exit diameter wear threshold of 1.10 mm being exceeded.

performance may be due to overfitting, or due to providing an insufficient parameter search space for exploration. LGBM, for example, which had a more in-depth search space, appears to have continued finding performance improvement with a greater number of iterations. For classification, every algorithm converged early, and LogR got a maximum F1 score on the first iteration.
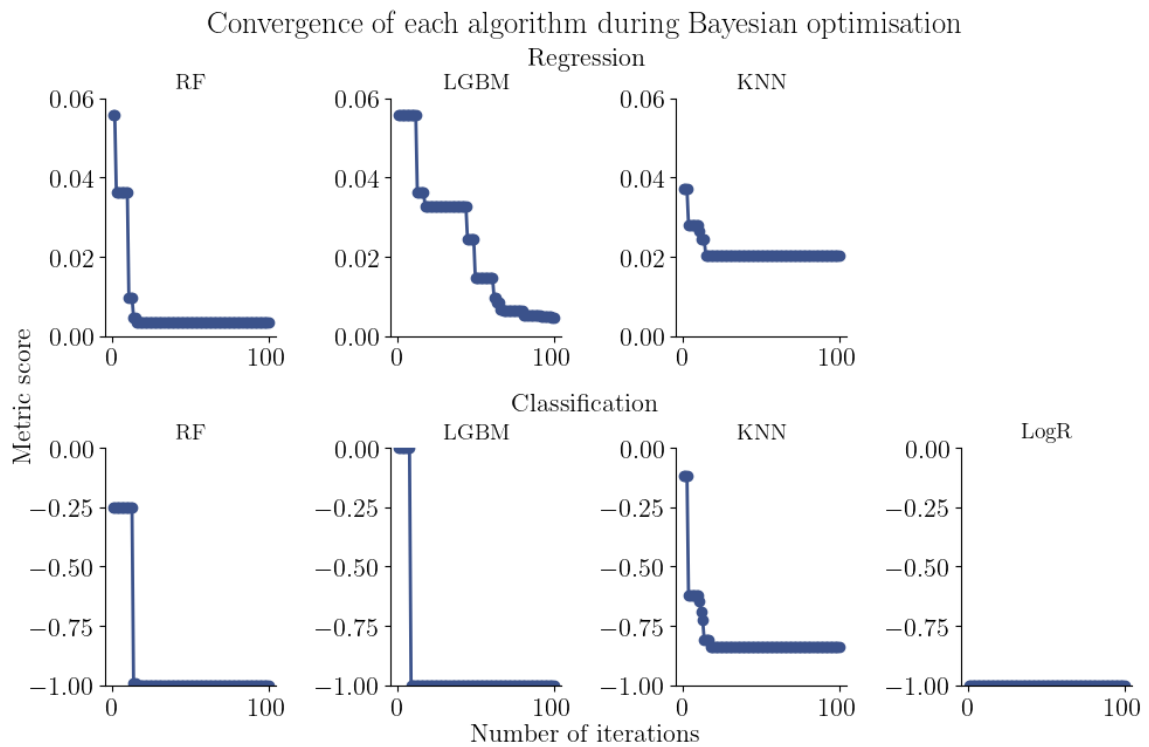
Figure 6.8: Bayesian optimisation convergence plots for each algorithm when optimised on the training set of dataset 1.

Model ensembling improved regression performance without model tuning, as seen in Figure 6.5. However, tuned LGBM outperformed both ensembling approaches. If hyperparameter tuning is not carried out, the results suggest ensembling predictions of multiple models either through stacking or averaging is suitable to achieve a small boost in regression performance. However, despite requiring lower training time due to the absence of tuning, the potential interpretability of the modelling method decreases as multiple models (and potentially the stacking algorithm) require interpretation instead of a singular model. Therefore, for regression, the use of a singular model may be preferred whether the models get tuned or not. For classification, LogR outperformed ensembling approaches.

Similar to Chapter 4, basic approaches using a singular wear time feature outperformed more complex methodologies despite a larger dataset being provided and the algorithmic performance of best models being improved via tuning. The result is significant, as it implies a TCM system can be developed for the AWJ system, capable of tool path compensation and tool state classification by simply recording the time the mixing tubes are worn for. Even when the time feature is added to the machine learning feature space, machine learning is outperformed by the simpler approaches, contradicting the results in Chapter 4. This result goes against the initial hypothesis that machine learning approaches would outperform time-based methods. The results are limited, as performance on regular wear trial tubes was not investigated.

6.4 Model generalisation to regular wear trial mixing tubes

While time recording appears to be a good way to start TCM of mixing tube wear, machine learning methods utilising inexpensive sensors may still hold value for AWJ users. Especially when the time of mixing tube use is not recorded. Datasets 2 and 3, for which wear time data was unavailable, can be used to assess generalisation performance to regular wear mixing tubes. The generalisation results are presented in Figure 6.9. Optimised LGBM was used for regression, and optimised LogR was used for classification tasks, with feature selection and hyperparameter optimisation performed from scratch on new training data. LGBM and LogR were selected as they were the strongest performers for their respective tasks on the accelerated wear trial data in Figure 6.5. Due to the presence of missing data for different sensors during data collection, missing data was imputed. KNN imputation was selected as

the preferred method. However, other methods were also tested to compare their performance.

Model generalisation to mixing tubes worn using regular wear trials
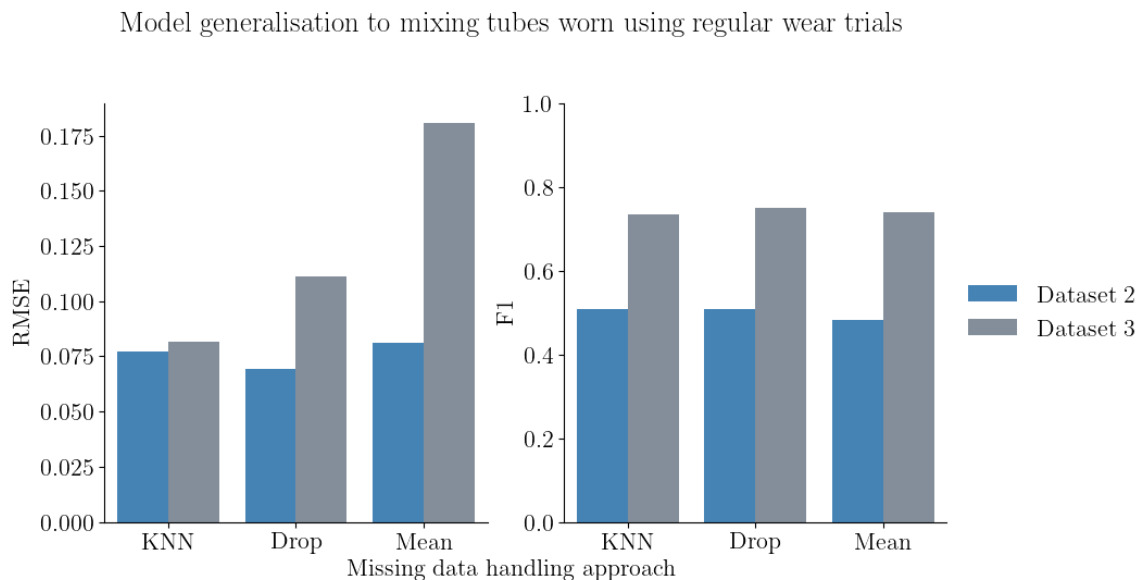
Figure 6.9: Generalisation performance of LGBM (left) for predicting exit diameter and LogR (right) for classifying mixing tube state on datasets 2 and 3, evaluated with different missing data imputation methods, including dropping columns with missing data ("Drop") and mean imputation ("Mean").

Figure 6.9 suggests KNN was a good choice as a data imputation method. Overall, the model generalisation ability for regression was poor, as performance was lower compared to dataset 1 evaluation in Figure 6.5. Meanwhile, the classification performance was comparable for dataset 3. For dataset 2, classification performance was lower, which was surprising considering dataset 2 had a greater training set size. The difference could potentially result from a larger class imbalance present for dataset 2, compared to datasets 1 and 3, as indicated by Table 6.1. However, dataset 3 also had additional sensors, which may have impacted classification performance. Finally, more mixing tubes were included in the dataset 3 test set, as additional tubes were brought for testing during Phase II of the main trial, on which dataset 3 is based. So performance may have been impacted by this additional evaluation data.

The generalisation prediction errors can be studied for insight into the metric performance. The regression and classification errors are presented in Figures 6.10 and 6.11. For regression, for both datasets, LGBM appears to generally over-predict the exit diameter. For mixing tubes 12-20, larger mixing tube length and wear profile inconsistencies (as seen in Figure 5.12) of mixing tubes in the test may have contributed to these errors. The longer length of the mixing tubes could have made an impact, as

156

the total wear of those mixing tubes would have been greater upstream of the exit diameter compared to shorter mixing tubes used for training the models. This will have impacted the sensor signal as discussed in Chapter 5 and suggested by Figure 5.23. Inconsistent wear for mixing tubes 12-20 also likely impacted the prediction error, as the mixing tubes used in the training set had higher wear consistency between wear progression along the profile and the exit diameter growth, as suggested by Figures 5.10, 5.12, 5.14 and 5.15. Mixing tube 12, which LGBM made large prediction errors on, had significant internal profile wear despite a small exit diameter expansion seen in Figure 5.12. Therefore, the model's regression error is likely caused by the exit diameter not being completely representative of total mixing tube wear. Lastly, the exit diameter of the shorter mixing tube 11 is under-predicted for both datasets. As Figure 5.12 in Chapter 5 suggests, this is likely due to the inconsistency between the internal wear profile of mixing tube 11 and its exit diameter.
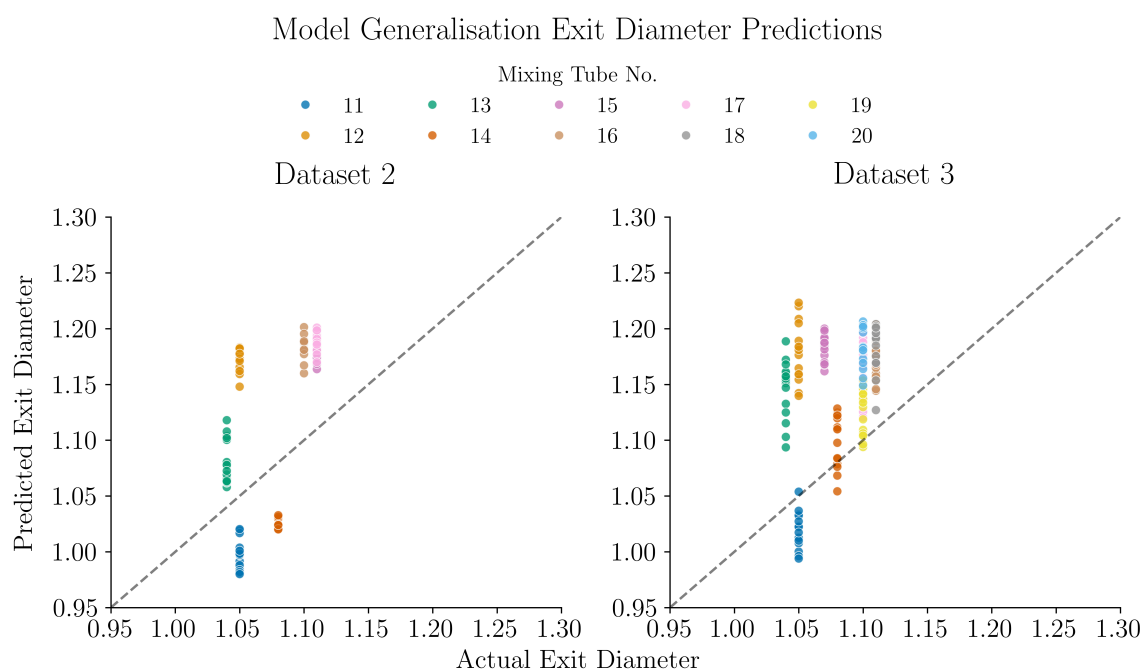
Figure 6.10: Predicted versus actual values per sample on test data during regression using LGBM algorithm on datasets 2-3. Each sample is coloured based on the mixing tube number.

Figure 6.11 and Table 6.6 break down the errors LogR made during tool state classification. For dataset 2, the model made more errors detecting the worn samples, while for dataset 3, the model overpredicted the worn state. When studying the misclassification Table 6.6, the wrong predictions appear clustered on several mixing

157

tubes for both datasets. Similar reasons as seen for regression may have resulted in this performance, with length and irregular wear profiles being potential contributors.

Generalisation Confusion Matrix
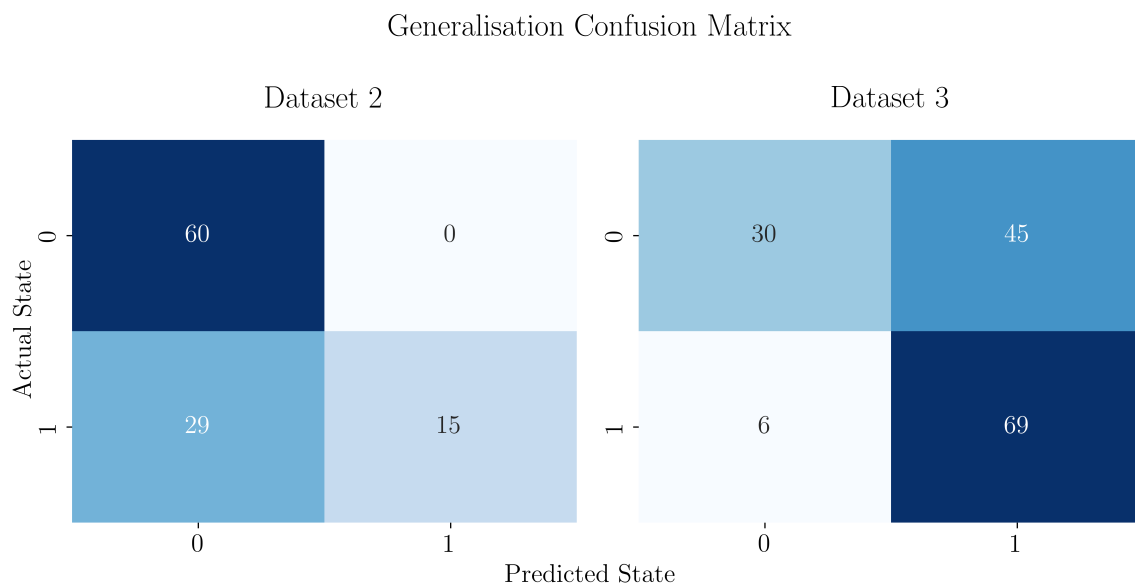
Figure 6.11: Confusion matrix of predictions and actual values during tool state classification using LogR algorithm on datasets 2-3.

Mixing tubes 11-20 were not worn as part of this research, so it is unknown whether poor wear practices may have resulted in uneven wear and impacted the exit diameter growth. However, if the regular wear profile is representative of the profile normally seen in industry, then similar to the observations on dataset 1, data drift mitigations are required. For example, by increasing the dataset size to account for possible variations that can be observed in practice. The exit diameter measurements may not directly correlate with indirect sensor data, which can be affect by total wear of the mixing tubes as shown in Figure 5.23.

Overall, for the collected dataset, generalisation was poor for both regression and classification. The evaluation was limited by the majority of mixing tubes in the test set being of longer length and by the mixing tubes in the test set being less consistent in their relationship between internal profile wear and exit diameter wear.

The regression model especially struggled on this dataset. LGBM, a tree-based model can struggle to extrapolate predictions, when the observed range of features in training differs from the range of feature in testing. As the structure of tree-based models involves recursive binary splits based on feature threshold. Introducing longer length mixing tubes with a different tube length value may have limited the models performance, as the values would fall into a feature space defined by these splits

Table 6.6: Classification predictions for studying misclassification of the LogR per mixing tube in datasets 2-3. The predictions are broken down by true positive (TP), true negative (TN), false positive (FP) and false negative (FN) values, with the sum of wrong predictions also provided.

Dataset	Tube No.	TP	TN	FP	FN	Wrong Predictions
2	11	0	15	0	0	0
2	12	0	15	0	0	0
2	13	0	15	0	0	0
2	14	0	15	0	0	0
2	16	1	0	0	14	14
2	17	0	0	0	15	15
2	18	14	0	0	0	0
3	11	0	15	0	0	0
3	12	0	0	15	0	15
3	13	0	0	15	0	15
3	14	0	15	0	0	0
3	15	0	0	15	0	15
3	16	15	0	0	0	0
3	17	15	0	0	0	0
3	18	15	0	0	0	0
3	19	9	0	0	6	6
3	20	15	0	0	0	0

in training. Regression may perform better in practice during generalisation when data for similar length tubes is also used in training. Alternatively, if mixing tubes of different lengths are used in practice, other models, which are more robust at handling extrapolation, might be better suited to the task.

6.5 Model explainability

Earlier, classification performance differences were seen in Figure 6.9 between datasets 2-3. The availability of additional sensor data was attributed as a potential reason for the disparity in performance. This section will review the utilisation of features in each dataset and study the impact of each feature on the models' predictions. This will help gain insight into the value of each sensor and understand how each feature contributes to the predictions during the TCM process.

The total utilisation of each sensor for each dataset is visualised in Figure 6.12. Not all features were available for each dataset. Dataset 1 had no nozzle pressure sensor available for selection due to a high percentage of missing data, while datasets

1 and 2 had no audio data.
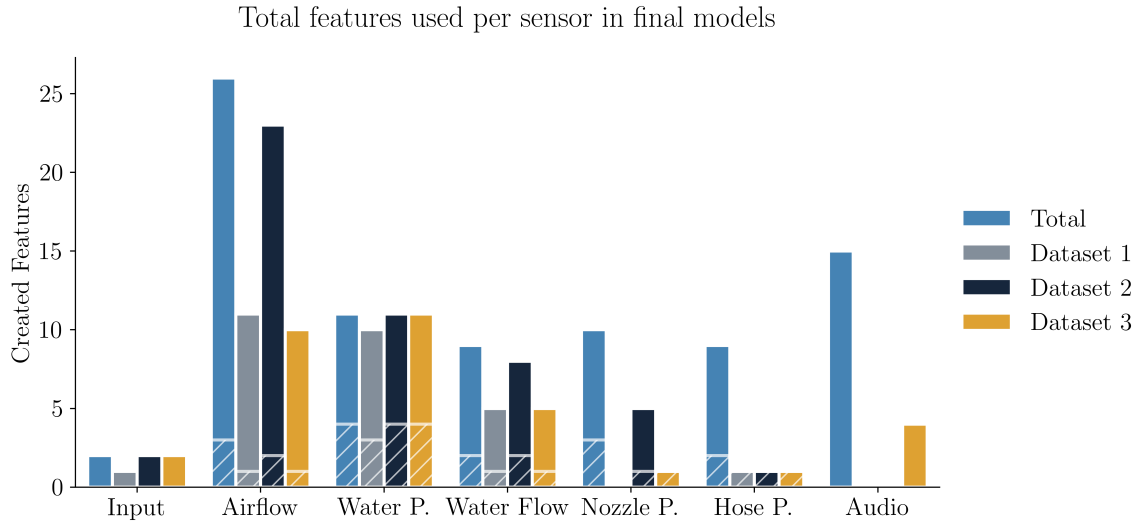
Figure 6.12: Feature count per sensor selected by LASSO for datasets 1-3, out of all created features. Ratio features are counted for both sensors in the ratio, with shading indicating their count.

Airflow, water pressure and water flow stand out in Figure 6.12 as the three sensors whose features are selected the most among the datasets. The figure suggests these sensors should be prioritised when creating a TCM system. On the other hand, nozzle and abrasive hose pressure data appear less important. The introduction of audio data may have made an impact, as LASSO selected audio features on the training set of dataset 3, which may have provided the difference to boost the classification performance of dataset 3 during generalisation in Figure 6.9.

However, studying the selected features does not provide a comprehensive account of the utilisation of the features during model training, as the model may have suppressed the features' importance after feature selection. The present state of the model is characterized by its "black-box" nature, wherein the internal mechanisms and processes are not interpretable. Model explainability methods can be used to help interpret how each feature contributes to the predictions for each model [158, 159]. Feature importance and SHAP summary plots are suitable methods to better understand features' relative significance and contribution in a machine learning model [159]. While feature importance plots help evaluate which features matter to a model, SHAP summary plots can also help understand how each feature matters, thus providing additional detail [160].

Figures 6.13, 6.14 and 6.15 show the SHAP summary plots for datasets 1-3, plotted using the SHAP library [181]. On the figures, each dot corresponds to a single predic-

tion instance. Colour shows whether the magnitude was high or low for an instance for its respective feature. The horizontal placement along the feature axis indicates whether the instance pushes the model's prediction above or below the baseline. The features are sorted by their overall contribution to the model's output.

(a) Regression
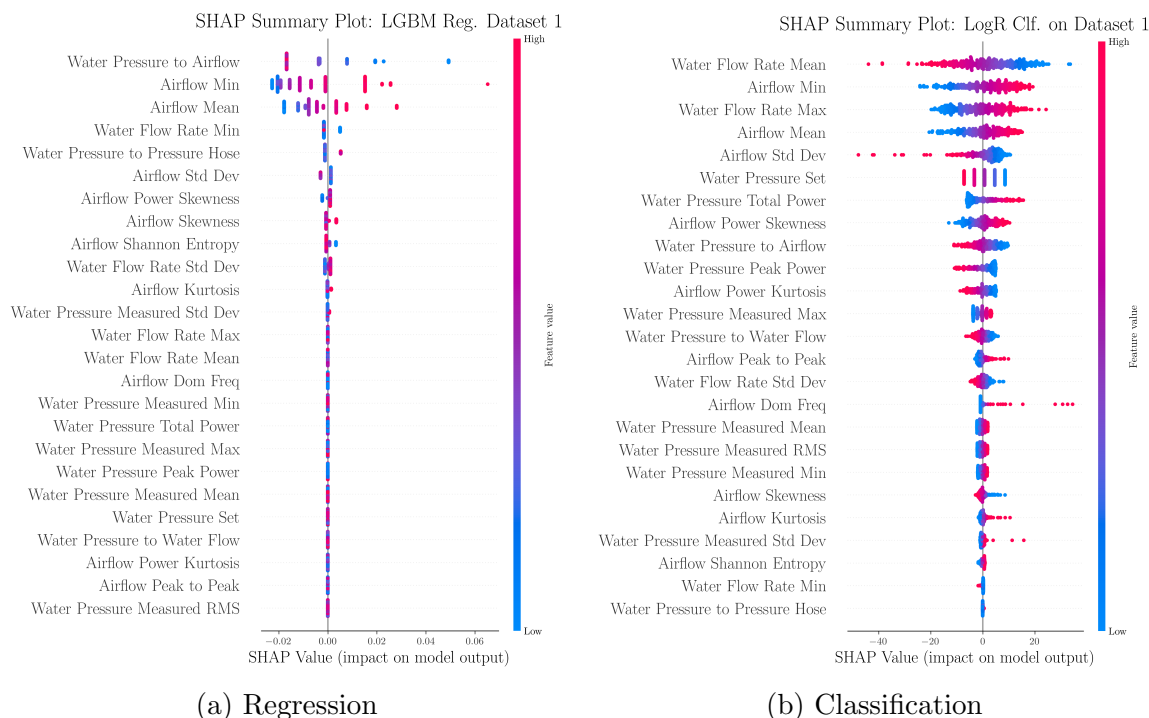
(b) Classification

Figure 6.13: SHAP summary plots for dataset 1 regression and classification.

For the three SHAP figures, the first observation is that for LGBM regression, the SHAP plots have more discreet buckets - a result of how tree-based models train. A second initial observation is that not all features are used by every model after LASSO feature selection, indicated by the clustering of dots around the 0 SHAP value. For most models, there are a few features that appear most important. Airflow features, in particular, appear to dominate the importance of features throughout. As was observed in Chapter 5, airflow data was influenced by process inconsistencies, so the poor model performance compared to time-based models may have resulted from these inconsistencies, which would have impacted the minimum value even though the first 0.5 seconds of recordings were segmented out.

Audio features for dataset 3 classification have little impact on the model's predictions, as seen in Figure 6.15. First, this suggests that the disparity in classification performance between datasets 2 and 3 was not additional audio data related. Second, it suggests that the introduction of a microphone to the setup is unnecessary as the

(a) Regression

(b) Classification

Figure 6.14: SHAP summary plots for dataset 2 regression and classification.

algorithms do not utilise the features to a great extent. Considering the challenges of using a microphone for audio data collection (fixing the position in the enclosure, protecting the microphone from humidity, and data processing) as well as the additional cost, the results indicate that the introduction of this recording device is not desirable.

Figures 6.13, 6.14 and 6.15 have a few examples where some features appear to have a very similar effect on the predictions, such as RMS and mean features in classification of dataset 2 in Figure 6.14. Multicollinearity of these features was observed in Chapter 4 and is likely a contributing factor here - a limitation of using LASSO for feature selection. This may have limited the model's performance due to the model struggling to differentiate the individual contribution of each feature in predicting the target, which can also be seen on the SHAP plots as the features provide a very similar effect on predictions.

(a) Regression   (b) Classification
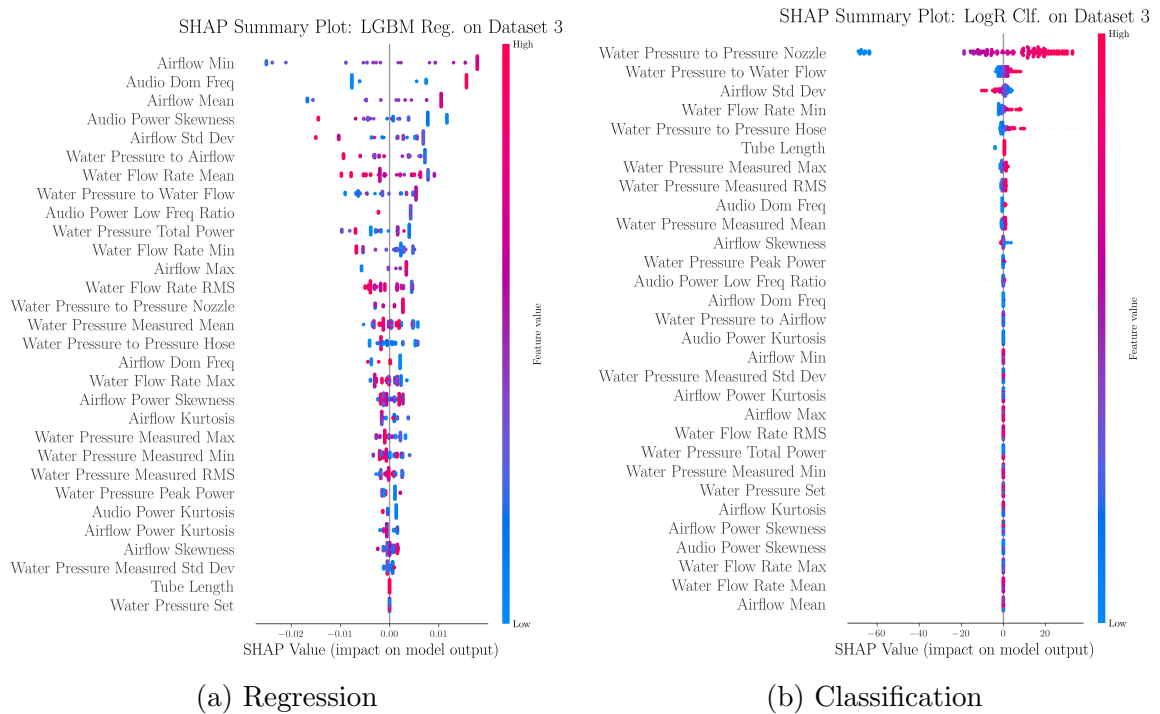
Figure 6.15: SHAP summary plots for dataset 3 regression and classification.

The highest-scoring datasets for regression and classification were datasets 1 and 3, respectively. From Figures 6.13, 6.14 and 6.15, these two solutions also appear to utilise the lowest number of available features. The models were successful in identifying what features are important. As a result, their solutions may have been less complex and, therefore, better at generalising to unseen data.

Time domain features appear to dominate feature importance, potentially a result of the low sampling rate used for airflow and machine sensors, limiting the effectiveness of frequency domain features. Ratio features also appear valuable to the model for learning the relationships within the data, suggesting it was right to include them during the feature engineering process. Finally, for TCM the three sensors that standout throughout in their utilisation by LGBM and LogR in Figures 6.13, 6.14 and 6.15, are airflow, water pressure and water flow sensors. Prioritising these three sensors should form a strong foundation if choosing to go down the indirect monitoring route. Sensor fusion plays a part, and the overall indication is to use multiple sensors together to predict exit diameter wear. A set of exact "best" features does not stand out in Figures 6.13, 6.14 and 6.15. Nozzle and abrasive hose pressure sensors do appear to be valuable to several models as well.

To summarise, airflow, water pressure, and water flow sensors appear to be the biggest contributors to the models for predicting mixing tube wear. For AWJ TCM

163

users, sensor fusion of these three sensors should form a good foundation for wear prediction. The use of audio sensors is not recommended.

6.6   Mitigating data drift

In Chapter 5, data distribution drift was observed in Figure 5.23 with changes in process conditions. Data drift is important and is a problem as it is likely to affect both the sensor-based and wear time-based TCM solutions in practice. The current approach of assuming that drift will not be present in the test data is insufficient. Model performance presented earlier in Figures 6.5 and 6.9, was likely affected by changes in the data. Further supporting the use of drift mitigating practices. The TCM system will not have a static dataset, and it will be unrealistic to expect the data distribution to stay stable over an extended period of time. Therefore, understanding the effects of data drift on the model performance, as well as potentially reducing its effects, is important.

Data drift refers to the situation where the statistical properties of the input data used by a machine learning model change over time [182]. This change in the data distribution can impact the model's performance. The model may be trained on one distribution but later deployed in an environment where the data distribution has shifted. The particular drift observed in Chapter 5 was concept drift, a situation where the relationship between input features and the target variable changes over time [182]. The drift in the collected data was perhaps more obvious due to significant changes to the process, such as a waterjet change or part change. However, in practice, drift can develop over time.

Data distribution shifts are only a problem if they cause the performance of the model to degrade [182, 183]. Therefore, the first step to mitigating drift is to validate its presence and the effect of it on model performance. A method that can be used for detecting data drift in the test set is adversarial validation. Adversarial validation popularised through a machine learning competition platform - Kaggle, is a technique to assess the similarity between training and test data. Adversarial validation is carried out by dropping the target column, labelling the training and test data as 0 and 1, combing the training and test sets and performing binary classification via an algorithm such as RF [132, 184, 185]. The performance of the model can then be evaluated using the Receiver Operating Characteristic - Area Under the Curve (ROC-AUC) metric, which measures the ability of a model to distinguish between the positive and negative classes by plotting the true positive rate (sensitivity) against

the false positive rate (specificity) across different probability thresholds [132, 185]. If the classifier cannot correctly distinguish between the two sets of data, a ROC-AUC score closer to 0.5 will be observed, indicating randomness in predictions. A score closer to 1.0 indicates the test set is distinguishable from the training data. According to Banachewicz et al., a ROC-AUC score greater than 0.8 would alert peculiarity in the test data [132].

By using adversarial validation, the concept drift in this thesis's collected data can be verified. Three different dataset splits were identified from all the collected data which contain drift, following the analysis in Chapter 5. These are summarised in Table 6.7. Only mixing tubes 1-10, worn using Al_2O_3, were used. An attempt was made for the dataset splits to only contain one major difference which would contribute to drift: using a separate AWJ, changing the orifice holder component and changing the MC to a more worn state. The AWJ change training set contained data for mixing tubes 1-8 recorded during WDC and ATD during Phase I of the main trial, while the test data included data collected during the preliminary trial. For the orifice holder change, the training set included main trial Phase I WDC and ATD data for mixing tubes 1-10 and WDC data for mixing tube 9 from Phase II. The test set included Phase II data of mixing tube 10 WDC and mixing tubes 1-10 ATD. Finally, for the MC change, the worn MC data was used in the test set, with the test set of the orifice holder dataset used for the training set. The same unreliable data was removed as for datasets 1-3 earlier in the Chapter.

Table 6.7: Summary of the three dataset splits containing concept drift between the train and test sets.

Drift Reason (Dataset)	Train/Test Set	Total Samples	Worn
AWJ	Train	767	23%
AWJ	Test	209	29%
Orifice Holder	Train	899	28%
Orifice Holder	Test	249	40%
MC	Train	249	40%
MC	Test	149	30%

Adversarial validation was performed on each of the three datasets, and the results are presented in Figure 6.16.

Figure 6.16 confirms the presence of concept drift, as the model was capable of confidently differentiating between the training and test sets. Figure 6.17 checks for the presence of drift in the dataset used for predicting wear under the same wear

Adversarial Validation of Different Datasets Experiencing Drift
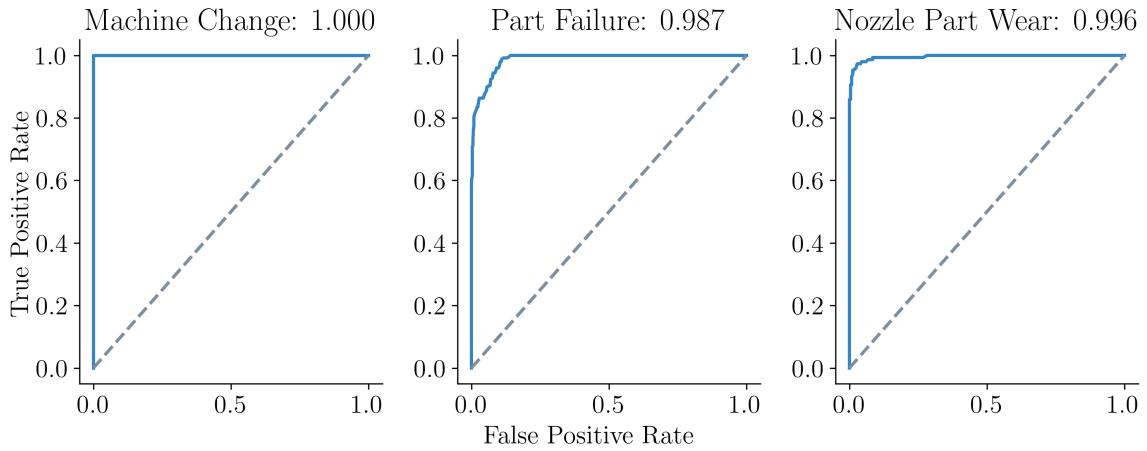
Figure 6.16: ROC-AUC scores and ROC curves after adversarial validation. The scores were calculated over 5 CV folds using the RF algorithm.

conditions of dataset 1. Even though the assumption was made that drift was not present, a significant difference in data distribution between the training and test sets appears to exist. The ROC-AUC score of 0.81 is above the 0.80 threshold defined by Banachewicz et al. [132]. Therefore, the performance of the models on dataset 1 was likely affected by this drift.
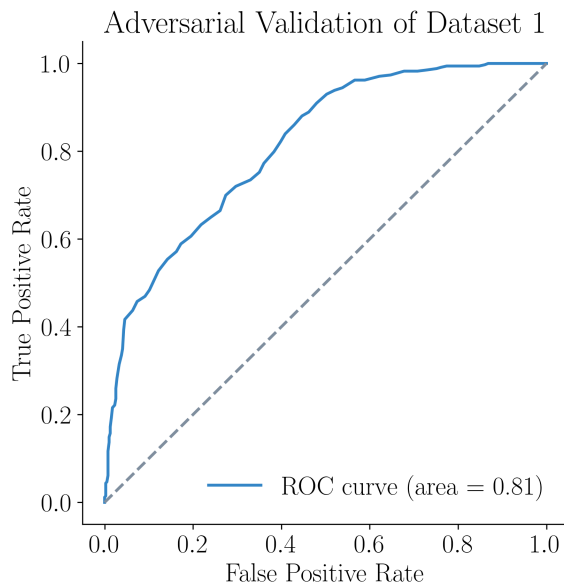
Figure 6.17: ROC curve of adversarial validation on dataset 1. The scores were calculated over 5 CV folds using the RF algorithm.

While drift is present in the data, it does not necessarily matter if it does not

impact performance. The model performance on each dataset is compared in Figure 6.18. When comparing the performance to that achieved on dataset 1 seen in Figure 6.5, for both regression and classification, all models (machine learning and wear-time based) performed worse relative to their counterparts of the same model type on the aforementioned dataset. The only exception was for the classification solution on the MC change dataset. The wear-time-based model still outperformed optimised machine learning.

Model Performance During Data Drift
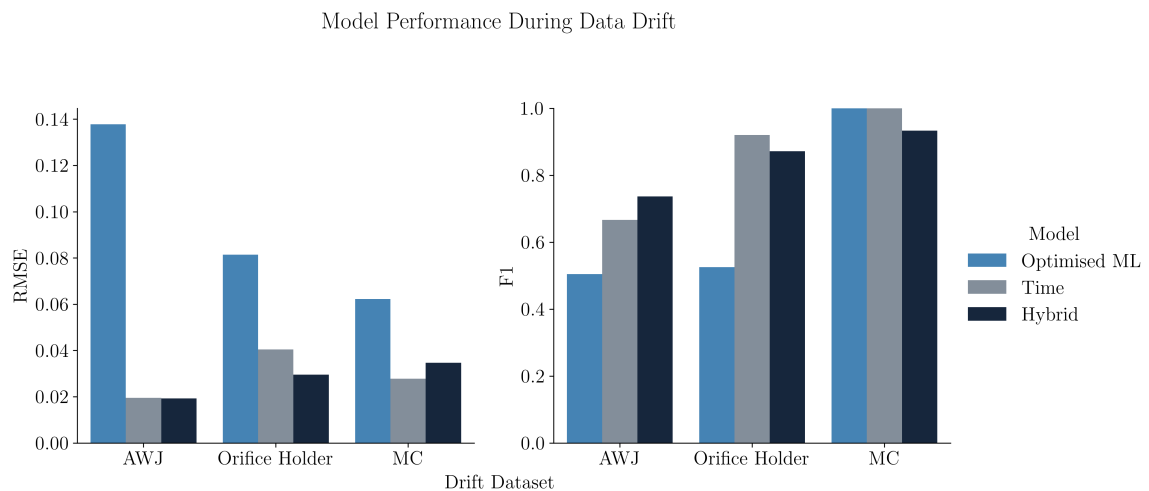
Figure 6.18: Effect of drift on model performance on different datasets for optimised machine learning (ML) algorithms, wear time-based solutions, and a hybrid approach incorporating wear time into the machine learning pipeline. For machine learning, LGBM was used for regression and LogR for classification, with KNN for missing data imputation. The wear-time approach also had the tube length feature added, due to varying tube sizes.

In Figure 6.18 a hybrid approach was also tested which included both wear time and sensor data for training machine learning models. The hybrid approach did not have its hyperparameters tuned, following the results presented in Figure 6.5, which indicated this step to be unnecessary when wear time is used as a feature. The hybrid method stood out for comparable and sometimes better performance than the simpler time-based model in Figure 6.18. The accuracy of the wear-time model decreased in comparison to earlier results, likely due to the changing wear rates between different datasets.

The results suggest the real performance of the evaluated models could be worse in practice when the data collection process is not as controlled, even for the simple wear-time model. Data drift is, therefore, a significant potential limitation to the TCM system, which must be addressed.

With drift identified and quantified and its significance established, the next stage is to discuss how this limitation can be mitigated. There are multiple existing practices for tackling data drift and several will be tested in this thesis.

A common approach in research and industry is to train the models using massive datasets in the hope that the dataset covers a comprehensive distribution with all newly encountered data points likely coming from the same distribution [182].

A second method is to remove the features most affected by drift from the model [132, 173]. This method is sometimes referred to as suppression[132]. In suppression, first the feature importance of the adversarial validation model is plotted, next the feature that is most important is removed before re-evaluating for the presence of drift. These steps are repeated until the distributions are the same again. This approach might make the model more resilient over time and easier to maintain, however it can also drastically reduce the models performance [132].

A third approach that again is popular in industry is to re-train the model using the labelled data from the test distribution [182]. Re-training can be done from scratch or by fine-tuning the model on new data. The challenge here is having labelled data from the test distribution. For the AWJ TCM system, this can be done via a sort of calibration, where an AWJ user can manually measure the exit diameter of a mixing tube before collecting dwell data on it in a controlled exercise. This labelled data can then be supplied to the model for re-training. Essentially allowing the model to calibrate to the new AWJ state. As most machine learning algorithms allow for a sample weight to be supplied, which can enable the prioritisation of individual samples, re-training can also be done with new data given a larger per-sample importance.

A fourth potential solution is to use a technique known as domain adaptation, which is a subfield of transfer learning focussed on adapting a model to perform well on the target distribution [186]. Domain adaptation methods can be supervised, unsupervised, or semi-supervised, depending on the availability of labels from the target domain. A variety of methods exist for carrying out domain adaptation, including shallow and deep approaches [187–192]. Deep approaches utilize neural networks and can involve convolutions and autoencoders [193]. Shallow approaches on the other hand can use feature-based techniques to learn domain-invariant feature representations to align data distribution [193, 194]. Conducting a thorough review of all the available domain adaptation methods is outside the scope of this thesis. A common shallow method used is to align the distributions by minimising the distance between

the domains, for example, by using the maximum mean discrepancy (MMD) distance measure with the kernel mean matching (KMM) approach [187, 192, 193, 195]. KMM minimises the difference between the source (training data) and target (test data) domains by re-weighting the samples in the source domain and adjusting their importance [192, 195]. KMM was applied in this thesis using the ADAPT python toolbox for domain adaptation [196].

The results of applying each of the four approaches to mitigating data drift are presented in Figure 6.19. The hybrid approach incorporated wear-time as a feature of the machine learning pipeline, while the time approach used wear-time and tube length as sole features.
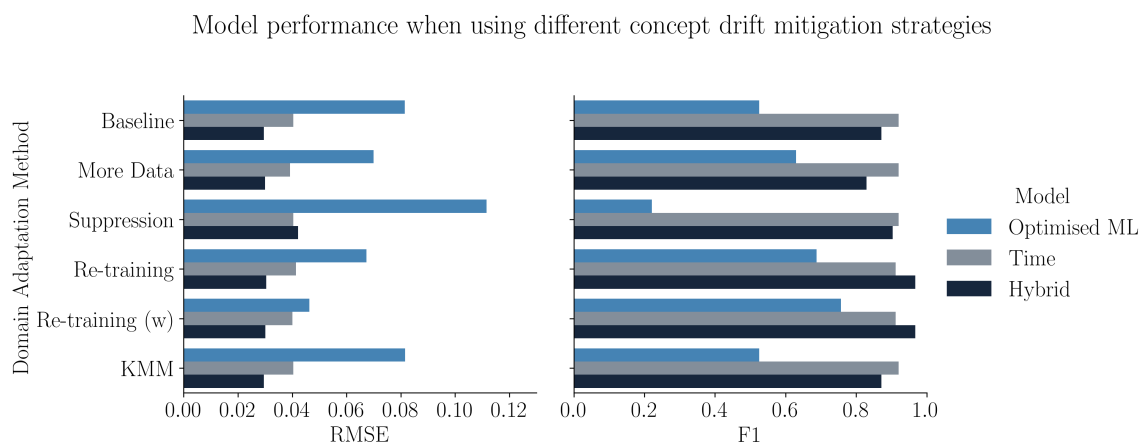
Figure 6.19: Performance of different models when using different strategies to combat drift in data. For machine learning, LGBM was used for regression and LogR for classification. For the weighted re-training method ("Re-training(w)") new data was given a larger sample importance weight of 5 with all training data given a weight of 1.

In figure 6.19, the orifice holder dataset was chosen for the evaluation of each approach, as it was the largest of the three datasets available, as seen in Table 6.7. An additional 209 samples were used from the preliminary trial to evaluate the "More data" approach. ATD data for mixing tubes 3 and 8 from Phase II of the main trial was used in the training set when testing the "Re-training" approaches. The effect of dropping features on the adversarial validation ROC-AUC score is visualised in Figure 6.20. While Banachewicz et al. suggested that a threshold of 0.8 is a better choice for stopping feature removal, a higher threshold of 0.9 was used due to many features already dropped after crossing the 0.9 threshold [132]. During suppression, missing data was only imputed after the features were dropped to avoid data leakage.
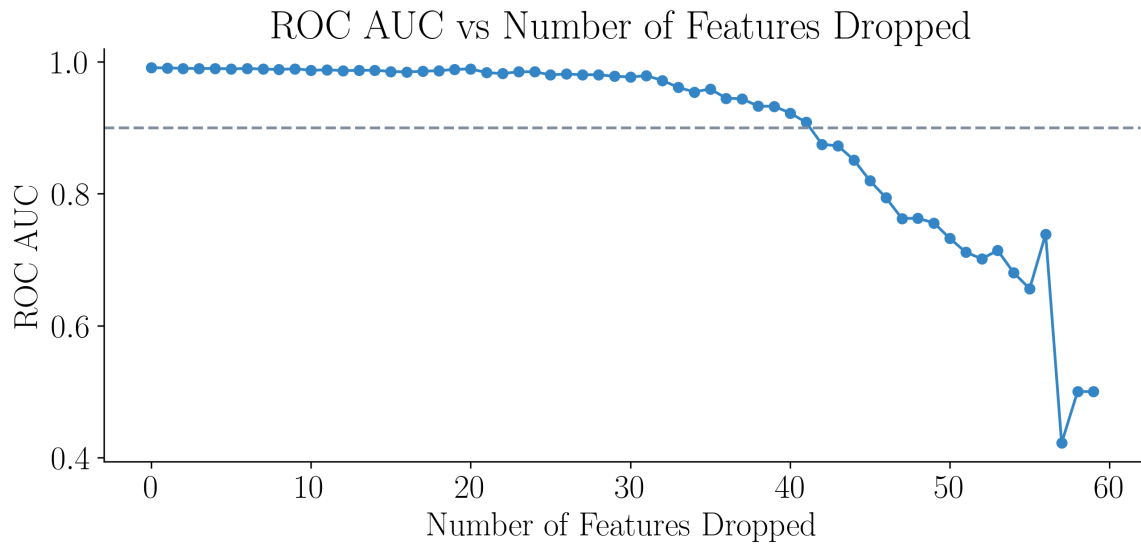
Figure 6.20: The adversarial validation ROC-AUC score during suppression, with the highest feature importance feature for the RF algorithm being continuously dropped. A dashed threshold line is drawn at 0.9 ROC-AUC score.

Figure 6.19 suggests that the best method for mitigating drift is re-training the model using additional data collected during the "calibration" stage. By giving the new data a higher weight, the performance can be further improved. However, both the hybrid and time-based approaches saw little improvement with drift adaptation. In addition, the re-training method used more data in the training set and less data in the test set, which was a limitation of this result. Training on more data also performed well and could be a viable solution for AWJ users. Potentially used in tandem with weighted model re-training when a drift in machine learning performance is observed. Overall, the best-performing model relied on the use of both sensor and time data for both regression and classification. Judging by the drift results, future work could look at collecting time data during regular wear and seeing how a hybrid model trained on accelerated wear trial data can adapt to regular wear trial data. Domain adaptation could be applied to help the model improve performance.

6.7   Wear prediction summary

To summarise, machine learning can be used with inexpensive indirect sensors for both regression and classification. However, the models are outperformed by a simpler methodology of using wear time recordings together with algorithms such as LR and LogR. Machine learning can generalise well to classification on longer mixing tubes

worn using regular wear. However, the models struggle during regression. This conclusion is limited by the fact regular wear mixing tubes were worn by separate AWJ users with different input parameters and most tubes in the test set were of longer length than the mixing tubes used to train the model.

Data distribution shifts were found to affect the modelling accuracy, however different strategies such as training on more data and calibrating the models (re-training) were shown to both be successful in mitigating the effect of drift, especially for classification. However, this needs further validation on mixing tubes collected under regular wear, ideally with time recorded so that the best performing hybrid approach, which used both sensor and wear time data, could be used.

If having to choose the best-value sensors, the results indicate that airflow, water pressure and water flow sensors form a good starting point. Ratio features between the sensors can also help machine learning models learn relationships within the data. The solutions are also not "black-box", as SHAP summary plots can help explain the prediction values of the models. Ensembling methods were shown not to be required for TCM of mixing tubes.

Both regression and classification approaches were compared throughout. Regression can achieve scores up to 0.011 - 0.023 RMSE for hybrid and optimised machine learning approaches, as indicated by Figure 6.5 and 6.19. The error equates to around 3 - 6 hours of machining time during regular wear at 3000 bar pressure and an abrasive feed rate of 6g/s [162]. For classification, pure machine learning could achieve close to 0.7 F1 score, with closer to 0.9 F1 score for hybrid approaches as seen in Figure 6.5. Both machine learning tasks have potential for application in industry with regression for tool path compensation and classification for designing a sustainable mixing tube replacement strategy. However, the TCM models may need further development and improvement in generalisation.

Recording wear-time only is a great way to start monitoring, with the potential of perfect classification performance and small errors of 0.01 RMSE for regression. This performance may slip with data drift, as seen in Figure 6.19.

Chapter 7

Conclusions

The main aim of this research was to design a framework for building a mixing tube process monitoring system for the AWJ machining process. The hypothesis was that this could be achieved via accelerated wear data collection, indirect sensor monitoring and the use of machine learning. The goal was to work towards more sustainable, efficient and accurate AWJ machining.

Chapter 1 introduced the background of AWJ machining and TCM. Next, Chapter 2 addressed the initial objective by conducting a comprehensive literature review on mixing tube wear, wear monitoring in AWJ machining, and the construction of TCM systems. The literature review identified a research gap in developing and evaluating a monitoring application for the AWJ process, which accounts for multiple data collection challenges and can predict wear.

The subsequent objective centred on developing a data collection methodology for creating a dataset based on indirect sensor data for predictive model training. The methodology had to address the challenges of measuring mixing tube wear, the long wear time of the mixing tubes and the large input parameter space of the AWJ machining process. This objective was tackled in Chapter 3, where a data collection framework was presented. The framework leveraged exit diameter measurements via pin gauges for recording wear directly to correlate with indirect sensor measurements, Al_2O_3 abrasive for reducing the wear time during data collection and relied on recording the data during dwell cycles when no abrasives were flowing through the system, simplifying the input parameter space. The proposed framework is built on previous research on mixing tube wear to create a novel, feasible methodology for building an AWJ TCM system. Utilising dwell cycles for monitoring has not been previously explored, with the designed framework presenting an opportunity for a new outlook on monitoring the AWJ process.

With the framework established, the following objective involved the selection of a suitable and inexpensive sensor for data collection. The sensors were selected based on the literature review, with airflow, pressure sensors, and a condenser microphone being preferred for the task. These sensors are inexpensive, easy to set up, do not interfere with the process and can be mounted in the harsh AWJ environment. The airflow setup was adjusted from literature, to be housed at the air inlet, instead of in the abrasive hose, allowing for data collection during standard operation.

After the framework was established, the next objective was to gather data and explore the effectiveness of chosen sensors in monitoring wear. A preliminary study was conducted to validate the methodology before larger data collection trials were conducted. The methodology was deemed successful after two mixing tubes were worn for 60 minutes and a preliminary analysis was carried out in Chapter 4. A wear threshold of 10% exit diameter growth was successfully exceeded within an hour of wear using Al_2O_3 abrasive. The used sensors experienced a change in magnitude during the dwell cycles with changing wear. The built machine learning models on data from a singular mixing tube could predict the exit diameter and classify the state of the tool under varying water pressure for a separate mixing tube. The lowest RMSE error for regression on unseen data was 0.03, equating to an error of around 8 hours of tool life. An F1 score of 0.91 was achieved for classification, with the model making 12/105 false predictions.

The preliminary trial helped narrow the scope of machine learning, helping select the LASSO algorithm as a feature selection approach over manual feature selection and narrowing down the number of machine learning models explored. The data also suggested that collecting additional data under varying water pressure was worthwhile, even if the end user only uses one input water pressure.

Chapter 4 made an original contribution to research by quantifying how well airflow sensors can predict mixing tube wear. A small dataset limited the conclusions, but it suggested that a TCM system can be built for exit diameter prediction and tool state classification by recording the time the mixing tubes are worn. A wear-time-based system would allow for a simplified data collection process and potentially outperform indirect sensor-based models.

Following, the preliminary trials the main data collection effort, split into two phases, was carried out with an additional 8 mixing tubes worn. Six tubes were worn for up to 90 minutes, with 15-minute wear intervals. Two mixing tubes of a shorter length were worn for 60 minutes. Data was also collected on 10 mixing tubes worn by other researchers using regular wear with garnet abrasive. The wear progression

of the worn mixing tubes was studied in Chapter 5, as per an outlined objective. The wear was found to be consistent between mixing tubes with good internal and tube exit wear profiles. The internal wear patterns observed during accelerated wear were more consistent but similar to regular wear.

Both garnet and Al_2O_3 abrasive were also studied in Chapter 5 to validate the assumptions made after the literature review, in line with the stated objective. The literature results were confirmed, with the two abrasives found to be similar in shape, size and density [7, 50]. A further contribution to the research field was made by comparing the flow of the two abrasives via angle of repose tests. The results again indicated a similarity between the two abrasives, confirming Al_2O_3 is a suitable alternative to garnet to achieve a similar wear pattern and accelerated wear.

Before building predictive models, a thorough data analysis of all collected data was carried out in Chapter 5. The observed exit diameter wear trend was not linear, with accelerated wear at the beginning and towards the end of mixing tube life. The condenser microphone, airflow and pressure sensors all responded to a change in exit diameter and water pressure. The airflow was higher for mixing tubes of the same exit diameter but greater internal wear. The airflow recordings also changed with changing nozzle components or worn AWJ parts above the orifice. This finding of changes in data distributions meant the data could be affected in production, and a developed TCM system would have to account for potential data drift.

In Chapter 6, the remaining objectives were addressed. Multiple novel contributions to the research field were made. The performance of various machine learning methodologies in exit diameter prediction and tool state classification of the AWJ mixing tube were assessed. The feasibility of the framework was evaluated by comparing machine learning performance with linear wear time-based model performance. Generalisation performance of machine learning models trained on accelerated trial data to mixing tubes worn by separate researchers, on separate machines using separate wear conditions was also evaluated to see how well machine learning models adapt to industry conditions. And finally, data drift effect and mitigation were explored, to suggest methods of maintaining any developed TCM system in production. During all validation, the training and test data were kept separate with mixing tubes used for training the models not used in testing of model performance. Overcoming limitations in earlier work in AWJ TCM [42, 43].

Machine learning algorithms had their hyperparameters optimised via Bayes optimisation and used features selected via the LASSO algorithm. In regression, the machine learning models, including RF, LGBM, KNN, and LogR, achieved the best

RMSE score of 0.023 on data collected under the same conditions via an optimised LGBM model. For classification, performance was close to 0.7 F1 score via an optimised LogR model. During generalisation to mixing tubes worn using regular wear, the regression performance was poor, with the best RMSE close to 0.075. However, the best-performing model achieved an F1 score of around 0.7 for classification. The results were limited by the fact the wear of garnet-worn mixing tubes was conducted by other AWJ users, with the process not controlled. Nine out of ten mixing tubes in the test set were also of longer length than the mixing tubes in the training data, which could have impacted the model performance further.

Machine learning models evaluated under the same wear conditions were outperformed by a linear model based on wear-time data, which achieved an RMSE score of 0.01 and an F1 score of 1.0. However, when addressing the issue of data drift, a hybrid approach which used machine learning models with both sensor data and wear-time data was seen to outperform the time-based approach. Recording sensor data could be of value. To mitigate drift, training on large datasets with varying process conditions and periodic calibration of the model with additional data could provide the best solution. An exit diameter RMSE of around 0.04 can be expected. For classifying the tool state, an almost perfect predictor could be built.

While machine learning shows potential, the performance of wear time-based models suggests a good foundation for TCM of AWJ mixing tube wear would be to build a system around wear-time recordings. Especially due to the complexity of the problem. The wear-time models would need adjusting for generalisation to regular wear. If choosing to incorporate sensor data, model explainability analysis suggested airflow, water pressure, and water flow sensors offer the most value to the machine learning models. Ratio features were also seen to be powerful predictors based on their feature importance. The use of a condenser microphone is not recommended.

The hypothesis of this thesis was that indirect sensor data from an accelerated wear trial could be used to accurately predict mixing tube wear of the AWJ process via machine learning. The hypothesis was confirmed, as the exit diameter and tool state could be predicted. However, simpler methods such as recording wear time of the mixing tubes and using a linear model outperformed pure machine learning approaches. Machine learning performance fluctuated between different datasets; however, solutions based on wear time, whether using sensor data or not, were more consistent in their performance.

The presented work had several limitations. The methodology limitations are discussed first. First, only one water pressure was used to wear the mixing tubes

despite the dwell data being recorded under multiple pressures. While it was shown in Chapter 4 that if only one pressure were recorded the performance of the models would not drastically change, it would be beneficial to understand how the wear profile may adjust under different water pressure over time, if at all, in the 3000 - 5000 bar water pressure range. If the wear profile does change, it may lead to data drift and require accounting for in the data collection strategy. A secondary limitation was that the jet was stationery during wear, and nozzle movement was assumed not to affect the wear profile. In practice, the jet could have a traverse rate greater than 0, and the nozzle may be at an angle during machining. Whether these two factors affect the wear profile was not studied. The proposed framework also only works for cutting. This framework may need adjusting for drilling where the vacuum assist port would not be connected to the nozzle pressure sensor. A wear threshold of 10% exit diameter growth was chosen for feasibility reasons in this thesis. However, a higher threshold of 25% exit diameter growth may be appropriate for certain applications, for which the model accuracy may differ [7]. Finally, the study lacks an understanding of the effect of replacing the mixing tubes on the recorded data. A gauge repeatability and reproducibility study is required to understand the potential effect on the collected data. Which may mean variation to the proposed framework if a significant impact is observed. Understanding the effect of replacing the mixing tube was part of the initial data collection plan, but this was impacted by part failure during the data collection trial, which affected the data.

From the perspective of machine learning, there were further limitations. Sequential models, utilising previous predictions, were not explored. Wavelet analysis was also not performed for feature engineering. Both approaches may have improved performance. Finally, deep learning models were not tested in their predictive ability on main trial data. These models may have extrapolated better during generalisation analysis, as the models are inherently better at extrapolating outside the range of training data compared to tree-based models. Tube length was increased for most tubes in the test set during generalisation, which deep learning models may have been better at adapting to.

An additional limitation of this research arises from the exclusion of several data points prior to model training and evaluation due to various issues encountered with the AWJ process during data collection. While these exclusions were essential to ensure data reliability, they also meant that process instabilities were not fully accounted for during model performance evaluation.

To summarise, the research presented in this thesis proposed a novel methodology for monitoring AWJ mixing tube wear by recording data during dwell cycles. A framework for data collection was also designed to address AWJ data collection challenges that had not previously been addressed. A novel contribution was made by assessing the predictive capabilities of machine learning models in inferring mixing tube wear from airflow, water pressure, water flow, nozzle pressure, abrasive hose pressure and audio data. A further contribution was made by assessing how well the created machine learning models can adapt to mixing tubes worn under industry conditions. The effect of data drift was also assessed, suggesting how future TCM efforts can maintain models in production. Analysis of model feature importance highlighted the best sensors to invest in.

This research forms a foundation for further efforts to translate previous AWJ monitoring research into production, which can aid in the industry adoption of the AWJ machining process. AWJ users can also use the modelling results presented in this thesis to help them choose a TCM direction for monitoring mixing tube wear and designing a smarter tool path compensation system.

Based on the work carried out, a foundation framework for AWJ TCM is set out below, with a visual representation of the framework shown in Figure 7.1:

1. Collect data.

   - Select input parameters based on typical running conditions of water pressure, abrasive flow rate, and abrasive mesh size. If common parameters are unclear, repeat data collection for varying parameter sets.

   - Airflow sensors (100 Hz) and water pressure and flow sensors (50 Hz) are recommended as a baseline. Nozzle and hose pressure sensors can be optionally added for enhanced monitoring. Figures 3.5 and 3.8 illustrate the sensor setup.

   - Decide on a wear threshold. A 10% exit diameter increase is recommended as a threshold for wear, but a higher exit diameter wear of 25% can be used.

   - Use Al_2O_3 abrasive to wear mixing tubes with selected input parameters. Reinforce the catcher tank to prevent damage (Figure 3.6).

   - Record sensor data and measure exit diameter at 0 minutes and every 5 or 10 minutes. Use pin gauges in 0.01 mm increments. Detailed data collection methodology is available in Chapter 3, Section 1.1.

177

- Wear at least 2 mixing tubes past a defined wear threshold. The wear of additional mixing tubes is recommended to expand the dataset. Additional tubes can be worn to different points of wear to facilitate future ATD data collection and capture data under varying orifice and mixing chamber conditions.

2. Process data.

    - Segment the data, removing the first 0.5 seconds and retaining 4 seconds of each recording.

    - Create input, time-domain, frequency-domain and ratio features from segmented data.

    - Remove unreliable data points.

    - Handle missing sensor data with KNN imputation if required.

    - Use LASSO for selecting the most predictive features.

3. Train machine learning models.

    - Use LogR for tool state classification and LGBM for exit diameter regression.

    - Optimise hyperparameters using Bayesian optimisation. Refer to Table 6.5 for the parameters to tune.

    - Split data into training and test sets, ensuring that data from different mixing tubes is separated to prevent data leakage.

    - Evaluate trained model performance on test set using F1-score for tool state classification and RMSE for exit diameter regression.

    - If satisfied with performance, retrain the final model on the full dataset to leverage all available data.

4. Use in production.

    - Track wear time in operation. Once data from multiple mixing tubes is available, incorporate wear-time and wear mode (accelerated or regular wear) as additional features in future models. The wear mode feature is included to allow the model to adapt to different wear progression rates.

- Monitor model performance for concept drift. When performance deviation is observed or after a significant process change (e.g. part failure), collect new data using pre-worn tubes and apply weighted retraining as described in Chapter 6, Section 6, to mitigate drift.

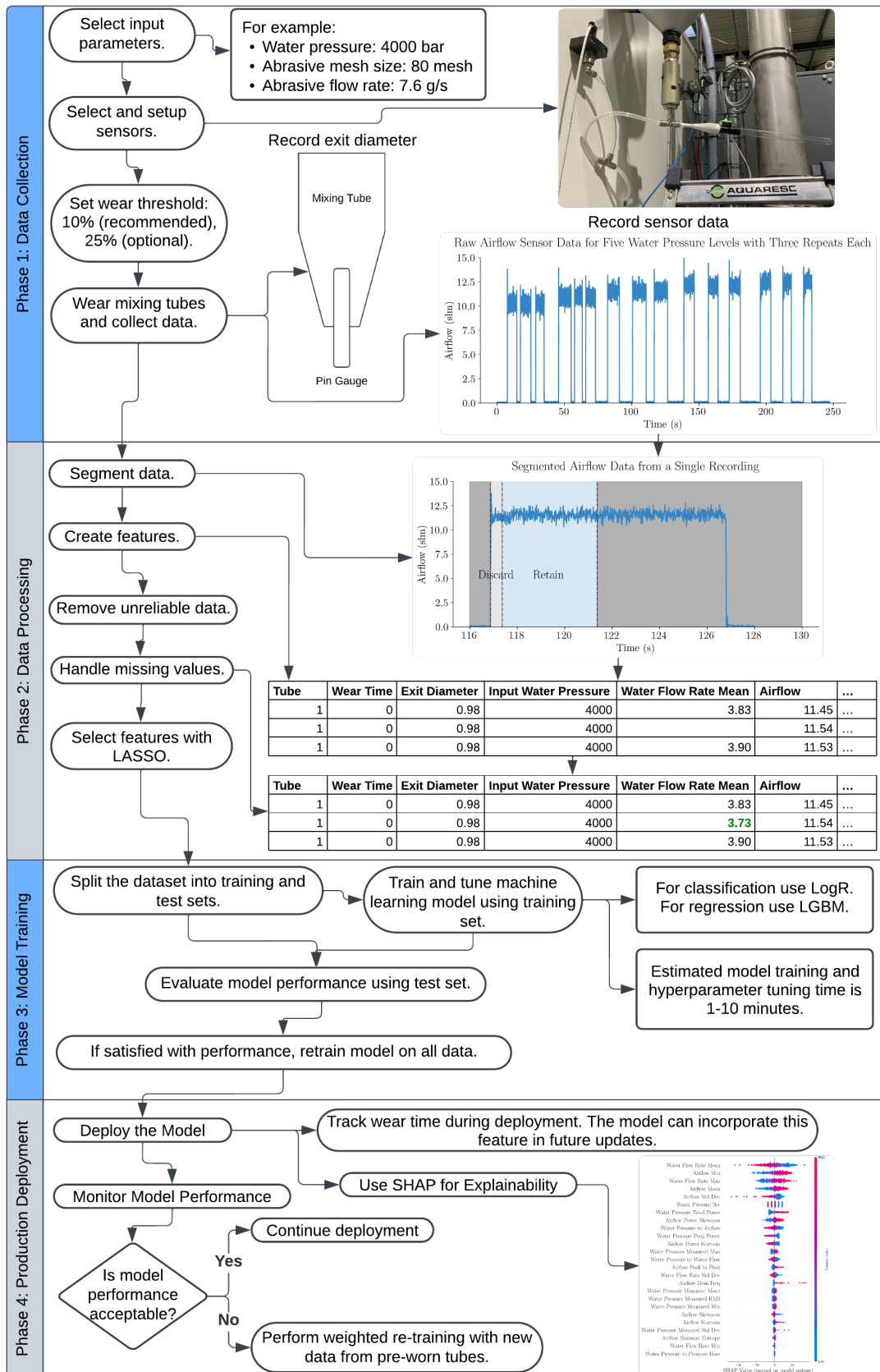- For model explainability, consider using SHAP summary plots.

Figure 7.1: Framework for AWJ TCM.

7.1 Future work

This research has presented a viable framework for TCM of AWJ mixing tubes and proposed a data collection strategy based on dwell cycles. However, the framework did not focus on wear of two other critical AWJ components, the MC and orifice. Both the MC and orifice have a greater tool life of 500 and 1000 hours respectively, so were not studied [23–25]. The orifice is also only subject to water, meaning accelerated wear cannot be used - making potential data collection efforts both expensive and time consuming. Limited research has attempted to develop a method for real-time monitoring of these components and can be explored.

In addition, while generalisation performance to regular wear mixing tubes has been presented, the test data had several differences from the training data. Therefore, a more accurate evaluation of accelerated wear trial model generalisation to regular wear trial data should be assessed, where the mixing tube length is not varied, and the test data is collected in the same environment. Performance evaluation should also be conducted on mixing tubes worn for a longer period of time, with a higher wear threshold of 25%.

The limitations of the data collection framework should also be addressed. The effect of nozzle angle, traverse speed, and water pressure on the internal wear profile of mixing tubes should be studied. If either is found to affect the wear profile, this parameter may have to be factored into the data collection design.

While the research provided a foundation for tool path compensation, the relationship between exit diameter, jet properties and cutting performance on different materials should be explored. This would allow for a better understanding of what the prediction error means for tool path compensation and also would allow for the translation of the predictions into suggested offset values for the AWJ operator. The use of a high-speed camera may be required to understand the jet's properties better. The challenge here would be providing sufficient lighting in the AWJ enclosure and a suitable background for seeing the jet.

As mentioned in the limitations discussion, a gauge repeatability and reproducibility study is needed for the proposed framework to assess how replacing the mixing tubes affects the collected data. Mixing tube orientation and nut tightening torque can be varied.

During the data collection trials, the bottom of the AWJ tank was damaged. This part of the data collection method could be optimised by studying the particle impact on the bottom of the AWJ catcher tank. To minimise damage, the height effect of
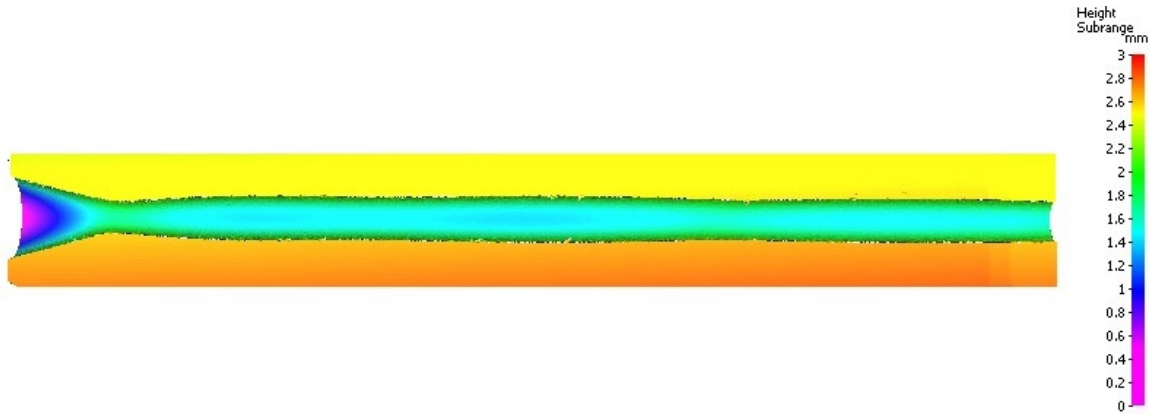
Figure 7.2: Alicona scan of mixing tube 8. The Alicona scan is of the top half of the mixing tube, taken after the mixing tube was sectioned via EDM.

the AWJ above the water level can be explored, together with the water depth, steel thickness, and angle of the catcher tank.

In Chapter 5, the internal profiles of the mixing tubes were studied after the tubes were sectioned using EDM. Further work can look at sine wave analysis of these profiles to better characterise the wave pattern and its potential flow-related causes. Alicona scans, which use high-resolution optical 3D surface measurement technology, can be employed to achieve higher resolution of the internal mixing tube profiles. Compared to using digital photography for contour detection, as shown in Figure 5.13. A sample Alicona scan of mixing tube 8 is presented in Figure 7.2. Alicona scans can also help quantify the wear profile progression through roughness and wear depth measurements. Challenges associated with using Alicona include the length of the mixing tubes, requiring a balance between processing time and final scan resolution. Multiple scans may be required per mixing tube to capture the entire length of the tube.

The use of computational fluid dynamics (CFD) for further research should be considered. CFD can be used to investigate the effect of mixing tube inlet cone angle and inlet cone length on abrasive particle trajectories and resulting wear patterns, providing valuable insights for optimising tool design and reducing mixing tube wear. This analysis would extend the findings presented in Chapter 5 and help explain variations observed in Figures 5.11 and 5.12, which compare mixing tubes with different inlet angles.

By integrating CFD, future work could also build on the machine learning research presented in this thesis. CFD offers physics-based insights into the wear process, complementing data-driven machine learning approaches to achieve more robust and

interpretable predictions. It could be used to generate synthetic data representing various flow conditions, wear patterns, design parameters and abrasive properties. This additional data could enhance machine learning models by providing both new features (such as velocity gradients) and larger datasets for training, improving generalisation by simulating diverse wear scenarios. Using CFD to expand the dataset size would directly address the data drift limitations discussed in Chapter 6.

When collecting the data and conducting data quality validation in Chapter 5, it was noted that the airflow sensor was suitable for spotting different operational faults on the AWJ. For example, the presence of humidity in the abrasive hose, unstable pressure, or non-mixing tube part wear and failure. It was also previously successful in detecting orifice wear [86]. Therefore, using a similar framework discussed in this thesis, the sensor can be used to diagnose process faults, for example, via clustering algorithms or autoencoders for anomaly detection. Fault diagnosis could also be applied during the running of a machine.

Despite an extensive exploration of machine learning methods in this thesis, a significant number of alternative approaches are available and could be explored. The application of computer vision algorithms together with converted sensor data via spectorgrams or gramian angular field, as seen in Figure 7.3, can be studied. Neural networks, sequential models and the use of wavelet analysis for feature engineering should also be considered. The prediction of remaining useful life was not done in this thesis and can be explored.

GADF images of ATD data at different levels of wear
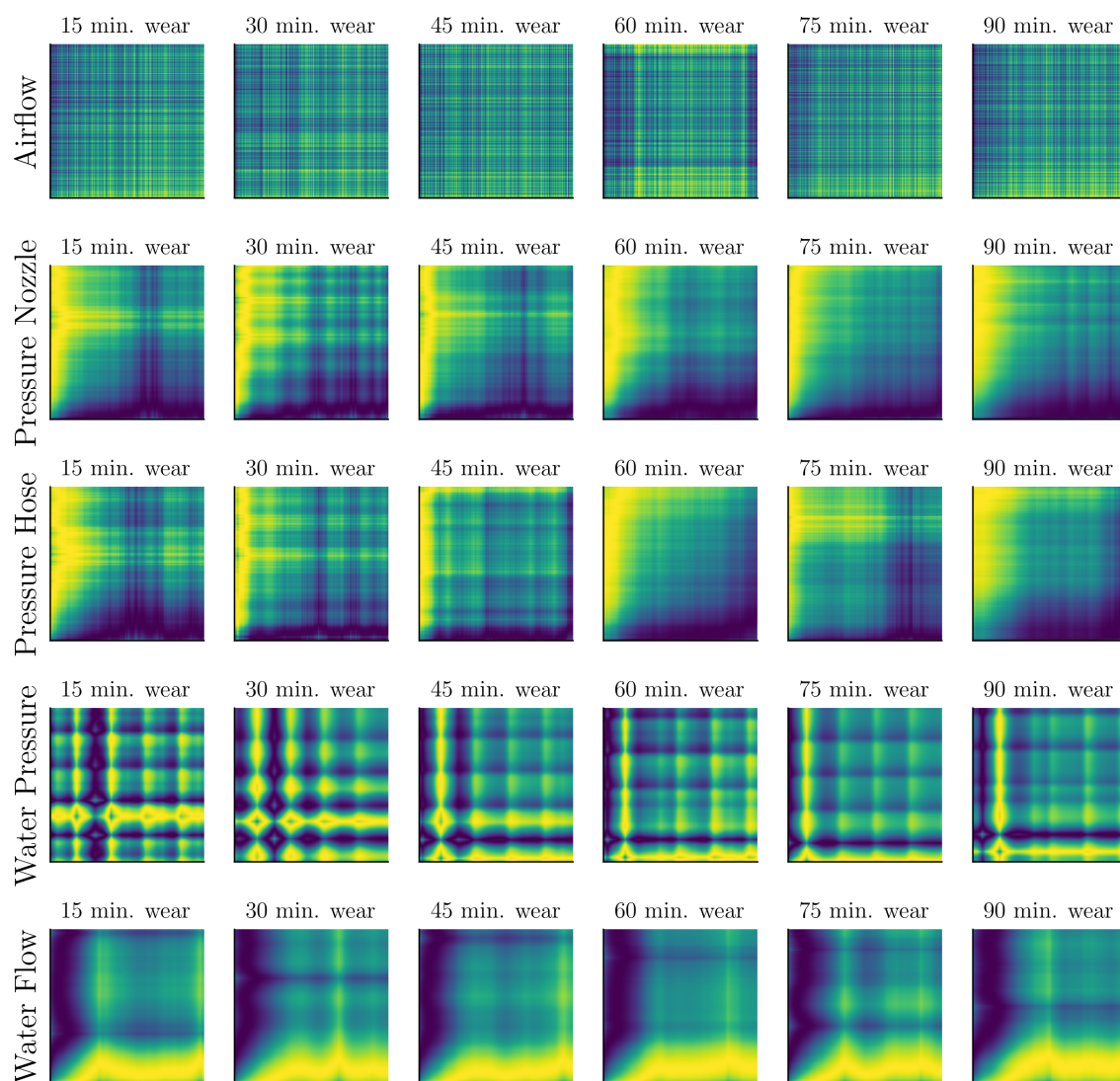
Figure 7.3: Gramian angular difference field encoded images from raw sensor data at different stages of mixing tube wear. The data used to encode the images was from the ATD data recorded in Phase II of the main trial at 4000 bar water pressure for mixing tubes 3 (15 min. wear), 4 (30 min. wear), 5 (45 min. wear), 6 (60 min. wear), 7 (75 min. wear) and 8 (90 min. wear).

References

[1]   CIRP, ed. "Dictionary of Production Engineering II - Material removal processes". 1st. Vol. 2. Springer, 2004.

[2]   Mohamed Hashish. "Method and apparatus for forming a high velocity liquid abrasive jet".

[3]   Andreas W. Momber and Radovan Kovacevic. "Generation of Abrasive Water Jets". *Principles of Abrasive Water Jet Machining*. 1998, pp. 20–76. DOI: `10.1007/978-1-4471-1572-4{\_}3`.

[4]   Shijin Zhang, Xiaohong Li, and Yilei Gu. "Air flow exploration of abrasive feed tube". *Acta Mechanica Sinica* 25.6 (2009), pp. 761–768. DOI: `10.1007/s10409-009-0290-2`.

[5]   Mohamed Hashish. "Suction Characteristics of Abrasive-Waterjet Nozzles". Tech. rep. Flow Industries, Inc., 1984.

[6]   Xiang Zou, Liandong Fu, Lin Wu, and Wenhao Zuo. "Research on Multiphase Flow and Nozzle Wear in a High-Pressure Abrasive Water Jet Cutting Head". *Machines* 11.6 (2023). DOI: `10.3390/machines11060614`.

[7]   M. Hashish. "Observations of wear of abrasive-waterjet nozzle materials". *Journal of Tribology* 116.3 (1994), pp. 439–444. DOI: `10.1115/1.2928861`.

[8]   Mohamed Hashish, A. Kotchon, and M. Ramulu. "Status of AWJ machining of CMCs and hard materials". *Proceedings of Intertech*. Indianapolis, 2015.

[9]   Tae Min Oh, Gun Wook Joo, Yohan Cha, and Gye Chun Cho. "Effect of garnet characteristics on abrasive waterjet cutting of hard granite rock". *Advances in Civil Engineering* 2019 (2019). DOI: `10.1155/2019/5732649`.

[10]   James G. Evans and Phillip R. Moyle. "U.S. Industrial Garnet". *Contributions to Industrial-Minerals Research*. 2006.

[11]   "Product Data Sheet GMA ClassicCut 80". *GMA Garnet*.

[12]   Andrzej Perec. "Environmental aspects of abrasive water jet cutting". *Rocznik Ochrona Srodowiska* 20 (2018), pp. 258–274.

[13]   Andrzej Perec, Frank Pude, Anton Grigoryev, Michael Kaufeld, and Konrad Wegener. "A study of wear on focusing tubes exposed to corundum-based abrasives in the waterjet cutting process". *International Journal of Advanced Manufacturing Technology* 104.5-8 (2019), pp. 2415–2427. DOI: `10.1007/s00170-019-03971-0`.

[14]   Madhusarathi Nanduri, David G. Taggart, and Thomas J. Kim. "The effects of system and geometric parameters on abrasive water jet nozzle wear". *International Journal of Machine Tools and Manufacture* 42.5 (2002), pp. 615–623. DOI: `10.1016/S0890-6955(01)00147-X`.

[15]   M. Adam Khan, Hargovind Soni, P. M. Mashinini, and M. Uthayakumar. "Abrasive water jet cutting process form machining metals and composites for engineering applications: A review". *Engineering Research Express* 3 (2021). DOI: `10.1088/2631-8695/abfe98`.

[16]   P. P. Badgujar and M. G. Rathi. "Abrasive Waterjet Machining-A State of Art". *IOSR Journal of Mechanical and Civil Engineering* 11.3 (2014), pp. 59–64.

[17]   Duane Snider and Mohamed Hashish. "AWJ Trimming of Composites and Cutting of Other Materials Using 6-Axis Robots". *WJTA-IMCA Conference and Expo.* 2011.

[18]   Jamal Y. Sheikh-Ahmad. "Machining of polymer composites". Springer US, 2009, pp. 1–315. DOI: `10.1007/978-0-387-68619-6`.

[19]   Kevin Kerrigan and Garret E. O'Donnell. "On the Relationship between Cutting Temperature and Workpiece Polymer Degradation during CFRP Edge Trimming". *Procedia CIRP.* Vol. 55. Elsevier B.V., 2016, pp. 170–175. DOI: `10.1016/j.procir.2016.08.041`.

[20]   Madhusarathi Nanduri, David G. Taggart, and Thomas J. Kim. "A study of nozzle wear in abrasive entrained water jetting environment". *Journal of Tribology* 122.2 (2000), pp. 465–471. DOI: `10.1115/1.555383`.

[21]   H. Syazwani, G. Mebrahitom, and A. Azmir. "A review on nozzle wear in abrasive water jet machining application". *IOP Conference Series: Materials Science and Engineering* 114 (2016). DOI: `10.1088/1757-899X/114/1/012020`.

[22]   E. A. Ness, E. Dubensky, C. Haney, G. Mort, and P. J Singh. "New Developments in ROCTEC Composite Carbides for Use in Abrasive Waterjet Applications". *Proceedings of the 12th International Conference on Jet Cutting Technology.* 1994, pp. 195–211.

[23]   "Waterjet Cutting With The Purest Almandine Garnet - Maximise Production". URL: `https://www.gmagarnet.com/en-gb/waterjet-cutting/waterjet-parts/waterjet-orifices`. *(accessed on: 21-08-2023).*

[24]   J. John Rozario Jegaraj and N. Ramesh Babu. "Condition Monitoring of Orifice in Abrasive Waterjet Cutting System Using High Pressure Sensor". *44th Proceedings of the North American Manufacturing Research Institution of SME.* Vol. 5. 2016, pp. 578–593. DOI: `10.1016/j.promfg.2016.08.048`.

[25]   Mohamed Hashish. "Inside AWJ Nozzles". *WJTA American Waterjet Conference.* Waterjet Technology Association, 2003.

[26] Hakan Wiklund. "Bayesian and regression approaches to on-line prediction of residual tool life". *Quality and Reliability Engineering International* (1998), pp. 303–309.

[27] Adam G Rehorn, Jin Jiang, and Peter E Orban. "State-of-the-art methods and results in tool condition monitoring: a review". *International Jorunal of Advanced Manufacturing Technology* 26 (2005), pp. 693–710. DOI: 10.1007/s00170-004-2038-2.

[28] R. Teti, K. Jemielniak, G. O'Donnell, and D. Dornfeld. "Advanced monitoring of machining operations". *CIRP Annals - Manufacturing Technology* 59.2 (2010), pp. 717–739. DOI: 10.1016/j.cirp.2010.05.010.

[29] Mo A. Elbestawi, Mihaela Dumitrescu, and Eu-Gene Ng. "Tool Condition Monitoring in Machining". *Condition Monitoring and Control for Intelligent Manufacturing*. 2006, pp. 55–82.

[30] Radovan Kovacevic and Yu Ming Zhang. "On-Line Fuzzy Recognition of Abrasive Waterjet Nozzle Wear". *Jet Cutting Technology*. Ed. by A. Lichtarowicz. Vol. 13. 1992, pp. 329–345. DOI: 10.1007/978-94-011-2678-6{_}22.

[31] G. Byrne, D. Dornfeld, I. Inasaka, G. Ketteler, W. Konig, and R. Teti. "Tool Condition Monitoring (TCM) - The Status of Research and Industrial Application". *Annals of the CIRP*. 1995, pp. 541–567.

[32] Miha Prijatelj, Marko Jerman, Henri Orbanić, Izidor Sabotin, Joško Valentinčič, and Andrej Lebar. "Determining focusing nozzle wear by measuring AWJ diameter". *Strojniski Vestnik/Journal of Mechanical Engineering* 63.10 (2017), pp. 597–605. DOI: 10.5545/sv-jme.2017.4424.

[33] Ananda Mohon Ghosh and Katarina Grolinger. "Edge-Cloud Computing for Internet of Things Data Analytics: Embedding Intelligence in the Edge with Deep Learning". *IEEE Transactions on Industrial Informatics* 17.3 (2021), pp. 2191–2200. DOI: 10.1109/TII.2020.3008711.

[34] Ashwani Kumar, T. V.K. Gupta, Rajib Kumar Jha, and Subrata Kumar Ghosh. "Wear analysis of abrasive waterjet nozzle using suprathreshold stochastic resonance technique". *Proceedings of the Institution of Mechanical Engineers, Part E: Journal of Process Mechanical Engineering*. 2020, pp. 3–8. DOI: 10.1177/0954408920968354.

[35] R. Kovacevic, R. Mohan, and H. E. Beardsley. "Monitoring of thermal energy distribution in abrasive waterjet cutting using infrared thermography". *Journal of Manufacturing Science and Engineering, Transactions of the ASME* 118 (1996), pp. 555–563. DOI: 10.1115/1.2831067.

[36] Jiyue Zeng and José P Muñoz. "Feasibility of monitoring abrasive waterjet conditions by means of a vacuum sensor". *Jet Cutting Technology*. 1994, pp. 553–565.

[37] H. Louis and G. Meier. "Methods of Process Control for Abrasive Water Jets". *Proceedings of the 6th American Water Jet Conference*. 1991, pp. 427–437.

[38] Andreas W. Momber and Radovan Kovacevic. "Control and Supervision of Abrasive Water-Jet Machining Processes". *Principles of Abrasive Water Jet Machining*. 1998, pp. 333–375. DOI: 10.1007/978-1-4471-1572-4{_}10.

[39] R. Prabu and A. Manivannan. "Condition Monitoring of Focusing Nozzle in Abrasive Water Jet Machine using Sound Sensor". *Indian Journal of Science and Technology* 10.17 (2017), pp. 1–12. DOI: 10.17485/ijst/2017/v10i17/112583.

[40] M. Bauer, H. J. Maier, T. Hassel, and O. Grünzel. "Full Automatization of Waterjet Cutting". *WJTA American Waterjet Conference*. 2017.

[41] Edoardo Copertaro, Francesco Perotti, and Massimiliano Annoni. "Operational vibration of a waterjet focuser as means for monitoring its wear progression". *The International Journal of Advanced Manufacturing Technology* 116 (2021), pp. 1937–1949. DOI: 10.1007/s00170-021-07534-0/Published.

[42] R. S. Mohan and R. Kovacevic. "Real Time Monitoring of AWJ Nozzle Wear Using ANN". *Transactions of the North American Manufacturing Research Institute of SME* 12 (1994), pp. 253–258.

[43] Jeong Uk Kim, Roh Won Kim, Sung Ryul Kim, Hyun Hee Kim, and Kyung Chang Lee. "Nozzle Condition Monitoring System Using Root Mean Square of Acoustic Emissions during Abrasive Waterjet Machining". *Journal of Manufacturing and Materials Processing* 6.2 (2022). DOI: 10.3390/jmmp6020031.

[44] Aurélien Géron. "Hands-on machine learning with Scikit-Learn, Keras and TensorFlow: concepts, tools, and techniques to build intelligent systems". 2019.

[45] Darek Kłeczek, Bryan Bischof, and Hamel Husain. "MLOps: A Holistic Approach". Tech. rep. Weights & Biases.

[46] John Branch. "Water Jet Pump Maintenance Series – Part 3: High Pressure Seal Change/Repair". URL: https://blog.jetedgewaterjets.com/water-jet-pumps/pump-maintenance-series-part-3-high-pressure-seal-change-repair. *(accessed on: 18-01-2024)*.

[47] Mohamad Hashish, David Monserad, and Steve Craigen. "Abrasive-waterjet nozzle for intelligent control".

[48] Mohamed Hashish. "Wear Performance of Alternative Materials for AWJ Nozzles". Tech. rep. Flow Industries Inc, 1985.

[49] E. J. Chalmers. "Effect of Parameter Selection on Abrasive Waterjet Performance". *6th American Water Jet Conference*. Water Jet Technology Association, 1991, pp. 345–354.

[50] M. Hashish. "Optimization Factors in Abrasive-Waterjet Machining". *Journal of Engineering for Industry* 113 (1991), pp. 29–37.

[51] Andreas W. Momber. "Energy transfer during the mixing of air and solid particles into a high-speed waterjet: An impact-force study". *Experimental Thermal and Fluid Science* 25 (2001), pp. 31–41. DOI: 10.1016/S0894-1777(01)00057-7.

[52] A. H. Osman, T. Mabrouki, B. Théry, and D. Buisine. "Experimental analysis of high-speed air-water jet flow in an abrasive water jet mixing tube". *Flow Measurement and Instrumentation* 15.1 (2004), pp. 37–48. DOI: `10.1016/j.flowmeasinst.2003.08.001`.

[53] U. Himmelreich and W. Riess. "Hydrodynamic Investigations on Abrasive-Waterjet Cutting Tools". *Proceedings of the 10th International Symposium on Jet Cutting Technology*. Elsevier Science Publishing, 1991.

[54] W. F. Gale and T. C. Totemeier. "Friction and wear". *Smithells Metals Reference Book*. 8th ed. Butterworth-Heinemann, 2004. DOI: `10.1016/B978-075067509-3/50028-2`.

[55] J. G. A. Bitter. "A study of erosion phenomena Part I". *Wear* 6.3 (1963), pp. 5–21.

[56] J. G. A. Bitter. "A study of erosion phenomena Part II". *Wear* 6.3 (1963), pp. 169–190.

[57] M. Ramulu, M. G. Jenkins, T. L. Stevens, and J. A. Salem. "Wear Performance of Monolithic and Composite Mixing Tubes for Abrasive Water Jet Cutting of Ceramics". *Ceramic Engineering and Science Proceedings*. Ed. by Don Bray. July 2020. 1998, pp. 45–54. DOI: `10.1002/9780470294499.ch6`.

[58] Andrzej Perec, Aleksandra Radomska-Zalas, and Anna Fajdek-Bieda. "Experimental research into marble cutting by abrasive water jet". *Facta Universitatis, Series: Mechanical Engineering* 20.1 (2022), pp. 145–156. DOI: `10.22190/FUME210203037P`.

[59] "ROCTEC Abrasive Waterjet Nozzles: Composite Carbide Mixing Tubes".

[60] Xiaochen Chen, Songsheng Deng, Jinfa Guan, and Weixing Hua. "Experiment and simulation research on abrasive water jet nozzle wear behavior and anti-wear structural improvement". *Journal of the Brazilian Society of Mechanical Sciences and Engineering* 39.6 (2017), pp. 2023–2033. DOI: `10.1007/s40430-017-0707-y`.

[61] Mingming Du, Haijin Wang, Huiyue Dong, Yingjie Guo, and Yinglin Ke. "Numerical research on multi-particle movements and nozzle wear involved in abrasive waterjet machining". *The International Journal of Advanced Manufacturing Technology* 117 (2021), pp. 2845–2858. DOI: `10.1007/s00170-021-07876-9/Published`.

[62] Naqib Hakim Kamarudin, A. K. Prasada Rao, and Azmir Azhari. "CFD Based Erosion Modelling of Abrasive Waterjet Nozzle using Discrete Phase Method". *IOP Conference Series: Materials Science and Engineering* 114.1 (2016). DOI: `10.1088/1757-899X/114/1/012016`.

[63] Xinping Long, Xiaofeng Ruan, Qi Liu, Zhengwen Chen, Shengxiong Xue, and Ziquan Wu. "Numerical investigation on the internal flow and the particle movement in the abrasive waterjet nozzle". *Powder Technology* 314 (2017), pp. 635–640. DOI: `10.1016/j.powtec.2016.09.089`.

[64] Ruslan Melentiev and Fengzhou Fang. "Recent advances and challenges of abrasive jet machining". *CIRP Journal of Manufacturing Science and Technology* 22 (2018), pp. 1–20. DOI: 10.1016/j.cirpj.2018.06.001.

[65] Mohamed Hashish. "Pressure effects in abrasive-waterjet (AWJ) machining". *Journal of Engineering Materials and Technology, Transactions of the ASME* 111.3 (1989), pp. 221–228. DOI: 10.1115/1.3226458.

[66] B. Nedić and J. Baralić. "The wear of the focusing tube and the cut-surface quality". *Tribology in Industry* 32.2 (2010), pp. 38–48.

[67] M. Hashish. "Singulation of micro SD cards with AWJ". Tech. rep. Flow International Corporation, 2006.

[68] D. K. Shanmugam, J. Wang, and H. Liu. "Minimisation of kerf tapers in abrasive waterjet machining of alumina ceramics using a compensation technique". *International Journal of Machine Tools and Manufacture* 48.14 (2008), pp. 1527–1534. DOI: 10.1016/j.ijmachtools.2008.07.001.

[69] Mehdi Zohoor and S. Hadi Nourian. "Development of an algorithm for optimum control process to compensate the nozzle wear effect in cutting the hard and tough material using abrasive water jet cutting process". *International Journal of Advanced Manufacturing Technology* 61.9-12 (2012), pp. 1019–1028. DOI: 10.1007/s00170-011-3761-0.

[70] Sam Ashworth and Nicolas Duboust. "The effect of platform and process on machining CFRP for High Value Manufacturing Catapult UK". Tech. rep. AMRC, 2021.

[71] D. G. Taggart, M. Nanduri, and T. J. Kim. "Evaluation of an accelerated wear test for AWJ nozzles". *9th American Waterjet Conference*. 1997, pp. 239–250.

[72] Randall S Lynn, Kien K Wong, and Hector MCI Clark. "On the particle size effect in slurry erosion". *Wear* 149 (1991), pp. 55–71.

[73] H. McI. Clark and Ryan B. Hartwich. "A re-examination of the 'particle size effect' in slurry erosion". *Wear* 248 (2001), pp. 147–161.

[74] Jianxin Deng, Zeliang Ding, Houming Zhou, and Yuanqiang Tan. "Performance and wear characteristics of ceramic, cemented carbide, and metal nozzles used in coal-water-slurry boilers". *International Journal of Refractory Metals and Hard Materials* 27.5 (2009), pp. 919–926. DOI: 10.1016/j.ijrmhm.2009.05.007.

[75] Jianxin Deng, Xihua Zhang, Pingzhang Niu, Lili Liu, and Jinghai Wang. "Wear of ceramic nozzles by dry sand blasting". *Tribology International* 39.3 (2006), pp. 274–280. DOI: 10.1016/j.triboint.2004.07.026.

[76] R. Kovacevic, L. Wang, and Y. M. Zhang. "Identification of abrasive waterjet nozzle wear based on parametric spectrum estimation of acoustic signal". *Proceedings of the Institution of Mechanical Engineers, Part B: Journal of Engineering Manufacture*. Vol. 208. B3. 1994, pp. 173–181.

[77] M. Abudaka and P. S. Crofton. "Theoretical analysis and preliminary experimental results for an abrasive water jet cutting head". *Proc. 5th American Water Jet Conference, WJTA*. 1989, pp. 79–87.

[78] M. Nanduri, D. Taggart, T. Kim, C. Haney, and Waterjet Technology Association. "Effect Of The Inlet Taper Angle On AWJ Nozzle Wear". *Proceedings of the 9th American Water Jet Conference*. American waterjet conference. 1997, pp. 223–238.

[79] K. Yanaida. "Flow Characteristics of Waterjets". *2nd International Symposium on Jet Cutting Technology*. BHRA, 1974, A2/19–A2/32.

[80] "Private communication with Dr Pierre Ricco, University of Sheffield".

[81] A. Evans and D. Marshall. "Fundamentals of Friction and Wear of Materials". Ed. by David Rigney. American Society for Metals, 1981, pp. 439–452.

[82] Jose Vicente Abellan-Nebot and Fernando Romero Subirón. "A review of machining monitoring systems based on artificial intelligence process models". *International Journal of Advanced Manufacturing Technology* 47.1-4 (2010), pp. 237–257. DOI: 10.1007/s00170-009-2191-8.

[83] P. Hreha, A. Radvanská, J. Cárach, D. Lehocká, K. Monková, G. Krolczyk, A. Ruggiero, I. Samardzić, D. Kozak, and S. Hloch. "Monitoring of focusing tube wear during abrasive waterjet (AWJ) cutting of AISI 309". *Metalurgija* 53.4 (2014), pp. 533–536.

[84] R. Kovacevic. "Development of opto-electronic sensor for monitoring the abrasive waterjet nozzle wear". *The ASME's Winter Annual Meeting, Symposium on Sensors, Controls, and Quality Issues in Manufacturing*. 1991.

[85] M. Annoni, F. Arleo, and C. Malmassari. "CFD aided design and experimental validation of an innovative Air Assisted Pure Water Jet cutting system". *Journal of Materials Processing Technology* 214.8 (2014), pp. 1647–1657. DOI: 10.1016/j.jmatprotec.2014.01.020.

[86] M. Putz, M. Dittrich, and M. Dix. "Process Monitoring of Abrasive Waterjet Formation". *Procedia CIRP* 46 (2016), pp. 43–46. DOI: 10.1016/j.procir.2016.03.189.

[87] J. Colgan, H. Chin, K. Danai, and S. R. Hayashi. "On-Line Tool Breakage Detection in Turning: A Multi-Sensor Method". *Journal of Engineering for Industry* 116 (1994), pp. 117–123.

[88] M. S. Lan and D. A. Dornfeld. "In-Process Tool Fracture Detection". *Journal of Engineering Materials and Technology* 106 (1984), pp. 111–118.

[89] S. H. Yeo, L. P. Khoo, and S. S. Neo. "Tool condition monitoring using reflectance of chip surface and neural network". *Journal of Intelligent Manufacturing* 11 (2000), pp. 507–514.

[90] Yuchen Zhou, Peter Orban, and Suwas Nikumb. "Sensors for intelligent machining - a research and application survey". *Proceedings of the IEEE International Conference on Systems, Man and Cybernetics*. Vol. 2. IEEE, 1995, pp. 1005–1010. DOI: `10.1109/ICSMC.1995.537900`.

[91] Shang-Liang Chen and Y W Jen. "Data fusion neural network for tool condition monitoring in CNC milling machining". *International Journal of Machine Tools & Manufacture* 40 (2000), pp. 381–400.

[92] E. J. Cross. "On Structural Health Monitoring in Changing Environmental and Operational Conditions in the Faculty of Engineering". PhD thesis. The University of Sheffield, 2012.

[93] Yuqing Zhou and Wei Xue. "Review of tool condition monitoring methods in milling processes". *International Journal of Advanced Manufacturing Technology* 96.5-8 (2018), pp. 2509–2523. DOI: `10.1007/s00170-018-1768-5`.

[94] Nitin Ambhore, Dinesh Kamble, Satish Chinchanikar, and Vishal Wayal. "Tool condition monitoring system: A review". *Materials Today: Proceedings*. Vol. 2. 4-5. Elsevier Ltd, 2015, pp. 3419–3428. DOI: `10.1016/j.matpr.2015.07.317`.

[95] D. T. Thinh, N. B. H. Quan, and N. Maneetien. "Implementation of Moving Average Filter on STM32F4 for Vibration Sensor Application". *4th International Conference on Green Technology and Sustainable Development*. 2018, pp. 627–631.

[96] Myeongsu Kang and Jing Tian. "Machine Learning: Data Pre-processing". *Prognostics and Health Management of Electronics*. John Wiley & Sons Ltd., 2018, pp. 111–130.

[97] H. S. Obaid, S. A. Dheyab, and S. S. Sabry. "The Impact of Data Pre-Processing Techniques and Dimensionality Reduction on the Accuracy of Machine Learning". *9th Annual Information Technology, Electromechanical Engineering and Microelectronics Conference (IEMECON)*. 2019, pp. 279–283.

[98] Gustavo E.A.P.A. Batista and Maria Carolina Monard. "An analysis of four missing data treatment methods for supervised learning". *Applied Artificial Intelligence* 17.5-6 (2003), pp. 519–533. DOI: `10.1080/713827181`.

[99] Nicholas J Horton and Ken P Kleinman. "Much ado about nothing: A comparison of missing data methods and software to fit incomplete data regression models". *Am Stat.* (2007). DOI: `10.1198/000313007X172556`.

[100] Shichao Zhang. "Nearest neighbor selection for iteratively kNN imputation". *Journal of Systems and Software* 85.11 (2012), pp. 2541–2552. DOI: `10.1016/j.jss.2012.05.073`.

[101] Keith Worden, Wieslaw J. Staszewski, and James J. Hensman. "Natural computing for mechanical systems research: A tutorial overview". *Mechanical Systems and Signal Processing* 25 (2011), pp. 4–111. DOI: `10.1016/j.ymssp.2010.07.013`.

[102] Henri J. Nussbaumer. "The Fast Fourier Transform". *Fast Fourier Transform and Convolution Algorithms*. Springer, 1982, pp. 80–111. DOI: `10.1007/978-3-642-81897-4{\_}4`.

[103] Paul Heckbert. "Fourier Transforms and the Fast Fourier Transform (FFT) Algorithm".

[104] Emiel Por, Maaike Van Kooten, and Vanja Sarkovic. "Nyquist-Shannon sampling theorem". Tech. rep. 2019.

[105] G. Serin, B. Sener, A. M. Ozbayoglu, and H. O. Unver. "Review of tool condition monitoring in machining and opportunities for deep learning". *The International Journal of Advanced Manufacturing Technology* 109 (2020), pp. 953–974. DOI: `10.1007/s00170-020-05449-w/Published`.

[106] Andrew K.S. Jardine, Daming Lin, and Dragan Banjevic. "A review on machinery diagnostics and prognostics implementing condition-based maintenance". *Mechanical Systems and Signal Processing* 20.7 (2006), pp. 1483–1510. DOI: `10.1016/j.ymssp.2005.09.012`.

[107] Xiang Wang, Yuan Zheng, Zhenzhou Zhao, and Jinping Wang. "Bearing fault diagnosis based on statistical locally linear embedding". *Sensors (Switzerland)* 15.7 (2015), pp. 16225–16247. DOI: `10.3390/s150716225`.

[108] "Signal Features - MATLAB & Simulink - MathWorks United Kingdom". URL: `https://uk.mathworks.com/help/predmaint/ug/signal-features.html`. *(accessed on: 27-12-2023)*.

[109] Onur Surucu, Stephen Andrew Gadsden, and John Yawney. "Condition Monitoring using Machine Learning: A Review of Theory, Applications, and Recent Advances". *Expert Systems with Applications* 221 (2023). DOI: `10.1016/j.eswa.2023.119738`.

[110] Melvin Alexis Lara de Leon, Jakub Kolarik, Radek Byrtus, Jiri Koziorek, Petr Zmij, and Radek Martinek. "Tool Condition Monitoring Methods Applicable in the Metalworking Process". *Archives of Computational Methods in Engineering* (2023). DOI: `10.1007/s11831-023-09979-w`.

[111] Indivarie Ubhayaratne, Michael P. Pereira, Yong Xiang, and Bernard F. Rolfe. "Audio signal analysis for tool wear monitoring in sheet metal stamping". *Mechanical Systems and Signal Processing* 85 (2017), pp. 809–826. DOI: `10.1016/j.ymssp.2016.09.014`.

[112] Constantin Constantinescu and Remus Brad. "An Overview on Sound Features in Time and Frequency Domain". *International Journal of Advanced Statistics and IT&C for Economics and Life Sciences* 13.1 (2023), pp. 45–58. DOI: `10.2478/ijasitels-2023-0006`.

[113] Mrinmoy Bhattacharjee, S. R. M. Prasanna, and Prithwijit Guha. "Time-Frequency Audio Features for Speech-Music Classification" (2018).

[114] Krzysztof Jemielniak, Tomasz Urbański, Joanna Kossakowska, and Sebastian Bombiński. "Tool condition monitoring based on numerous signal features". *International Journal of Advanced Manufacturing Technology* 59.1-4 (2012), pp. 73–81. DOI: `10.1007/s00170-011-3504-2`.

[115] D. Sandoval, U. Leturiondo, F. Pozo, Y. Vidal, and O. Salgado. "Trends in condition monitoring for pitch bearings". *16th International Conference on Condition Monitoring and Asset Management.* British Institute of Non-Destructive Testing, 2019. DOI: `10.1784/cm.2019.113`.

[116] A. M. Sayeed, A. Papandreou-Suppappola, S. B. Suppappola, X. G. Xia, F. Hlawatsch, G. Matz, Boualem Boashash, G. Azemi, and N. A. Khan. "Detection, Classification, and Estimation in the (t,f) Domain". *Time-Frequency Signal Analysis and Processing.* Second Edition. Academic Press, 2016. Chap. 12, pp. 693–743. DOI: `10.1016/B978-0-12-398499-9.00012-1`.

[117] O. M. Solomon. "PSD Computations Using Welch's Method". Tech. rep. Sandia National Lab, 1991.

[118] Peter D. Welch. "The Use of Fast Fourier Transform for the Estimation of Power Spectra: A Method Based on Time Averaging Over Short, Modified Periodograms". *IEEE Transactions on Audio and Electroacoustics* 15.2 (1967), pp. 70–73. DOI: `10.1109/TAU.1967.1161901`.

[119] "Welch spectrum - MATLAB spectrum.welch - MathWorks United Kingdom". URL: `https://uk.mathworks.com/help/signal/ref/spectrum.welch.html`. *(accessed on: 03-01-2024)*.

[120] Jorge R. Vergara and Pablo A. Estévez. "A review of feature selection methods based on mutual information". *Neural Computing and Applications* 24 (2014), pp. 175–186. DOI: `10.1007/s00521-013-1368-0`.

[121] Daniel E Kirby, Zhe Zhang, and Joseph C. Chen. "Development of an Accelerometer-Based Surface Roughness Prediction System in Turning Operations Using Multiple Regression Techniques". *Journal of Industrial Technology* 20.4 (2004).

[122] A. Al-Habaibeh and N. Gindy. "A new approach for systematic design of condition monitoring systems for milling processes". *Journal of Materials Processing Technology* 107 (2000), pp. 243–251.

[123] Yu Quan, Meng Chu Zhou, and Zhenbi Luo. "On-line robust identification of tool-wear via multi-sensor neural-network fusion". *Engineering Applications of Artificial Intelligence* 11 (1998), pp. 717–722. DOI: `10.1016/S0952-1976(98)00046-3`.

[124] Thomas M Cover and Joy A Thomas. "Elements of Information Theory". Wiley & Sons, 2006.

[125] Valeria Fonti and Eduard Belitser. "Feature Selection using LASSO". PhD thesis. VU Amsterdam, 2017.

[126] Kim Esbensen and Paul Geladi. "Principal Component Analysis". *Chemometrics and Intelligent Laboratory Systems* (1987), pp. 37–52.

[127] Dong Hyeon Kim, Thomas J.Y. Kim, Xinlin Wang, Mincheol Kim, Ying Jun Quan, Jin Woo Oh, Soo Hong Min, Hyungjung Kim, Binayak Bhandari, In-soon Yang, and Sung Hoon Ahn. "Smart Machining Process Using Machine Learning: A Review and Perspective on Machining Industry". *International Journal of Precision Engineering and Manufacturing - Green Technology* 5.4 (2018), pp. 555–568. DOI: 10.1007/s40684-018-0057-y.

[128] Alexei Botchkarev. "A new typology design of performance metrics to measure errors in machine learning regression algorithms". *Interdisciplinary Journal of Information, Knowledge, and Management* 14 (2019), pp. 45–76. DOI: 10.28945/4184.

[129] Guy S. Handelman, Hong Kuan Kok, Ronil V. Chandra, Amir H. Razavi, Shiwei Huang, Mark Brooks, Michael J. Lee, and Hamed Asadi. "Peering into the black box of artificial intelligence: Evaluation metrics of machine learning methods". *American Journal of Roentgenology* 212.1 (2019), pp. 38–43. DOI: 10.2214/AJR.18.20224.

[130] Corinna Cortes, Vladimir Vapnik, and Lorenza Saitta. "Support-Vector Networks". *Machine Learning* 20 (1995), pp. 273–297.

[131] Fabian Pedregosa, Gaël Varoquaux, Alexandre Gramfort, Vincent Michel, Bertrand Thirion, Olivier Grisel, Mathieu Blondel, Peter Prettenhofer, Vincent Dubourg, Alexandre Passos, Jake Vanderplas, Alexandre Passos, David Cournapeau, Matthieu Brucher, Matthieu Perrot, and Edouard Duchesnay. "Scikit-learn: Machine Learning in Python". *Journal of Machine Learning Research* 12 (2011), pp. 2825–2830.

[132] Konrad Banachewicz, Luca Massaron, and Anthony Goldbloom. "The Kaggle Book: Data analysis and machine learning for competitive data science". 2022.

[133] Pierre Geurts, Damien Ernst, and Louis Wehenkel. "Extremely randomized trees". *Machine Learning* 63.1 (2006), pp. 3–42. DOI: 10.1007/s10994-006-6226-1.

[134] Jerome H Friedman. "Greedy Function Approximation: A gradient boosting machine". *The Annals of Statistics* 29.5 (2001), pp. 1189–1232.

[135] Tianqi Chen and Carlos Guestrin. "XGBoost : A Scalable Tree Boosting System". *KDD '16: Proceedings of the 22nd ACM SIGKDD International Conference on Knowledge Discovery and Data Mining*. 2016. DOI: 10.1145/2939672.2939785.

[136] Guolin Ke, Qi Meng, Thomas Finley, Taifeng Wang, Wei Chen, Weidong Ma, Qiwei Ye, and Tie-Yan Liu. "LightGBM: A Highly Efficient Gradient Boosting Decision Tree". *31st Conference on Neural Information Processing Systems*. California, 2017.

[137] Liudmila Prokhorenkova, Gleb Gusev, Aleksandr Vorobev, Anna Veronika Dorogush, and Andrey Gulin. "CatBoost: unbiased boosting with categorical features". *32nd Conference on Neural Information Processing Systems*. 2018.

[138] Haithm Alshari, Abdulrazak Yahya Saleh, and Alper Odabaş. "Comparison of Gradient Boosting Decision Tree Algorithms for CPU Performance". *Journal of Institute Of Science and Technology* 37.1 (2021).

[139] Noah Hollmann, Samuel Müller, Katharina Eggensperger, and Frank Hutter. "TabPFN: A Transformer That Solves Small Tabular Classification Problems in a Second". *ICLR*. 2023.

[140] T. M. Cover and P. E. Hart. "Nearest Neighbor Pattern Classification". *IEEE Transactions on Information Theory* (1967), pp. 21–27.

[141] María Teresa García Ordás. "Wear characterization of the cutting tool in milling processes using shape and texture descriptors". PhD thesis. Universidad de León, 2017.

[142] Sohyung Cho, Shihab Asfour, Arzu Onar, and Nandita Kaundinya. "Tool breakage detection using support vector machine learning in a milling process". *International Journal of Machine Tools and Manufacture* 45.3 (2005), pp. 241–249. DOI: 10.1016/j.ijmachtools.2004.08.016.

[143] Dazhong Wu, Connor Jennings, Janis Terpenny, Robert X. Gao, and Soundar Kumara. "A Comparative Study on Machine Learning Algorithms for Smart Manufacturing: Tool Wear Prediction Using Random Forests". *Journal of Manufacturing Science and Engineering, Transactions of the ASME* 139.7 (July 2017). DOI: 10.1115/1.4036350.

[144] P. Krishnakumar, K. Rameshkumar, and K. I. Ramachandran. "Tool wear condition prediction using vibration signals in high speed machining (HSM) of Titanium (Ti-6Al-4V) alloy". *Procedia Computer Science*. Vol. 50. Elsevier B.V., 2015, pp. 270–275. DOI: 10.1016/j.procs.2015.04.049.

[145] Doriana M. D'Addona, A. M.M.Sharif Ullah, and D. Matarazzo. "Tool-wear prediction and pattern-recognition using artificial neural network and DNA-based computing". *Journal of Intelligent Manufacturing* 28.6 (2017), pp. 1285–1301. DOI: 10.1007/s10845-015-1155-0.

[146] N. Thomas Rincy and Roopam Gupta. "Ensemble learning techniques and its efficiency in machine learning: A survey". *2nd International Conference on Data, Engineering and Applications*. Institute of Electrical and Electronics Engineers Inc., 2020. DOI: 10.1109/IDEA49133.2020.9170675.

[147] Zhi Hua Zhou. "Ensemble methods: Foundations and algorithms". *Ensemble Methods: Foundations and Algorithms* (2012), pp. 1–218. DOI: 10.1201/B12207/ENSEMBLE-METHODS-ZHI-HUA-ZHOU.

[148] Giovanna Martínez-Arellano, German Terrazas, and Svetan Ratchev. "Tool wear classification using time series imaging and deep learning". *International Journal of Advanced Manufacturing Technology* 104.9-12 (2019), pp. 3647–3662. DOI: 10.1007/s00170-019-04090-6.

[149] Matthias Feurer and Frank Hutter. "Hyperparameter Optimization". 2019, pp. 3–33. DOI: 10.1007/978-3-030-05318-5{_}1.

[150] Gábor Melis, Chris Dyer, and Phil Blunsom. "On the State of the Art of Evaluation in Neural Language Models" (2017). URL: http://arxiv.org/abs/1707.05589.

[151] Ron Kohavi and George H. John. "Automatic Parameter Selection by Minimizing Estimated Error". *Proceedings of the 12th International Conference on Machine Learning* (1995), pp. 304–312. DOI: 10.1016/B978-1-55860-377-6.50045-1.

[152] Randal S. Olson, William La Cava, Zairah Mustahsan, Akshay Varik, and Jason H. Moore. "Data-driven advice for applying machine learning to bioinformatics problems". *Pacific Symposium on Biocomputing. Pacific Symposium on Biocomputing* 23.212669 (2018), p. 192. DOI: 10.1142/9789813235533{_}0018.

[153] Rafael G. Mantovani, Tomas Horvath, Ricardo Cerri, Joaquin Vanschoren, and Andre C.P.L.F. De Carvalho. "Hyper-Parameter Tuning of a Decision Tree Induction Algorithm". *Proceedings - 5th Brazilian Conference on Intelligent Systems* (2017), pp. 37–42. DOI: 10.1109/BRACIS.2016.018.

[154] Li Yang and Abdallah Shami. "On hyperparameter optimization of machine learning algorithms: Theory and practice". *Neurocomputing* 415 (2020), pp. 295–316. DOI: 10.1016/j.neucom.2020.07.061.

[155] James Bergstra, James Bergstra@umontreal Ca, and Yoshua Bengio@umontreal Ca. "Random Search for Hyper-Parameter Optimization Yoshua Bengio". Tech. rep. 2012, pp. 281–305.

[156] Jasper Snoek, Hugo Larochelle, and Ryan P. Adams. "Practical Bayesian Optimization of Machine Learning Algorithms" (2012). URL: http://arxiv.org/abs/1206.2944.

[157] MohammadNoor Injadat, Fadi Salo, Ali Bou Nassif, Aleksander Essex, and Abdallah Shami. "Bayesian Optimization with Machine Learning Algorithms Towards Anomaly Detection" (2020). DOI: 10.1109/GLOCOM.2018.8647714.

[158] "Model Explainability with AWS Artificial Intelligence and Machine Learning Solutions". Tech. rep. AWS, 2024.

[159] Umang Bhatt, Alice Xiang, Shubham Sharma, Adrian Weller, Ankur Taly, Yunhan Jia, Joydeep Ghosh, Ruchir Puri, José M.F. Moura, and Peter Eckersley. "Explainable machine learning in deployment". *Proceedings of the Conference on Fairness, Accountability, and Transparency.* Association for Computing Machinery, Inc, 2020, pp. 648–657. DOI: 10.1145/3351095.3375624.

[160] Dan Becker and Alexis Cook. "Advanced Uses of SHAP Values — Kaggle". URL: https://www.kaggle.com/code/dansbecker/advanced-uses-of-shap-values. *(accessed on: 04-03-2024)*.

[161] Lloyd Shapley. "A Value for n-Person Games". *Contributions to the Theory of Games II.* 1953, pp. 307–317.

[162] "ROCTEC™ Abrasive Waterjet Nozzles: Composite Carbide Mixing Tubes".

[163] "Setting recording and playback levels - Audacity Support". URL: `https://support.audacityteam.org/basics/recording-your-voice-and-microphone/setting-recording-levels-and-playback-levels`. *(accessed on: 09-01-2024)*.

[164] "scipy.signal.welch — SciPy v1.11.4 Manual". URL: `https://docs.scipy.org/doc/scipy/reference/generated/scipy.signal.welch.html`. *(accessed on: 03-01-2024)*.

[165] "NumPy documentation — NumPy v1.26 Manual". URL: `https://numpy.org/doc/stable/`. *(accessed on: 16-11-2023)*.

[166] "pandas documentation — pandas 2.1.3 documentation". URL: `https://pandas.pydata.org/docs/`. *(accessed on: 16-11-2023)*.

[167] "SciPy documentation — SciPy v1.11.3 Manual". URL: `https://docs.scipy.org/doc/scipy/`. *(accessed on: 16-11-2023)*.

[168] "scikit-learn: machine learning in Python — scikit-learn 1.4.2 documentation". URL: `https://scikit-learn.org/stable/`. *(accessed on: 07-05-2024)*.

[169] "XGBoost Documentation — xgboost 2.0.3 documentation". URL: `https://xgboost.readthedocs.io/en/stable/`. *(accessed on: 07-05-2024)*.

[170] "LightGBM 4.0.0 documentation". URL: `https://lightgbm.readthedocs.io/en/stable/`. *(accessed on: 07-05-2024)*.

[171] "CatBoost". URL: `https://catboost.ai/en/docs/`. *(accessed on: 07-05-2024)*.

[172] Gabriel Samuel. "TabPFN". URL: `https://github.com/automl/TabPFN`. *(accessed on: 07-05-2024)*.

[173] Jeremy Howard, Sylvain Gugger, and Soumith Chintala. "Tabular Modeling Deep Dive". *Deep learning for coders with fastai and PyTorch : AI applications without a PhD*. 2020, pp. 277–327.

[174] "sklearn.ensemble.StackingRegressor — scikit-learn 1.4.1 documentation". URL: `https://scikit-learn.org/stable/modules/generated/sklearn.ensemble.StackingRegressor.html`. *(accessed on: 24-02-2024)*.

[175] "sklearn.ensemble.StackingClassifier — scikit-learn 1.4.1 documentation". URL: `https://scikit-learn.org/stable/modules/generated/sklearn.ensemble.StackingClassifier.html`. *(accessed on: 24-02-2024)*.

[176] Iaroslav Shcherbatyi, Gilles Louppe, and Tim Head. "Scikit-learn hyperparameter search wrapper". URL: `https://scikit-optimize.github.io/stable/auto_examples/sklearn-gridsearchcv-replacement.html`. *(accessed on: 23-02-2024)*.

[177] "scikit-optimize: sequential model-based optimization in Python — scikit-optimize 0.8.1 documentation". URL: `https://scikit-optimize.github.io/stable/index.html`. *(accessed on: 23-02-2024)*.

[178] Philipp Probst, Marvin N. Wright, and Anne Laure Boulesteix. "Hyperparameters and tuning strategies for random forest". *Wiley Interdisciplinary Reviews: Data Mining and Knowledge Discovery*. ISSN: 19424795. DOI: `10.1002/widm.1301`.

[179] Kohei Ozaki. "LightGBM Tuner: New Optuna Integration for Hyperparameter Optimization". URL: `https://medium.com/optuna/lightgbm-tuner-new-optuna-integration-for-hyperparameter-optimization-8b7095e99258`. *Optuna, Medium*.

[180] "Parameters Tuning — LightGBM 4.3.0.99 documentation". URL: `https://lightgbm.readthedocs.io/en/latest/Parameters-Tuning.html`. *(accessed on: 24-02-2024)*.

[181] "SHAP documentation". URL: `https://shap.readthedocs.io/en/latest/`. *(accessed on: 29-02-2024)*.

[182] Chip Huyen. "Designing machine learning systems: an iterative process for production-ready applications" (2022). Ed. by Gregory Hyman Nicole Butterfield Jill Leonard, p. 389.

[183] Indre Zliobait, Mykola Pechenizkiy, and João Gama. "An overview of concept drift applications". Tech. rep. 2016.

[184] Wen Zhang, Zhengjiang Liu, Yan Xue, Ruibo Wang, Xuefei Cao, and Jihong Li. "An Improved Cross-Validated Adversarial Validation Method". *16th International Conference, KSEM*. Vol. 14117 LNAI. Springer Science and Business Media Deutschland GmbH, 2023, pp. 343–353. DOI: `10.1007/978-3-031-40283-8{\_}29`.

[185] Carl McBride Ellis. "What is Adversarial Validation? — Kaggle". URL: `https://www.kaggle.com/code/carlmcbrideellis/what-is-adversarial-validation`. *(accessed on: 29-02-2024)*.

[186] Wouter M. Kouw and Marco Loog. "An introduction to domain adaptation and transfer learning". Tech. rep. Delft University of Technology, 2018.

[187] Arthur Gretton, Karsten Borgwardt, Malte J. Rasch, Bernhard Scholkopf, and Alexander J. Smola. "A Kernel Method for the Two-Sample Problem". *Journal of Machine Learning Research* (May 2008).

[188] S. J. Pan, I. W. Tsang, J. T. Kwok, and Q. Yang. "Domain adaptation via transfer component analysis". *IEEE Transactions on Neural Networks* (2011), pp. 199–210.

[189] Raghuraman Gopalan, Ruonan Li, and Rama Chellappa. "Domain Adaptation for Object Recognition: An Unsupervised Approach". 2011.

[190] Yaroslav Ganin, Evgeniya Ustinova, Hana Ajakan, Pascal Germain, Hugo Larochelle, François Laviolette, Mario Marchand, and Victor Lempitsky. "Domain-Adversarial Training of Neural Networks". *Journal of Machine Learning Research* (2016). URL: `http://arxiv.org/abs/1505.07818`.

[191]   Mingsheng Long, Yue Cao, Jianmin Wang, and Michael I. Jordan. "Learning Transferable Features with Deep Adaptation Networks" (2015). URL: http://arxiv.org/abs/1502.02791.

[192]   Arthur Gretton, Alex Smola, Jiayuan Huang, Marcel Schmittfull, Karsten Borgwardt, and Bernhard Schölkopf. "Covariate Shift by Kernel Mean Matching". *Neural Information Processing Systems*. 2009.

[193]   Abolfazl Farahani, Sahar Voghoei, Khaled Rasheed, and Hamid R. Arabnia. "A Brief Review of Domain Adaptation" (Oct. 2020). URL: http://arxiv.org/abs/2010.03978.

[194]   Junhyuk Choi, Dohyeon Kong, and Hyunbo Cho. "Weighted Domain Adaptation Using the Graph-Structured Dataset Representation for Machinery Fault Diagnosis under Varying Operating Conditions". *Sensors* 24.1 (2023), p. 188. DOI: 10.3390/s24010188.

[195]   Jiayuan Huang, Alexander J Smola, Arthur Gretton, Karsten M Borgwardt, and Bernhard Schölkopf. "Correcting Sample Selection Bias by Unlabeled Data". *NeurIPS Proceedings*. 2006.

[196]   "adapt.instance_based.KMM — adapt 0.1.0 documentation". URL: https://adapt-python.github.io/adapt/generated/adapt.instance_based.KMM.html. *(accessed on: 01-03-2024)*.

Appendices

Appendix A

Brown Fused Alumina Informational Sheet

NK.A NK.B

Brown fused alumina

Brown fused alumina in the qualities NK.A and NK.B are economical alternatives to our premium quality.

Both products can be used especially for applications where iron-free blasting medium is no requirement.

Physical properties

Hardness	9 mohs
Grain shape	Angular
Melting point	approx. 1,950 C
Specific gravity	approx. 3.9 – 4.1 g/cm^3
Bulk density	approx. 1.5 – 2.1 g/cm^3

* depending on granular size

Typical chemical properties

	NK.A	NK.B
Al_2O_3	93- 94%	87 %
TiO_2	3 %	3,5 %
Fe_2O_3	1,5 %	3,5 %
SiO_2	0,3 %	2 %

Metric	Average grain size (mm)
	0,06 – 0,12
	0,12 – 0,25
	0,25 – 0,50
	0,50 – 1,00
	1,00 – 2,00
	1,00 – 3,00

Areas of application

- Reusable abrasive

Blasting systems

- Pressure blast systems
- Injector blast cabinets

Packaging

- 25 kg sacks on pallet up to 1 t
- 1 t loose in a big bag

Available grain size

Brown fused alumina macro			
FEPA	Grain size range (µm)	FEPA	Grain size range (µm)
F008	2000 - 2800	F046	300 – 425
F010	1700 – 2360	F054	250 – 350
F012	1400 – 2000	F060	212 – 300
F014	1180 – 1700	F070	180 – 250
F016	1000 – 1400	F080	150 – 212
F020	850 – 1180	F090	125 – 180
F022	710 – 1000	F100	106 – 150
F024	600 – 850	F120	90 – 125
F030	500 – 710	F150	63 – 106
F036	425 – 600	F180	53 – 90
F040	355 – 500	F220	45 – 75

Appendix B

GMA ClassicCut™80 Datasheet

Product Data Sheet
GMA ClassicCut™ 80

Average Chemical Composition (Typical)

SiO_2*	36%
Al_2O_3	20%
Fe_2O_3	35%
MgO	6%
CaO	2%
TiO_2	3%
MnO	1%

*Refers to SiO_2 bound within the lattice of the homogeneous garnet crystal (not free silica)

Mineral Composition (Typical)

Garnet (predominately Almandine)	> 96%
Ilmenite	< 3%
Quartz (free silica)	< 0.1%
Others	< 1%

Product Range (typical weight % retained)

Mesh	Microns	Cumulative	Discrete
40	425	0	0
45	355	3	3
50	300	23	20
60	250	55	32
70	212	78	23
80	180	92	14
100	150	98	6
PAN	PAN	100	2

Physical Characteristics (Typical)

Bulk Density	2.3 T/m³
Specific Gravity	4.1
Hardness (Mohs)	7.5 – 8.0
Melting Point	1250°C / 2250°F
Shape of Natural Grains	Sub-Angular

Other Characteristics (Typical)

Radioactivity	Non-detectable above background
Moisture Absorption	Non-hygroscopic, Inert
Total Chlorides	10 – 20 ppm
Conductivity	100 – 150 µS/cm (10 – 15 mS/m)

Packaging

- 25kg bags shrink wrapped onto a 1 metric ton or 2 metric ton pallet
- Loose bulk form in 1 metric ton or 2 metric ton bulk bag with an inner plastic liner on a pallet.

Source

- Made in Australia
- Product Code: GMA-AUS 80

Appendix C

SFM3000 Datasheet

Datasheet SFM3000

Low Pressure Drop Digital Flow Meter

- Low pressure drop
- Flow range: +/- 200 slm (bidirectional)
- Accuracy 1.5% m.v. (typical)
- Very fast update time (0.5ms)
- Fully calibrated & temperature compensated
- Zero offset, no drift

Product Summary

The SFM3000 sensor is Sensirion's digital flow meter designed for high-volume applications. It measures the flow rate of **air, oxygen and other non-aggressive gases** with superb accuracy. A special design of the flow channel results in the very low pressure drop through the flow body of the sensor making it extremely suitable for very demanding applications, such as medical ventilation and respiratory applications.

The SFM3000 operates from a 5 Volt supply voltage and features a digital 2-wire I²C interface. The measurement results are internally **linearized** and **temperature compensated**.

The outstanding performance of this sensor is based on Sensirion's patented **CMOSens® sensor technology**, which combines the sensor element, signal processing and digital calibration on a single microchip. The flow rate of the gas is measured by a thermal sensor element which assures **very fast signal processing time and bi-directional measurement with best-in-class accuracy**.

The well-proven CMOS technology is perfectly suited for high-quality mass production and is the ideal choice for demanding and cost-sensitive OEM applications.

Applications

- Medical
- Process automation
- Burner control
- Fuel cell control
- Spectroscopy
- Environment monitoring
- Laboratory

OEM options

A variety of custom options can be implemented for high-volume OEM applications (custom flow rates, calibration for other gases, different body form factor etc.). Contact Sensirion for more information.

Sensor chip

The SFM3000 flow meter features a fifth-generation silicon sensor chip SF05. In addition to a thermal mass flow sensor element, the chip contains an amplifier, A/D converter, EEPROM memory, digital signal processing circuitry, and interface. Due to seamless integration of signal acquisition and processing on the single silicon die significant performance and cost benefits are achieved.

Connection diagram
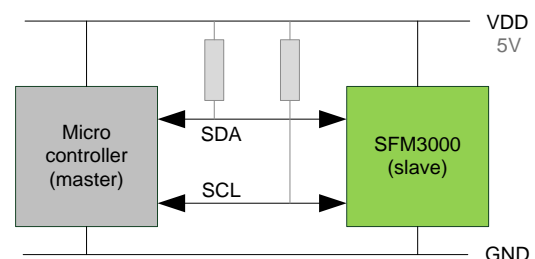
SFM3000 with bidirectional digital communication (I²C bus)

1. Sensor performance

1.1 Physical specifications [1]

Parameter	Condition	Value		Unit
Flow Ranges	Air/N_2/O_2	-200 … +200 [2]		slm [3]
Update Time	14 bit	0.5		ms
		Max.	Typ.	
Accuracy [4,5,6,7]	span	± 2.5	± 1.5	% m.v. [8]
	offset	± 0.1	± 0.05	slm
Repeatability [4,7]	span	± 1	± 0.5	% m.v.
	offset	± 0.05	± 0.02	slm
Noise Level [4,7]	span	± 1	± 0.5	% m.v.
	offset	± 0.1	± 0.05	slm
Accuracy Shift Due to Temperature Variation [9]	span	± 0.75	± 0.25	% m.v./10°C
	offset	± 0.0	± 0.0	slm
Position sensitivity [10]	non-horizontal position	< 0.05		slm
Pressure Drop	@60slm	< 100 / < 0.4		Pa / inH_2O
	@200slm	< 600 / < 2.4		

1.2 Media compatibility and materials

Parameter	Value
Calibration [11]	Air, N_2, O_2
Media Compatibility	Air (non-condensing), N_2, O_2, non- aggressive gases
Wetted Materials	PPE+PS blend (medical grade: biocompatible; ISO 10993 or USP Class VI), Si, Si_3N_4, SiO_x, Gold, Epoxy, Polyurethane, stainless steel (annealed)
RoHS, REACH	RoHS and REACH compliant
Sensor Weight with Cap	< 18 gram

1.3 Temperature and pressure conditions

Parameter	Condition	Value	Unit
Calibrated Temperature Range[11]	T(environment) = T(gas)	-20 … +80	°C
Operating Temperature Range[11]	Non-condensing	-20 … +80	°C
Storage Temperature	Non-condensing	-20 … +80	°C
Operating Pressure Range	absolute	0.7 – 1.3	bar
Operating Overpressure	gauge	± 0.2	bar
Burst Overpressure	gauge	> 1	bar

[1] Unless otherwise noted, all sensor specifications are valid at 25°C with Vdd = 5V and absolute pressure = 966 mbar.
[2] Other calibration ranges are available for large volume projects
[3] In standard liter per minute at 20°C and 1013 mbar
[4] With ideal inlet and outlet conditions, at VDD = 5V, 25°C, absolute pressure = 966 mbar
[5] Including offset, non-linearity, hysteresis
[6] Sensor position horizontal (see Section 4.1)
[7] Span or offset value, whichever is larger
[8] In % of measured value (m.v.) = of rate = of reading
[9] Shift due to temperature variation compared to calibration temperature
[10] See Section 4.1
[11] Contact Sensirion for information about other gases, wider calibrated and operating temperature ranges

2. Electrical specifications

2.1 Electrical characteristics

Electrical properties	Condition	Value		Unit
Interface		I²C		
Default Sensor Address		64 (0x40)		
Soft Reset Time		80		ms
Start-up Time [12]	Max.	100		ms
Supply Voltage (VDD)		5V +/-5%		V
I²C Communication Level	High	Min.	Max.	V
	Low	2.5	VDD	
		GND	1.1	
I²C Bus clock frequency	Max.	400		kHz
Power Consumption		< 50		mW
Electrical Connector		2 mm pitch, 4 pins in a row		
Output signal resolution		14[13]		bit
Scale Factor Flow	Air, N2	140		1/slm
	O2	142.8		
Offset Flow		32'000		

---

[12] After 4.75V is reached
[13] 16 bit with two least significant bits always zero

2.2 Pin layout and mechanical concept of the electrical connection

SDA   GND   VDD   SCL

Positive flow direction
(as marked on the sensor body)
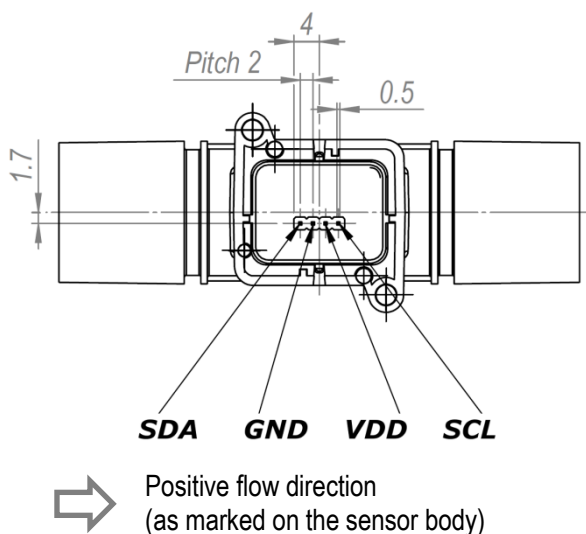
The SFM3000 is designed for both connector attachment and through-hole technology hand-soldering to a PCB.

2.2.1 Connector attachment

The SFM3000 sensor's 4-pin 2 mm pitch electrical connector is compatible with Molex DuraClik™ socket (Molex product number: 502351-0400). For this type of connection please order the SFM3000 with a cap (according to the ordering information in Chapter 5). Diverse 4-core flat ribbon cables with crimp fittings can be used for electrical connection.

2.2.2 PCB soldering

Standard selective soldering systems may be used for soldering SFM3000 sensors. Reflow soldering is not feasible and may damage the sensor. The sensor ports must be protected from solder splash and flux during soldering. The characteristics of selective soldering machines vary, so any soldering setup must be tested before production use.

2.3 Conversion to physical values

In order to obtain the measured flow in [slm], the measured value needs to be converted using the following formula:
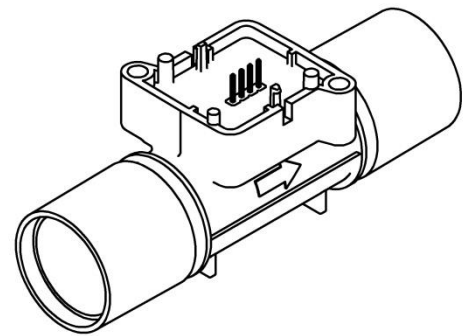
$$flow \text{ [slm]} = \frac{measured\ value - offset\ flow}{scale\ factor\ flow}$$

Please note that the first measurement performed directly after chip initialization is not valid.

3. Mechanical specifications

All dimensions are in millimeters (mm).

3.1 SFM3000 without cover (PCB mount)

82

31,5

33,5

11,5

22mm Cone conforming to ISO5356

14

19,75

∅ 3,2

21

2,6

26

∅ 19,8
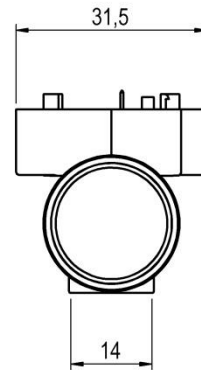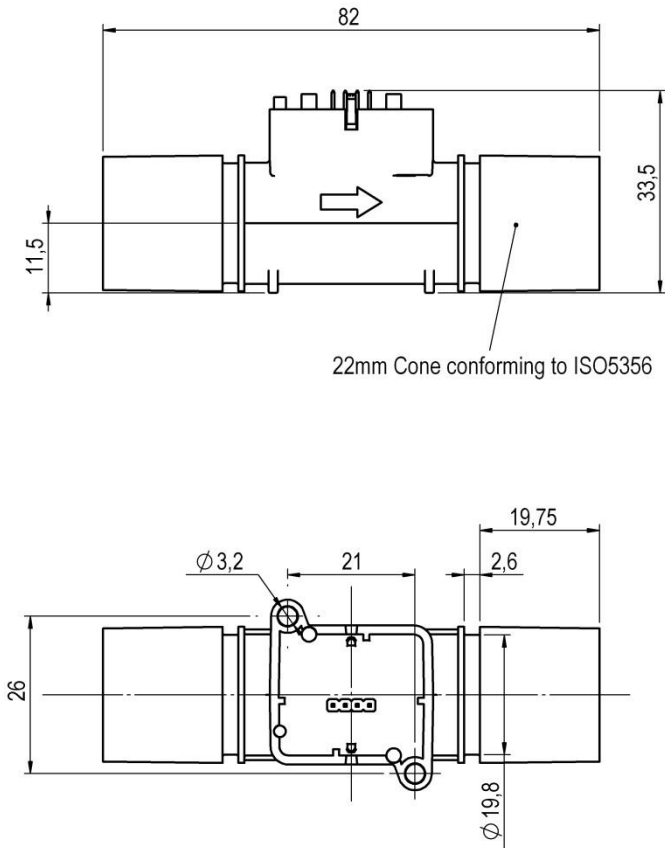
3.2 Footprint

Please refer to the mask given below for reliable PCB attachment using the dedicated snap-in feet.
Consider using the screw holes of the SFM3000 for a sturdy integration of the sensor.

Flow Direction

Bottom view

1.65

13 10 7.7 6 1.7 0 7.7 10 13

∅ 2.2
∅ 0.8

∅ 2.7
∅ 2.5
∅ 2.5

11.8
10.5
7
3
1
0
1
3
7
10.5
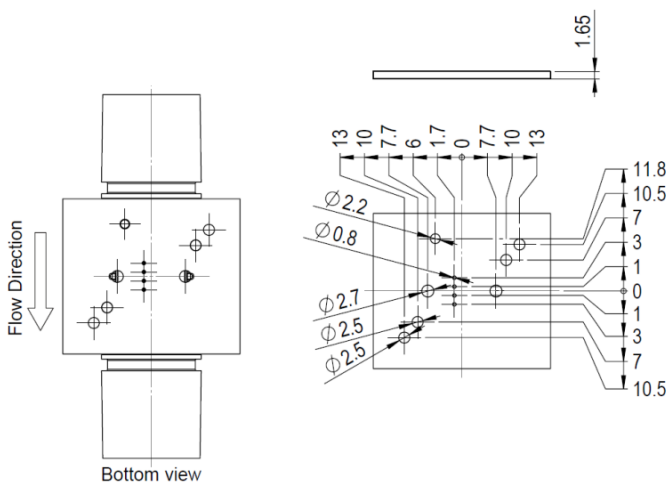
3.3 SFM3000 with cover

If used with cover, sensor height is 34.4 mm instead of 33 mm. All the other dimensions are the same

82

34.4

11.5
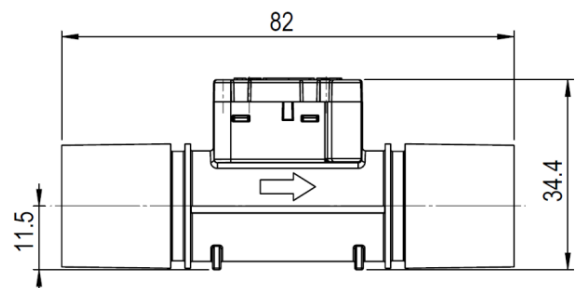
3.4 Mechanical fitting

Fittings of the SFM3000 sensor correspond to the international standard ISO5356-1:2004. Details about this type of connection can be found in the description of the standard. To minimize the risk of connectors being accidentally disconnected, latching connectors can be suggested.

It is also possible to insert O-rings in the grooves and attach tubes with an inner diameter of 23 mm to the SFM3000.

d_1 = 19mm
d_2 = 2mm

Cross section of recommended O-ring

4. Instructions for use

4.1 Calibration orientation

The sensors are calibrated horizontally as depicted in the following graph:

4.2 Inlet flow conditions

In order to provide good flow conditions, the inner diameter of the connecting tube has to be approximately the same as the inner diameter of the SFM3000 main flow channel. The inlet tube has to be straight and at least 10 cm in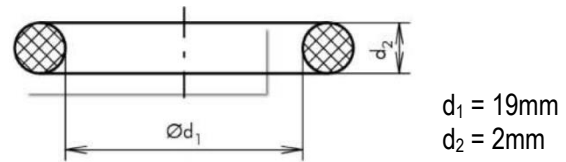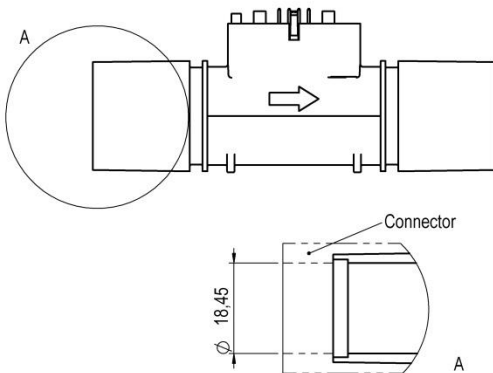 length. The SFM3000 is equipped with meshes on the in- and outlets of the flow channel to reduce turbulences and thus improve the stability.

Please refer to the application note "Inlet conditions for the SFM3000 Mass flow meters" for more information.

4.3 Temperature compensation

The SFM3000 sensor features digital temperature compensation. The temperature is measured on the CMOSens® chip by an on-chip temperature sensor. This data is fed to a compensation circuit that is also integrated on the CMOSens® sensor chip. Thus, no external temperature compensation is necessary.

4.4 Sensor handling

The SFM3000 sensor is designed to be robust and shock resistant. Nevertheless, the accuracy of the high-precision SFM3000 can be degraded by rough handling. Sensirion does not guarantee proper operation in case of improper handling. **Note:** avoid applying any mechanical stress to the solder joints of the sensor during or as a result of PCB assembly.

4.5 ESD

The electronics of the SFM3000 sensor consist of a single automotive qualified chip. It complies with the following ESD norms:
- AEC Q 100 002 (4kV HBM)
- AEC Q 100 003 (200V MM)

Although the sensor complies with these norms, it does not mean the sensor is immune against ESD.

The sensor is shipped in an antistatic tray to prevent electrostatic discharge. To avoid damage to the sensor, ground yourself using a grounding strap or by touching a grounded object before touching the sensor. Furthermore, store the parts in an antistatic package when not in use.

4.6 I²C Interface and communication

Due to I²C interface restrictions, the cable length from the sensor to the microprocessor is recommended to be as short as possible and certainly not above 30 cm. For wires longer than 10 cm it is mandatory to shield the SDA and SCL.

In case data is read from the sensor, the first data byte of the transaction must always be acknowledged by the master.

It must be possible to reset the sensor through a hard reset, i.e. powering off and on the sensor, in case the sensor freezes.

I²C Communication details are given in the application note "I²C Functional Description for SFM3000".

Appendix D

SEK-SensorBridge Technical Guide

SEK-SensorBridge Technical Guide

Connecting Bridge with 2 Sensor Ports

Highlights

- I2C Bus with speeds up to 1MHz
- 1.2V-5.5V Selectable supply in voltage steps
- Connect up to 2 Sensor Evaluation Kits

- Micro USB Virtual COM Port
- RS485 Serial Connector

The SEK-SensorBridge (referred to as SensorBridge) is the universal tool of Sensirion when it comes to evaluation. Sensirion offers a huge variety of sensors and SensorBridge is used to connect the different Evaluation Kits and the different evaluation tools and drivers Sensirion offers.

Scan me to provide feedback

1 Quick Start Guide

To connect a Sensor Evaluation Kit (SEK) via SensorBridge to your computer follow the next steps:

1. Use the adapter cable supplied with your SEK and connect it to the female connector on the evaluation board
2. Connect the RJ45 connector of the adapter cable to either of the two RJ45 ports on the SensorBridge
3. Use the supplied Micro USB to USB cable to power and connect the SensorBridge to your computer
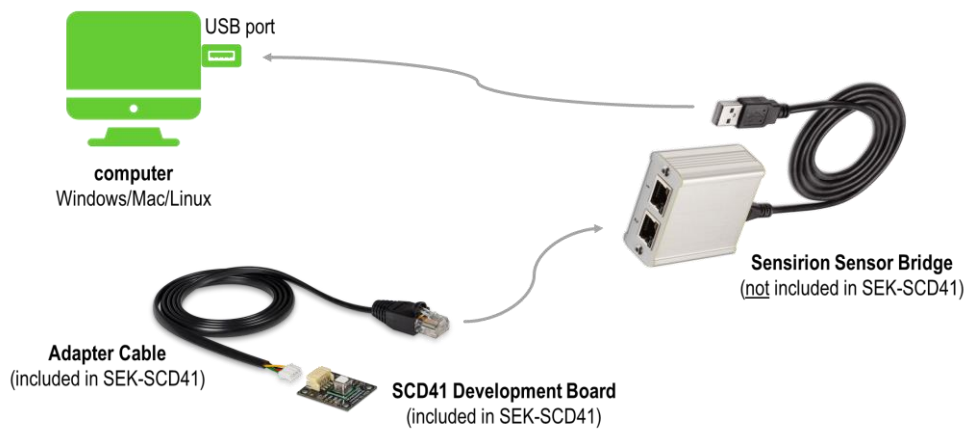4. Launch ControlCenter

Figure 1. Typical connection diagram to a computer with a SensorBridge and Sensor Evaluation Kit.

Find about the evalution kits on Sensirion Website: Sensor evaluation (sensirion.com)
Find about the compatibility list of SensorBridge in the Evaluation Kit Compatibility list

Appendix E

PA3029 Pressure Transmitter Datasheet

PA3029

Pressure transmitter with ceramic measuring cell

PA-0-1-RBR14-A-ZVG/US/   /V
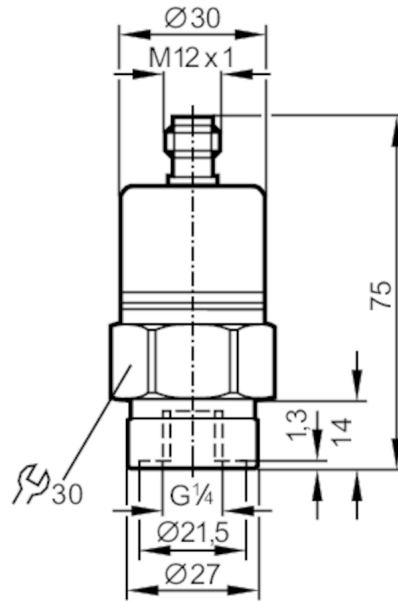
Product characteristics				
Number of inputs and outputs	Number of analogue outputs: 1			
Measuring range	-1...0 bar	-1000...0 mbar	-14.5...0 psi	-100...0 kPa
Process connection	threaded connection G 1/4 internal thread			
Application				
Special feature	Gold-plated contacts			
Application	for industrial applications			
Media	liquids and gases			
Medium temperature [°C]	-25...90; (on request: -40...90 °C)			
Min. bursting pressure	30 bar	435 psi		3 MPa
Pressure rating	10 bar	145 psi		1 Mpa
Type of pressure	relative pressure; vacuum			
Electrical data				
Operating voltage [V]	9.6...32 DC			
Min. insulation resistance [MΩ]	100; (500 V DC)			
Protection class	III			
Reverse polarity protection	yes			
Inputs / outputs				
Number of inputs and outputs	Number of analogue outputs: 1			
Outputs				
Total number of outputs	1			
Output signal	analogue signal			
Number of analogue outputs	1			
Analogue current output [mA]	4...20			

PA3029

Pressure transmitter with ceramic measuring cell

PA-0-1-RBR14-A-ZVG/US/   /V

Max. load	[Ω]	720; (Ub = 24 V; (Ub - 9,6 V) / 20 mA)			
Overload protection		yes			

Measuring/setting range

Measuring range	-1...0 bar	-1000...0 mbar	-14.5...0 psi	-100...0 kPa

Accuracy / deviations

Repeatability	[% of the span]	< 0,1; (with temperature fluctuations < 10 K)
Characteristics deviation [% of the span]		< ± 0,25 (BFSL) / < ± 0,5 (LS); (BFSL = Best Fit Straight Line; LS = limit value setting)
Long-term stability [% of the span]		< ± 0,05; (per 6 months)
Temperature coefficient zero point [% of the span / 10 K]		0,1; (0...80 °C)
Temperature coefficient span [% of the span / 10 K]		0,2; (0...80 °C)

Response times

Step response time analogue output	[ms]	3

Operating conditions

Ambient temperature	[°C]	-25...80
Storage temperature	[°C]	-40...100
Protection		IP 65

Tests / approvals

EMC	EN 61000-4-2 ESD	4 kV CD / 8 kV AD
	EN 61000-4-3 HF radiated	30 V/m
	EN 61000-4-4 Burst	2 kV
	EN 61000-4-6 HF conducted	10 V
	radiation of interference	according to the automotive directive 2004/104/EC
	CISPR 25	
	immunity	according to the automotive directive 2004/104/EC
	ISO 11452-2 HF radiated	100 V/m
	ISO 7637-2 pulse	severity level 4
Shock resistance	DIN EN 60068-2-27	50 g (11 ms)
	DIN EN 61373	category 3
Vibration resistance	DIN EN 60068-2-6	20 g (10...2000 Hz)
	DIN EN 61373	category 2
MTTF	[years]	506
Pressure Equipment Directive	Sound engineering practice; can be used for group 2 fluids; group 1 fluids on request	
Railway applications	DIN EN 50155 / IEC 60571	Klasse T3, C1, S1

Mechanical data

Weight	[g]	222.5
Materials		stainless steel (1.4404 / 316L); FKM; PA; EPDM/X
Materials (wetted parts)		stainless steel (1.4305 / 303); ceramics; FKM
Min. pressure cycles		100 million
Process connection		threaded connection G 1/4 internal thread

Appendix F

HP-2 Pressure Sensor Datasheet

Pressure sensor
For highest-pressure applications to 15,000 bar [217,500 psi]
Model HP-2

EAC for further approvals, see page 6

Applications

- Test bench construction
- Water-jet cutting
- High-pressure pasteurisation
- High-pressure cleaning

Special features

- High number of load cycles through patented design
- Exchangeable process connection in case of hairline cracks
- Suitable for highly dynamic pressure due to diaphragm protection system
- Reduced recalibration costs thanks to excellent long-term stability

Pressure sensor model HP-2

Description

For highest pressures
The model HP-2 pressure sensor has been specifically developed for demanding high-pressure applications up to 15,000 bar [217,500 psi]. This makes it one of the few pressure measuring instruments in the world that can reliably measure pressures of this magnitude.

High accuracy
This pressure sensor features a very high long-term stability and offers extremely high accuracy for the highest pressures. Measuring ranges up to and including 0 ... 10,000 bar [145,000 psi] can, as an option, be supplied with an even higher accuracy of 0.25 %.

Long service life
Thanks to its excellent load cycle stability, the model HP-2 has a particularly long service life, even with dynamic pressure profiles.
A protection against cavitation and pressure spikes, specifically developed for highly dynamic pressure profiles, further extends the service life. For water as a medium, this protection is particularly recommended.

WIKA
Part of your business

Specifications

Overview of versions	
Model HP-2-S	Standard version
Model HP-2-D	Additionally with DIPS (diaphragm impact protection system) DIPS protects the pressure sensor from cavitation and micro-diesel effects; it is particularly recommended for use with water as a medium.
Model HP-2-E	Additionally with EPC (exchangeable pressure connection) EPC enables the changing of the process connection without having to change the entire pressure sensor. This system is particularly recommended when hairline cracks can occur.

Further details on DIPS and EPC on request.

Accuracy specifications		
Accuracy	→ See "Max. measured error per IEC 61298-2"	
Max. measured error per IEC 61298-2	Measuring ranges < 10,000 bar [145,000 psi]	■ ≤ ±0.5 % of span ■ ≤ ±0.25 % of span
	Measuring range 10,000 bar [145,000 psi]	■ ≤ ±0.5 % of span ■ ≤ ±0.25 % of span, typical
	Measuring ranges 12,000 bar and 15,000 bar [217,500 psi]	≤ ±0.5 % of span, typical
Adjustability of current and voltage output	Zero point	±5 % of span
	Adjustment is made using potentiometers inside the instrument	
Adjustability of USB output	Zero point	-5 ... +20 % of span
	Span	-50 ... +5 % of span
	Adjustment is made via "EasyCom 2011" software	
Temperature error at 0 ... 80 °C [32 ... 176 °F]		
Typical	≤ ±1 % of span	
	≤ ±2 % of span for special measuring ranges	
Maximum	≤ ±2.5 % of span	
Long-term stability per DIN 16086	≤ 0.1 % of span/year	
	≤ 0.2 % of span/year for special measuring ranges	
Reference conditions	Per IEC 61298-1	

Measuring ranges

Gauge pressure						
bar	**Measuring range**	**0 ... 1,600**	**0 ... 2,500** [1]	**0 ... 4,000** [1]	**0 ... 5,000** [1]	**0 ... 6,000**
	Overload safety	2,300	3,500	5,000	6,000	7,000
	Burst pressure	4,000	6,000	8,000	10,000	11,000
	Measuring range	**0 ... 7,000**	**0 ... 8,000**	**0 ... 10,000** [1]	**0 ... 12,000**	**0 ... 15,000** [2]
	Overload safety	8,000	10,000	11,000	12,500	15,500
	Burst pressure	11,000	12,000	12,000	14,000	16,000
psi	**Measuring range**	**0 ... 23,000**	**0 ... 36,000** [1]	**0 ... 58,000** [1]	**0 ... 72,000** [1]	**0 ... 87,000**
	Overload safety	33,300	50,500	72,500	87,000	101,500
	Burst pressure	58,000	87,000	116,000	145,000	159,500
	Measuring range	**0 ... 100,000**	**0 ... 115,000**	**0 ... 145,000** [1]	**0 ... 217,500** [1] [2]	
	Overload safety	116,000	145,000	159,000	224,750	
	Burst pressure	159,500	174,000	174,000	232,000	

1) Optionally also with a measuring cell from Elgiloy®
2) Adjustment at max. 12,500 bar [181,250 psi], 15,000 bar [217,500 psi] is calculated.

Further details on: Measuring range	
Units	bar, psi, MPa
Special measuring ranges	On request, special measuring ranges between the listed ranges 0 ... 1,600 and 0 ... 10,000 bar are possible. These special measuring ranges, however, have a higher temperature error and a reduced long-term stability.

Process connection				
Standard	Process connection	Max. measuring range	Overpressure limit	Type of sealing
-	M16 x 1.5 female thread, with sealing cone	7,000 bar [100,000 psi]	8,000 bar [115,000 psi]	60° sealing cone
-	M20 x 1.5 female thread, with sealing cone	15,000 bar [217,500 psi]	16,000 bar [224,750 psi]	60° sealing cone
-	9/16-18 UNF, female thread	7,000 bar [100,000 psi]	8,000 bar [115,000 psi]	60° sealing cone

The maximum permissible pressure at the installation point is dependent on the high-pressure pipes used.
For the valid values, see the high-pressure pipe manufacturer's documentation.

Other process connections on request.

Output signal		
Signal type		
Analogue	Current (2-wire)	4 ... 20 mA
	Voltage (3-wire)	■ DC 0 ... 5 V ■ DC 0 ... 10 V
Digital	USB 2.0	
Load in Ω		
Current (2-wire)	≤ (supply voltage - 10 V)/0.02 A	
Voltage (3-wire)	> max. output signal/1 mA	
Voltage supply		
Supply voltage	Output signal 4 ... 20 mA	DC 10 ... 30 V
	Output signal DC 0 ... 5 V	DC 10 ... 30 V
	Output signal DC 0 ... 10 V	DC 14 ... 30 V
	Output signal USB 2.0	DC 5 V
Current supply	Current (2-wire)	Signal current, max. 35 mA
	Voltage (3-wire)	8 mA
	USB 2.0	40 mA
Overvoltage resistance	■ DC 36 V ■ DC 5.25 V with USB output	
Dynamic behaviour		
Settling time per IEC 61298-2	Current and voltage output	< 1 ms
	USB output	< 10 ms [1]
Warm-up time	< 10 min	

1) Other values on request

Other output signals on request.

Electrical connection

Connection type	IP code [1]	Wire cross-section	Cable diameter	Cable lengths
Angular connector DIN 175301-803 A	IP65	Max. 1.5 mm²	6 ... 8 mm [0.24 ... 0.32 in]	-
Circular connector M12 x 1 (4-pin)	IP67	-	-	-
USB connector type A	IP67 (instrument), IP20 (connector)	-	-	2 m [6.5 ft]
Cable outlet	IP67	0.5 mm² (AWG 20)	6.8 mm [0.27 in]	1.5 m [16.4 ft]

1) The stated IP codes only apply when plugged in using mating connectors that have the appropriate IP code.
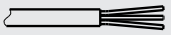
Further details on: Electrical connection

Connection type	→ See above
Wire cross-section	→ See above
Cable diameter	→ See above
Pin assignment	→ See below
Ingress protection (IP code) per IEC 60529	→ See above
Short-circuit resistance	S_+ vs. 0V
Reverse polarity protection	UB vs. 0V
Insulation voltage	DC 500 V

Pin assignment

Angular connector DIN 175301-803 A		2-wire	3-wire
	U_B	1	1
	0V	2	2
	S_+	-	3

USB connector type A		
	+5V	1
	GND	4
	D_+	3
	D-	2

Circular connector M12 x 1 (4-pin)		2-wire	3-wire
	U_B	1	1
	0V	3	3
	S_+	-	4

Cable outlet		2-wire	3-wire
	U_B	Brown	Brown
	0V	Green	Green
	S_+	-	White

Legend
UB, +5V   Positive supply voltage
0V, GND   Reference potential
S+   Positive output terminal
D+, D-   Data link USB 2.0

Material

Material (wetted)	
Process connection	Stainless steel 1.4534
Sensor	■ Stainless steel 1.4534 ■ 2.4711 Elgiloy®

For hydrogen as a medium, see "Options for specific media".

Operating conditions

Medium temperature limit	0 ... +80 °C [32 ... 176 °F]
Ambient temperature limit	-20 ... +80 °C [-4 ... +176 °F]
Storage temperature limit	-40 ... +85 °C [-40 ... +185 °F]
Vibration resistance per IEC 60068-2-6	0.35 mm (10 ... 55 Hz)
Shock resistance per IEC 60068-2-27	100 g (2.4 ms)
Ingress protection (IP code) per IEC 60529	→ See "Electrical connection"
Service life	On request, since the service life depends on the actual pressure profile.

Options for specific media

Hydrogen		
Measuring ranges	2,500, 4,000, 5,000 and 10,000 bar.	
Long-term drift	On request	
Material	Process connection	MP35N
	Sensor	2.4711 Elgiloy

Packaging and instrument labelling

Packaging	Individual packaging
Instrument labelling	■ WIKA product label, lasered ■ Customer-specific product label on request

Approvals

Logo	Description	Country
CE	**EU declaration of conformity**	European Union
	EMC directive	
	Pressure equipment directive	
	RoHS directive	
EAC	**EAC** EMC directive	Eurasian Economic Community
-	**CRN** Safety (e.g. electr. safety, overpressure, ...)	Canada

Manufacturer's information and certificates

Logo	Description
-	**China RoHS directive**

Test report

Test report	
Test report	5 measuring points

Appendix G

8081 Water Flow Rate Sensor Datasheet

bürkert
FLUID CONTROL SYSTEMS

Type   8081

Water flow rate transmitter
Wasser-Durchfluss-Transmitter
Transmetteur de débit d'eau

Operating Instructions

Bedienungsanleitung
Manuel utilisateur

⚠️

Various dangerous situations

To avoid injury take care:

▪ not to use the type 8081 ultrasound flow rate transmitter in a potentially explosive atmosphere.

▪ not to use fluid that is incompatible with the materials of which the transmitter is made.

▪ not to subject the device to mechanical loads (e.g. by placing objects on top of it or by using it as a step).

▪ not to make any external modifications to the device. Do not paint or varnish any part of the device.

NOTICE

Elements / Components sensitive to electrostatic discharges

This device contains electronic components sensitive to electrostatic discharges. They can get damaged if they are touched by an electrostatically charged person or object. In the worst case scenario, these components are instantly destroyed or go out of order as soon as they are activated.

▪ To minimise or even avoid all damage due to an electrostatic discharge, take all the precautions described in the EN 61340-5-1 norm.

▪ Also ensure that you do not touch any of the live electrical components.

4. GENERAL INFORMATION

4.1. Manufacturer's address and international contacts

To contact the manufacturer of the device use following address:

Bürkert SAS

Rue du Giessen

BP 21

F-67220 TRIEMBACH-AU-VAL

You may also contact your local Bürkert sales office.

The addresses of our international sales offices can be found on the last pages of this manual. They are also available on the Internet at: country.burkert.com

4.2. Warranty conditions

The condition governing the legal warranty is the conforming use of the 8081 in observance of the operating conditions specified in this manual.

4.3. Information on the Internet

You can find the user manuals and technical data sheets regarding the type 8081 at: country.burkert.com

1   DESCRIPTION

4.4.   Area of application

The ultrasonic flow rate transmitter type 8081 is intended for the measurement of water flow rates which may be slightly charged with contaminants.

4.5.   General description

4.5.1.   Design

The 8081 ultrasonic flow rate transmitter consists of an electronic module and a brass fitting with a built-in measuring tube. When combined with a controller and a control loop, it enables a control loop to be established.

The electrical connection is made via a 5-pin M12 fixed connector.

The transmitter features, depending on the version:

▪ a pulse output or

▪ a pulse output and a 4...20 mA current output;

Each version is available for 5 different flow rate ranges:

▪ model QN 0.6 DN15: 0.06 to 20 l/min
  (nominal flow rate 0.6 m³/h namely 10 l/min)

▪ model QN 1.5 DN15: 0.1 to 50 l/min
  (nominal flow rate 1.5 m³/h namely 25 l/min)

▪ model QN 2.5 DN20: 0.16 to 82 l/min
  (nominal flow rate 2.5 m³/h namely 41 l/min)

▪ model QN 3.5 DN25: 0.6 to 116 l/min
  (nominal flow rate 3.5 m³/h namely 58 l/min)

▪ model QN 6 DN25: 1 to 200 l/min
  (nominal flow rate 6 m³/h namely 100 l/min)

4.5.2.   Measuring item and principle

The 8081 flow meter is based on the transit time method. This consists in measuring the transit times of the sound from emitter 1 to receiver 2 and from emitter 2 to receiver 1 and subsequently comparing both values. The calculated transist time difference is directly proportional to the flow speed of the fluid.
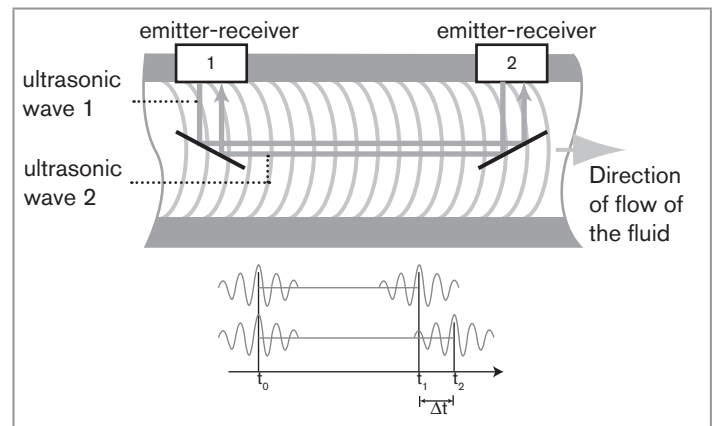
The electronic module then delivers a pulse signal proportional to the volume or an industry-standard 4...20 mA signal, proportional to the flow rate or to the temperature.

4.6. Description of the name plate

1. Measured quantity, type of flow meter
2. Supply voltage
3. Measuring principle
4. Nominal flow rate
5. Output data
6. Process connection
7. Flow rate range
8. Manufacturing code
9. Serial number
10. Article number
11. Materials: housing, seal

5. TECHNICAL DATA

5.1. Conditions of use

Ambient temperature:	+5...+55 °C
Storage temperature:	+5...+55 °C
Air humidity:	< 80 %, not condensated
Protection rating:	IP65 with cable plug plugged-in and tightened

5.2. Conformity to standards and directives

The applied standards, which verify conformity with the EU directives, can be found on the EU-type examination certificate and/or the EU declaration of conformity (if applicable).
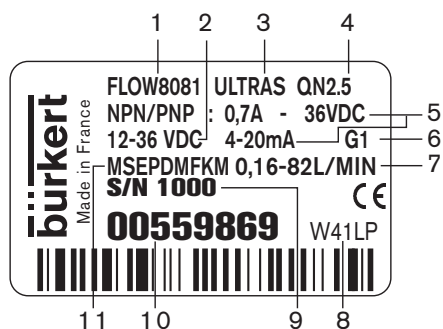
5.3. Conformity to the pressure equipment directive

- Make sure that the device materials are compatible with the fluid.
- Make sure that the pipe DN is adapted for the device.
- Observe the fluid nominal pressure (PN) for the device. The nominal pressure (PN) is given by the device manufacturer.

The device conforms to Article 4, Paragraph 1 of the Pressure Equipment Directive 2014/68/EU under the following conditions:

- Device used on a piping (PS = maximum admissible pressure; DN = nominal diameter of the pipe)

Type of fluid	Conditions
Fluid group 1, Article 4, Paragraph 1.c.i	Forbidden
Fluid group 2, Article 4, Paragraph 1.c.i	DN $\leq$ 32 or PSxDN $\leq$ 1000 bar
Fluid group 1, Article 4, Paragraph 1.c.ii	Forbidden
Fluid group 2, Article 4, Paragraph 1.c.ii	DN $\leq$ 200 or PS $\leq$ 10 bar or PSxDN $\leq$ 5000 bar

5.4. General technical data

5.4.1. Mechanical data

Item	Material
Housing, cover	PPS
Seal in contact with the environment	Silicone
M12 connector	PA
Fitting	Brass
Measuring tube	PES
Seal in contact with the fluid	EPDM, FKM

5.4.2. Dimensions

→ Please refer to the technical data sheets related to the device at: country.burkert.com

5.4.3. Fluid data

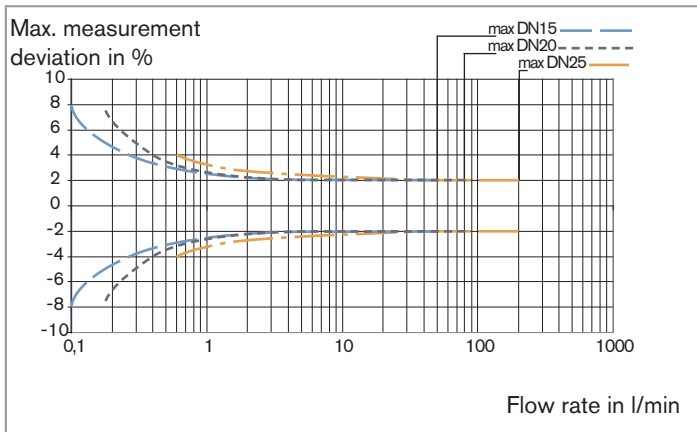| Pipe diameter	DN15 to DN25
Type of fluid	water (or neutral liquids on request)
Fluid temperature	+5...+90 °C
Fluid pressure	PN 16
Measuring range	0.06...200 l/min

Accuracy (see curves on next page)	± (0.01 % of Full Scale* +2 % of measured value) [1]
Repeatability	1 % of measured value
Measuring element	2 ultrasound emitter-receiver cells

Full Scale, see measuring range on the diagram of measurement accuracy.

[1] *Reference conditions: fluid = water, water and ambient temperatures = 20 °C*

Measurement accuracy

5.4.4.   Electrical data

Supply voltage (V+)	12...36 V DC
Current consumption	▪ Own consumption: < 4 mA ▪ Consumption with load: < 1 A
Pulse output (transistor) ▪ version without current output ▪ version with current output	▪ NPN as default setting; (PNP on request), open collector, 5 mA min., 700 mA max., NPN output: 0,2...36 V DC ▪ PNP as default setting; (on request: NPN for the pulse output and sinking mode for the current output), open collector, 5 mA min., 700 mA max., PNP output: supply voltage (V+) If QN=0.6 or 1.5: 1 pulse corresponds to a volume V = 0.002 l (K factor = 500 pulse/litre) If QN=2.5 or 3.5: 1 pulse corresponds to a volume V = 0.005 l (K factor = 200 pulse/litre) If QN=6: 1 pulse corresponds to a volume V = 0.01 l (K factor = 100 pulse/litre)

Current output	4...20 mA (sourcing mode as default setting; on request: sinking mode for the current output and NPN for the pulse output) corresponding to the flow rate range of the selected model max. loop resistance: 1100 Ω at 36 V DC 610 Ω at 24 V DC 100 Ω at 12 V DC Accuracy: ±0.4 % of Full Scale (16 mA)
Protection against: reversed polarity voltage peaks short-circuits	 yes yes yes, for the pulse output
Recommended cable type	max. cross section of 1.5 mm²

5.4.5. Electrical connections

Flow rate meter version	Type of cable plug
Any version	female 5-pin M12 cable plug (available as an accessory; Article number 438680)

6. INSTALLATION AND WIRING

6.1. Safety instructions

⚠️ **DANGER**

Risk of injury due to high pressure
- Cut off the pressure and depressurize the pipes before loosening the pipes and connections.

Risk of injury due electrical discharge.
- If the device is installed either in a wet environment or outdoors, all the electrical voltages must be of max. 35 V DC.
- Before starting work, make sure that you switch off the supply voltage and secure it to prevent restarting.
- Observe all applicable accident protection and safety guidelines for electrical equipment.

⚠️ **WARNING**

Risk of injury due to non-conforming installation.
- The electrical and fluid installation can only be carried out by qualified and skilled staff with the appropriate tools
- Install appropriate safety devices (correctly rated fuse and/or circuit-breaker).
- Use cables with an operating temperature limit which is suitable for your application.
- Under normal conditions of use, cables with a 0.75 mm² cross section should be enough to transmit the signal.

Appendix H

C-1U User Manual

User Manual

C-1U

USB Studio Condenser Microphone

3. Installing the Microphone

3.1 Technical requirements

Your C-1U microphone comes with a USB connector. The audio signal is sent from the microphone to the computer through this connection. At the same time the computer uses the USB connection to supply the microphone with the necessary power. A connection is made by using the included USB cable with type-B connector.

◊   **Use only the included cable to ensure an optimal signal quality and a reliable power supply.**

To operate the C-1U, your computer needs to meet the following system requirements:

PC	Mac
Intel or AMD CPU, 1 GHz or higher	G4/G5, 800 MHz or higher
minimum 512 MB RAM	minimum 512 MB RAM
USB 2.0 interface	USB 2.0 interface
Windows XP/Vista	Mac OS X 10.3.9 (Panther) or higher

3.2 Initial operation

Before you can use your C-1U, connect it to a free USB port on your computer.

For initial operation of your C-1U, complete the following steps:

1)   Power up your computer.

2)   Connect your C-1U to a free USB port on your computer.

◊   **Your operating system automatically installs the required drivers.**

3)   Select the C-1U as input source in your preferred audio software application.

Windows:

4)   Adjust the recording level as required, using the Windows **Volume Control** panel. (Shortcut: Loudspeaker icon found in the taskbar)

Mac OS:

5) Adjust the recording level as required, using **Audio Midi Setup** in Mac OS.

◊ **Your C-1U is now ready for use.**

Complete the following steps should you want to use your C-1U by default in other applications:

Windows:

- Select the C-1U in the pull-down menu of **Sound recording** by clicking on **Sounds and Audio Devices** in the **Control Panel** and then clicking the tab **Audio**

Mac OS:

- Select C-1U as **Default Input** found under the tab **Audio Devices** in **Audio Midi Setup** of Mac OS

4. Using the Microphone

To get the sound you want, try changing the mic position relative to the sound source or even move the microphone around in the recording room of your studio. Adjusting the angle at which walls face the sound source can also be helpful. Only when the desired basic sound has been achieved, should you start to use equalizers and signal processors, if any at all (remember: less is often more!).

Due to the extremely linear frequency response and the high sonic resolution of your C-1U, there is no need for high-frequency "EQing" that can heavily influence the signal and unnecessarily increase the noise level. The C-1U provides that much-desired transparency which often gets lost during recording and mixing.
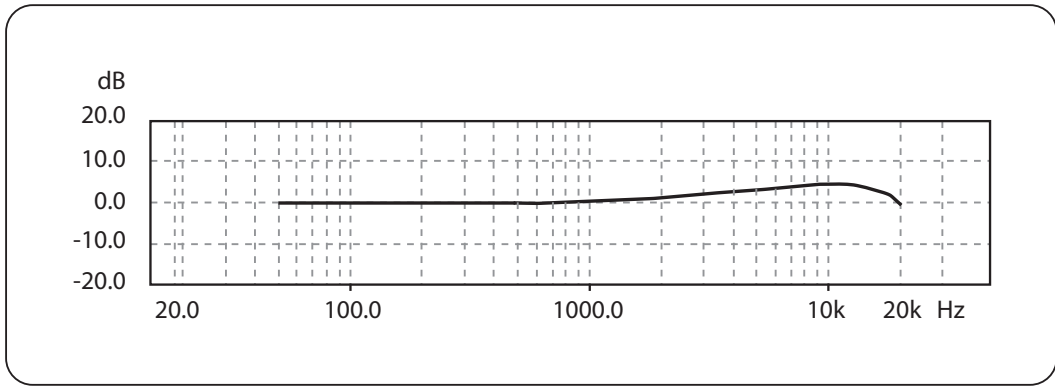
Frequency response
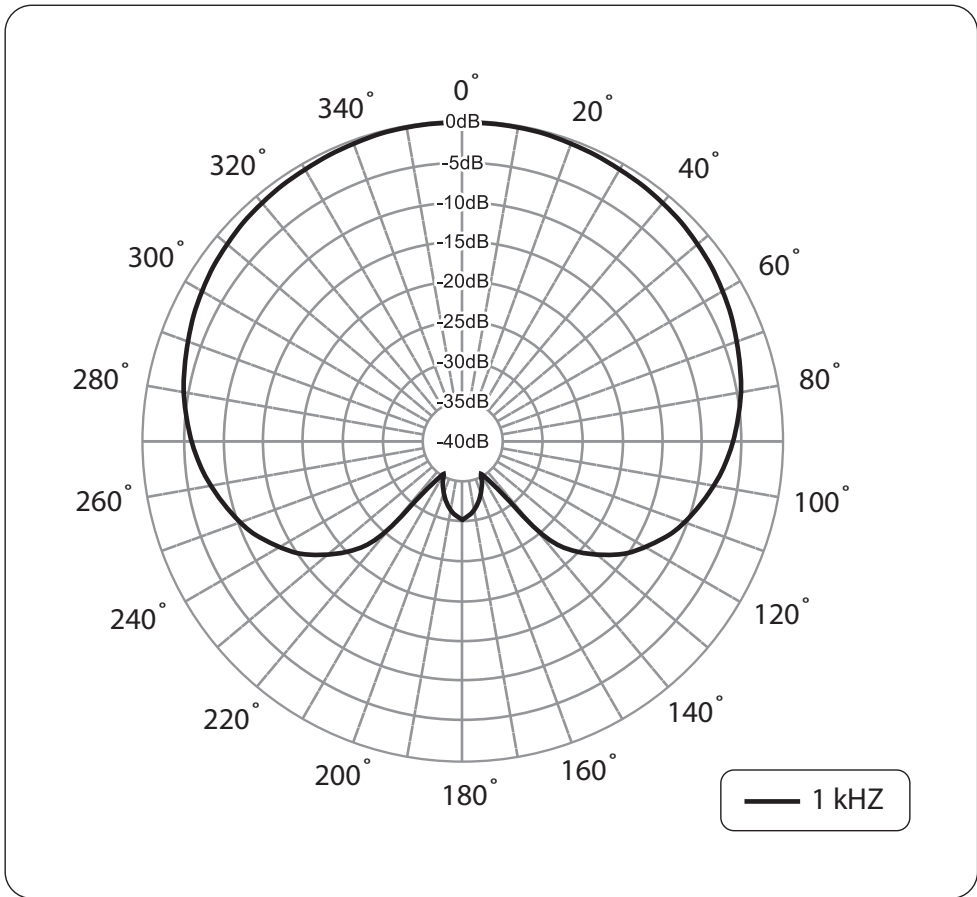
Polar pattern

5. Specifications

Transducer type	condenser, 16 mm (0.63'')
Polar pattern	cardioid
Frequency response	40 Hz to 20 kHz
Max. SPL (1% THD @ 1 kHz)	136 dB
Connector	USB connector type B
Power supply	5 V, max. 50 mA (via USB)

Physical/Weight	
Dimensions	Ø shaft: 2.1", length: 6.7" Ø shaft: 54 mm, length: 169 mm
Weight (net)	approx. 1.17 lbs / 0.53 kg

BEHRINGER is constantly striving to maintain the highest professional standards. As a result of these efforts, modifications may be made from time to time to existing products without prior notice. Specifications and appearance may differ from those listed or illustrated.

Appendix I

Python Libraries and Modules Used

This appendix provides a comprehensive list of all external Python libraries used throughout this thesis.

```python
# General Purpose
import os
import pandas as pd
import numpy as np
from datetime import timedelta

# Data Visualisation
import matplotlib.pyplot as plt
import seaborn as sns

# Data Processing
from scipy.signal import welch
from scipy.stats import skew, kurtosis, iqr
from scipy.fftpack import fft, fftfreq
import librosa

# Machine Learning Preprocessing
from sklearn.preprocessing import StandardScaler
from sklearn.impute import KNNImputer
from sklearn.feature_selection import mutual_info_regression,
    mutual_info_classif
from sklearn.decomposition import PCA, KernelPCA
from sklearn.model_selection import StratifiedKFold,
    cross_val_predict
from sklearn.pipeline import Pipeline
```

```python
# Machine Learning Models
from sklearn.linear_model import LinearRegression,
    LogisticRegression, Lasso, Ridge, RidgeClassifier
from sklearn.neighbors import KNeighborsRegressor,
    KNeighborsClassifier
from sklearn.svm import SVR, SVC
from sklearn.neural_network import MLPRegressor, MLPClassifier
from sklearn.tree import ExtraTreeRegressor,
    ExtraTreeClassifier
from sklearn.ensemble import RandomForestRegressor,
    RandomForestClassifier, GradientBoostingRegressor,
    GradientBoostingClassifier, StackingRegressor,
    StackingClassifier
from xgboost import XGBRegressor, XGBClassifier
from lightgbm import LGBMRegressor, LGBMClassifier
from catboost import CatBoostRegressor, CatBoostClassifier
from tabpfn import TabPFNClassifier

# Evaluation Metrics
from sklearn.metrics import mean_squared_error,
    mean_absolute_error, f1_score, accuracy_score,
    confusion_matrix, roc_curve, auc

# Hyperparameter Optimisation
import skopt
from skopt import BayesSearchCV, dump, load
from skopt.plots import plot_evaluations
from skopt.space import Real, Categorical, Integer

# Specialised Tools
import joblib
from custom_cross_validator import CustomStratifiedKColumnFold
from adapt.instance_based import KMM
import shap
from pyts.image import GramianAngularField
import cv2
```

Appendix J

Excluded Sensor Data

Table J.1: Collected data that was not used when training or evaluating the performance of different models for tool wear prediction and classification. Each row represents a single dwell cycle repeat. This data was excluded for various reasons, including operator errors and issues with the AWJ process that affected the data quality. Detailed reasoning for the unreliability of certain data points can be found in Chapter 5 of this thesis. Abbreviations: P = Preliminary, M1 = Main – Phase I, M2 = Main – Phase II, Change = MC or orifice change, B. Ch. 5 = Before Chapter 5 analysis, A. Ch. 5 = After Chapter 5 analysis.

Tube No.	Trial	Event	Wear Time (min.)	Water Pressure (bar)	Excluded	Reason
1	P	WDC	40	4000	B. Ch. 5	Unreliable
3	M1	WDC	0	5000	A. Ch. 5	Unreliable
3	M1	WDC	15	5000	A. Ch. 5	Unreliable
3	M1	WDC	15	5000	A. Ch. 5	Unreliable
3	M1	WDC	15	5000	A. Ch. 5	Unreliable
3	M1	WDC	5	5000	A. Ch. 5	Unreliable
3	M1	WDC	5	5000	A. Ch. 5	Unreliable
3	M1	WDC	5	5000	A. Ch. 5	Unreliable
4	M1	WDC	20	4000	B. Ch. 5	Operator error
4	M1	Change	30	4000	B. Ch. 5	Operator error
5	M1	WDC	10	3000	A. Ch. 5	Unreliable
5	M1	WDC	15	3000	A. Ch. 5	Unreliable
5	M1	WDC	15	5000	A. Ch. 5	Unreliable
5	M1	WDC	25	5000	A. Ch. 5	Unreliable
5	M1	WDC	30	3000	A. Ch. 5	Unreliable
5	M1	WDC	40	3000	A. Ch. 5	Unreliable
7	M1	WDC	25	3000	A. Ch. 5	Unreliable
7	M1	WDC	30	5000	A. Ch. 5	Unreliable
7	M1	WDC	30	5000	A. Ch. 5	Unreliable
7	M1	WDC	30	5000	A. Ch. 5	Unreliable
7	M1	WDC	40	3000	A. Ch. 5	Unreliable
7	M1	WDC	45	4000	B. Ch. 5	Operator error
7	M1	WDC	55	3000	B. Ch. 5	Operator error
7	M1	WDC	5	3500	B. Ch. 5	Operator error
7	M1	WDC	65	3000	A. Ch. 5	Unreliable
8	M1	WDC	40	3000	A. Ch. 5	Unreliable
8	M1	WDC	40	4000	B. Ch. 5	Operator error
8	M1	WDC	50	3000	A. Ch. 5	Unreliable
8	M1	WDC	70	3000	A. Ch. 5	Unreliable
8	M1	WDC	90	3000	A. Ch. 5	Unreliable
18	M1	ATD	70	5000	A. Ch. 5	Unreliable
6	M2	Change	60	5000	B. Ch. 5	Operator error
9	M2	WDC	20	1500	B. Ch. 5	Operator error
9	M2	WDC	20	5000	B. Ch. 5	Operator error
9	M2	WDC	50	5000	A. Ch. 5	Unreliable
9	M2	WDC	50	5000	A. Ch. 5	Unreliable
10	M2	WDC	0	3500	B. Ch. 5	Operator error
10	M2	WDC	0	5000	A. Ch. 5	Unreliable
10	M2	WDC	10	5000	A. Ch. 5	Unreliable
10	M2	WDC	20	3000	A. Ch. 5	Unreliable
10	M2	WDC	30	3000	A. Ch. 5	Unreliable
10	M2	WDC	30	3500	A. Ch. 5	Unreliable
10	M2	WDC	30	4500	A. Ch. 5	Unreliable
19	M2	ATD	70	4000	B. Ch. 5	Operator error